CHARACTERIZING HOST TARGETED ANTIVIRALS THAT IMPAIR INFLUENZA A VIRUS PROTEIN SYNTHESIS

By

Patrick D. Slaine

Submitted in partial fulfilment of the requirements
for the degree of Doctor of Philosophy

at

Dalhousie University
Halifax, Nova Scotia
September 2021

Dalhousie University is located in Mi'kma'ki, the
ancestral and unceded territory of the Mi'kmaq.
We are all Treaty people.

DEDICATION

I dedicate this thesis to my friends and family.

Your unwavering support and love enabled me to complete this degree.

TABLE OF CONTENTS

LIST OF TABLES ix

LIST OF FIGURES x

ABSTRACT xii

LIST OF ABBREVIATIONS USED xiii

ACKNOWLEDGEMENTS xix

CHAPTER 1: INTRODUCTION 1

1.1 Overview of Influenza 1

1.2 Influenza A Virus Structure and Replication Cycle 4

1.3 The Viral Envelope Proteins HA, NA, and M2 8

1.3.1 Haemagglutinin 8

1.3.2 Neuraminidase 11

1.3.3 Matrix 2 11

1.4 The Mechanisms of Antigenic Shift and Drift 13

1.5 Direct Acting Antivirals Against Influenza 14

1.5.1 NA Inhibitors 14

1.5.2 M2 Inhibitors 17

1.5.3 Polymerase Inhibitors 17

1.5.4 The Need for New Antivirals 18

1.6 Generation of Host mRNA, mRNA Processing, and Translation 20

1.6.1 Overview 20

1.6.2 mRNA Synthesis and Export 21

1.6.3 mRNA Stability and Degradation 23

1.6.4 Translation Initiation *24*

1.6.5 tRNA Abundance and Translation *26*

1.6.6 Translation Regulation *26*

1.6.7 The Integrated Stress Response *27*

1.6.8 Stress Granules *29*

1.6.9 IAV and Host Translation *31*

1.7 TRANSLATION AND THE ER 34

1.7.1 Post-Translational Modifications *35*

1.8 THE THREE ARMS OF THE UPR 37

1.8.1 BiP *38*

1.8.2 IRE1 ..... *39*

1.8.3 PERK *43*

1.8.4 ATF6 ..... *44*

1.8.5 ER Associated Degradation *45*

1.8.6 Prolonged UPR Signaling and the Induction of Apoptosis *46*

1.8.7 UPR and IAV Infection *48*

1.9 RATIONALE AND OVERVIEW 49

CHAPTER 2: MATERIALS AND METHODS 55

2.1 CELL CULTURE 55

2.2 INFLUENZA VIRUSES AND INFECTIONS 55

2.3 PLAQUE ASSAY 57

2.4 HEMAGGLUTINATION ASSAY 58

2.5 CHEMICALS 58

2.6 CYTOTOXICITY ASSAY 59

2.7 IMMUNOFLUORESCENCE 60

2.8 IMMUNOBLOTTING 60

2.9 SEMIQUANTITATIVE XBP1 MRNA SPLICING ASSAY 61

2.10 SEQUENCING AND ANALYSIS 62

2.11 GENERATION OF RECOMBINANT VIRUSES 64

2.12 MINIGENOME ASSAY 65

2.13 GENERATING CRISPR KO CELL LINES 66

2.14 MLD_{50} CALCULATION IN THE BALB/C MOUSE MODEL 67

2.15 6-TG TREATMENT IN MURINE CHALLENGE STUDY 68

2.16 FLOW CYTOMETRY ANALYSIS 69

2.17 STATISTICAL ANALYSIS 69

2.18 ACCESSION NUMBERS 70

2.19 ANIMAL ETHICS 70

CHAPTER 3: THE EIF4A INHIBITORS SILVESTROL AND PATEAMINE A IMPAIR THE ACCUMULATION OF VIRAL PROTEINS AND REDUCE VIRUS PRODUCTION 71

3.1 INTRODUCTION 72

3.2 RESULTS 77

3.2.1 Sil and PatA Impaired IAV Replication 77

3.2.2 Sil and PatA are Cytotoxic in Treated Cells 80

3.2.3 Sil and PatA Impaired Viral Protein Synthesis 81

3.2.4 SG Formation is Inversely Correlated with Viral Protein Accumulation 82

3.2.5 Sil and PatA Treatment Induced Apoptosis in Treated Cells 83

3.2.6 PatA Reduced Virus Production from Different Influenza Viruses 85

3.2.7 PatA Inhibited Translation from the NanoLuc Reporter Virus 86

3.3 DISCUSSION 87

CHAPTER 4: THE THIOPURINES 6-TG AND 6-TGO ACTIVATE AN ANTIVIRAL UNFOLDED PROTEIN RESPONSE THAT BLOCKS INFLUENZA A VIRUS GLYCOPROTEIN ACCUMULATION 101

4.1 INTRODUCTION 101

4.2 RESULTS 112

4.2.1 6-TG and 6-TGo are Cytostatic 112

4.2.2 Treating Infected Cells with 6-TG and 6-TGo Impaired Virus Production 114

4.2.3 6-TG And 6-TGo Treatment Impaired the Accumulation of Viral Glycoproteins 118

4.2.4 6-TG And 6-TGo Treatment Induced the UPR in Treated Cells 119

4.2.5 Modulating the UPR Restored Viral Glycoprotein Accumulation but Failed to Restore Virus Production 121

4.2.6 Knocking Out PERK Increased the Antiviral Effects of 6-TG 123

4.2.7 6-TG Is More Effective Than the Rac1 Inhibitor V 126

4.2.8 Calculating the MLD_{50} of CA/07-MA 127

4.2.9 Drug Delivery and 6-TG Tolerance in Mice 128

4.2.10 6-TG Did Not Protect Against Lethal Infection 130

4.2.11 6-TG Treatment Altered the Immune Response of Infected Mice 131

4.2.12 6-TG Failed to Induce the UPR in Mouse Cell Lines 133

4.2.13 Treating Infected MEFs with 6-TG did not Impair Virus Production 134

4.3 DISCUSSION 135

CHAPTER 5: ANALYSIS OF ADAPTIVE MUTATIONS FOUND IN THE INFLUENZA A VIRUS POLYMERASE SUBUNITS 158

5.1 INTRODUCTION 158

5.2 RESULTS 164

5.2.1 Swiss-Webster Mice Lack Functional Mx1 164

5.2.2 Utilizing the Illumina MiSeq Platform for Deep Sequencing 165

5.2.3 Deep Sequencing of the Mouse Adapted Viruses Identified Unique Mutations 166

5.2.4 CA/07-MA Virus Displayed Differential Junction Sites and Read Coverage Compared to Parental CA/07 167

5.2.5 Identification and Quantification of Adaptive Mutations in CA/07-MA 169

5.2.6 All Identified Adaptation Mutations on the RdRp are Surface Exposed in Viral RdRp 172

5.2.7 Generation the Infectious Clone of CA/07 173

5.2.8 Generation of Mouse Adaptation Mutations in PA and PB1 Using Site Directed Mutagenesis 174

5.2.9 PA E349G Enhanced Viral Polymerase Activity in the Minigenome Replicon Assay 175

5.2.10 Recombinant Virus Harbouring the Polymerase Adaptation Mutations in PB1 and PA Replicated Efficiently in Mouse Cells 177

5.2.11 Bioinformatic Analysis of Clinical Isolates of H1N1 Shows Low Abundance of PA E349G 178

5.3 DISCUSSION 179

CHAPTER 6: CONCLUSIONS 205

6.1 CONCLUSIONS AND LIMITATIONS 205

6.2 TESTING SIL, PATA, AND 6-TG ON PRIMARY CELL LINES THAT FAITHFULLY REPRESENT THE HUMAN RESPIRATORY TRACT 208

6.3 Further Investigation into the Effects of 6-TG Treatment on the UPR and Cell Fate 209

6.4 Identification of the GTPase Responsible for 6-TG Mediated UPR Activation 211

6.5 Further Characterization of IAV RdRp Adaptation Mutations in the Mouse Model will Confirm an Increase in Virus Fitness 213

6.6 Further Studying the Effects of RdRp Mutations on Viral Polymerase Activity Will Identify Key Viral Processes 214

BIBLIOGRAPHY 218

LIST OF TABLES

Table 4.1 Average concentrations of chemokine/cytokine from the BALF of infected mice at 3 dpi 143

Table 5.1 Primers used for deep-sequencing IAV 188

Table 5.2 Deep sequencing overview for parental CA/07 and CA/07-MA..... 189

Table 5.3 Hierarchical indexing for spliced alignment of transcripts 2 (HISAT2) analysis of junction reads..... 190

Table 5.4 Nucleotide substitutions identified by deep sequencing..... 191

LIST OF FIGURES

Fig 1.1 Simplified overview of a single round of IAV replication in the host cell 52

Fig 1.2 Translation initiation requires the 43S preinitiation complex and the eIF4F complex 53

Fig 1.3 ER stress induces the unfolded protein response (UPR) 54

Fig 3.1 Bond line structures of the eukaryotic initiation factor 4A inhibitors Pateamine A and Silvestrol. 92

Fig 3.2 Dose-dependent reduction of viral replication, cytotoxicity, and stress-granule formation from treatment with Pateamine A 94

Fig 3.3 Dose-dependent reduction of viral replication, cytotoxicity, and stress-granule formation from treatment with Silvestrol 96

Fig 3.4 Pateamine A and Silvestrol treatment cause cytotoxicity and induce apoptosis in treated cells 97

Fig 3.5 Pateamine A treatment reduces Udorn replication and may reduce the proliferation of different IAV subtypes across different IAV subtypes 98

Fig 3.6 Silvestrol treatment reduces accumulation of A/Udorn/72 (H3N2) 99

Fig 3.7 Pateamine A treatment may reduce the synthesis of viral encoded Nanoluciferase 100

Fig 4.1 6-Thioguanine and 6-Thioguanosine demonstrate cytostatic effects on treated cells 144

Fig 4.2 6-TG and 6-TGo treatment impairs replication of genetically diverse influenza subtypes 145

Fig 4.3 Characterization of 6-TG and 6-TGo antiviral effects over time and at different concentrations 146

Fig 4.4 6-TG and 6-TGo impair viral glycoprotein synthesis 147

Fig 4.5 6-TG and 6-TGo activate the UPR 148

Fig 4.6 ISR inhibition restores NA synthesis in the presence of 6-TG but NA processing and virion production remain impaired 149

Fig 4.7 Knocking out of PERK enhances inhibition of viral replication by 6-TG 150

Fig 4.8 Rac1 inhibitor V may not be as effective as 6-TG at reducing viral titers 151

Fig 4.9 Determining the MLD_{50} of CA/07-MA 152

Fig 4.10 Testing the intranasal route of administration in infected mice and testing different concentrations of 6-TG intraperitoneal 153

Fig 4.11 IP injection of 0.3 mg/kg 6-TG does not protect against a lethal dose of CA/07-MA 154

Fig 4.12 Multiplex ELISA from mouse BALF showed changes in 6-TG treated mice 155

Fig 4.13 Representative flowcytometric analysis of immune cells found in the BALF of treated mice 156

Fig 4.14 6-TG fails to induce the UPR in murine cells and fails to reduce virus production from infected mouse cells 157

Fig 5.1 Murine adaptation of CA/07 increases virus replication in the lung over time and spread to brain 197

Fig 5.2 Outbred Swiss Webster mice have non-functional Mx1 198

Fig 5.3 Successful multi-segment amplification of the IAV genome 199

Fig 5.4 Differential generation of defective viral genomes between parental CA/07 and CA/07-MA 200

Fig 5.5 Identification of adaptive mutations in CA/07-MA by MiSeq Illumina deep sequencing 201

Fig 5.6 CA/07 mouse adaptation mutations are surface exposed in the ternary RdRp complex 202

Fig 5.7 PA E349G substitution enhances viral RNA polymerase activity 203

Fig 5.8 Rescued virus harbouring the mouse adapted PA and PB1 increase replication in mouse cells 204

Fig 6.1 Potential GTPases that 6-TG may be inhibiting in the secretory pathway 216

Fig 6.2 Illustration of the air-liquid interface model using primary cell lines 217

ABSTRACT

The plasticity of influenza A virus (IAV) genomes enables rapid evolution of resistance to antivirals that directly target viral proteins. By contrast, host-targeted antivirals have the potential to disrupt key steps in viral replication and alert the immune system in a manner that is not so easily overcome by rapid viral evolution. Like all viruses, IAV uses host protein synthesis machinery to produce viral proteins. IAV mRNAs access this machinery by incorporating host 5'-cap structures and mimicking host 3'-polyadenylate tails. Host cap-dependent translation requires the RNA helicase eIF4A. Here, I demonstrate that treating infected cells with eIF4A inhibitors silvestrol or pateamine A inhibits IAV replication by preventing the accumulation of viral proteins required to support viral genome replication. However, these compounds were also cytotoxic, limiting their utility as host-targeted antivirals. The McCormick lab identified the thiopurines 6-thioguanine (6-TG) and 6-thioguanosine (6-TGo) as candidate molecules that stimulate host stress responses. I showed that these thiopurines inhibited IAV replication by activating the host unfolded protein response and selectively preventing the accumulation of IAV glycoproteins. Importantly, these molecules were not cytotoxic at doses required to disrupt viral replication. Finally, I directly investigated the plasticity of the IAV genome by identifying host adaptation mutations required to support viral replication in a murine infection model. I characterized novel substitutions in the viral polymerase subunits that increased polymerase activity and viral replication in cultured murine cells. Together, these studies have advanced understanding of the molecular basis of host adaptation and identified vulnerabilities that can be exploited by host-targeted antivirals.

LIST OF ABBREVIATIONS USED

˚C	Degree Celsius
~	Approximately
%	Percent
µg	Microgram
µM	Micromolar
1x	One-times
2x	Two-times
4-PBA	4-phenylbutyrate acid
5x	Five-times
5’ cap	5’-7-Methylguanosine cap
5-FU	5-Flurouracil
6-MP	6-Mercaptopurine
6-TG	6-Thioguanine
6-TGN	6-Thioguanine nucleotides
6-TGo	6-Thioguanosine
10x	Ten-times
A	Adenosine
ADP	Adenosine diphosphate
ALG7	Asparagine linked glycosylation 7
AmantS	Amantadine sensitive
ANOVA	Analysis of variance
ANP32A	Acidic nuclear phosphoprotein 32A
AP-1	Activator protein-1
As	Sodium Arsenite
ARDS	Acute respiratory distress syndrome
ASK1	Apoptosis signal-regulating kinase 1
ATF3	Activating transcription factor 3
ATF4	Activating transcription factor 4
ATF6	Activating transcription factor 6
ATF6-FL	Activating transcription factor 6 full-length
ATF6-N	Activating transcription factor 6-N-terminus
ATP	Adenosine triphosphate
Aza	Azathioprine
BALF	Bronchiolar alveolar lavage fluid
BcL	B-cell lymphoma-2
BCL2L11	Bcl-2-like protein 11
BiP	Binding immunoglobulin protein
bp	Base pair
Brisbane	A/Brisbane/57/2007 (H1N1)
BSA	Bovine serum albumin
BSL	Bio-safety level
bZIP	Basic Leucine Zipper Domain
C	Cytosine
Ca^{2+}	Calcium

CA/07	A/California/07/2009 (H1N1)
CARE	C/EBP-ATF Response Elements
CBC	Cap binding complex
CD	Cluster of differentiation
cDNA	Complementary DNA
CFI	Cleavage factor I
CHO	Chinese hamster ovary
CHOP	C/EBP homology protein
CNS	Central nervous system
COP II	Coat protein II
COVID-19	Coronavirus-19
CPSF	Cleavage and polyadenylation specificity factor
CREB	cAMP-response element binding protein
CRISPR	Clustered regulatory interspaced short palindromic repeats
cRNA	Complementary RNA
C-terminus	Carboxyl terminus
CTD	C-terminal domain
CXCL	Chemokine (C-X-C motif) ligand
d	Day(s)
DI	Defective interfering
DMEM	Dulbecco's modified Eagle's medium
DMSO	Dimethyl sulfoxide
DNA	Deoxyribonucleic acid
dpi	Days post-infection
dsDNA	Double-stranded deoxyribonucleic acid
dsRNA	Double-stranded ribonucleic acid
DTT	Dithiothreitol
DVG	Defective viral genomes
EDEM1	ER Degradation Enhancing Alpha-Mannosidase Like Protein 1
EDTA	Ethylenediaminetetraacetic acid
eIF	Eukaryotic initiation factor
eIF4E-BP	eIF4E-binding protein
EJC	Exon junction complex
ELISA	Enzyme-linked immunosorbent assay
ER	Endoplasmic reticulum
ERAD	ER-associated degradation
ERSE	ER stress responsive element
FBS	Fetal bovine serum
FDA	Food and Drug Administration
FFU	Focus forming unit
Fig	Figure
G	Guanosine
G3BP1	Ras-GTPase-activating protein binding protein 1
GADD34	Growth and arrest DNA damage protein 34
GADD153	Growth arrest and DNA damage inducible gene 153
GCN2	General control nonderepressible 2

GDP	Guanosine diphosphate
GEF	Guanine nucleotide exchange factor
GFP	Green fluorescent protein
GlcNAc	N-acetylglucosamine
GMP	Guanosine monophosphate
GRP78	Glucose regulated protein 78
GTP	Guanosine triphosphate
GTPase	Guanosine triphosphate hydrolase
h	Hour(s)
HA	Hemagglutinin
HCV	Hepatitis C virus
HEK	Human embryonic kidney
HGPRT	Hypoxanthine guanine phosphoribosyl transferase
HPAI	Highly pathogenic avian influenza
HRI	Heme-regulated inhibitor
HRP	Horse radish peroxidase
HSP	Heat shock protein
HTA	Host-targeted antiviral
IAV	Influenza A virus
IBD	Inflammatory bowel disease
IBV	Influenza B virus
IC_{50}	Inhibitory concentration 50
IFN	Interferon
Ig	Immunoglobulin
IL-6	Interleukin-6
I.N	Intranasal
I.P	Intraperitoneal
IP3R1	Inositol 1,4,5-trisphosphate receptor type 1
IRE1	Inositol-requiring enzyme 1
IRES	Internal ribosomal entry site
ISG	Interferon-stimulated gene
ISR	Integrated stress response
ISRIB	ISR inhibitor
JNK	c-Jun N-terminal kinase
Kb	Kilobase
kDa	Kilodalton
kg	kilogram
KO	Knock out
LC3	Light chain 3
log	Logarithmic
Ly6G	Lymphocyte antigen 6 complex locus G
M1	Matrix protein 1
M2	Matrix protein 2
MA	Mouse adapted
Man	Mannose
MARK2	Microtubule affinity-regulating kinase 2

MDCK	Madin-Darby Canine Kidney
MEF	Mouse embryo fibroblast
mg	Milligram
MHC	Major histocompatibility complex
miRNA	Micro RNA
mL	Milliliter
MLD_{50}	Mean lethal dose 50
mM	Millimolar
MOI	Multiplicity of infection
mRNA	Messenger ribonucleic acid
mTORC	Mammalian target of rapamycin complex
MW	Molecular weight
MxA	Myxovirus resistance protein 1
N	nucleotide
NA	Neuraminidase
NBD	Nucleotide binding domain
NDV	Newcastle disease virus
NEP	Nuclear export protein
ng	Nanogram
NLG	N-Linked glycosylation
NLS	Nuclear localization signal
nm	Nanometer
nM	Nanomolar
NNTB	Number needed to benefit
NNTH	Number needed to harm
NP	Nucleoprotein
NS1	Non-structural 1
nt	Nucleotide
NT	Non targeting
N-terminal	Amino terminal
OOR	Out of range
ORF	Open reading frame
PA	Polymerase acid
PABP	Poly(A)-binding protein
PAMP	Pathogen-associated molecular pattern
PAP	Poly adenosine polymerase
PARP	Poly (ADP-ribose) Polymerase
PatA	Pateamine A
PA-X	Polymerase acid-X ORF
PB1	Polymerase basic protein 1
PB1-F2	Polymerase basic protein frame 2
PB2	Polymerase basic protein 2
PBS	Phosphate buffered saline
PCR	Polymerase chain reaction
PDI	Protein disulfide isomerase
PERK	PKR-like ER kinase

PFU	Plaque forming unit
pH	Power of hydrogen
PIC	Pre-initiation complex
PKA	Protein kinase A
PKR	Protein kinase R
PM	Plasma membrane
Pol I	RNA polymerase I
Pol II	RNA polymerase II
Pol III	RNA polymerase III
PP1	Protein phosphatase 1
PP2A	Protein phosphatase 2A
PR8	A/Puerto Rico /08/1934 (H1N1)
Pre-mRNA	Pre-messenger RNA
PRRs	Pattern recognition receptor
PTM	Post-translational modification
Q	Quality score
qPCR	Quantitative polymerase chain reaction
R	Purine
Rac1	Ras-related C3 botulinum toxin substrate 1
RACK1	The Receptor for Activated C Kinase 1
RBC	Red blood cell
RBD	Receptor binding domain
RBM8A	RNA-binding protein 8A
RdRp	RNA dependent RNA polymerase
RE	Restriction enzyme
RIDD	Regulated IRE1-dependent decay
RIP	Regulated intramembrane proteolysis
RNA	Ribonucleic acid
RNP	Ribonucleic protein
rRNA	Ribosomal RNA
RT-PCR	Reverse-transcription polymerase chain reaction
RT-qPCR	Quantitative reverse-transcription polymerase chain reaction
S1P	Site-1 protease
S2P	Site-2 protease
SARS-CoV-2	Severe acute respiratory syndrome coronavirus 2
SD	Standard deviation
SDS-PAGE	Sodium dodecyl sulfate polyacrylamide gel electrophoresis
SERCA	Sarco/endoplasmic reticulum Ca^{2+}ATPase
SG	Stress granule
Sil	Silvestrol
SIP	Semi-infectious particle
snRNA	Small nuclear RNA
SRP	Signal recognition particle
SREBPs	Sterol regulatory element-binding proteins
SR	SRP receptor
s/s/r	Substitutions/site/replication

Stau1	Staufen
T	Thymine
TC	Ternary complex
$TCID_{50}$	Tissue culture dose 50
TFIIH	Transcription factor II human
Tg	Thapsigargin
TGN	Trans-Golgi network
TIA-1	T-cell intracellular antigen 1
TIAR	TIA-related protein
TLR7	Toll-like receptor
TM	Tunicamycin
TMEM38B	Transmembrane Protein 38B
TMPRSS2	Transmembrane protease, serine 2
TPCK	Tosyl phenylalanyl chloromethyl ketone
tRNA	Transfer ribonucleic acid
TUDCA	Tauroursodeoxycholic acid
U	Uracil
Udorn	A/Udorn/1972 (H3N2)
UDP	Uracil diphosphate
Uni12	Universal 12
Uni13	Universal 13
uORF	Upstream open reading frame
UPR	Unfolded protein response
UPRE	Unfolded protein response element
USP10	Ubiquitin specific peptidase 10
UTR	Untranslated region
vRNA	Viral RNA
vRNP	Viral ribonucleoprotein
XBP1	X box binding protein 1
XBP1s	Spliced XPB1
XBP1u	Unspliced XBP1
Xrn1	5′-3′ exoribonuclease 1

ACKNOWLEDGEMENTS

Foremost, I would like to thank my supervisor, Dr. Craig McCormick, from the bottom of my heart. Thank you for supporting me as we went through the last six years together. Thank you for letting me pursue science, building a wonderful lab that I was could be a part of, and teaching me many things both inside and outside the lab. Thank you for taking me on and letting me explore the world of science under you.

I would like to thank Dr. Denys Khaperskyy. Your work laid the groundwork for my entire thesis. Without you, I would not be here today. You helped with almost every assay I completed, thank you for imparting your wisdom on me. Thank you for your guidance and words of enlightenment.

I would like to thank the members of the McCormick lab, past and present. Thank you for making the lab a supportive environment and a joy to participate in. I would like to thank Mariel Kleer for all her help and support during her time with the McCormick lab. I would like to thank Dr. Eric Pringle and Dr. Brett Duguay for their help, mentorship, and ideas to complete the work done here.

I would like to thank my committee members, Dr. Todd Hatchette, Dr. Brent Johnston, and Dr. Andrew Makrigiannis. Thank you for helping me over the years. Thank you Dr. Hatchette for providing me training/resources for my experiments, and volunteering with you was incredible. Thank you, Dr. Johnston for supporting me over the years and collaborating with me on the mental health working group. Thank you Dr. Makrigiannis for our collaborative projects and discussions. Thank you, Dr. Valerie Chappe, we made good progress on mental health support systems, and thank you FMGSS members, specifically Adrian Herod and Prathyusha Konda for your help.

I would like to thank my parents Dr. Kathleen Cavanaugh and David Slaine for installing in me an undying desire to learn and explore. Thank you for showing me love and being good role models for how to live a fulfilling life.

I would like to thank my friends that I have made along the way. My friends helped me get through every aspect of this degree, and I owe them everything. Tupper Mixer allowed us to socialize, thank you all who participated. Thank you, Michal Scur and Alexa Wilson, you two helped me through this. And lastly, I would like to acknowledge Luke Hattie, we miss you and may you rest in peace.

CHAPTER 1: INTRODUCTION

1.1 Overview of Influenza

The influenza viruses generally causes mild illness, but it can lead to severe morbidity and mortality with annual epidemics associated with ~200,000-500,000 deaths worldwide (Paget et al., 2019). The virus is spread through respiratory droplets, aerosols, and less frequently, fomites (Kutter et al., 2018; Richard & Fouchier, 2016). Influenza virus infection typically leads to the onset of a fever, headache, cough, muscle aches, and fatigue. In most healthy individuals, infection resolves in 7-10 days with minimal long-term effects. However, infection can result in severe immune dysregulation and tissue injury, resulting in hospitalization and on death. Infection can also lead to immune suppression in the lung, resulting in secondary bacterial infections. These secondary bacterial infections can lead to further complications, leading to a worse prognosis for the infected patient. Furthermore, some bacterial infections can enhance influenza's infection of the lung by secreting co-factors that aid in viral replication. Several co-morbidities increase the risk for influenza complications; these include obesity and infection with human immunodeficiency virus (Honce & Schultz-Cherry, 2019).

Influenza viruses belong to the *Orthomyxoviridae* Family and are separated into four different Genera. The *Alphainfluenzavirus* Genus contains the influenza A virus (IAV), which is further divided into different subtypes based on their glycoprotein make-up. IAV species are subtyped by antigenic properties of surface glycoproteins haemagglutinin (HA) and neuraminidase (NA). There are 18 different subtypes of HA, and 11 different subtypes of NA. Currently, H1N1 and H3N2 co-circulate in humans and cause seasonal outbreaks (Y. Wu et al., 2014). However more broadly, IAV infects a

plethora of species beyond humans including waterfowl, horses, pigs, and bats. IAV can jump from a reservoir species into humans; this event is termed zoonosis. The large number of reservoir species currently makes the eradication of IAV impossible. The *Betainfluenzavirus* Genus contains the Influenza B virus species (IBV), which instead of diverging into two subtypes based on HA and NA clustering. The two subtypes are the Victoria and Yamagata lineages. IBV only circulates in humans and seals, with the mass majority of IBV infections arising from human-to-human transmission. Interestingly, both lineages of IBV cocirculate along with IAV in humans. The pandemic potential of IBV is much less than IAV due to its lack of extraneous genetic diversity in the restricted reservoir species (Paules & Subbarao, 2017). The antigenic sites in IBV evolve at a slower rate than IAV as well (Matsuzaki et al., 2004). The *Deltainfluenzavirus* Genus contains the Influenza D viruses that are found in pigs and cattle and do not circulate in humans. The last Genus, *Gammainfluenzavirus*, contains the influenza C virus, which rarely causes disease in humans. Among influenza species, IAV has caused the greatest damage to our civilization, in terms of economic loss and cost of human life. I have focused my thesis research on IAV due to its clinical relevance.

Influenza infection can lead to viral pneumonia, which can be accompanied or followed by a secondary bacterial pneumonia (Short et al., 2014). Pneumonia can lead to acute respiratory distress syndrome (ARDS), a fatal complication of viral infection. ARDS is characterized by low oxygen in the blood (hypoxaemia), respiratory failure, and pulmonary edema (fluid in the lungs) which can result in multiorgan failure. ARDS can deadly, with a fatality rate up to 60% in some studies (Short et al., 2014). Damage to the alveoli reduces gas exchange as the alveolar space fills with fluid containing

inflammatory immune cells, fibrin, and red blood cells. The tight junctions made by the type I and type II epithelial cells of the alveoli are disrupted by infection, progressing to edema of the lung (Short et al., 2014). Influenza virus infection results in the death of the epithelial cells, weakening the cell layer. Influenza primarily damages bronchial or bronchiolar epithelial cells but the damage is not limited to this area. Neutrophils and monocytes also infiltrate the alveolar space, adding immunological pathology. Here, the activated immune cells directly damage the epithelium of the alveoli, furthering the disease manifestation. Damaged epithelial cells and activated leukocytes release more chemokines and cytokines to further recruit more monocytes and neutrophils, leading to a positive feedback loop that further damages the lung (Duan et al., 2017).

IAV is responsible for five major pandemics in the last century. The first, and most notable, was the 1918 H1N1 pandemic, commonly referred to as the "Spanish flu". This outbreak occurred as World-War I was coming to an end, enabling the virus to disseminate across the globe following troop movements. The 1918 H1N1 pandemic is estimated to have ended 20-50 million lives (Barry, 2004; Flahault & Zylberman, 2010). The H1N1 virus circulated in the human population until it was replaced in 1957 by an H2N2 virus. In 1957, a H2N2 virus emerged into the human population, leading to the deaths of 1 to 1.5 million individuals. This outbreak is generally referred to as the "Asian flu". H2N2 then circulated alone until 1968, when it was replaced by an H3N2 virus during the "Hong Kong flu" outbreak (Flahault & Zylberman, 2010). This H3N2 established transmission within the human population and is still in circulation today. In 1977, H1N1 re-emerged in the USSR and re-entered the human population. Anyone older than 30 years had pre-existing immunity to this virus, due to its circulation two decades

earlier. Retroactive investigation has determined that the H1N1 virus that emerged in the USSR in 1977 was almost identical to the H1N1 in circulation in 1950, with little genetic evolution over the two decades. Because of this, researchers speculate that H1N1 re-entered the human population accidentally through artificial means. There are two likely hypotheses on how this happened. The first is a laboratory-acquired infection from a laboratory worker handling the extinct virus, and the second being a failed attempt to cold-adapt a H1N1 isolate from 1950 and its subsequent use in a vaccine trial. The evidence for the latter hypothesis is supported by genetic analysis of the earliest samples from this outbreak harbouring cold-adapted mutations seen in live-attenuated vaccines (Palese, 2004; Rozo & Gronvall, 2015). Irrespective of how H1N1 re-emerged into the human population, it co-circulated with H3N2 until it was replaced in 2009 by an antigenically distinct H1N1 during the swine flu pandemic. The H1N1 virus that emerged in 2009 continues to co-circulate with H3N2. Interestingly, the transmission of IAV has been limited during COVID-19 pandemic due to the implementation of non-pharmaceutical interventions, including reduced inter- and intra-national mobility, social distancing, mask wearing, shutting down high risk sectors of the economy, and hand washing.

1.2 Influenza A Virus Structure and Replication Cycle

IAV is an enveloped virus composed of a 13.6 Kilobase (Kb) negative-sense RNA genome that contains 8 different ribonucleoprotein (RNP) complexes. IAV encodes at least 12 proteins across 8 genome segments. The viral proteins are polymerase basic protein 1 (PB1), polymerase basic protein 1-frame 2 (PB1-F2), polymerase basic protein

2 (PB2), polymerase acidic (PA), polymerase acidic protein X (PA-X), hemagglutinin (HA), neuraminidase (NA), nucleoprotein (NP), matrix protein 1 (M1), matrix protein 2 (M2), non-structural protein 1 (NS1), and nuclear export protein (NEP). The viral polymerase is a heterotrimeric complex composed of PB1, PB2, and PA. The trimeric polymerase complex forms an RNA dependent RNA polymerase (RdRp) that synthesises viral mRNA and viral genomic RNA (vRNA). Each genome segment carries its own polymerase complex. The viral genome segment is also coated by NP. Together, the vRNA, RdRp, and NP form viral ribonucleoprotein complexes (vRNPs). The envelope of influenza is derived from the host plasma membrane. The viral envelope contains three viral transmembrane domain proteins, HA, NA, and M2. HA makes up the majority of viral glycoproteins in the envelope, followed by NA, then followed by M2. Like all matrix proteins, M1 is found under the viral envelope, where it interacts with both the viral glycoproteins and the packaged vRNPs.

IAV enters host cells through receptor-mediated endocytosis after binding its receptor, sialic acid, on the cell surface. Sialic acid is found as a terminal linkage on N-linked glycans and on lipids in the phospholipid bilayer. IAV can infect the cell using clathrin mediated endocytosis, clathrin independent, and caveolin independent pathways (Lakadamyali et al., 2004). The endosome travels along the recycling endocytic pathway and becomes an acidic late endosome. The reduction in pH deprotonates HA, subsequently changing its conformation and activating intrinsic fusogenic properties. HA penetrates the endosomal membrane with its fusion peptide and promotes the fusion of viral envelope to host membranes (Lai & Freed, 2015). Tetrameric M2 also channels protons across the viral envelope to acidify the viral core. The acidification of the virion

core reduces the affinity of M1 for the vRNPs, allowing proper uncoating of viral genome segments. IAV transcribes viral mRNA and replicates its genome in the nucleus of its host cell. Therefore, the vRNPs must migrate to the nucleus via known nuclear localization signals (NLS) found on several proteins in the vRNP complex. The influenza virus is one of only two RNA viruses that replicate in the nucleus, the second being human immunodeficiency virus; all other RNA viruses replicate in the cytoplasm. Replication in the nucleus provides IAV with access to essential host machinery for viral mRNA synthesis and replication of vRNA.

Each genome segment carries its own trimeric polymerase complex. All eight segments of the IAV genome have conserved 12 and 13 nucleotide sequences on their 3' and 5' ends respectively. These sequences show partial complementarity and form a duplex. These nucleotides are thought to create a 3-D corkscrew structure that is essential for polymerase binding and function (Cauldwell et al., 2014). The incoming vRNPs are recruited to host RNA polymerase II (Pol II). PA has affinity to the C-terminal domain (CTD) of host Pol II, giving the viral polymerase privileged access to nascent host transcripts. IAV transcription is likely activated by the binding of PA to the CTD of RNA Pol II (Serna Martin et al., 2018). The viral polymerase uses the 5'-7-methylguanosine cap (5' cap) from host mRNAs as a primer to synthesize its own mRNA. The trimeric polymerase complex binds the 5' cap of host transcripts through the PB2 cap-binding domain. Viral PA then cleaves the transcript ~10-14 nucleotides downstream of the cap through its endoribonuclease domain. The endonuclease domain of PA is strongly activated by manganese ions. Furthermore, the endonuclease domain of PA resembles the type II class of restriction endonucleases (Dias et al., 2009). PB1 contains an RdRp

domain that is responsible for synthesizing new RNA molecules. mRNAs from segments 7 and 8 are spliced by host factors to synthesize alternative ORFs. Viral mRNA is exported from the nucleus to the cytoplasm where it is translated into viral proteins. The viral glycoproteins HA and NA are targeted to the endoplasmic reticulum (ER) for imbedding into membranes and appropriate PTMs. M2 is also targeted to the ER but is not glycosylated. HA, NA, and M2 then localizes to the plasma membrane through the Golgi apparatus following the secretory pathway. All other viral proteins are synthesized on free cytoplasmic ribosomes. Some proteins contain a nuclear localization signal (NLS) to target them to the nucleus to fulfill their function.

During genome replication, the full-length negative sense genome is copied to a replicative intermediate, termed complementary RNA (cRNA). cRNA is then used as the template to further synthesize full length genomic RNA (vRNA) (Dadonaite et al., 2019). Synthesizing the cRNA and subsequently vRNA requires newly synthesized polymerase complexes and NP. The new polymerase complex and NP stabilize the replicative intermediates and allow replication of the viral genome. Newly synthesized polymerase complexes form asymmetric heterodimer complexes, with one “old” RdRp complex dimerizing with the newly synthesized RdRp complex. The heterodimeric complex initiates primer-independent synthesis and stabilization of cRNA. The formation of the heterodimeric complex also utilizes host factors as scaffolds to form higher level structures (Carrique et al., 2020). cRNA is then used as a template to synthesis genomic vRNA with, again, newly synthesized RdRp subunits to form progeny vRNPs. Progeny vRNPs are then exported into the cytoplasm and traffic to the plasma membrane for packaging in budding particles (Lakdawala et al., 2014). vRNPs rely on host recycling

endosomes for the migration from the nucleus to the plasma membrane. Specifically, the small GTPase Rab11 is responsible for concentrating vRNPs on small intracellular vesicles and their subsequent migration to the plasma membrane where they are packaged into budding particles (Bhagwat et al., 2020).

1.3 The Viral Envelope Proteins HA, NA, and M2

IAV virions can assume two distinct morphologies, spherical or filamentous. The spherical morphology is often observed in laboratory settings. Serial passaging in embryonated eggs rapidly selects against the production of filamentous virus. By contrast, serial passaging laboratory strains in animal models selects for filamentous particle formation. Filamentous virus is significantly longer than spherical virions, ranging upwards of 30 μm, and is thought to be a general feature of the orthomyxovirus family (Dadonaite et al., 2016). It is thought that filamentous particles incorporate significantly more HA into the virion, which aids infiltration of mucosal surfaces by increasing binding to sialic acid receptors. Consistent with this idea, filamentous viral particles also require higher levels of secreted immunoglobulin A (IgA) to be neutralized (Lakdawala et al., 2011).

1.3.1 Haemagglutinin

Haemagglutinin (HA) is the most abundant glycoprotein on the virion. HA is a homotrimer and is responsible for attachment to the host cell and membrane fusion in the late endosome. HA has a N-terminal signal sequence that allows it to be translated at the ER as a pro-protein known as HA0 (Elder et al., 1979). HA undergoes post-translational

modifications during its synthesis and is embedded into the ER membrane by a C-terminal stop transfer sequence (Grabherr & Ernst, 2010; Schmidt, 1982). The trimerization of HA is required before it translocates to the Golgi apparatus (Gething et al., 1986). The farthest section of HA from the membrane is a globular head which contains the receptor binding domain (RBD), while the membrane proximal area contains a stretch of hydrophobic amino acids that compose the fusion peptide (Wilson et al., 1981). HA0 is cleaved by the host protease TMPRSS2 and other trypsin-like proteases into HA1 and HA2, with the globular head comprising HA1, while the fusion peptide resides in HA2 (Klenk et al., 1975; Limburg et al., 2019; Meyer et al., 2013). HA cleavage is essential to generate an infectious virion, because cleavage liberates the hydrophobic fusion peptide in HA enabling its fusogenic properties. Secreted bacterial secreted proteases can also activate HA. Thus, a co-infection with Staphylococcus can enhance IAV disease progression through its secreted protease and subsequent activation of HA0 (Tashiro et al., 1987).

The RBD of HA recognizes and binds to terminal sialic acid, which can also be referred to as neuraminic acid, on plasma membrane resident glycoproteins on the surface of host cells. Glycoproteins contain N-linked glycosylation, where oligosaccharides are added to asparagine residues post-translationally in the ER lumen. The N-linked oligosaccharides are further trimmed and modified in the Golgi apparatus. Most mature oligosaccharides are terminally modified with sialic acid bonded to galactose. Sialic acid can be linked to galactose via α-2,3 or α-2,6-linked sialyl-galactosyl bond. Human adapted IAVs generally have a high affinity for α-2,6 linked sialic acid, whereas avian adapted strains preferentially bind α-2,3 linkages (Rogers & Paulson, 1983). IAV binds

these sialic acid linkages as its receptor, which leads to receptor mediated endocytosis into an endosome. The endosome acidifies, which deprotonates key amino acids within HA, leading to a conformational change of cleaved HA resulting in exposure of the fusion peptide in HA2 (Russell et al., 2018). The exposed fusion peptide penetrates the host endosome membrane, resulting in the fusion of the viral envelope and the endosomal membrane. Once the viral envelope has mixed with the host endosomal membrane, the internal viral ribonucleoprotein (vRNP) complexes are released allowing them to transit to the nucleus, initiating infection.

Highly pathogenic avian influenzas (HPAI) contain a polybasic cleavage site in HA, allowing it to be recognized and proteolytically cleaved by the host protease furin (Luczo et al., 2015). Furin is a protease that is highly abundant in most human tissues. Both H5N1 and H7N9 are classified as HPAI. HPAI viruses disseminate from the site of infection and replicate in multiple tissues across the body, leading to systemic infection resulting in a high mortality rate (Luczo et al., 2015). Estimates of case fatality ratio range from 14%-60% (F. C. K. Li et al., 2008). Conversely, the case fatality rate of seasonal H1N1 is 0.3%. If H5N1 entered the human population and established transmission human-to-human, the results could be catastrophic. Zoonosis occurs through direct contact with a reservoir (waterfowl) species or an intermediate host (swine) (Richard & Fouchier, 2016). Several key adaptations must occur in zoonotic viruses to overcome evolutionary bottlenecks and establish sustained transmission between humans. HPAI struggle to establish human-to-human transmission due to HA's affinity to α-2,6 sialic acid residues, adaptive polymerase mutations, and resistance mutations against innate antiviral restriction factors.

1.3.2 Neuraminidase

Neuraminidase (NA) also binds sialic acid modifications on glycoproteins. NA destroys the sialic acid receptor by removing it from surface glycoproteins, glycolipids, and off HA. The removal of the sialic acid receptor prevents viral aggregation at the plasma membrane during egress, enabling efficient viral release from the host cell (Gamblin & Skehel, 2010). NA shows unique antigenic properties across different IAV subtypes. Antibodies against NA prevent its sialidase activity and impair the virus from budding from infected cells. The NA glycoprotein forms tetrameric shape, with the head of the protein harbouring the sialidase activity (Gamblin & Skehel, 2010). NA is a type II transmembrane glycoprotein. NA requires N-linked glycosylation for its proper folding, dimerization, and maturation.

Previous reports show that impairing the glycosylation of NA dramatically reduces the formation of tetrameric NA. Monomers form dimers through the formation of an intermolecular disulfide linkage in the stalk (Saito et al., 1995). NA dimers then oligomerize further to form a tetramer. The IAV strain WSN (H1N1) NA has been identified to harbour 3 N-linked glycosylations at positions asparagine 44, 72, and 219 (Bao et al., 2021). Mutating the asparagine residues to a glycine on NA resulted in a product that migrated at a lower MW and with reduced protein accumulation. Furthermore, the asparagine 219 mutant could not be rescued as an infectious virus when reverse engineered into the virus (Saito et al., 1995).

1.3.3 Matrix 2

The matrix 2 (M2) protein is the least abundant protein found of the surface of virions, only accounting for ~1% of protein. The 97 amino acid protein forms a homotetramer that is stabilized by disulfide bridges. The N-terminus of M2 is surface exposed, whereas the C-terminus is positioned in the virion interior (Manzoor et al., 2017, p. 2). The transmembrane domain of the homotetramer forms the proton channel. The channel selectively transfers protons form the late endosome to the virion interior. The acidification of the virion core dissociates the M1 protein from the vRNPs, allowing their migration to the nucleus (To & Torres, 2019). M2 is essential for IAV entry and uncoating into a host cell.

M2 also deprotonates the *trans*-Golgi network, preventing the activation of the pH sensitive HA during its migration to the plasma membrane (Ciampor et al., 1995). The viroporin shows unidirectionality for proton migration across the channel, with protons moving from the N-terminus to the C-terminus. M2 also facilitates egress by scission of the viral membrane off the host plasma membrane. Antibody responses against M2 have shown protection in animal models, primarily thought to target infected cells for antibody dependent cellular cytotoxicity (Velappan et al., 2020). The viroporin is also thought to perturb the activity of other cellular ion channels such as the cystic fibrosis transmembrane conductance regulator (CFTR) that is present in the apical membrane in the lung. Impairing CFTR is thought to affect the absorption and secretion of fluids in the air space, inducing pulmonary edema (To & Torres, 2019).

1.4 The Mechanisms of Antigenic Shift and Drift

The segmented genome allows the virus to reassort its segments with other lineages to generate a novel virus. Any segment can undergo reassortment; the easiest to detect is the reassortment of HA and NA due to their prevalence on viral particles and subsequent detection by antibodies. If NA or HA is re-assorted, then the antigenicity of the progeny virus may change sufficiently enough to evade immune surveillance in a process termed antigenic shift. (Van Poucke et al., 2010; Wille & Holmes, 2020). Reassortment requires one cell to be infected with two different viruses. Genome reassortment have created viruses responsible for previous pandemics, such as the H3N2 outbreak. Intermediate animals may serve as vessels for reassortment. For instance, pigs have equal abundance of α-2,3 sialic and α-2,6 sialic acid terminal linkages (Ito et al., 1998). Pigs are permissive to infection by both avian and human-tropic viruses, and subsequent segment switching can lead to antigenic shift. Interestingly, α-2,3 linkages are dominate in the chicken, but α-2,6 sialic acid linkages are found at lower concentrations in the respiratory and gastrointestinal tract of domestic chickens (Costa et al., 2012).

The RdRp encoded by IAV has poor fidelity and lacks 3' to 5' proofreading capabilities, resulting in an exceptionally high mutation rate of $4.5x10^{-3}$ to $0.5x10^{-3}$ substitutions/site/replication (s/s/r) (Nobusawa & Sato, 2006). At this rate, one-to-two mutations are introduced into the IAV genome every time it is copied. The low fidelity polymerase allows the rapid generation of mutant viral genotypes. At one given time point, there is one dominant genotype (>50% prevalence) in the viral population. Due to the high level of mutation from the RdRp, mutations quickly arise. Any mutation that is not immediately selected against exists within the viral population as a quasispecies.

These mutations are quickly selected for through evolutionary pressures, with the rare mutations quickly becoming fixed as the dominant genotype if they show an advantage over their parental genotype. This rapid generation of mutations and their subsequent fixation allows the virus to "drift" an immunogenic epitope away from immune surveillance or enhance the viruses fitness (R. Chen & Holmes, 2006; Nobusawa & Sato, 2006). The accumulation of mutations in antigenic sites in HA and NA is termed antigenic drift. Lam and co-authors have shown that vaccination in itself changes the antigenic landscape of viruses through selection (Lam et al., 2017). H3 subtypes evolve away from selective antibody pressures faster than H1 subtypes and B lineages, with new H3 variants replacing older strains quickly (Hay et al., 2001; Petrova & Russell, 2018; Z. Xu et al., 2010).

1.5 Direct Acting Antivirals Against Influenza

Current vaccine strategies against IAV are not highly efficacious at preventing IAV infections. Overall, vaccine coverage remains poor across the general population. IAV, as stated in 1.4, intrinsically generate mutations in their populations, allowing for the rapid generation and selection for immune escape mutations. The high rates of annual IAV infection necessitates antiviral therapies to treat infected individuals. If an infected individual requires medical attention or hospitalization, the active viral infection can be treated with antivirals. Direct acting antiviral therapy uses a small molecule that specifically impairs the function of a viral protein, which in turn inhibits viral replication.

1.5.1 NA Inhibitors

The class of NA inhibitors are the most common antivirals used against IAV infection. This class of sialidase inhibitors contains oseltamivir carboxylate (TamiFlu™), zanamivir (Relenza™), laninamivir (Inavir™), and peramivir (Rapivab™). TamiFlu is stockpiled by governments in preparation for the next influenza pandemic (Heneghan et al., 2016). NA activity is essential to the creation of infectious progeny by destroying the cellular receptor and liberating budding viral particles. Oseltamivir carboxylate mimics sialic acid, allowing it to bind to the sialidase domain of NA and prevents its receptor destroying capabilities. Therefore, oseltamivir carboxylate acts as a receptor decoy specifically for NA that blocks its enzymatic activity.

Oseltamivir phosphate is taken as an oral tablet and is absorbed into the blood stream. Oseltamivir phosphate undergoes ester hydrolysis by hepatic esterases, which converts it into the active metabolite oseltamivir carboxylate. Roughly 75% of oseltamivir phosphate is converted to oseltamivir carboxylate (He et al., 1999). Oseltamivir must be taken within 2 days of symptom onset for antiviral efficacy (Moscona, 2005). Oseltamivir carboxylate shows variable inhibitory concentration 50 (IC_{50}) concentrations across different viral isolates, with the IC_{50} concentration ranging from 0.01 to 70 nM (Davies, 2010). Current administration of 75 mg twice daily leads to a concentration of ~330 nM in the plasma with a half-life of 6-10 hours (He et al., 1999). Secretion is thought to be through the kidneys, with individuals with renal failure showing a reduction in oseltamivir carboxylate secretion (He et al., 1999).

An unbiased systematic review of randomized control trials showed a modest reduction in disease when oseltamivir was taken therapeutically, with a reduction of symptoms from 7 to 6.3 days (Jefferson et al., 2014). However, oseltamivir showed

significant protection against symptomatic infection when taken prophylactically (Jefferson et al., 2014). The number needed to treat to benefit (NNTB) is 100 in preventing the development of pneumonia, while the number needed to treat to harm (NNTH) is 28 to cause a mild side effect (Jefferson et al., 2014). The increase in risk of side effects due to oseltamivir is nearly four times greater than the associated decrease in risk of pneumonia. Zanamivir is administered to the site of infection through nasal spray or inhalation shows similar effects as oseltamivir, with a reduction in disease manifestation by 16 hours (Jefferson et al., 2014). There is strong evidence that oseltamivir reduces viral replication and disease manifestation when applied to a sensitive virus. Interestingly, oseltamivir enhanced infection of some viruses *in vitro*, where impairing the receptor destroying enzymatic activity of NA improved the virus's ability to bind to its host cell (Lin et al., 2009).

The use of oseltamivir selects for resistance mutations within the viral genome. The N1 H274Y mutation has been found to dramatically reduce the pharmacological effect of oseltamivir carboxylate. The H274Y mutation has been found to arise within treated patients with ARDS, which resulted in higher mortality rates over individuals infected with sensitive viruses during treatment (Behillil et al., 2020). The prevalence of resistance in currently circulating IAVs is low (~1%), but resistance was found in upwards of ~99% of H1N1 isolates during the 2007/2008 H1N1 influenza season in some locations (Casalegno et al., 2010; Dharan et al., 2009). Fortunately, the H1N1 that entered the human population in 2009 is sensitive to oseltamivir, with no significant increase in the prevalence of antiviral resistance to date. Other mutations that reduce NA inhibitor effectiveness can also arise in HA, with mutations showing decreased affinity to

sialic acid and subsequently reducing the need for NA (Renaud et al., 2011). Here, HA can compensate for impaired NA activity by reducing its affinity to sialic acid, reducing the threshold of liberation during budding.

1.5.2 M2 Inhibitors

Amantadine and Rimantadine are the two clinically approved M2 inhibitors. M2 is a homo-tetrameric proton channel that promotes the acidification of the viral core during entry. Amantadine and Rimantadine work by preventing the translocation of protons into the virus core, preventing successful uncoating of the genome during entry. The proton channel spans from the 25^{th} to 46^{th} amino acid, which also includes the transmembrane domain. The homotetramer structure makes a pore across the envelope for protons to migrate through. Resistance to M2 inhibitors is caused by S31N, V27A, and L26F substitutions within the proton channel (Schnell & Chou, 2008). These mutations are neutral to the fitness of the virus, meaning there is no negative selection to revert sensitivity to the antiviral. IAV quickly evolves to resist amantadine treatment. The generation of antiviral resistant virus can occur within a few rounds of replication within an infected individual (Schilling et al., 2004).

1.5.3 Polymerase Inhibitors

The most recently developed direct acting antiviral against IAV is baloxavir acid, the active form of baloxavir marboxil, which specifically inhibits the viral heterotrimer polymerase. This new antiviral has yet to be approved by the FDA and subsequently is not used in clinical settings in North America, although evidence supports its safety in

adults (Koshimichi et al., 2018). Transcription of viral mRNAs requires the virus to "snatch" the 5' cap from host mRNAs. PB2 in the polymerase has a cap-binding domain, which allows the first 10-14 nucleotides to be cleaved by the endonuclease domain in PA. The 5' cap is used as a primer to synthesize viral mRNA; the mRNA is synthesized through the activity of PB1 RdRp. Baloxavir acid binds and impairs the endonuclease activity of PA (Noshi et al., 2018). Baloxavir acid effective IC_{50} values against diverse influenza viruses is around ~0.5-3.5 nM concentrations(Noshi et al., 2018).

Serial passaging IAV in the presence of baloxavir acid generated a PA I38T substitution that reduced the virus's sensitivity to baloxavir acid by 30 to 40-fold. Interestingly, the PA I38T mutation reduced viral polymerase activity, indicating that this adaptation may have a detrimental effect on viral fitness (Noshi et al., 2018). Baloxavir marboxil is administered as a single oral dose, where it is absorbed by the GI tract and metabolized into its active compound baloxavir acid. The half-life of baloxavir acid is ~40-90 hours and is excreted into the feces. No significant side effects were identified, several liver enzymes were asymptomatically elevated (Koshimichi et al., 2018).

1.5.4 The Need for New Antivirals

Clinicians currently use NA inhibitors as a direct acting antiviral to treat IAV infections. Fortunately, the virus that caused the swine flu pandemic in 2009 was sensitive to neuraminidase inhibitors. Previous experiences with oseltamivir resistance in circulating H1N1 during the 2007-2009 period should prove a warning to the worldwide spread of antiviral resistant IAV. This highlights the need for new antivirals to treat IAV infections. Medicinal chemistry studies are currently underway to modify the oseltamivir

carboxylate structure to optimize its antagonistic effects (Ai et al., 2020). Baloxavir marboxil also shows promise as a direct acting antiviral, although drug-resistance emerges rapidly in experimental evolution experiments. Furthermore, The PA I38T mutation has been identified in viral isolates from treated individuals (Takashita et al., 2019). Other new antivirals that are currently in development include favipiravir, which acts as a broad antiviral. Favipiravir is a purine analog that mutagenizes the genome of IAV by increasing the frequency of C-to-U and G-to-A mutations in the genome (Baranovich et al., 2013). Favipiravir treatment may also encourage the viral polymerase to terminate chain synthesis during viral replication if the nucleoside analog is incorporated numerous times (Shiraki & Daikoku, 2020). Resistance to favipiravir has already been identified, with resistance mutations arising within the PB1 and PA polymerase units (Goldhill et al., 2018). Direct acting antivirals have a low genetic barrier against resistance, with the established antivirals generating antiviral resistance rapidly during circulation. The rapid generation of antiviral resistance to direct acting antiviral treatments continue to plague IAV treatment regiments in clinical settings (Toots & Plemper, 2020).

Targeting host factors during viral replication may provide a higher genetic barrier for the emergence of resistance. Here, I aim to develop a host-targeted antiviral (HTA) that will impair viral replication. Several new antiviral strategies seek to specifically target host factors that are essential for viral replication. Current research programs aim to identify and impair host factors that are essential to viral replication. Blocking these host factors that are essential to viral replication will likely inhibit viral replication. Previous studies have demonstrated antiviral properties of HTAs against

IAV, enterovirus, parainfluenza virus, SARS-CoV-2, dengue, and HCV (L. Bauer et al., 2017; H.-H. Hoffmann et al., 2017; Seyedpour et al., 2021; Villareal et al., 2015; Watanabe et al., 2014). HTAs may also be effective across different virus families, with broad-spectrum effects by targeting a common host factor that supports viral replication (Chitalia & Munawar, 2020). IAV relies upon host translation and the ER, making these host factors appropriate targets for antiviral therapies. Both pathways can be targeted with pharmaceuticals to temporarily block their function. I also outline potential cytotoxic effects that may arise during treatment. In Chapters 3 and 4, I characterize candidate antiviral compounds that impair host factors that disrupt cellular function to subsequently impair viral replication. The first host target is the RNA helicase eukaryotic initiation factor 4A (eIF4A) to reduce viral protein translation. The second host target is the host's ER, which is responsible for synthesizing viral glycoproteins. I will now cover the background, pathways, and stress responses in host translation and the ER. I finish my thesis by further studying the extent of host-IAV interactions during the adaptation of IAV to a new host.

1.6 Generation of Host mRNA, mRNA Processing, and Translation

1.6.1 Overview

To target host translation as a therapeutic against IAV replication, we must first understand the biological processes during homeostasis and infection. Translation is essential to the host cell, with every protein originating in an almost identical fashion. Almost every cellular process is reliant upon the synthesis of proteins. Here, I describe

mRNA synthesis, translation initiation, the control of translation initiation, and the stress responses that are involved in translation.

1.6.2 mRNA Synthesis and Export

mRNA is synthesized by cellular Pol II. Pol II is recruited to a promoter through several transcription factors to initiate primer-independent RNA synthesis downstream of the promoter (X. Liu et al., 2013). Pol II contains a large unstructured CTD. In humans, the CTD contains a seven amino acid sequence that is repeated 52 times. The seven amino acid repeat contains two serine residues at position 2 and 7 (Harlen & Churchman, 2017). Both serine residues are targets for phosphorylation, which dramatically increases the acidic nature of the CTD. The CTD is mostly unphosphorylated at initiation of transcription. The CTD is heavily phosphorylated during elongation by TFIIH and the elongation factor P-TEFb. The phosphorylated CTD recruits the factors responsible for capping, splicing, and synthesizing the poly A tail (Buratowski, 2009; Harlen & Churchman, 2017; McCracken et al., 1997).

The 5’ cap is added co-transcriptionally, with the transcript receiving the 5’ cap after 20-30 nucleotides have been polymerised (Ghosh & Lima, 2010). The addition of the 5’ cap occurs through three different steps. RNA triphosphatase hydrolyzes the γ phosphate off the first nucleotide leaving a diphosphate. RNA guanylyltransferase then catalyzes attachment of a GMP to the first nucleotide through a 5’ -5’ triphosphate linkage. Finally, RNA guanine-N7 methyltransferase methylates the N7 position on the guanosine (Proudfoot et al., 2002).

Most mammalian transcripts harbor introns, which are non-protein coding sequences that are spliced out to generate mature mRNAs. Splice sites are recognized by consensus sequences that flank the 5' and 3' exon-intron junction on the pre-mRNA. snRNPs are formed with five small nuclear RNAs (snRNAs) U1, U2, U4, U5, and U6 (Proudfoot et al., 2002). The snRNPs complex with the pre-mRNA to form the spliceosome to facilitate the removal of the intron. Splicing generates the exon junction complex (EJC) that forms ~20 nucleotides upstream of a splice junction on the mRNA. The EJC assists in the export and stability of mRNA. The EJC contains eIF4A3, which is locked onto the RNA by the other two components RBM8A and MAGOH. RBM8A and MAGOH also prevent eIF4A3 activation by blocking its ATPase domain (Schlautmann & Gehring, 2020). The EJC also aids in translation of the transcript; the protein PYM likely bridges the EJC to the 48S preinitiation complex and enhances translation initiation (Schlautmann & Gehring, 2020).

All encoding mRNAs have a ~200 adenosine nucleotide sequence at the 3' end of the transcript, termed the poly A tail. The pre-mRNA is cleaved before the poly A tail is added. The cleavage of the pre-mRNA occurs at the specific polyadenylation consensus sequence AAUAAA (Hamilton et al., 2019). The consensus sequence is recognized by multisegmented proteins, mainly the cleavage and polyadenylation specificity factor (CPSF). CPSF is formed from four different subunits, CPSF-160, CPSF-100, CPSF-73, CPSF-30. Cleavage factor I (CF I) and cleavage factor II (CF II) are essential in the cleavage of the pre-mRNA allowing the poly(A) polymerase (PAP), with assistance from the CPSF complex, to synthesize the poly A tail (Clerici et al., 2017). The mature mRNA has the 5' cap, a 5' untranslated region (5' UTR), a start codon to initiate translation, an

open reading frame (ORF) of in-frame codons that end at a stop codon, a 3' UTR, and a 3' poly A tail.

The 5' cap is then bound by the cap binding complex (CBC) composed of CBP20 and CBP80 (Rambout & Maquat, 2020). Newly synthesized mRNAs with CBC can support the pioneer round of translation (Gonatopoulos-Pournatzis & Cowling, 2014). The CBC protects the mRNA from Xrn1 mediated decay (Proudfoot et al., 2002). CBC bound mRNAs have been found with ribosomes on them. CBC is likely replaced by eIF4E during the first rounds of translation to licence the mRNA for bulk protein synthesis. The exon junction complex (EJC) is also likely removed during pioneer translation. eIF4F bound mRNAs are the source of most cellular protein synthesis.

1.6.3 mRNA Stability and Degradation

The number of protein molecules produced from each mRNA molecule is determined by the translation efficiency and half-life of the mRNA. mRNAs that lack a 5' cap or poly A tail do not form the eIF4F complex and therefore fail to be translated in a cap dependent manor. There is extensive cross talk between translation and mRNA decay, with efficient translation stabilizing the mRNA over time. Some mRNAs are degraded upstream of translation initiation, while others are degraded co-translationally. mRNA decay is initiated by de-capping or deadenylating the mRNA which targets the transcript for Xrn1 exonuclease or exosome mediated decay. Xrn1 specifically degrades transcripts from the 5' end, while exosomes degrade the mRNA from the 3' end (Clerici et al., 2017). Degradation from the 5' to 3' can happen co-translationally with the nuclease following the last ribosome, whereas degrading the mRNA 3'-5' is incompatible

during translation and must occur before ribosome loading. There are three mRNA surveillance pathways to recognize and degrade mRNAs that lack a stop codon, possess a premature stop codon, or contain a ribosomal stalling sequence. The three pathways are non-stop decay, no-go decay, and non-sense-mediated decay. The activation of the three pathways occurs during translation to recover ribosomes, prevent the synthesis of aberrant protein products, and control mRNA half-life (Simms et al., 2017). Non-sense mediated decay of mRNAs also occurs during pioneer translation. If a stop codon is found 25-35 nucleotides upstream of an EJC, then future translation initiation is blocked in the preinitiation complex (PIC) (Maquat et al., 2010).

1.6.4 Translation Initiation

Translation initiation requires the formation of the PIC and the eIF4F complex. The PIC is comprised of the ternary complex (TC), eIF5, eIF3, eIF1A, and the 40S small ribosomal subunit (Fig 1.1) (Brito Querido et al., 2020; Frosi et al., 2019; Rutkovsky et al., 2019). The TC itself is comprised of the heterotrimer eIF2, made from the alpha (α), beta (β), and gamma (γ) subunits, GTP, and a charged methionyl-initiator transfer RNA (Met-tRNA$_i^{Met}$) (Thakur et al., 2020). The PIC is recruited to the mRNA by eIF4F to form the 48S initiation complex (Brito Querido et al., 2020). The eIF4F complex is essential for cap dependent translation; it is comprised of eIF4E, eIF4G, and eIF4A. eIF4G is a large scaffolding protein that interacts with eIF4E, PABP, and RNA. Accordingly, eIF4G is responsible for the circularization of the mRNA. eIF4E binds to the 5’ cap, displacing the CBC and licensing the mRNA for bulk translation (Maquat et al., 2010). eIF4A is an Asp-Glu-Ala-Asp (DEAD)-box RNA helicase that is responsible

for melting the secondary RNA structures found in the 5' UTRs of mRNAs. eIF4A unwinds secondary RNA structures of the mRNA and recruits the 43S PIC forming the mRNA 48S initiation complex (Brito Querido et al., 2020). The binding of these complexes to the mRNA increases its stability. Furthermore, actively translated mRNAs are further stabilized.

Once the 48S initiation complex has formed with the mRNA, it scans for an AUG to initiate translation. The initiation machinery moves away from the 5' cap in a 5' to 3' direction searching for a suitable AUG codon. Once a suitable AUG codon is found, the GTP that is bound to eIF2 is hydrolyzed to GDP + phosphate (Pi) (Brito Querido et al., 2020). The hydrolysis of GTP greatly reduces eIF2's affinity for Met-tNRAi^{Met}, facilitating the release of eIF2-GDP and the Met-tRNA$_i^{Met}$ entry into the ribosomal P site (Merrick & Pavitt, 2018). eIF5B-GTP is then recruited which facilitates the joining of the 60S large ribosomal subunit. The hydrolysis of eIF5B GTP to GDP and its subsequent release forms the 80S ribosome on the mRNA to finalize translation initiation (Huang & Fernández, 2020). Translation is initiated from the AUG codon once binds the anti-codon on the Met-tRNA$_i^{Met}$. AUG is the canonical codon used to initiate translation, although alternative codons have been identified. The initial codon anti-codon binding occurs in the P-site of the ribosome. The A site then recruits an aminoacyl-tRNA to start hybridizing to downstream codons (Merrick & Pavitt, 2018). The recycling of eIF2-GDP to eIF2-GTP one of the rate-limiting steps in translation initiation. This exchange is mediated by the guanosine nucleotide exchange factor (GEF) eIF2B. During times of stress, the α subunit of eIF2 is phosphorylated on Ser 51, which changes its interaction

with the GEF eIF2B preventing the recycling of GDP to GTP (Anand & Walter, 2020; Costa-Mattioli & Walter, 2020).

1.6.5 tRNA Abundance and Translation

mRNA uses triplicate nucleotides to encode a codon, codons in turn are recognized by an anticodon within a charged tRNA in the ribosome. There are 61 nucleotide codons, that account for 20 different amino acids (Y. Liu, 2020). Most tRNAs can hybridize with more than one codon to encode one amino acid, because there are significantly more codons than amino acids. tRNAs that incorporate the same amino acid but recognize a different codon sequence are termed iso-acceptors (Schimmel, 2018). The concentration of specific tRNAs vary across different species. Highly expressed mRNAs are selected for codon optimization to match the available tRNA pool to improve protein synthesis. Translation rates were found to be slower on mRNAs that encoded rare tRNA codons when compared to mRNAs that used optimal codons, codon adapted mRNAs also showed higher ribosome density (Nakahigashi et al., 2014).

1.6.6 Translation Regulation

Translation control is essential for all cellular functions, with pathologies arising from inappropriate protein expression. Initiation of translation is highly regulated through two pathways. The first pathway is the sequestration of eIF4E away from the eIF4F complex to reduce cap-dependent translation. eIF4E is responsible for binding the 5’ cap and is the target of several regulatory proteins. eIF4E-binding proteins (4E-BPs) limit eIF4E’s ability to bind eIF4G, and thereby prevent the formation of eIF4F. 4E-BPs

competitively inhibit eIF4E by binding the eIF4G recognition domain (Diab-Assaf et al., 2015). 4E-BPs are known negative regulators of cap-dependent translation. 4E-BPs are the target of phosphorylation by several kinases, one of which is the mammalian target of rapamycin complex 1 (mTORC1). When 4E-BPs are phosphorylated, they do not associate with eIF4E, allowing translation to occur (Rutkovsky et al., 2019). Therefore, the hypo-phosphorylated 4E-BPs inhibit translation through the sequestration of eIF4E.

1.6.7 The Integrated Stress Response

The second pathway to reduce global translation is controlling the recycling of eIF2-GDP to eIF2-GTP through the phosphorylation of eIF2α in the integrated stress response (ISR). Four established sentinel kinases phosphorylate eIF2α on Ser 51, therefore eIF2α is the central axis of the ISR. The four kinases are protein kinase R (PKR) that is activated by double stranded RNA, PKR-like-ER resident kinase (PERK) that responds to ER stress, heme-regulated eIF2α kinase (HRI) that responds to oxidative stress, and general control nonderepressible factor 2 kinase (GCN2) that senses the depletion of charged tRNAs (Donnelly et al., 2013). A fifth kinase has recently been described as a functional sensor, the microtubule affinity-regulated kinase 2 (MARK2) is activated by proteotoxic stress (Y.-N. Lu et al., 2021). Although recently discovered, Further investigation is required to confirm MARK2 role in the ISR. The eIF4F complex and subsequently the 48S pre-initiation complex can still form during events where eIF2α is phosphorylated. In turn, the failure to recycle eIF2-GDP to eIF2-GTP blocks the recognition of the AUG start codon and stalls translation initiation and subsequently fails to recruit the 60S ribosome (Costa-Mattioli & Walter, 2020; Ivanov et al., 2019). This

results in the accumulation of stalled mRNPs. Stress granules (SGs) form from the accumulation of mRNPs containing stalled initiation factors.

In the absence of ISR activation, eIF2-GDP is readily recharged with GTP to reform the TC. This allows the 48S initiation complex to scan the 5' UTR for the AUG start codon of the ORF. Translation will start at that start codon and terminate at the stop codon. Sometimes, the small ribosomal subunit can initiate translation again at another AUG just downstream of the stop codon. The re-initiation at the next start codon requires the repriming of eIF2 with a GTP (Vattem & Wek, 2004). When eIF2α is phosphorylated, the recycling of eIF2-GDP to eIF2-GTP is significantly slower at recharging the TC. This increases the time needed for re-initiation. The ISR converges on eIF2α, which in turn preferentially translates a potent bZIP transcription factor ATF4. The translation of ATF4 is controlled by the presence short ORFs upstream of the start codon of ATF4. These short ORFs are called upstream ORFs (uORFs) (Costa-Mattioli & Walter, 2020). In humans, the ATF4 mRNA has two uORFs upstream of the canonical AUG start codon. In the absence of ISR signaling, uORF1 and uORF2 are translated, while the ATF4 ORF is bypassed. The AUG of ATF4 is in the coding sequence of uORF2. When the ISR is activated, the recharging of eIF2-GDP to eIF2-GTP is slowed down, encouraging the ternary complex to bypass the AUG in uORF2 and recognize the AUG in the ATF4 ORF (Vattem & Wek, 2004). mRNAs with shorter 5' UTRs are also preferentially translated when eIF2α is phosphorylated (Harding et al., 2003).

ATF4 is bZIP transcription factor in the CREB (cAMP responsive element-binding)/ATF family. The ISR converges on the phosphorylation of eIF2α, which in turn synthesizes ATF4, making it the master regulator of the ISR. ATF4 binds to the

ATF/CRE consensus sequence, along with the amino-acid response element. ATF4 upregulates ATF3 and the pro-apoptotic transcription factor C/EBP homology protein (CHOP). CHOP is generally responsible for initiating the apoptotic cascade (Marciniak et al., 2004; Novoa et al., 2001). The synthesis of CHOP occurs independent of ER stress resolution, which could be helpful in returning the cell to homeostasis or pushing the cell further towards apoptosis (Marciniak et al., 2004). One protein of interest that is expressed by CHOP is growth arrest and DNA damage-inducible protein 34 (GADD34), also known as protein phosphatase 1 regulatory subunit 15A. GADD34 is a cofactor for the protein phosphatase 1 (PP1) that removes the phosphorus of eIF2α, de-repressing translation. GADD34 is the cofactor that aids PP1 specificity to eIF2α (Novoa et al., 2001).

eIF2B is sequestered by phosphorylated eIF2α, with phosphorylated eIF2α acting as a non-competitive inhibitor of eIF2B. The ISR can be pharmaceutically inhibited through a drug called integrated stress response inhibitor (ISRIB) (Zyryanova et al., 2021). ISRIB shows favourable bioavailability and readily crosses the blood brain barrier. ISRIB stabilizes the GEF eIF2B, replenishing the available pool of eIF2B to recharge eIF2-GDP to eIF2-GTP in the TC. However, ISRIB is limited in effect if the pool of eIF2B components are depleted, observed when the ISR is strongly activated (Costa-Mattioli & Walter, 2020).

1.6.8 Stress Granules

Stress granules (SGs) are cytoplasmic aggregates of mRNA complexed with an array of different host RNA binding proteins, forming messenger ribonucleoprotein

(mRNP) complexes. mRNPs accumulate in SGs in response to stress-induced translation arrest. SG formation is the downstream product of the phosphorylation of eIF2α. SGs that form from ISR signaling contain most PIC factors, except eIF2 and eIF5 (Ivanov et al., 2019; Kedersha et al., 2002). SGs can also form independently of the ISR. Treating cells with eIF4A inhibitors such as pateamine A or the class of rocaglates (silvestrol) impair translation initiation. This results in the accumulation of mRNPs with all PIC factors, including eIF2 and eIF5 (Low et al., 2005; Sadlish et al., 2013). The formation of SGs are not required for translation arrest to occur (McCormick & Khaperskyy, 2017). SGs both rapidly form and dissolve depending on cellular stressors. Treating stressed cells with the polysome stabilizing agent cycloheximide dissolves SGs, indicating that mRNAs are cycled through SGs into readily translated pools of mRNAs (Wheeler et al., 2016).

SGs have characteristic markers, which allow for the visualization of SGs in cells. SGs contain T cell restricted intracellular antigen 1 (TIA1), TIA1-related protein (TIAR), and RAS GTPase-activating protein SH3 domain-binding protein 1 (G3BP1) (Kedersha et al., 2002). TIA and TIAR bind to mRNA and enable mRNP aggregation through their prion-like domains. G3BP1 also self-aggregates to further establish the formation of the SG. SGs are thought to maintain their aggregation through RNA-protein and protein-protein interactions. G3BP1 and TIA1 both show low complexity and contain intrinsically disordered domains that allow liquid-liquid phase separation. Both TIA1 and G3BP1 are extensively post-translationally modified, which aid in the formation and stability of the SG. Caprin1 promotes SG formation through interacting with G3BP1, whereas ubiquitin-specific-peptidase 10 (USP10) inhibits SG assembly (Kedersha et al., 2016). The C-terminus of G3BP1 is responsible for interacting with RNA. Knocking

down/out G3BP1 dramatically reduces the cells ability to form SGs during times of stress (Kedersha et al., 2020).

1.6.9 IAV and Host Translation

IAV uses several methods to outcompete host mRNAs to preferentially synthesize viral products. This technique is generally referred to as host shutoff. The IAV polymerase uses the first 10-14 nucleotides of a nascent host mRNAs with a 5' cap as a primer to synthesize viral mRNA. Here the viral polymerase complex is recruited to the CTD of RNA Pol II which localizes it to the targeted mRNA (Pflug et al., 2017). The PA subunit of the IAV polymerase directly binds the CTD of RNA Pol II through two highly conserved domains (Lukarska et al., 2017). The 5' cap on the host mRNA is bound by the PB2 subunit. The cap binding domain of PB2 shows some homology to eIF4E and CBC (Bier et al., 2011). Binding of the 5' cap is then subsequently cleaved by the endoribonuclease domain found in PA. Removal of the 5' cap from the host mRNA prevents the host mRNA from binding to CBC, export into the cytoplasm, and sensitizes the host mRNA to Xrn1 mediated degradation.

The NS1 protein impairs several host responses, such as the polyadenylation of host mRNA. NS1 inhibits the nuclear export of host mRNAs. The effector domain of NS1 interacts with CPSF30 kDa subunit, which prevents the cleavage of the 3' ends of host pre-mRNA, disallowing the PAP to synthesize the poly A tail (Nemeroff et al., 1998). The viral polymerase creates the poly A tail on its mRNA by reiterative copying of a poly-uracil tract in the RNA template (Poon et al., 1999). Therefore, NS1 does not affect the synthesis of viral mRNAs, while viral mRNA still mimic host mRNAs.

Evidence also suggests that IAV infection leads to the RNA Pol II to read through the transcription termination site. Reading through the termination site prevents the proper formation of the poly A tail. This specific phenomena was independent of NS1 and the exact mechanism remains unclear (D. L. V. Bauer et al., 2018).

NS1 has also been shown to interact with eIF4G (Arias-Mireles et al., 2018; Burgui et al., 2003). NS1 likely binds eIF4G to enhance viral translation by circularizing viral mRNAs. The expression of NS1 alone is enough to increase translation efficiency of viral mRNA. The mechanism of NS1's selectivity to viral transcripts is unknown (Aragón et al., 2000). NS1 was thought to have specificity to the 5'UTRs of viral mRNAs, but it was later shown that NS1 has affinity for all RNA with no specificity to viral mRNAs (Arias-Mireles et al., 2018). Interestingly, the viral polymerase PB2 subunit has been shown to interact with eIF4G. Furthermore, it appears that PB2 may functionally replace eIF4E *in vivo* (Yángüez et al., 2012). mRNA pull downs shows an interaction between viral mRNA and host PABP1, viral NS1, RNA export factors, and the 20 kDa subunit of CBC (Bier et al., 2011). These data indicate that viral mRNAs are likely exported from the nucleus through canonical RNA export pathways. NS1 also binds the E3 ubiquitin ligase TRIM25 to prevent the oligomerization of RIG-I (Gack et al., 2009). NS1 also interacts with the host factor staufen1 (Stau1), which binds secondary RNA structures in host mRNA (Cho et al., 2013). It is thought that Stau1 controls RNA stability by binding 3' UTR structures in mRNAs that result in rapid degradation of mRNA. NS1 binds Stau1 and likely impairs Stau1 mediated mRNA degradation, stabilizing the viral mRNAs and promoting translation and subsequently virus replication (Cho et al., 2013). Other research suggests NS1 hijacks Stau1 somehow

to further promote vRNA stability or vRNA packaging into the budding virion, with Stau1 knockdown cells yielding 5-10 times less virus (de Lucas et al., 2010).

IAV utilizes ribosomal frameshifting to synthesize a rare ORF from the PA mRNA. The mRNA encoding PA contains a U-rich region followed by a rare codon (CGU) that has a relatively rare tRNA, which promotes a +1 frame shift altering all down-stream amino acids (Jagger et al., 2012). The product of the ribosomal frameshift is the X ORF, producing PA-X. This occurs at the 191st amino acid, making PA-X identical to PA in the first 191 amino acids, while the X-ORF can contain 41 to 61 unique amino acids. The first 191 amino acids harbour the PA N-terminal endoribonuclease domain but lacks the C-terminal domain responsible for formation of the trimeric RdRp, preventing PA-X from interacting with PB1 and PB2. PA-X localizes to the nucleus, where it uses RNA splicing machinery to selectively cleave host mRNAs (Gaucherand et al., 2019). Cleaved mRNAs are then a target for host Xrn1 for degradation. PA-X is involved in impairing the hosts antiviral response against IAV infection. The half-life of PA-X varies from 30 minutes to 3.5 hours depending on the C-terminal sequence (Levene et al., 2021). Together, cap-snatching, NS1, and PA-X prevent host mRNAs from being translated, encouraging preferential translation of viral mRNAs.

Most viruses are highly sensitive to the arrest of global translation. IAV specifically encodes three proteins to prevent the formation of SGs. The first protein is PA-X, which is the second protein synthesized from PA mRNAs that selectively degrades host mRNA. Reducing the pool of host mRNAs prevents their translation and subsequent entry into SGs independent of eIF2α phosphorylation (Khaperskyy et al., 2014, 2016). NS1 binds viral RNA through its dsRNA binding domain to mask the

pathogen associated molecular pattern (PAMP) from PKR. Mutating the dsRNA binding domain of NS1 results in strong induction of PKR activation and ISR-mediated SG formation (Khaperskyy et al., 2012). The last viral protein that prevents the formation of SGs is NP. NP prevents the formation of SGs in an eIF2α independent fashion, but the exact mechanisms of SG inhibition remain unknown. The oligomerization of NP is required for its inhibition of SG formation (Khaperskyy et al., 2014). NP has also been demonstrated to colocalize with SGs (Onomoto et al., 2012).

1.7 Translation and the ER

The ER is responsible for numerous cellular processes. The ER is the site for lipid genesis, protein synthesis, the folding of proteins and their PTMs, and calcium storage. It is estimated that roughly 1 in 3 proteins in the mammalian genome are synthesized in the ER (Chitwood et al., 2018; Pobre et al., 2019). Translation initiation occurs on free-cytoplasmic ribosomes. The signal peptide is synthesized on the nascent polypeptide, which is recognized by the signal recognition particle (SRP). The binding of the SRP stalls translation while the mRNP relocates to the ER. The SRP is recognized on the cytoplasmic face of the ER by the SRP receptor (SR). Both the SRP and SR are small GTPases that require hydrolysis of a GTP to GDP for the attachment and insertion of the nascent polypeptide into the Sec61p translocon (Akopian et al., 2013; Linxweiler et al., 2017). Proteins that enter the ER are unfolded, protein folding in the ER lumen is assisted by numerous cellular chaperones and enzymes responsible for maintaining ER homeostasis (Pobre et al., 2019). The translocon spans the ER membrane and forms a channel for the polypeptide to integrate into the lipid bilayer, or for the protein to be

synthesized into the ER lumen to enter the secretory pathway. After the protein begins translation across the ER membrane, SRP and SR dissociate to engage in another round of signal peptide identification and relocation.

1.7.1 Post-Translational Modifications

Proteins that are synthesized in the ER require several PTMs for their proper folding and function. The most common PTM in the ER lumen is the covalent linkage of an oligosaccharide to an asparagine residue, termed N-Linked glycosylation. The oligosaccharides are transferred onto the amide group of an asparagine residue of nascent polypeptides by oligosaccharyltransferases in the ER lumen (X. Zhang & Wang, 2016). The oligosaccharides are built on a lipid intermediate called dolichol. The Asparagine linked glycosylation 7 (ALG7) protein is the first enzyme that adds the base GlcNAc on the dolichol. Tunicamycin (TM) is a bacterial toxin that specifically impairs ALG7, preventing the development of the oligosaccharide on dolichol, thereby preventing all N-linked glycosylation (J. Wu et al., 2018). TM contains a nucleoside homolog that specifically binds the nucleotide binding domain of ALG7, which transfers the N-acetylglucoamine-1-phosphate from UDP-N-acetylglucosamine onto dolichol. The impairment of N-linked glycosylation results in the accumulation of unfolded proteins and the activation of the unfolded protein response (UPR) (J. Wu et al., 2018).

The oligosaccharide undergoes glycan trimming in the ER by resident glucosidases and mannosidases. Glycans are specifically recognized by cellular lectins, which are essential for protein folding and transport. If the protein fails to be properly modified or folded, it is polyubiquitinated for degradation. Asparagine residues first

receive an oligosaccharide containing GlcNAc2Man9Glc3, which is trimmed by glucosidase 1 and glucosidase 2 to GlcNAc2Man9Glc1. GlcNAc2Man9Glc1 is recognized by calreticulin and calnexin lectin chaperones, which in turn promote protein folding (Cherepanova et al., 2016). The oligosaccharide is further trimmed to GlcNAc2Man8 with three glucose and one mannose molecules removed, before leaving the ER for the Golgi apparatus (Cherepanova et al., 2016). Proteins that fail to receive proper glycosylation can become misfolded and subsequently are marked for degradation.

The Golgi apparatus receives the protein output from the ER, which continues to modify and sort the proteins to their final destination. The Golgi contains the machinery to perform glycosylation modifications, sulfation, phosphorylation, and proteolysis of protein. The high mannose glycan is further trimmed in the *cis*-Golgi. The oligosaccharide can be branched by adding another GlcNAc onto one of the mannose molecules. Galactose, sialic acid, or fucose can be added in the *trans*-Golgi apparatus to create complex glycans on the glycoprotein (X. Zhang & Wang, 2016). Glycoproteins are then sorted and sent to their targeted location, such as the plasma membrane. Some cells direct glycoproteins to preferred locations on the plasma membrane, thereby facilitating cell membrane polarization and the generation of apical and basal membranes.

Proteins can also be further modified by O-linked glycosylation, where a glucose molecule is linked to a serine, threonine, or tyrosine residue in the ER, Golgi apparatus, and rarely the cytoplasm (Steen et al., 1998). Proteins are also modified with C-mannosylation, where a mannose molecule is attached to tryptophan (X. Zhang & Wang, 2016). Free-cytoplasmic proteins can be modified with one sugar molecule, β-N-

acetylglucosamine (O-GlcNAcylation) which is attached to a serine or threonine residue. This modification affects numerous functions of the protein including stability and protein-protein interactions.

Proteins synthesized in the ER can be modified with a cysteine-cysteine sulfide bridge that alters it folding and stability. The protein disulfide isomerases (PDI) catalyze an intra- or intermolecular disulfide bond formation between two cysteine amino acids. PDI is found in the lumen of the ER, where it acts on nascent proteins (Coe & Michalak, 2010). The formation of disulfide bridges is essential to the maturation of many glycoproteins, including HA and NA. Disulfide bonds can be broken by the reducing agent dithiothreitol (DTT).

1.8 The Three Arms of the UPR

All eukaryotic cells have mechanisms to sense and respond to ER stress. The stress responses upregulate the expression of genes that regulate protein folding, degradation, lipid synthesis, and can determine the cells fate. The UPR is responsible for the initiation and transduction of signaling to the nucleus. The binding immunoglobulin protein (BiP), also known as the glucose regulated protein 78 (GRP78), is the master regulator of the UPR. BiP is a member of the Hsp70 family of chaperones. BiP itself is upregulated by the UPR, where it acts as a chaperone in the ER lumen to aid in folding proteins. BiP mRNA contains an internal ribosomal entry site (IRES) to allow cap-independent translation during ISR signaling (Hellen & Sarnow, 2001). BiP binds to the hydrophobic domains of unfolded proteins independent of their glycosylation status, such as misfolded HA (Gething et al., 1986). There are three sensors in the UPR that work

together to reprogram the cell to alleviate ER stress. If the stress becomes chronic, the UPR becomes a proapoptotic response. The three sensors are Inositol-requiring enzyme 1 (IRE1), PERK, and activating transcription factor 6 (ATF6) (Fig 1.2).

Proteins enter the ER lumen in an unfolded state, where they are post-translationally modified and folded appropriately. Cellular chaperones bind and unbind these proteins to aid in their folding. There are two major chaperone families present in the ER, the lectin chaperones that analyze the glycosylation status of unfolded proteins, and BiP. The lectin chaperones contain calnexin and calreticulin that recognize monoglucosylated N-linked glycans on the unfolded protein. The last glucose molecule on the N-linked oligosaccharide is removed prior to the glycoproteins localization to the Golgi apparatus, preventing the glycoprotein from binding to calnexin or calreticulin (Pearse & Hebert, 2010). If a protein does not fold properly, then the ER resident UDP-glucose:glycoprotein glucosyltransferase binds to the unfolded protein and adds back a single glucose to the trimmed glycan, enabling the lectin chaperones to bind to the misfolded protein.

1.8.1 BiP

BiP is responsible for a variety of roles, such as aiding the retrograde translocation of misfolded proteins during ER associated degradation (ERAD) and the activation of the UPR. BiP is a highly stable protein with a long half-life that is >24 hours *in vitro* and *in vivo*. BiP can be sequestered into oligomeric structures when ER stress is absent. BiP oligomers disassemble when the concentration of unfolded proteins rises, increasing the available pool of BiP to aid in protein folding (Preissler & Ron, 2019). BiP

contains an N-terminal nucleotide binding domain (NBD) that has affinity for ATP. BiP's affinity for ATP is stabilized from an interaction with the ER localized DnaJ (ERdjs) family members. These ERdjs members also directly bind unfolded proteins in the ER lumen. ERdjs work with BiP to help enable BiP's diverse functions within the ER, including its role in UPR induction. ATP binding licences BiP to interact with client proteins and the binding of BiP to hydrophobic residues on a nascent protein initiates the hydrolysis of ATP to ADP. BiP then binds, releases, and rebinds the same protein until they fold, or they are marked for degradation (Lewy et al., 2017). The binding of ATP enables BiP to release its substrate, while ADP binding does not affect the release of the client protein. BiP requires a nucleotide exchange factor to recycle ADP to ATP (Pobre et al., 2019). BiP's nucleotide cycling also depends on the Ca^{2+} status of the ER. Declining Ca^{2+} levels favour dissociation of BiP from the UPR activators (Preissler et al., 2020). BiP itself is post-translationally modified through phosphorylation and ADP-ribosylation, both of which are removed during times of ER stress (Freiden et al., 1992). It is thought that BiP does not bind its target protein tightly while it is ADP ribosylated. BiP transiently binds the lumenal domain of the three UPR signal transducers IRE1, PERK, and ATF6 preventing their activation. BiP dissociates from the three sensors to bind nascent unfolded proteins, liberating the three activator molecules of the UPR.

1.8.2 IRE1

The first arm of the UPR is the inositol-requiring enzyme 1 (IRE1). IRE1 is a serine/threonine kinase and a ribonuclease. IRE1 is a type I transmembrane protein spanning the membrane of the ER with the N-terminal lumenal side acting as a sensor for

ER stress, while the Ser/Thr kinase and endoribonuclease domains are found in the cytoplasm (Calfon et al., 2002). Mammals express IRE1α and IRE1β through differential splicing. IRE1α is ubiquitously expressed across all tissues, while IRE1β is only expressed in intestinal epithelial cells (Tsuru et al., 2013). Hereafter, I will refer to IRE1α as IRE1.

The lumenal domain of IRE1 is sequestered by BiP in the absence of ER stress. BiP dissociates from IRE1 when unfolded proteins accumulate in the ER lumen. The liberation of IRE1 from BiP allows IRE1 to bind unfolded proteins directly through its lumenal domain, which in turn promotes IRE1 oligomerization. IRE1's lumenal domain contains an MHC I like groove that can directly bind unfolded proteins (Credle et al., 2005). IRE1 can also form higher level oligomeric structures. IRE1 is also repressed by the ER lumenal chaperone ERdj4. ERdj4 maintains IRE1 as a monomer by recruiting BiP and stimulates BiP's ATP hydrolysis, which disrupts IRE1 dimers (Amin-Wetzel et al., 2017). Oligomerization stimulates IRE1 transautophosphorylation leading to structural rearrangement and activation (Joshi et al., 2015). IRE1 is also activated during inositol depletion and ER membrane perturbations. IRE1 senses lipid bilayer stress through its transmembrane domain (Promlek et al., 2011).

IRE1 mediates the unconventional splicing of the *X-box binding protein 1 (XBP1)* mRNA. IRE1 removes a 26-nucleotide intron from the *XBP1* mRNA, changing the down-stream reading frame and creating a protein with a novel C-terminus called XBP1 spliced (XBP1s). Expression of *XBP1s* mRNA without the 26-nucleotide intron activates the UPR independent of IRE1 activation. XBP1s is a basic leucine zipper (bZIP) transcription factor. XBP1s contains two domains, the first is the α helical leucine zipper

that is responsible for forming dimers, and the second is a DNA binding domain that is comprised of basic amino acids. XBP1s can form homodimers or heterodimerize with other bZIP transcription factors (Newman & Keating, 2003). XBP1s upregulates genes involved in lipid metabolism, ERAD, and upregulates ER chaperones. IRE1 recognizes the splice sites on *XBP1* mRNAs through secondary stem-loop structures and a nucleotide consensus flanking the intron (Back et al., 2006). The ER-localized RtcB tRNA ligase is responsible for ligating the 5' and 3' ends of the cleaved *XBP1* mRNA, completing the splicing event. IRE1 likely recruits and activates RtcB (Y. Lu et al., 2014). IRE1 is also subjected to several PTMs to aid in dimer formation and dissolution. IRE1 is phosphorylated by protein kinase A (PKA), which aids in its oligomerization and stabilization independent of transautophosphorylation (Mao et al., 2011). The phosphorylation of IRE1 by PKA bridges metabolic signaling and the UPR. Dephosphorylation of IRE1 encourages the monomerization of IRE1. The receptor for activated C-kinase 1 (RACK1) acts as a scaffold for protein phosphatase 2 A (PP2A) to dephosphorylate IRE1. PP2A inactivates IRE1 by dephosphorylating dimers downstream of metabolic signaling (Qiu et al., 2010). Poly ADP-ribose polymerase 16 (PARP16) is anchored into the ER and activates IRE1 through ADP-ribosylation. The ADP-ribosylation of IRE1 is essential for IRE1 dimerization (Jwa & Chang, 2012).

The unspliced *XBP1* mRNA produces the XBP1 unspliced (XBP1u) protein. XPB1u is translated at low levels and has a short half-life, preventing significant XBP1u accumulation. XBP1u has been demonstrated to modulate early UPR signaling. During initial UPR signaling, XBP1u directly binds XBP1s and other bZIP transcription factors and reduces their stability. This prevents strong induction of the UPR from very short

stresses. In times of prolonged UPR signaling, XBP1u is quickly degraded due to its short half-life while the production of XBP1s and other bZIP transcription factors increase over time (Hinte et al., 2020). XBP1u is recruited to the ER by the SRP that recognizes a hydrophobic region in the N-terminus of XBP1u. IRE1 can directly bind the Sec61 translocon, allowing IRE1 to recognize and cleave mRNAs recruited to the SR. The mRNA is then spliced by IRE1 into *XBP1s* (Plumb et al., 2015).

IRE1 is also responsible for regulated IRE1 dependent decay (RIDD), where a subset of mRNAs is degraded by IRE1 during ER stress. RIDD can be activated by the over expression of IRE1, as well as strong induction of ER stress. mRNAs that are a targeted by RIDD are generally localized to the ER, reducing the translational burden within the ER. mRNAs that are targeted by RIDD must contain the secondary stem-loop structure found in *XBP1* mRNAs. Currently, 37 transcripts have been identified and confirmed as RIDD targets, most of which localize to the ER (Oikawa et al., 2010). Although the degradation of specific transcripts is highly variable across different types of ER stressors and across different cell types, RIDD is thought to reduce ER protein influx by ~15%. The 28S rRNA has also been identified as a target of RIDD, further reducing the translational output of the cell (Hollien et al., 2009). RIDD plays a role in the homeostasis of the cell, showing initial pro-survival affects across diverse stressors. However, RIDD can destroy anti-apoptotic micro-RNAs (miRNAs) (Bashir et al., 2021). An example of this is RIDD dependent degradation of miRNA-17, which is responsible for the suppression of Caspase-2 mRNA (Y. Chen & Brandizzi, 2013). Degrading miRNA-17 increases the expression of Caspase-2, which encourages the induction of caspase-mediated apoptosis.

1.8.3 PERK

PERK is the second sensor in the UPR. PERK can be activated by the accumulation of unfolded proteins and lipid perturbations in the ER membrane (Volmer et al., 2013). Activated PERK phosphorylates Ser 51 on eIF2α. In the absence of ER stress, PERK monomers are bound by BiP. During the onset of ER stress, PERK functions similarly to IRE1, with BiP dissociation leading to the homodimerization and autophosphorylation of PERK. PERK autophosphorylation promotes PERK dimerization and enables PERK to phosphorylate eIF2α. PERK may also form higher-order oligomers, which may bind unfolded proteins directly (P. Wang et al., 2018). PERK can also directly interact with hydrophobic domains in unfolded proteins, which promotes its oligomerization (P. Wang et al., 2018). The lumenal domain of PERK shows similarity to the lumenal domain of IRE1, while the cytoplasmic effector domain is most closely related to the eIF2α kinase PKR. The phosphorylation of eIF2α reduces global protein synthesis (Harding et al., 2000). PERK activation is responsible for reducing the translational burden of the ER, decreasing the accumulation of proteins entering the ER until ER stress is resolved. PERK activation and subsequent phosphorylation of eIF2α activates the ISR, which was described in detail previously.

PERK positively regulates RIDD activity during ER stress. Knocking down PERK results in reduced RIDD-mediated degradation of known RIDD targets (Bashir et al., 2021). RIDD activity was recovered by attenuating translation in PERK knock down cells. Actively translated mRNAs sequester the secondary stem-loop structure that is

essential for IRE1 recognition. Furthermore, knocking out PERK has been shown to increase IRE1 signalling (Harding et al., 2000).

1.8.4 ATF6

The third sensor in the UPR is the activating transcription factor 6 (ATF6). ATF6 spans the ER membrane, with the cytoplasmic face containing a N-terminal bZIP transcription factor. Like IRE1 and PERK, ATF6 is bound to BiP in the absence of ER stress. The accumulation of unfolded proteins dissociates BiP from ATF6, enabling ATF6 to migrate to the cis-Golgi. The transportation of ATF6 to the Golgi relies on coat protein-II (COP-II) vesicles. BiP masks a COP-II binding site (Golgi localization signal) on ATF6, preventing its recruitment to COP-II vesicles (J. Shen et al., 2002). ATF6 activation is also governed by protein disulfide isomerase A5 (PDIA5) by rearranging lumenal disulfide bonds, which in turn affects ATF6 migration to the Golgi. Further, PDIA5 promotes the recruitment and packaging of ATF6 into COPII vesicles (Higa et al., 2014). ATF6 is cleaved by the Golgi resident site-1 protease (S1P) and site-2 protease (S2P). The cleavage of ATF6 to release a transcription factor is referred to as regulated intramembrane proteolysis (RIP). RIP releases the N-terminal bZIP transcription factor from ATF6. ATF6 is not the only transcription factor that is controlled by proteolytic cleavage following Golgi trafficking. SREBP1 and SREBP2 are also ER bound transcription factors that migrate to the Golgi to undergo RIP to liberate their transcription factors. The N-terminal bZIP transcription factor of ATF6 contains an NLS, which translocates ATF6-N to the nucleus.

The bZIP ATF6-N transcription factor binds the ER stress response element-I (ERSE-I) and ERSE-II consensus element to upregulate UPR induced genes. ATF6-N binding to the ERSE requires the heterotrimeric transcription factor NF-Y (Yoshida et al., 2001). The ESRE-I sequence is comprised of 5' CCAAT-N9-CCACG 3', and the ESRE-II is comprised of 5' ATTGG-N-CCACG 3' (Shoulders et al., 2013). ATF6-N also heterodimerizes with XBP1s, which then can recognize ERSE-II and unfolded protein response element (UPRE) sequences (Shoulders et al., 2013). ATF6-N upregulates genes that encode chaperones, quality control proteins, protein degradation, and components of the redox pathway. ATF6-N is specifically known to upregulate BiP (Shoulders et al., 2013). Further, ATF6-N upregulates XBP1 expression, promoting XBP1 splicing during times of ER stress.

1.8.5 ER Associated Degradation

Proteins can be terminally misfolded in the ER and require degradation to reduce potential cytotoxicity and recycle essential amino acids. The ER associated degradation (ERAD) pathway targets misfolded proteins for translocation across the ER membrane for degradation in the 26S proteosome. Misfolded proteins fail to be transported to their targeted organelle, leading to their accumulation in the ER lumen and subsequently perturb ER homeostasis. ERAD is responsible for the identification and removal of terminally misfolded proteins. BiP likely is involved in recruiting the misfolded protein to ERAD machinery to assist in the identification and subsequent removal of a misfolded protein. Proteins are polyubiquitinated during their retrotranslocation across the ER

membrane to allow for their ubiquitin dependent degradation by the 26S proteasome (Qi et al., 2017).

There are several pathways responsible for targeting and removing different classes of misfolded proteins. Removing several mannose residues from N-linked oligosaccharides can direct a misfolded protein for degradation through the ERAD pathway. ER degradation enhancing α-mannosidase-like protein 1 (EDEM1) is another chaperone responsible for the identification and subsequent delivery to the Sel1L-Hrd1 ERAD complex. Hrd1 is an ER residential E3 ubiquitin ligase that forms a complex with Sel1L that is responsible for targeting a subset of misfolded proteins in the ER lumen. Hrd1 likely forms a retrotranslocation channel to export misfolded proteins from the ER lumen to the cytoplasm for proteasomal degradation (Qi et al., 2017). There are other lectins present in the ER lumen that recognize N-linked glycans that have not been successfully modified that divert the protein to the ERAD pathway. Lectin chaperones recognize specific glycosylations on glycoproteins (Kozlov & Gehring, 2020). The mannosidase Htm1 marks misfolded proteins for degradation by adding an α-1,6-linked mannose, which in turn marks it for an ERAD substrate recognition factor resulting in its degradation (Ruggiano et al., 2014). Proteins must stay within the ER for a prolonged time in order to be recognized for lectin dependent degradation.

1.8.6 Prolonged UPR Signaling and the Induction of Apoptosis

Prolonged ER stress and UPR induction can trigger apoptosis through one of two pathways. The first pathway involves activation of the effector procaspase 12, found on the cytosolic side of the ER (Nakagawa et al., 2000). Caspase-12 mediated cleavage of

caspase-9 is independent of mitochondrial damage, effectively being independent of cytochrome C (Morishima et al., 2002). During times of ER stress, reactive oxygen species accumulate in the ER lumen, which can activate the ER calcium release channel inositol-1,4,5-trisphosphate receptor 1 (IP3R1). Activation of IP3R1 results in the leakage of Ca^{2+} ions from the ER lumen to the cytoplasm (Tabas & Ron, 2011). High concentrations of cytoplasmic Ca^{2+} activates the Ca^{2+} sensitive cytoplasmic cysteine protease calpain. Activated calpain proteolytically cleaves and activates procaspase-12 to caspase-12, which cleaves caspase-9 or caspase-3 initiating the apoptotic cascade (Hitomi et al., 2004). Activated calpain also cleaves the anti-apoptotic factor Bcl-xL, turning the antiapoptotic protein into a proapoptotic molecule (Nakagawa & Yuan, 2000).

The second pathway in which prolonged UPR induction can result in apoptosis is through the ISR, with PERK activation preferentially translating ATF4 through the phosphorylation of eIF2α. The synthesis of ATF4 leads to the expression of CHOP, which is also referred to as growth arrest and DNA damage inducible gene 153 (GADD153). CHOP is another transcription factor that downregulates expression of anti-apoptotic proteins within the Bcl-2 family, while upregulating proapoptotic proteins such as BCL2L11 (McCullough et al., 2001). CHOP upregulates GADD34, which associates with protein phosphatase 1 (PP1) that works in concert to remove the phosphate on Ser 51 on eIF2α to relieve translation inhibition and restore translation in stressed cells. If stress is alleviated, then the cell returns to homeostasis, but if the stress continues, than this further promotes ER stress and cell death (Marciniak et al., 2004).

Prolonged XBP1s induction may induce apoptosis through the upregulation of specific response factors. The increased concentration of XBP1s changes its target from

canonical UPRE sequences to non-canonical sequences found in the promoter of KLF9. KLF9 then activates the expression of the transmembrane protein 38B (TMEM38B) and inositol 1,4,5-triphosphate receptor 1 (ITPR1). TMEM38B and ITPR1 form ion channels in the ER membrane to increase the efflux of Ca^{2+} from the ER lumen to the cytoplasm (Fink et al., 2018). Increasing the Ca^{2+} concentration in the cytoplasm may induce apoptosis through calpain activation as mentioned previously. Prolonged IRE1 activation can also promotes cell death by activating cJun-N-terminal kinase (JNK) and apoptosis signal-regulating kinase 1 (ASK1).

1.8.7 UPR and IAV Infection

The interaction between IAV and the host's UPR is not well understood. IAV replication is thought to activate IRE1, but not PERK or ATF6 (Hassan et al., 2012). XBP1s was notably higher in infected cells, along with the phosphorylation of JNK. Infection does not induce eIF2α phosphorylation, indicating that both PERK and PKR are not substantially activated by IAV. Furthermore, BiP and other cellular chaperones were not strongly induced during IAV infection. Treating cells with the chemical chaperone tauroursodeoxycholic acid (TUDCA) reduced the accumulation of XBP1s. Interestingly, TUDCA pre-treatment significantly reduced IAV virus production. When IRE1 was specifically inhibited, IAV replication was significantly decreased (Hassan et al., 2012). The advantages of IAV mediated IRE1 activation remain unknown. XBP1u may impair viral replication. IAV likely takes advantage of the pro-survival signaling from XBP1s and the upregulation of genes involved in protein synthesis and folding. IAV is not the

only virus that specifically triggers the IRE1, with adenoviruses activating IRE1 to utilize XBP1s as a transcription factor for early gene expression (Prasad et al., 2020).

Pharmacological induction of the UPR may create an antiviral environment for IAV replication. Goulding and coauthors demonstrated the antiviral properties of thapsigargin (Tg) on IAV infected mice (Goulding et al., 2020). Tg impairs the import of Ca2+ ions into the ER lumen from the cytoplasm which activates the three sensors in the UPR. UPR activation was found to be antiviral against IAV replication. Furthermore, selectively activating PERK in infected cells was demonstrated to impair virus production (Landeras-Bueno et al., 2016).

1.9 Rationale and Overview

Direct-acting antivirals quickly select drug-resistant viral genotypes. The emergence of resistant IAV strains has been observed for all current direct-acting antivirals. Some resistance mutations have no fitness cost to IAV replication, ensuring that there is no negative selective pressures for the virus to revert back to antiviral sensitivity. Fortunately, most circulating viruses are currently sensitive to NA inhibitors, but previous years have experienced a high degree of resistance in circulating strains (Casalegno et al., 2010). Billions of dollars are spent stockpiling NA inhibitors in the event of another pandemic, but emerging zoonotic IAVs are not guaranteed to be susceptible to antivirals. Thus, there is a desperate need for new antivirals against IAV.

A new class of antivirals is currently being investigated. All viruses are intracellular parasites that require numerous host factors to fulfill their replication cycles. Targeting a cellular pathway that is essential for viral replication may block virus

production. Impairing a viral pathway, instead of a directly targeting a viral protein, potentially creates a large genetic threshold for the development of antiviral resistance. Antiviral resistance against direct-acting antivirals in IAV can arise from the substitution of a single amino acid. Whereas forcing the virus to evolve to a new host factor would hypothetically pose a significantly higher threshold for resistance. Hypothetically, targeting a conserved host pathway instead of a specific viral protein would enable the antiviral to be effective against all influenza A viruses. The potential pantropic effectiveness against all IAV would be a cost-effective measure to prepare for future IAV pandemics. Genome wide CRISPR and RNAi screens have identified numerous host factors that are essential for IAV replication (Karlas et al., 2010, 2010; Su et al., 2013). These experiments demonstrate clear relationships between host factors and IAV replication. Many of these host factors are druggable targets, potentially allowing new HTA therapies (Watanabe et al., 2014). Virus replication is dependent on these host factors to synthesize new virions. The work presented in this thesis examines the interaction between IAV and its host and the potential to target these interactions as antiviral therapies. I examine several candidate HTAs that inhibit host pathways that may be essential to sustain virus replication. Finally, I directly investigated the plasticity of the IAV genome by identifying host adaptation mutations required to support viral replication in a murine infection model. Each Chapter in this thesis represents a peer-reviewed article and contain both published and unpublished figures.

In Chapter 3, I investigate the reliance of IAV protein synthesis on the host eIF4F cap-binding complex. IAV synthesises mRNA that is almost identical to host mRNA and requires similar translation initiation machinery to produce viral proteins. I hypothesize

that IAV translation critically relies on host cap-dependent machinery. I hypothesize that impairing eIF4A with pateamine A and the rocaglate silvestrol will reduce the accumulation of viral proteins and impair virus replication in all IAV infection model cell lines tested.

In Chapter 4, I investigate the ER as a potential target for an HTA. The ER is essential in synthesizing, modifying, and sending glycoproteins to their targeted organelle. Accordingly, viral glycoproteins are directed to the ER for their synthesis and subsequent translocation to the plasma membrane. Evidence suggests that perturbing the ER reduces virus production (Al-Beltagi et al., 2021). I hypothesize that perturbing the ER will impair the synthesis and modification of viral glycoproteins, which will subsequently reduce the production of virions.

In Chapter 5, I will continue my investigation into the interaction that IAV has with its host. The molecular adaptation of a virus to a new host can be essential in identifying key host pathways in which the virus relies upon. Previous adaptation studies have identified key sites within the IAV genome that harbour these adaptation mutations (Brown, 1990; Ilyushina et al., 2010). I aim to examine a mouse adapted virus using current next-generation sequencing to identify any mutation that may improve virus replication in a new host. I hypothesize that the adapted virus contains numerous mutations, some of which will improve virus replication specifically in murine cell lines.

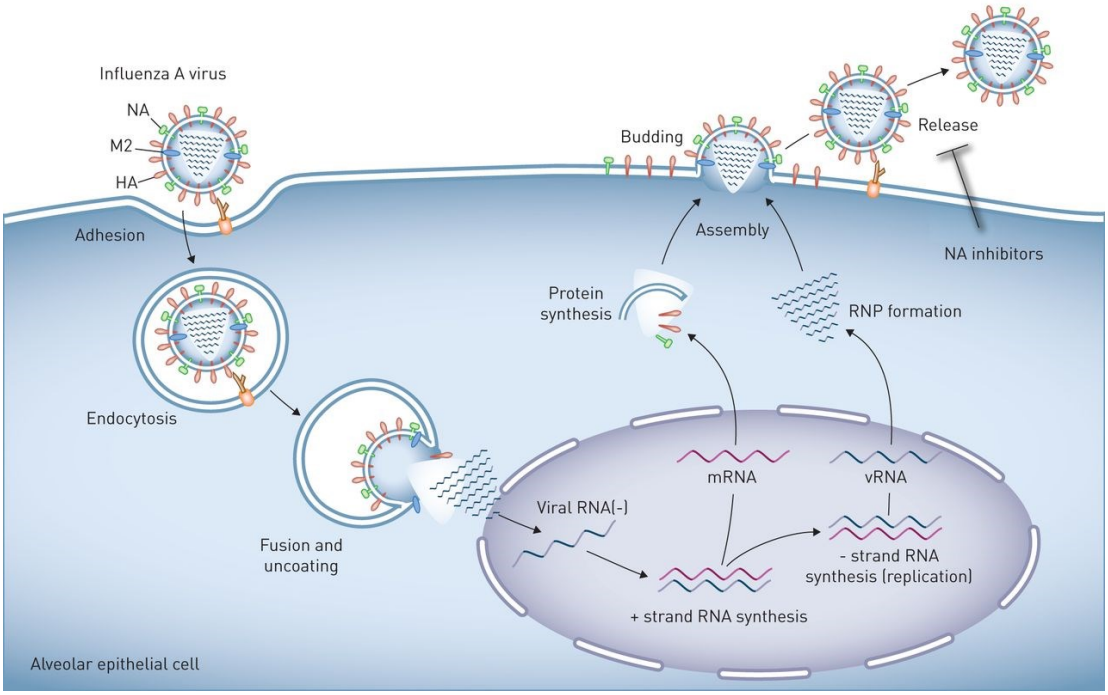

Figure 1.1: Simplified overview of a single round of IAV replication in the host cell. Influenza A virus (IAV) binds to sialic acid on the cell surface which results in receptor mediated endocytosis. As the endosome acidifies, viral HA irreversibly activates and promotes the fusion of the viral membrane and the late endosome, releasing the viral genome into the host's cytoplasm. The viral genomic segments are imported into the nucleus where they immediately synthesize viral messenger RNA (mRNA). Viral proteins are created from viral mRNA. Some viral proteins enter the nucleus to assist in genome replication and export of progeny genomes to the cytoplasm, while other proteins are localized to the plasma membrane to build progeny virions. The progeny viral genomes are transported to the plasma membrane, where they are packaged into budding progeny virions to form a fully infectious viral particle. NA enzymatically degrades the sialic acid receptor during egress, allowing the dissociation of the virion from the cell surface. This enzymatic cleavage is prevented by the NA inhibitor antivirals. Image was modified from (Herold et al., 2015).

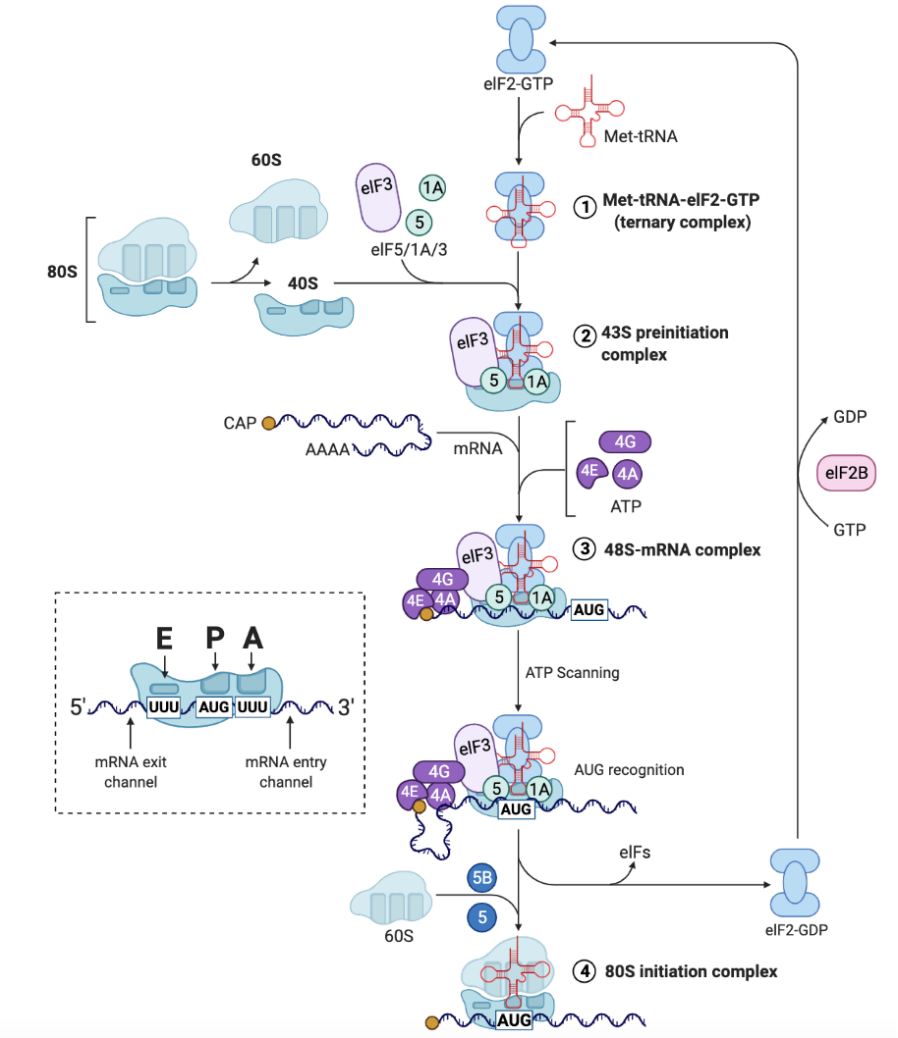

Figure 1.2: Translation initiation requires the 43S preinitiation complex and the eIF4F complex.

Cap-dependent translation requires the successful formation of the 43S preinitiation complex (PIC) and eIF4A. eIF2 is a heterotrimer initiation factor that is comprised of α, β, and gamma subunits. eIF2-GTP binds to the Met-tRNAi^{Met} to form the ternary complex (TC). The TC then binds the 40S ribosomal subunit and other initiation factors such as eIF3 to form the 43S PIC. eIF4F complex is built from eIF4A, eIF4G, and eIF4G. The eIF4F complex binds the 5'-7 methyl guanosine cap, melts secondary RNA structures in the 5' untranslated region (UTR), and circularizes the transcript by binding Poly A binding protein (PABP). The 48S PIC scans the 5' UTR for the AUG start codon, where it hydrolyses GTP to GDP to release eIF2-GDP. The 60S ribosomal subunit is then recruited and translation of the open reading frame (ORF) may begin. eIF2B is a guanosine exchange factor (GEF) that recycles the GDP to GTP on eIF2. The five sentinel kinases in the ISR can phosphorylate Ser 51 on the α subunit of eIF2, which inhibits the eIF2B GEF through higher affinity binding. This decreases the GTP charged pool of TC available for translation initiation, effectively reducing global translation. Adapted from "protein translation cascade", by BioRender.com (2021). Retrieved from https://app.biorender.com/biorender-templates.

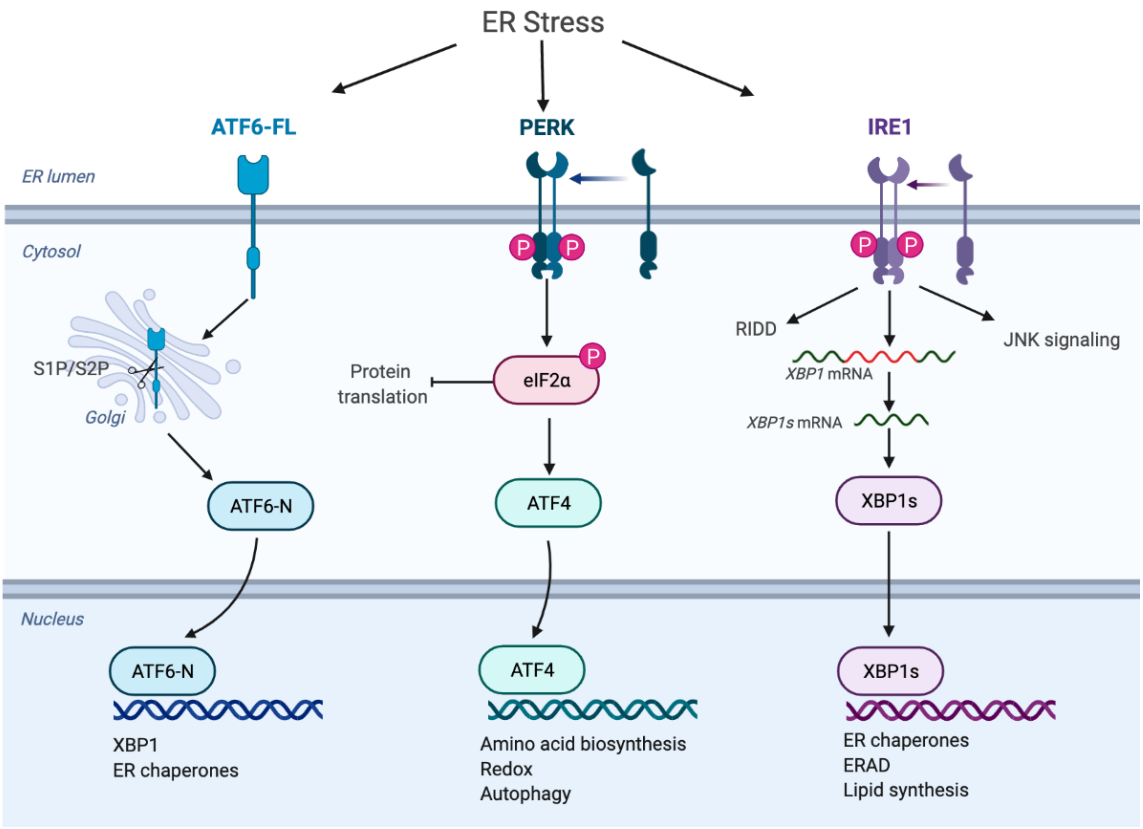

Figure 1.3: ER stress induces the unfolded protein response (UPR)
Misfolded proteins accumulate during times of stress. The accumulation of misfolded proteins activates the unfolded protein response (UPR) through ATF6, PERK, and IRE1. The activation of the three arms creates a transcriptional response by creating the transcription factors ATF6-N, ATF4, and XBP1s to upregulate response genes. ATF6-full length (ATF6-FL) leaves the ER during times of stress to the Golgi complex, where it is cleaved by the Golgi resident proteases. Proteolytic cleavage liberates the bZIP transcription factor to translocate to the nucleus. PERK undergoes autophosphorylation during ER stress, which enables it to phosphorylate eIF2α. The phosphorylation of eIF2α significantly reduces cap dependent translation to reduce protein synthesis into the ER. Phosphorylation of eIF2α preferentially translates the transcription factor ATF4. IRE1 autophosphorylates during times of ER stress, which enables it to non-canonically splice out a 26-nucleotide intron form the XBP1 mRNA. Removing the intron creates a frame shift that synthesizes the XBP1s transcription factor. Adapted from "UPR signaling", by BioRender.com (2021). Retrieved from https://app.biorender.com/biorender-templates.

CHAPTER 2: MATERIALS AND METHODS

2.1 Cell Culture

Madin-Darby canine kidney (MDCK) cells, human embryonic kidney 293T (HEK293T) cells, human lung adenocarcinoma A549 cells, Vero cells, and mouse L929 cells were purchased from the American Type Culture Collection (ATCC, Manassas, VA, USA). Mouse embryonic fibroblasts (MEF) were a gift from Dr. Nancy Kedersha (Brigham and Women's Hospital, Boston, MA, USA). All cells were maintained in Dulbecco's modified Eagle's medium (DMEM, HyClone, Mississauga, ON, Canada) supplemented with 10% fetal bovine serum (FBS, Life Technologies, Burlington, ON, Canada), 20 µM L-glutamine (Life Technologies, Burlington, ON, Canada), and 100 U/mL penicillin + 100 µg/mL streptomycin + 20 µg/mL glutamine (Pen/Strep/Gln; Wisent Bioproducts, St-Bruno, QC, Canada). Cells were incubated at 37°C in 5% CO_2 atmosphere. Generation of A549[EGFP-G3BP1] cells is described in (Khaperskyy et al., 2012). In brief, Dr. Khaperskyy generated A549 cells stably expressing EGFP-G3BP1 by transducing cells with the retrovirus vector pMSCV-EGFP-G3BP1-Puro. Once cells were transduced with the retrovirus, they were selected for resistance to puromycin treatment (10µg/mL) and clones were generated from single cells. Cells were further selected for EGFP expression, Clone #4 displayed strong cytoplasmic EGFP-G3BP1 foci following Silvestrol treatment, which was used for this study.

2.2 Influenza Viruses and Infections

Viruses used in this study include A/Puerto Rico/8/34/(H1N1) (PR8), A/Udorn/1972(H3N2) (Udorn), A/Brisbane/59/07(H1N1) (Brisbane),

A/California/07/2009(H1N1) (CA/07), A/California/07/2009(H1N1) (CA/07) Mouse-adapted (CA/07-MA), and A/California/07/2009(H1N1) (CA/07) PA-P2A Nanoluciferase (CA/07-NL). Wild-type PR8 stocks were generated using the 8-plasmid reverse genetic system (completed by Dr. Khaperskyy), which was provided by Dr. Richard Webby (St. Jude Children's Research Hospital, Memphis USA); Amantadine sensitive PR8 (PR8-AmantS) was engineered by mutating the 27th codon in M2 from GCU to GUU, which results in the A27V substitution and mutating the 31st codon from AAU to AGU, which results in the N31S substitution. The A27V and N31S amino acids in M2 confer antiviral susceptibility to amantadine. Amino acids were substituted using site-directed mutagenesis. PR8-AmantS was then generated using the 8-plasmid reverse genetic system (completed by Patrick Slaine), Udorn was rescued from the 12-plasmid system that was provided by Dr. Yoshi Kawaoka (University of Wisconsin-Madison, Madison, USA) (completed by Dr. Khaperskyy); CA/07 was provided by the Public Health Agency of Canada (PHAC) National Microbiology Laboratory; Brisbane was a gift from Dr. Todd Hatchette (Dalhousie University, Halifax Canada); CA/07-MA was mouse-adapted by serial passaging in Swiss-Webster mice, performed by Cara MacRae in the Hatchette lab (Slaine et al., 2018); CA/07-NL was a gift by Dr. Andrew Mehle (University of Wisconsin – Madison, Madison USA). Influenza virus stocks were propagated in MDCK cells in IAV infection media (DMEM supplemented with 0.5% [w/v] bovine serum albumin (BSA, Sigma, St. Louis, MO, USA) and 20 µg/mL L-glutamine, and 1 µg/ml N-tosyl-L-phenylalanine chloromethyl ketone (TPCK)-treated trypsin). TPCK treated trypsin activates IAV HA by cleaving HA0 into HA1 and HA2, liberating the fusion peptide. Supernatant was harvested at 48-72 hpi, centrifuged at

2,300 x g for 5 minutes to pellet cellular debris, aliquoted, and stored at -80˚C. Stocks of CA/07-MA for mouse experiments were generated using 10 day-old embryonated chicken eggs. 1:100 dilutions of CA/07-MA grown from a plaque purified stock grown in MDCKs were used to infect the embryonated eggs. Diluted virus was injected into the allantoic cavity of the egg using a 23-gauge 1mL syringe. After incubating the eggs for 3 days at 33˚C, the allantoic fluid was harvested and centrifuged at 3,000 x rpm for 5 minutes. An HA assay was performed on every egg (HA assay is described below). The allantoic fluid from all eggs were pooled if they yielded 64 HA units or above. The virus was aliquoted and stored at -80˚C. Plaque forming units (PFU) were calculated by plaque assay as described below.

For infections of cultured cells, cell monolayers were washed briefly with 1xPBS before inoculation with diluted virus. Virus inoculums were diluted in IAV infection media without TPCK-treated trypsin and added to cells for 1 h at 37ºC. Infections were conducted at a multiplicity of infection (MOI) of 0.1, or as indicated. After the diluted inoculum was removed, cell monolayers were washed with 1xPBS (Wisent, St-Bruno, QC, Canada) and fresh IAV infection media was added. Supernatants were harvested at 24 hpi unless indicated otherwise. Virus containing supernatant was incubated with TPCK-treated Trypsin at 1.5µg/mL for 1 hour at 37˚C to activate influenza HA.

2.3 Plaque Assay

Plaque assays were performed on confluent MDCK cells using 1.2% Avicel (FMC, Philadelphia, PA) overlays as described in (Matrosovich et al., 2006). Confluent MDCK cells were infected with serially diluted influenza samples for 1 hour at 37˚C. Virus was

aspirated off and cells were washed with 1xPBS. Overlay (1 (2.6% Avicel):1 (9:1 2xMEM:5%BSA in DMEM)) supplemented with 1µg/mL TPCK-treated trypsin was added to the wells and cells were incubated for 44-48 hours at 37˚C with 5% CO_2 atmosphere. Cells were washed twice with 1xPBS to remove the overlay before fixation with 5% formaldehyde for 30 minutes at room temperature. Cells were washed 3 times with 1xPBS for 5 minutes each before adding 1% crystal violet (w/v in 50% methanol:50% dH2O). Crystal violet was washed off after incubating for 15 minutes before counting plaques.

2.4 Hemagglutination Assay

Turkey red blood cells (RBC) (Cedar Lane-7209403) were washed with 1xPBS and diluted to 0.5% final concentration. In a round bottom 96 well plate, virus from each egg was serially diluted with a ratio of 1:2 with 1xPBS. 50µL of diluted red blood cells were then added to each well, shaken, and incubated at room temperature for an hour. Wells were observed for the formation of agglutination, where the RBCs fail to settle into a focus at the bottom of the well. HA units were calculated from the reciprocal of the highest dilution which agglutination was observed.

2.5 Chemicals

6-thioguanine (6-TG), 6-thioguanosine (6-TGo), also referred to as 2-Amino-6-mercaptopurine riboside hydrate, 6-mercaptopurine (6-MP), 5-fluorouracil (5-FU), ribavirin, integrated stress response inhibitor (ISRIB), 4-phenylbutyric acid (4-PBA), Tunicamycin (TM), sodium arsenite (As), and Thapsigargin (Tg) (all obtained from

Sigma-Aldrich Canada Co., Oakville, ON, Canada) were solubilized in dimethyl sulfoxide (DMSO) and stored at -80˚C. Stock concentrations were diluted to the indicated concentrations in media. PatA was a kind gift from Dr. Jerry Pelletier (McGill University, Montreal, QC, Canada); Silvestrol was obtained from MedChem Express (Princeton, NJ, USA).

2.6 Cytotoxicity Assay

A549 cells were seeded at 10,000 cells/well in a 96-well plate prior to drug treatment. Drugs were diluted in infection media at indicated concentration and incubated with the cells for 24 hours. At 20 hours post-treatment, 10% alamarBlue Cell Viability Reagent (ThermoFisher) was added to the cell monolayer followed by 4 additional hours of incubation. The active ingredient of the alamarBlue assay is resazurin, which is cell permeable and non-toxic. Resazurin is reduced to resorufin by the cellular enzymes in the mitochondria. Resorufin is highly fluorescent and can be detected in a florescence-based plate reader. Plates were incubated at 37˚C with 5% CO_2 atmosphere. Plates were analyzed on FLUOstar Omega 96 well plate reader or a Tecan Infinite M200 PRO microplate reader at an excitation of 544 nm, and an emission of 580-590 nm. The relative fluorescence units for cells treated with vehicle (DMSO) and compounds were first normalized to cells that were untreated. After this, treated cells were then normalized to DMSO treated cells to represent the overt cytotoxicity over the vehicle control.

2.7 Immunofluorescence

For immunofluorescence microscopy cells grown on glass coverslips were washed with 1xPBS, fixed using 4% paraformaldehyde at room temperature for 15 minutes before permeabilizing with -20˚C methanol. Cells were then stained using mouse monoclonal antibody to G3BP (clone 23, BD Biosciences, Mississauga, ON, Canada), goat polyclonal antibody to influenza virus antigens haemagglutinin (HA), nucleoprotein (NP), and matrix protein 1 (M1) (ab20841, Abcam Inc., Toronto, ON, Canada), and rabbit monoclonal antibody to TIAR (clone D32D3, New England Biolabs Ltd., Whitby, ON, Canada) at the manufacturer's recommended dilutions. Donkey Alexa Fluor-conjugated secondary antibodies (Molecular Probes) were used at 1:1000 dilution in combination with 5 ng/mL Hoechst dye. Images were captured using Zeiss Axioplan II microscope or Zeiss LSM 510 laser scanning microscope.

2.8 Immunoblotting

Cell monolayers were washed once with ice-cold PBS and lysed in 2x Laemmli buffer (4% [w/v] sodium dodecyl sulfate [SDS], 20% [v/v] glycerol, 120 mM Tris-HCl [pH 6.8]). DNA was sheared by repeated passage through a 21-gauge needle before 100 mM dithiothreitol (DTT) addition and boiling at 95˚C for 5 min. Samples were stored at -20˚C until analysis. Total protein concentration was determined by DC protein assay (Bio-Rad) and equal quantities were loaded in each SDS-PAGE gel. Proteins were transferred to polyvinylidene difluoride (PVDF) membranes (Bio-Rad) with the Trans-Blot Turbo transfer apparatus (Bio-Rad). Membranes were blocked with 5% [w/v] bovine serum albumin in TBS-T (Tris-buffered saline, 0.1% [v/v] Tween) before probing

overnight at 4˚C with primary antibodies to the following targets: β-actin (rabbit, HRP-conjugated, Cell Signaling, #5125); ATF6 (Mouse, Abcam, ab122897); BiP (Rabbit, Cell Signaling, #3177); CHOP (Mouse, Cell Signaling, #2895); eIF2α (Rabbit, Cell Signaling, #5324); Serine 51 phosphorylation eIF2α (Rabbit, Abcam, E90); influenza A virus polyclonal antibody against HA, NA, and M1 (Goat, Abcam, ab20841); influenza virus NA (Rabbit, GeneTex, GT288); influenza NS1 (Mouse, Kerafast, clone 13D8); IRE1 (Rabbit, Cell Signaling, #3294); PARP (Rabbit, Cell Signaling, #9542); PERK (Rabbit, Cell Signaling, #5683); phospho-S51-eIF2α (Rabbit, Cell Signaling, #3398); XBP1s (Mouse, Cell Signaling, #12782). Membranes were washed with TBS-T and incubated with HRP-linked secondary antibodies prior to detection with Clarity-ECL chemiluminescence reagent (Bio-Rad). All blots were imaged on a Bio-Rad ChemiDoc-Touch system. Molecular weights were determined using protein standards (New England Biolabs, P7719). Each protein target was probed independently of each other, except cellular actin and the poly-IAV antibody. Unless indicated otherwise, all western blot images represent two independent biological experiments.

2.9 Semiquantitative XBP1 mRNA Splicing Assay

The semiquantitative XBP1 mRNA splicing assay was performed as described previously (Johnston et al., 2019). Specifically, total RNA was isolated from treated A549 cells with the RNeasy kit (Qiagen). Five hundred nanograms of total RNA was reversed-transcribed (RT) using the Maxima H RT kit (Thermo) to complementary DNA (cDNA) using the oligo-dT primer. Oligo-dT anneals to mRNA poly A tails, facilitating the conversion of the entire mRNA pool to cDNA. A 473-bp PCR product was amplified

from the cDNA using the XBP1 forward primer 5'-AAACAGAGTAGCAGCTCAGACTGC-3' and the XBP1 reverse primer 5'-TCCTTCTGGGTAGACCTCTGGGA-3' from cDNA. The PCR product of the unspliced XBP1 mRNA contains the 26-nucleotide intron, while the PCR product of XBP1s is lacking the 26-nucleotides. The dsDNA copy of the 26-nucleotide intron contains a PstI cut site, allowing digestion of the unspliced XBP1 cDNA while XBP1s cDNA is resistant to the restriction enzyme. The PCR product was digested overnight with PstI-HF to cleave the unspliced XBP1 product into XBP1u1 and XBP1u2. The digested PCR product was resolved on a 2.5% agarose gel made with 1xTris-acetate-EDTA (1xTAE) and stained with ethidium bromide (Sigma-Aldrich). Data was captured on a ChemiDoc imaging station (Bio-Rad).

2.10 Sequencing and Analysis

Total RNA was isolated from virus-infected MDCK cells using the RNeasy Plus Mini Kit (Qiagen Inc., Toronto, ON, Canada), and the viral genomic RNA was reverse-transcribed as described in (Khaperskyy et al., 2016) using the Maxima H Minus First Strand cDNA Synthesis Kit (Thermo Fisher Scientific, Grand Island, NY, USA) with the Uni12 primer (5′-AGC AAA AGC AGG-3′) (E. Hoffmann et al., 2001). The first 12 nucleotides on the 3' end of the genome is highly conserved across all eight genome segments; this conservation is observed across all IAV subtypes. The universal consensus sequence at the 3' end of the negative sense RNA genome is 5' TCGYTTTCGTCC 3'. The fourth nucleotide is R, the single letter code for pyrimidine (T or C), with the first three segments of the genome harbouring a C at the fourth nucleotide, while the last five

segments carry an T. Accordingly, the primer used to generate the cDNA library and subsequent amplification is 5’ AGCRAAAGCAGG 3’ (referred to as Universal 12, or Uni12), with the fourth nucleotide being an R, the single letter code for purine (A or G). The primer pool contains both the 5’ AGCGAAAGCAGG 3’ and 5’ AGCAAAAGCAGG 3’ in equal concentrations, enabling all segments to be amplified without introducing artificial selection of one segment over the others. Similar to Uni12, all IAVs have the last 13 nucleotides (Uni13) at the 5’ end of the genome universally conserved across all eight segments and IAV subtypes. cDNAs were amplified for 10 cycles with Phusion High Fidelity DNA Polymerase (NEB) using primers (specific parts underlined) containing Illumina Nextera Transposase adapters: R1-Uni12 (5′-TCG TCG GCA GCG TCA GAT GTG TAT AAG AGA CAG AGC GAA AGC AGG-3′) and R2-Uni13 (5′-GTC TCG TGG GCT CGG AGA TGT GTA TAA GAG ACA GAG TAG AAA CAA GG-3′) using 20-s 48 °C annealing and 7-min 72 °C extension steps (adaptor and barcode oligonucleotide sequences from Illumina, Inc., San Diego, CA, USA) (Slaine et al., 2018). Products were purified using the PCR Purification Kit (Qiagen), and 1 ng was used for Nextera XT (Illumina) library preparation according to the manufacturer’s instructions, except that the kit’s bead-based clean-up and normalization (two steps) were completed using the Just-a-Plate 96 PCR Purification and Normalization Kit (CharmBiotech, San Diego, CA, USA) in one step. Complete libraries were pooled and sequenced in a portion of a 300 + 300 bp PE MiSeq run (Illumina 600-cycle v3 kit) by the CGEB-IMR (Centre for Genomics and Evolutionary Biology Integrated Microbiome Resource; (http://cgeb-imr.ca). Raw reads were imported into Geneious R 8.1.8 (Kearse et al., 2012). Reads were trimmed at default settings and filtered for a quality (Q) score of

30, selecting reads that have an error probability less than 0.001. Reads were aligned to reference genomes for each individual segment. Once aligned, single nucleotide polymorphisms (SNPs) were identified using Geneious variations/SNPs at 1% abundance (McGinnis et al., 2016). SNP frequencies and locations were imported into R (www.r-project.org) for final analysis.

The internal sequences of the larger viral segments sometimes are removed, resulting with the 5' and 3' ends of the segment ligated together missing the majority of the internal coding capacity of the segment. I refer to the 5' sequence that is ligated to a 3' downstream sequence, deleting the internal portion of the segment, as a junction. Junctions of internally deleted viral genomes were called manually in Geneious by identifying incorrectly aligned reads that spanned the junction. Illumina reads cover 150-350 base pairs allowing them to cover these junctions. Reads that showed homology to the 3′ and 5′ ends of the viral genome were used to identify the nucleotide positions of the breaks similarly to (Saira et al., 2013).

2.11 Generation of Recombinant Viruses

Eight genomic segments for the parental CA/07 virus were amplified individually from the multi-segment cDNA using universal primer sets described in (E. Hoffmann et al., 2001)and cloned into the pHW2000 vector (E. Hoffmann et al., 2000), yielding eight constructs named pHW-C71–pHW-C78. Subsequently, T156A and F740L amino acid substitutions were introduced into the PB1 construct to create pHW-C72 (T156A, F740L) and E349G in the PA construct to create pHW-C73 (E349G) using the Phusion site-directed mutagenesis PCR protocol (NEB). All constructs were verified by Sanger

sequencing. Recombinant viruses were rescued from 8 plasmids using HEK293T and MDCK cells as described in (E. Hoffmann et al., 2000; Neumann et al., 1999). For production of CA/07 virus, the original pHW-C71–pHW-C78 plasmids were used. pHW-C72 (T156A, F740L) and pHW-C73 (E349G) were substituted for pHW-C72 and pHW-C73 constructs, respectively, to produce CA/07-PA, PB1-MA virus. I co-cultured HEK 293T cells with MDCK cells to rescue infectious viral progeny. To generate stocks, virus was then passaged in MDCKs twice with observable cytopathic effects. Virus production was quantified using a plaque assay and stored at -80˚C for future experiments.

2.12 Minigenome Assay

Viral RNA polymerase activity was tested in HEK293T cells using the reconstituted minigenome assay with the pPolI-WSN-NA-firefly-luciferase reporter construct (gift from Dr. Yoshihiro Kawaoka, University of Wisconsin-Madison, Madison, WI, USA) and in mouse L929 cells using the pHL-NS-FF-Luc reporter construct (gift from Dr. Georg Kochs, University of Freiburg, Freiburg, Germany). The assay was performed as described in (Z. Li et al., 2009), except the pHW-C71, pHW-C72, pHW-C73 and pHW-C75 plasmids were used for the expression of CA/07 PB2, PB1, PA and NP proteins, respectively, and the pGL4.74 (hRluc/TK) plasmid (Promega, Madison, WI, USA) for control Renilla luciferase expression. The

The dual luciferase assay was performed 24 h post-transfection using the Dual-Glo Luciferase Assay System (Promega). I engineered the amino acid substitutions into PB1 and PA expression vectors pHW-C72 and pHW-C73 by site-directed mutagenesis and tested effects on viral polymerase activity in the minireplicon assay.

2.13 Generating CRISPR KO Cell Lines

The lentiCRISPR-v2 plasmid was acquired from Addgene (Addgene plasmid # 52961; http://n2t.net/addgene:52961; RRID:Addgene_52961) (Sanjana et al., 2014). The lentiCRISPR-v2 plasmids encoding guide RNAs targeting human PERK or non-targeting guide RNA control were cloned with primer sequences designed using Broad Institute GPP Web Portal (https://portals.broadinstitute.org/gpp/public/analysis-tools/sgrna-design). Guide RNA insert sequences: PERK guide-1 5'-GAATATACCGAAGTTCA AAG; PERK guide-2 5'- GGACCAAGACCGTGAAAGCA; non-targeting (NT) guide 5'- GCACTACCAGAGCTAACTCA (sequence similar to scrambled guide RNA in pCas-Guide-CRISPRi-Scramble vector from OriGene Technologies). The parental cell line was a pool of A549s passaged from an original stock purchased from the ATCC. A549 cells were transduced with lentiviruses generated with these vectors at MOI 1.0 and stably transduced cells were selected with 1 μg/ml puromycin for 48 h. Resistant cells were diluted to 0.5 cells/100μL and seeded 100 μL into 96-well dishes for singe-cell clone isolation. This dilution allowed 1 out of 2 wells to contain a single cell. Each well was confirmed to contain a single cell through brightfield microscopy. Knock out (KO) clones were confirmed using western blotting and subsequently used in experiments. NT-control A549 cells were also clonally selected for.

2.14 Mean lethal dose 50(MLD_{50}) Calculation in the BALB/c Mouse Model

BALB/c mice (Charles River-028) were purchased at 4 weeks of age and acclimatized for a week in the Carlton Animal Care Facility. Mice were separated into their respective groups with their ears marked for identification. CA/07-MA virus was 10-fold serial diluted in PBS (10^{-1} to 10^{-8}) before infecting mice. Groups of 5 mice were sham-infected or infected intranasally with 50 µL of serially diluted virus in PBS. Mice were anesthetized with 5% isoflurane before adding 12.5 µL of virus to each nostril. Mice were allowed a brief recovery period before adding the second amount of virus to their nostril. Mice were monitored for the clinical manifestation of influenza infection, which include; weight loss, dehydration, reduction in body temperature, lethargy, hunched postures, and laboured breathing. These were categorized into the following six quantifiable clinical outcomes: physical appearance, posture, activity/behaviour, body temperature, hydration, and body weight. Mice were observed and received a score of 0-3 for the listed clinical outcomes. If mice received a score of 12 or greater, or lost 20% or greater of their body weight, then they were euthanized by cervical dislocation after isoflurane induction and marked as a fatality. Survival rates were graphed and MLD_{50} units were calculated using the Reed-Muench method (Reed & Muench, 1938). The MLD_{50} of the stock of CA/07-MA was calculated to be 162 181 MLD_{50}/50 µL, which is approximately 3 virions/50 µL.

2.15 6-TG Treatment in Murine Challenge Study

BALB/c mice (Charles River-024) were purchased at 4 weeks of age and acclimatized for a week in the Carlton Animal Care Facility. Mice were separated into their trial groups with ears marked for identification. Mice were treated with 6-TG (0.3 mg/kg), Ribavirin (40 mg/mL), or vehicle control (PBS) by intraperitoneal (I.P.) injection two days prior to infection. Ribavirin was shown previously to be antiviral against H1N1 in the murine model (Rowe et al., 2010). Ribavirin and 6-TG were solubilized in PBS. Injections continued every day until 10 days post-infection, alternating sides each day. Mice were infected on day 0 with ~5xMLD_{50} units. A cohort of mice were mock infected to provide a healthy example. Mice were monitored and weighed frequently and euthanized if ethical endpoints were exceeded. Mice were sacrificed on day 3, 5, and 7 to obtain Bronchoalveolar Lavage Fluid (BALF), and harvest lungs for histopathology scoring. 500 µL of sterile 1xPBS was used to lavage mice post-mortem. To harvest samples, mice were anesthetized with 5% isoflurane. BALF was centrifuged to pellet cells for flow cytometry analysis, and supernatants were sterile filtered to enumerate the infectious progeny by plaque assay. BALF was also used to quantify the cytokines and chemokine profile from healthy mice, mock treated-infected mice, and 6-TG-treated infected mice. BALF was treated with 20 mJ/cm2 UV light (254 nm, UVC) in a HL-2000 Hybrilinker chamber (UVP) (equates to 3 minutes) to inactivate any virus present in the BALF. Chemokine and cytokine profile were quantified using a Multiplex ELISA for murine targets. Working with the Marshall lab, inactivated BALF was diluted in PBS and analyzed for 23 different targets using the ProcartaPlex™ Multiplex Immunoassay (Targets are listed in table 4.1).

2.16 Flow Cytometry Analysis

BALF was centrifuged at 500xg for 5 minutes to pellet cells. Cells were washed with FACS buffer (0.5% BSA and 1% azide w/v in 1xPBS) before trypan blue staining and counting viable cells with on a hemocytometer. Cells were probed for CD45 (Rat, PerCP Cy5-5-A, Cat # 103126, Biolegend), CD11c (Armenian Hamster, APC A, Cat # 117306, Biolegend), CD11b (Rat, FITC A Cat #101216, Biolegend), SigLig F (Rat, PE A, 1RNM44N, Thermo Fisher), and Ly6G (Rat APC eFluor 780, Cat # 127607, Biolegend). Cells were analyzed on the BD LSR Fortessa instrument. A total of 300,000 events were captured and cells were gated from forward and side scatter, CD45 and side scatter to enumerate leukocytes, CD11c and SigLig F to enumerate alveolar macrophages, and Ly6G and CD11b to enumerate neutrophils.

2.17 Statistical Analysis

Statistical analysis was performed on values obtained from at least three independent biological replicates with PRISM GraphPad 8, using a one-way ANOVA followed by a Tukey multiple comparison test or two-way ANOVA followed by Dunnett's multiple comparison test. Statistical analysis was also performed with paired t tests, with Welch's correction for standard deviation. Significance is indicated with * (p-value of <0.05), ** (p-value of <0.01), *** (p-value of <0.001), **** (p-value of <0.0001).

2.18 Accession Numbers

Sequences used for each segment of A/California/07/2009 (H1N1) are as follows; Segment 1-PB2 (NC_026438), Segment 2-PB1 (FJ969531), Segment 3-PA (NC_026437), Segment 4-HA (FJ981613), Segment 5-NP (NC_026436), Segment 6-NA (GQ377078), Segment 7-M (FJ969527) and Segment 8-NS (NC_026432). The protein accession number used for 3D modeling was 4WSB. Images were generated using PyMOL Version 2.0.4 (The PyMOL Molecular Graphics System, Schrödinger, LLC. (http://pymol.sourceforge.net/faq.html)). Mutations were identified in 5 out of 8 segments of CA/07-MA. The genomic segments harboring adaptation mutations are the Non-Structural (NS), Polymerase Acid (PA), Polymerase Basic 2 (PB2), Hemagglutinin (HA), and Nucleoprotein (NP) were submitted to GenBank and can be accessed as MG027911, MG027912, MG027913, MG027914 and MG027915, respectively.

2.19 Animal Ethics

Female BALB/c mice were purchased form Charles River Laboratories. Mice were maintained under specific pathogen-free conditions in the Carleton Animal Care Facility at Dalhousie University. All experimental procedures were approved by the University Committee on Laboratory Animals following the guidelines of the Canadian Council on Animal Care (approval number:15-057).

CHAPTER 3: THE eIF4A INHIBITORS SILVESTROL AND PATEAMINE A IMPAIR THE ACCUMULATION OF VIRAL PROTEINS AND REDUCE VIRUS PRODUCTION

3.1 Introduction

Current antivirals against IAV directly target viral proteins NA, M2, and PA. Identifying new antiviral therapies against IAV is essential in combating yearly epidemics or global pandemics because resistance mutations quickly become fixed in viral populations. The RdRp of IAV lacks 3' to 5' exonuclease activity and has an exceptionally high mutation rate of $4.5x10^{-3}$ to $0.5x10^{-3}$ s/s/r (Nobusawa & Sato, 2006). This results in the rapid generation of mutant genotypes in the virus population, any of which will be rapidly selected for if they confer resistance to an antiviral. Therefore, IAV can quickly become resistant to direct-acting antivirals. If there is no fitness cost for antiviral resistance, the mutation that confers resistance will remain fixed in the virus population. An example of this is IAV resistance to amantadine. Amantadine blocks the M2 ion channel from acidifying the virus core, an essential step during entry. However, amantadine is no longer effective in clinical settings due to single amino acid substitution (S31N) in the ion channel (To & Torres, 2019). Because of this, only one class of antiviral is used in clinical settings against IAV in North America, necessitating the need for new antivirals.

Since IAV has demonstrated the ability to develop resistance to all direct-acting antivirals, research has shifted to selectively targeting host factors to impair virus replication. IAV is an obligate intracellular parasite that does not encode any proteins

dedicated to metabolism and protein synthesis. Therefore, IAV must hijack its hosts translation and metabolic pathways to support virus replication. Genome-wide CRISPR KO studies have identified hundreds of host factors that are essential to sustain virus replication (B. Li et al., 2020). Targeting host translation may be effective at impairing the synthesis of viral proteins, and subsequently reduce the production of progeny virus. The genetic bottleneck to develop resistance against a HTA is presumably greater than that of a direct-acting antiviral because the virus will be forced to evolve around host processes. IAV may not be able to overcome the large genetic barrier generated by HTAs. The generation of HTA resistant IAV may force the virus to utilize new host processes will likely require numerous substitutions across the genome to arise concurrently.

IAV generates mRNA that closely resembles host mRNA, allowing efficient protein synthesis by host translation machinery. The IAV RdRp utilizes the first 10-14 nucleotides from nascent host mRNAs as a primer to synthesize the positive sense mRNA (Dias et al., 2009). Importantly, the first 10-14 nucleotides contain the 5' cap that promotes eIF4F dependent translation. Host mRNAs contain the 3' poly A tail, which are recognized by cellular PABPs during translation. IAV NS1 inhibits cellular CPSF30, which impairs the formation of the 3' poly A tail on host mRNAs (Nemeroff et al., 1998). IAV is able to bypass NS1 mediated host shutoff by reiterative copying from a stretch of uracil nucleotides in its genome to synthesize the 3' poly A tail. The 5' cap and the 3' poly A tail on viral mRNAs protect it from degradation by host factors such as Xrn1 (Clerici et al., 2017). NS1 also plays an important role in recruiting ribosomes to viral mRNAs (Panthu et al., 2017).

Translation is the cellular process of synthesizing a polypeptide, a step that is essential to all cellular functions. For bulk translation, the host mRNA is bound by the eIF4F complex. The eIF4F complex is comprised of the cap binding protein eIF4E, the scaffolding protein eIF4G, and the ATPase DEAD-box RNA helicase eIF4A. eIF4E recognizes mRNA specifically by binding to the 5' cap, which enables cap-dependent translation (Iwasaki et al., 2016, p. 4). eIF4G binds eIF4E, along with PABP to circularize the mRNA to allow efficient translation. The eIF4A helicase is responsible for unwinding the secondary RNA structures found in the 5' UTR of the mRNA, aiding in translation initiation.

For translation initiation to occur the TC binds eIF3, eIF5, eIF1, eIF1A, and the 40S ribosomal subunit to form the 43S PIC. The 43S PIC is then recruited to eIF4F-mRNA (Ivanov et al., 2019). Together, the initiation machinery scans the 5' of the mRNA for an AUG start codon. Once there is established codon-anticodon binding, the 48S initiation complex forms (Brito Querido et al., 2020). eIF5 induces the hydrolysis of eIF2-GTP to eIF2-GDP which results in the partial dissociation of eIF2 from the 40S subunit, allowing the recruitment of the 60S subunit (Brito Querido et al., 2020). Together, the 40S and 60S ribosomal subunits form the 80S, which processes incoming charged tRNAs to synthesize the polypeptide. After translation initiation occurs, eIF2-GDP must be recharged to eIF2-GTP to reform the ternary complex before the next round of initiation (Hinnebusch, 2011; Holcik & Pestova, 2007).

Translation is resource-intensive and highly demanding on cellular metabolism. Accordingly, translation is tightly regulated to prevent the synthesis of unneeded and potentially harmful products. Translation is primarily regulated during initiation through

controlling the functions of eIF4F and eIF2. As noted above, eIF4F consists of three subunits that work in concert to bind the 5' cap and 3' poly A tail of a mRNA and recruits the 43S preinitiation complex. eIF4F assembly and function can be regulated by mTORC signaling, which phosphorylates 4E-BPs (P. Shen et al., 2018). 4E-BPs sequester eIF4E away from the eIF4F complex, disallowing translation initiation (Cencic & Pelletier, 2016). mTORC phosphorylates 4E-BPs, which dissociates 4E-BP from eIF4E, allowing eIF4E to participate in the formation of eIF4F subsequently allowing cap-dependent translation (Diab-Assaf et al., 2015). The ISR controls translation through eIF2B, a GEF through the phosphorylation of eIF2α on Ser-51 (Costa-Mattioli & Walter, 2020). The recycling of GDP to GTP on eIF2 is a rate limiting step to translation initiation, and it is regulated by the GEF eIF2B. ISR signaling results in the phosphorylation of the α subunit of eIF2, which prevents the recycling of eIF2-GDP to eIF2-GTP in the ternary complex. There are five kinases responsible for phosphorylating eIF2α, each acting as a sentinel for specific cellular stresses (Hinnebusch, 2011; Y.-N. Lu et al., 2021, p. 2).

My first investigation into new HTAs was characterizing translation inhibitors silvestrol (Sil) and pateamine A (PatA) (Fig 3.1). Both of these compounds impair global translation and likely pose a large evolutionary bottleneck for the generation of antiviral resistance. Both Sil and PatA specifically inhibit the eIF4A helicase. Silvestrol is a member of the rocaglate family of compounds, known for their central cyclopenta[b]benzofuran skeleton. Rocaglates can be isolated from plants in the Aglaia genus. Impairing eIF4A can affect global protein synthesis, with previous studies showing downregulation of pro and anti-inflammatory cytokines in human macrophages

(Blum et al., 2020; Kim et al., 2007). Numerous studies have shown that eIF4A is the molecular target of silvestrol (Chambers et al., 2013; Chu et al., 2016). It is thought that Silvestrol specifically increases the helicase activity of eIF4AI, effectively locking the helicase to the mRNA and depleting the pool for future translation (Sadlish et al., 2013). Treating cells with Sil dramatically increase the number of ribosomes fixed to the 5' sequences of transcripts. Furthermore, sequencing the mRNAs that accumulated ribosomes after Sil treatment show that almost all sensitive mRNA contain G-quadruplexes in which four guanines fold in a planar arrangement (Wolfe et al., 2014). G-quadruplex structures are thought to regulate the expression of a subset of mRNAs. It is thought that sequences with G-quadruplexes pose a barrier to translation and requires eIF4A to melt the higher-level RNA structure to initiate translation. Previous work has demonstrated that adding G-quadruplex sequences to the 5' UTRs of a reporter gene increases its susceptibility to Sil treatment (Wolfe et al., 2014). Recent work argues that Sil increases eIF4A's affinity to polypurine sequences over mRNAs with the G-quadruplex. The authors show that eIF4A "fixes" onto mRNA independently of the eIF4F complex (Iwasaki et al., 2016). Cellular-MYC and a number of other oncogenes contain 5' UTR sequences that can form a G-quadruplex structure. Therefore, the translation of C-MYC and other oncogenes highly suspectable to eIF4A inhibitors (Wolfe et al., 2014). Sil is being pursued as a potential anti-cancer agent because of its ability to impair translation of oncogenes. Some cancer cells show resistance to Sil by upregulating ABCB1 and P-glycoprotein (Pgp), which are involved in the efflux of small molecules. Impairing Pgp or knocking down ABCB1 sensitizes cells to Sil (Gupta et al., 2011).

PatA is a natural compound isolated from the marine sea sponge *Mycale hentscheli* that irreversibly binds eIF4A (Low et al., 2007). PatA has shown remarkable effectiveness against actively replicating cells, whereas quiescent cells are 1000-to-2000-fold less sensitive to PatA. The primary mechanism of action of PatA is eIF4A inhibition, although studies have demonstrated that PatA also impairs host DNA polymerase and actin polymerization at much higher concentrations (Kuznetsov et al., 2009; Matthews et al., 2013). PatA is not subjected to Pgp and ABCB1 mediated efflux (Kuznetsov et al., 2009). Similar to Sil, PatA shows preferential inhibition against highly metabolically active cells.

There are three isoforms of eIF4A, eIF4AI, II, and III, which are synthesized through differential splicing. eIF4A I and II show a high degree of homology (~90% amino acid similarity) with each other, while eIF4AIII shows lesser homology. Previous work has shown that with their high degree of homology, eIF4AI and II likely have similar, but ultimately unique roles in translation (Galicia-Vázquez et al., 2012). eIF4A resides within the helicase superfamily 2 and is found bound to other factors such as eIF4B and eIF4H. Furthermore, eIF4A has ATPase activity that enhances RNA binding. eIF4F stimulates eIF4A's ability to bind to ATP, effectively stimulating the helicases affinity to RNA and subsequent melting of RNA structures in the 5' sequence of mRNAs (García-García et al., 2015). Both eIF4AI and eIF4AII are targets of Sil and PatA. For the duration of this chapter, I will refer to eIF4AI and eIF4AII as eIF4A.

Impairing eIF4A I or eIF4A II with Sil or PatA can result in the formation of cytoplasmic stress granules (SGs), independent of the phosphorylation of eIF2α and dephosphorylation of 4E-BPs (Iwasaki et al., 2016). SGs characteristically arise from the

phosphorylation of eIF2α from one of the 5 kinases during ISR signaling. SGs typically contain stalled 48S preinitiation complexes and their associated mRNA. Stalled mRNPs recruit several nucleating and aggregation prone proteins, such as Ras-GAP SH3 domain binding protein (G3BP), T-cell intracellular antigen-1 (TIA-1), and TIA-related protein (TIAR) (Kedersha et al., 2016). Aggregates of stalled mRNP form into SGs. SGs can release mRNAs back into the actively translating pool once the stress is resolved (Ivanov et al., 2019). mRNAs in SGs can also be degraded through processing bodies.

In this chapter, I investigated the efficacy of eIF4A inhibitors as HTAs against IAV infection. The work in this chapter is published in the peer reviewed journal "Viruses" and some experiments from that publication were performed by other members of the McCormick lab (Slaine et al., 2017). The work completed by my co-authors is explored in the discussion. In this chapter I explored host translation as a target for HTAs against IAV infection. I demonstrated that targeting eIF4A impaired the synthesis of viral proteins, which subsequently reduced virus production. I methodically analyzed the eIF4A inhibitors across three different model cell lines and quantified the antiviral properties across several different influenza viruses. I demonstrated that eIF4A inhibitors Sil and PatA induced the formation of SGs in infected cells in a dose-dependent manner. I also identified significant cytotoxicity of the eIF4A inhibitors on my model cell lines, limiting their application to clinical settings.

3.2 Results

3.2.1 Sil and PatA Impaired IAV Replication

All viruses are obligate intracellular parasites and require a host organism's cellular translation machinery to synthesize all viral proteins. IAV synthesizes mRNAs that are almost identical to host mRNAs and are sensitive to translation arrest (Khaperskyy et al., 2014). It has been demonstrated that Sil has been shown to impair the replication of Zika virus (Elgner et al., 2018), coronaviruses and picornaviruses (Müller et al., 2018), and hepatitis E virus (Glitscher et al., 2018). I treated PR8-infected cells with Sil and PatA to determine the compounds potential antiviral effects. An effective antiviral, be it direct-acting or host-targeting, must show efficacy in cell models before moving to an animal model. Accordingly, I utilized three cell line models for IAV infection: human lung adenocarcinoma (A549), African Green Monkey kidney (Vero), and Madin-Darby canine kidney (MDCK), with the laboratory adapted IAV A/Puerto Rico/08/1934 (H1N1) (PR8) to quantify the effectiveness of these compounds. The A549 cell line supports IAV replication and is a type II pulmonary epithelial cell model (Foster et al., 1998). The MDCK cell line polarizes with apical and basal membranes with the associated trafficking to each membrane. IAV infection specifically utilizes the apical membrane for both entry and egress, with viral glycoproteins targeted to the apical membrane for budding (Barman & Nayak, 2000; Sato et al., 2019). Apical trafficking of viral proteins occurs during typical infection, allowing the budding virions to be aerosolized and transmitted to the next individual. Accordingly, the MDCK cell line supports the replication of laboratory adapted and clinical isolates of influenza viruses. The Vero cell line is also used to propagate IAV. Vero cells have a 9-megabase deletion on chromosome 12, which removes the type I interferon gene cluster resulting in a significantly impaired antiviral response (Osada et al., 2014). The interferon gene cluster

contains IFN-α and IFN-β response genes, many of which are antiviral (Farrar, 2014). The lack of the type I interferon cluster allows the propagation of attenuated viruses that have NS1 mutations (Egorov et al., 1998). These cell lines were infected with a low multiplicity of infection (MOI), of 0.1, to analyze a single replication cycle of the virus. Infected cells were treated with serially diluted concentrations of PatA for 23 hours. Infectious viral progeny was enumerated at 24 hpi from cellular supernatant with a plaque assay using confluent MDCK cells and overlaid with Avicel. PatA showed a dose-dependent impairment of PR8 replication equally in all three cell types (Fig 3.2A), with ~2.5 log reduction at the highest concentration of 20 nM. The EC_{50} values are roughly around 3 nM across all three cell lines. Sil treatment showed variable effectiveness across the three different cell lines, with A549s showing the highest degree of sensitivity to Sil, whilst Sil showed almost no effect on the Vero cell line (Fig 3.3A). Sil treatment at its highest concentration of 640 nM in A549 cells reduced the viral titre over 2.5 log (~ 500-fold reduction), whereas infected Vero cells treated with 640 nM yielded 3-fold less virus compared to cells treated with vehicle control. Virus production in the A549 cell line was significantly impaired even at the lowest concentration of Sil. MDCK cells showed some degree of sensitivity to Sil treatment, with the 640 nM treatment group showing ~ 1 log reduction in viral replication. Accordingly, the EC_{50}values varied dramatically across the three different cell lines, with Vero EC_{50}=~500 nM, A549 EC_{50}=<40 nM, and MDCK EC_{50}=~80nm (Fig 3.3A). The reason why the three different cell lines demonstrate such variable responses to Sil treatment remains unknown.

These data indicated that treating infected cells with PatA universally reduced virus production across all three cell lines tested. However, treating infected cells with Sil

reduced virus production significantly in the A549 cell line, moderately in the MDCK cell line, and had little effect on virus production in the Vero cell line.

3.2.2 Sil and PatA are Cytotoxic in Treated Cells

Both Sil and PatA are under investigation as candidate anti-cancer agents. Cancer cells require high rates of translation to maintain cell replication and are sensitive to translation inhibition. I demonstrated that treating PR8-infected cancer cells with Sil and PatA significantly reduced virus production. I utilized transformed cell lines to perform these experiments, which may be especially sensitive to translation inhibition. Transformed cells rely on high translation rates to produce necessary cellular factors and transcription factors such as C-MYC. I evaluated the potential cytotoxic effects of Sil and PatA because antivirals must be non-cytotoxic at effective concentrations. I performed an alamarBlue assay on treated cells to determine cell viability following Sil and PatA treatment.

I quantified cell viability of the three model cell lines in the presence of eIF4A inhibitors using the alamarBlue™ assay, which quantifies the aerobic metabolism of the treated cells by measuring the conversion of resazurin to resorufin, which is a fluorescent compound that can be detected by a spectrophotometer. Thus, the alamarBlue assay quantifies cellular anaerobic metabolic activity which reflects the overall viability of a treated cell population when compared to an untreated population. I serially diluted Sil and PatA to similar concentrations in Fig 3.2A and Fig 3.3A. PatA showed different cytotoxicity profiles across the three different cell lines. The A549 cell line showed the highest cell viability after PatA treatment, whereas the MDCK cell line showed the

lowest cell viability (Fig 3.2B). The IC_{50} values of PatA in the three different cell lines are as follows Vero IC_{50}=0.94 log10, A549 IC_{50}=0.97 log10, and MDCK IC_{50}=0.42 log10 (Fig 3.3B). Treating infected cells with 5 nM PatA showed minimal cytotoxicity in the A549 cell line while impairing virus production from the A549 cell line by ~10 fold (Fig 3.2B). Sil also showed a high degree of variability in cell viability across the three different cell lines. The A549 cell line had the lowest degree of cell viability, whereas the Vero cell line had almost no reduction in cell viability (Fig 3.3B). The IC_{50} values of Sil in the three different cell lines are as follows Vero IC_{50}=2.17 log10, A549 IC_{50}=1.1 log10, and MDCK IC_{50}=1.41 log10 (Fig 3.3B)These data indicated that treating IAV model cell lines with Sil and PatA reduce cell viability.

3.2.3 Sil and PatA Impaired Viral Protein Synthesis

Both Sil and PatA inhibit the eIF4A, a helicase that is important for cap-dependent translation. Whether viral protein synthesis was sensitive to the eIF4A inhibitors had yet to be fully explored. To ascertain the effects of Sil and PatA treatment on infected cells, I analyzed the accumulation of viral proteins. The three different cell lines; MDCK, A549, and Vero cells, were infected with PR8 at a MOI of 0.1 for one hour and treated with increasing levels of Sil and PatA for 23 hours. Total protein was harvested at 24 hpi to allow me to analyze the accumulation of viral proteins with a western blot. Treating infected cells with PatA reduced the accumulation of viral proteins in a dose-dependent relationship equally across all three cell lines (Fig 3.2C). The reduction of viral protein synthesis strongly correlated with the reduction in virion release (Fig 3.2A). NP showed the highest degree of resistance to Sil and PatA treatment, while

M1 and HA accumulation was reduced at lower concentrations. I also probed for cellular actin, a loading control, which showed some reduction in cells treated with higher concentrations of PatA. The accumulation of viral proteins from Sil-treated cells varied across the three different cell lines (Fig 3.3C). Vero cells, which showed almost no impairment of viral replication following Sil treatment, showed no reduction of viral protein accumulation. By contrast, A549 cells showed a dose-dependent inhibition of viral protein synthesis that correlated well with impairment of viral replication. Treating infected MDCK cells with Sil reduced viral protein accumulation.

3.2.4 SG Formation is Inversely Correlated with Viral Protein Accumulation

The McCormick lab has previously demonstrated that treating IAV infected cells with PatA caused the formation of SGs (Khaperskyy et al., 2014). To further understand how eIF4A inhibitors can trigger the formation of SGs and impair viral protein synthesis, I treated PR8-infected cells with Sil and PatA and quantified SG formation. I treated PR8-infected A549, Vero, and MDCK cells with 1:2 dilutions of Sil and PatA and probed for the canonical SG marker TIAR. I probed infected cells for HA, M1, and NP (poly-IAV antibody). Using these two stains, I quantified SG formation and the accumulation of viral proteins. Treating PR8-infected cells with PatA universally induced SGs in all three cell lines, which directly correlated to the reduction of viral protein accumulation (Fig 3.2D). SG formation arose in cells treated PatA at 2.5 nM-5 nM concentrations. Treating infected cells with Sil variably induced SG formation across the three different cell lines. Treating infected cells with Sil failed to induce SG formation in Vero cells,

whereas Sil strongly induced SGs in A549 and MDCK cell lines (Fig 3.3D). Sil and PatA mediated SG induction tightly correlated with the inhibition of viral protein synthesis across all three cell lines. Taken together, these data indicate that PatA equally impaired the accumulation of viral proteins across all three cell types, which strongly correlated with the formation of SGs. Treating infected cells with Sil reduced the accumulation of viral proteins in A549 and MDCK cells. However, these data indicated that Vero cells are resistant to Sil mediated translation arrest and SG formation. Both Sil and PatA are known to form SGs in the A549 cell line independent of infection (Khaperskyy et al., 2014, Slaine et al., 2021). I used the A549 cell line as my infection model due to its sensitivity to both Sil and PatA for the remainder of this chapter.

I investigated the primary amino acid sequence of eIF4A across the three different species from which the cell lines originated from to determine the mechanism of resistance in the Vero cell line. I obtained and aligned the amino acid sequence from the human, canine, and green monkey genome. I discovered that the sequences across the three species are 100% identical. These data indicated that the molecular target of Sil is unperturbed in Vero cells.

3.2.5 Sil and PatA Treatment Induced Apoptosis in Treated Cells

My previous results indicated that Sil and PatA treatment reduced cell viability but did not differentiate between the potential cytostatic or cytotoxic side effects. Translation inhibition may slow down the cell cycle of the transformed cells or it may cause cell death due to the dramatic reduction in the translation of essential host factors.

Previous work demonstrates that translation inhibitors may induce apoptosis in transformed cells (W.-L. Chen et al., 2016). To further analyze potential detrimental side effects of Sil and PatA treatment, I incubated the adherent A549 cell line with vehicle control (DMSO) or Sil for 24 hours and captured brightfield images to observe any physiological changes in the cell monolayer (Fig 3.4A). The A549 cell monolayer in the vehicle control group displayed normal cellular morphology and the monolayer was unaffected. The cells were equally spread out and adherent to the cell culture dish. The cell monolayer in the Sil treatment was no longer evenly distributed, with numerous cells detached from the dish. The cells that were attached to the dish did not show typical morphology, with the cell membrane retracting and a fading cytoplasm (Fig 3.4A). To further analyze the potential cytotoxic effects of Sil and PatA treatment on host cells, A549 cells were mock infected or infected with PR8 and treated with Sil and PatA for 10 and 16 hours. Apoptosis can be observed by probing cellular lysate for poly-ADP-ribose polymerase (PARP) cleavage products, as PARP is cleaved by activated caspase and is considered an indicator of apoptosis (Nicholson et al., 1995). Whole protein lysates were harvested from treated cells and probed for PARP and its cleaved product. Both Sil and PatA treatment resulted in PARP cleavage at 16 hours post treatment, independent of infection (Fig 3.4B). In agreement with previous results, treating infected cells with Sil and PatA significantly impaired the accumulation of NP and M1, with complete reduction of HA. Taken together, these data indicated that both Sil and PatA are cytotoxic to both infected and non-infected cells and treatment with these compounds resulted in the induction of apoptosis.

3.2.6 PatA Reduced Virus Production from Different Influenza Viruses

My previous data demonstrated that PR8 is sensitive to translation inhibition, but the antiviral efficacy of eIF4A inhibitors across diverse influenza viruses remained unknown. To confirm the pan-antiviral activity of translation inhibitors, I treated A549 cells that were infected with diverse IAVs and quantified virus production. I infected A549 cells with three different IAVs; A/Udorn/1973 (H3N2) (Udorn), A/Brisbane/57/2007 (H1N1) (Brisbane), and A/California/07/2009 (H1N1) (CA/07). I treated infected cells with three different concentrations of PatA at concentrations that did not markedly reduce cell viability, as previously demonstrated in Fig 3.2. Sil was not used in this experiment because of its sub-optimal therapeutic window demonstrated in Fig 3.3. Udorn, another lab-adapted virus, showed a dose-dependent sensitivity to PatA treatment. Treating Udorn-infected cells with PatA reduced virus production by 50-fold at the 10 μM concentration (Fig 3.5A). Both Brisbane and CA/07 are not lab-adapted viruses and they closely resemble viruses that circulate in the human population. Because these two viruses are not lab adapted, they did not replicate to high titers *in vitro*, preventing the accurate quantification of virus production. I performed only one biological replicate on these two viruses to assess the antiviral effectiveness of PatA. Even with one biological replicate, treating infected cells with PatA demonstrated a clear dose-dependent antiviral response against Brisbane (Fig 3.5B) and CA/07 (Fig 3.5C). These data indicate that Sil and PatA broadly inhibit IAVs.

My previous results demonstrated that treating infected cells with PatA and Sil reduced the accumulation of viral proteins. To confirm this for the genetically diverse

IAVs, I treated Udorn-infected A549 cells with Sil and harvested total protein at 0, 4, 8, and 12 hpi. Protein lysates were probed for viral proteins NP, M1, and NS1. Similar to PR8, Udorn showed a high degree of sensitivity to Sil treatment. The accumulation of viral proteins was abolished in Sil treated cells (Fig 3.6). Taken together, these data demonstrate that Sil and PatA impair the accumulation of viral proteins and subsequently block the production of infectious progeny in sensitive cell lines.

3.2.7 PatA Inhibited Translation from the NanoLuc Reporter Virus

CA/07 failed to replicate to high titers in A549 cells, meaning it was difficult to ascertain the degree of antiviral effects of PatA on infected cells. To investigate the antiviral effects of PatA on CA/07 infected cells, I infected A549 cells with a reporter virus that harbours a Nanoluciferase (NanoLuc) open reading frame to directly quantify the inhibitory effects of PatA on viral translation. This reporter virus was built with the coding sequence for NanoLuc in the PA segment, NanoLuc is in the same reading frame as PA. The NanoLuc enzyme is liberated from the viral protein by a self-cleavage sequence from the porcine teschovirus (P2A), which allows direct quantification of viral translation using a Nanoluciferase assay (Fig 3.7A). Performing a Nanoluciferase assay on infected cells allows for the direct quantification of viral translation rates. Treating CA/07-NanoLuc-infected A549 cells with three different concentrations of PatA demonstrated a dose-dependent reduction of viral translation, as seen with a reduction in luciferase activity (Fig 3.7B). These data further provide evidence that inhibiting eIF4A directly reduces viral translation.

3.3 Discussion

IAV mRNA generally mimics that of host mRNA, allowing efficient translation by host machinery. Since IAV mRNA closely resembles host mRNA, they are susceptible to stress-induced translation arrest. Previous work has demonstrated that IAV protein synthesis requires eIF4A and eIF4G for viral protein synthesis (Yángüez et al., 2011). Here, I demonstrate that the synthesis of viral proteins is highly sensitive to Sil and PatA treatment in sensitive cell lines. The data collected in this chapter supports host translation as an effective target to impair virus replication. Here, I look to repurpose Sil and PatA as antivirals against IAV replication. Both Sil and PatA treatment reduced virus production of our laboratory adapted virus PR8, while PatA appeared to reduce viral titers across genetically diverse strains, including non-laboratory adapted viruses. All cells infected in this study showed equal sensitivity to PatA treatment, which correlated strongly with a similar dose-dependent impairment of viral replication. SG formation in treated cells was inversely correlated with impaired virus protein accumulation. By contrast, Vero cells showed almost complete resistance against the translation inhibition of Sil. Accordingly, Sil showed little antiviral effects on infected Vero cells.

In this chapter, I fully characterized the cytotoxic effects of Sil and PatA on both infected and non-infected cells. PatA showed variable cytotoxic profiles across the different cell lines, but all cells experienced some degree of cytotoxicity in response to PatA treatment. By contrast, Vero cells showed almost complete resistance to Sil-mediated SG induction, which directly correlated with the inability of Sil to reduce virus production from infected Vero cells. I demonstrated that treating cells with Sil and PatA

induced apoptosis in both infected and non-infected cells. Because of the cytotoxicity of both Sil and PatA, the clinical use of Sil and PatA as an antiviral is unlikely.

Some mRNAs contain a G-quadruplex and require eIF4A to reduce secondary RNA structures prior to translation. Recent work has predicted G-quadruplex formation in several IAV mRNAs. Predicted G-quadruplex sequences were hypothesized to be in the 5' sequence of mRNAs that encode M, NA, and HA (Brázda et al., 2021). The complexes are most conserved across HA and M. The authors of this study did not specifically analyze A/Puerto Rico/1934 (H1N1), so whether the laboratory adapted virus contains the advanced RNA structures is unknown. The authors found that the predicted G-quadruplexes may vary significantly across different viral isolates. The 5' UTRs of viral mRNAs are relatively short and comprised of divergent host-derived mRNA segments that contain the 5' cap. The divergence of the first 10-14 nucleotides make calculating the secondary structure of the 5' UTR more difficult.

Further work was completed in the McCormick lab by Dr. Denys Khaperskyy and Mariel Kleer demonstrated that treating infected cells with Sil and PatA reduced the replication of viral genomic RNA (vRNA) (Slaine et al., 2017). Blocking translation prevented the accumulation of viral proteins essential for switching the viral RdRp from synthesizing viral mRNA to synthesizing genomic RNA (Slaine et al., 2017). PatA irreversibly impairs eIF4A, whereas Sil reversibly binds eIF4A. Dr. Khaperskyy and I observed that the removal of Sil led to the rapid dissolution of SGs which returned viral protein synthesis. By contrast, Removing PatA from infected cells resulted in the persistence of SGs and the accompanied inhibition of viral protein synthesis (Slaine et al.,

2017). The rapid formation of SGs in infected cells reliably indicated the disruption of viral protein accumulation and impaired virus replication.

The transformed cells used in this study do not perfectly reflect the translation environment within the human body. Transformed cell lines may show a higher degree of sensitivity to eIF4A inhibitors due to their high metabolic requirements and their "addiction" to translation. To better ascertain the cytotoxic side effects of these compounds in clinically relevant settings, experimentation on primary, non-transformed, cells would be necessary. PatA shows less effectiveness in cells that are not actively dividing, giving evidence that primary cell lines may show a more favourable therapeutic window. Therefore, PatA and Sil may be more efficacious in the human lung, with primary human cells potentially tolerating translation inhibition. Further research is required to determine the replication rate, and subsequently the sensitivity of IAV to translation inhibition in primary cell lines.

During my investigation of Sil and PatA as potential HTAs, I infected cells with a low MOI to allow for the optimal analysis of a single round of replication. Infecting cells with a higher MOI would increase the viral load per cell, as well as increase the number of defective interfering particles in the experiment. Because I only analyzed a single round of replication, I cannot make any conclusions on the effectiveness of eIF4A inhibitors on multi-round replication of influenza. Presumably, PatA and Sil treatment would show equal to or greater impairment of viral replication, due to the poisoning of eIF4A in cells that would be infected in the second round of replication. The cytotoxic side effects of the compounds would also have to be re-evaluated at these longer time points. Furthermore, I did not assay the antiviral properties of Sil or PatA in later time

points during infection, it remains unknown whether Sil and PatA are antiviral during established IAV infection.

Sil treatment showed a high degree of variability across the three different cell lines, with infected Vero cells showing almost complete resistance. Treating Vero cells with high concentrations of Sil did not trigger SG formation, nor did treatment affect the accumulation of viral proteins and the subsequent production of virus. I observed that the Vero cell line showed resistance to translational arrest following Sil treatment. *In silico* analysis of eIF4AI across the three different species showed 100% amino acid homology. This indicated that the Vero cell lines resistance to Sil treatment was not due to a difference in the drug target, but likely a failure of the compound to be taken-up by the cell. Previous work has identified that Sil is targeted for efflux through Pgp and ABCB1 (Gupta et al., 2011). The action of the efflux pump reduces the efficacy of Sil dramatically in the authors model cell line. The expression and function of the Pgp and ABCB1 efflux pumps remain unknown in the Vero cell line. To determine the status of the two pumps, I would co-treat cells with the Pgp inhibitor verapamil and subsequently characterizing the cells sensitivity to Sil by analyzing SG formation and translation rates of treated cells. The Pgp efflux pathway must be considered in future experiments as potential resistance for antiviral therapies.

In this chapter, I demonstrated the feasibility of targeting global translation as an antiviral with a significant reduction in viral replication, but significant off-target cytotoxicity. My data indicated that disrupting viral protein synthesis potently blocks the IAV replication cycle. History has demonstrated, on numerous occasions, that direct-acting antivirals often select for antiviral resistance. HTAs may thwart the rise of antiviral

resistance by impairing a host factor that the virus relies upon. Proteomics and genetic screens have demonstrated that IAV replication relies on thousands of host genes, some of which encode proteins that are known drug targets (Heaton et al., 2017; B. Li et al., 2020; Watanabe et al., 2014). The potential cytotoxic effects on bystander cells represents a limitation of pharmacological inhibition of host factors in a clinical setting is the potential cytotoxic effects on bystander cells. Currently, antivirals are delivered orally, intravenously, or through a nebulizer in clinical settings. These different modes of administration affect bioavailability and tolerance. As an example, oseltamivir phosphate is generally administered orally, since it must be metabolized into its active form, oseltamivir carboxylate, by the patient's liver before circulation to the lungs. Since Sil and PatA are cytotoxic to uninfected cells, they would still be toxic even if applied right to the site of infection. Because of these limitations, superior HTAs must be identified with more favourable cytotoxic profiles.

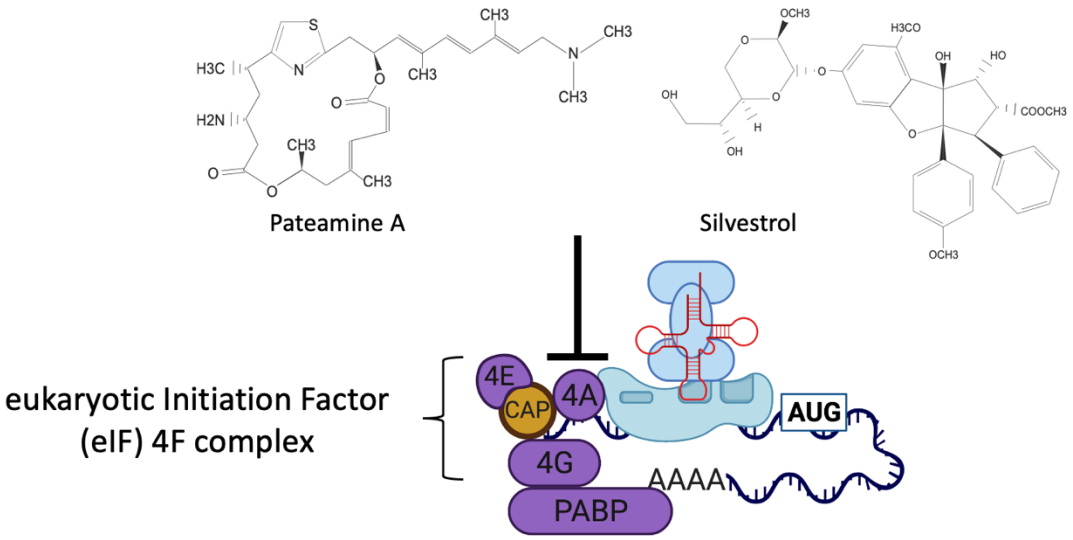

Figure 3.1: Bond line structures of the eukaryotic initiation factor 4A inhibitors Pateamine A and Silvestrol. Illustrations completed by Patrick Slaine. Image was created with BioRender.com.

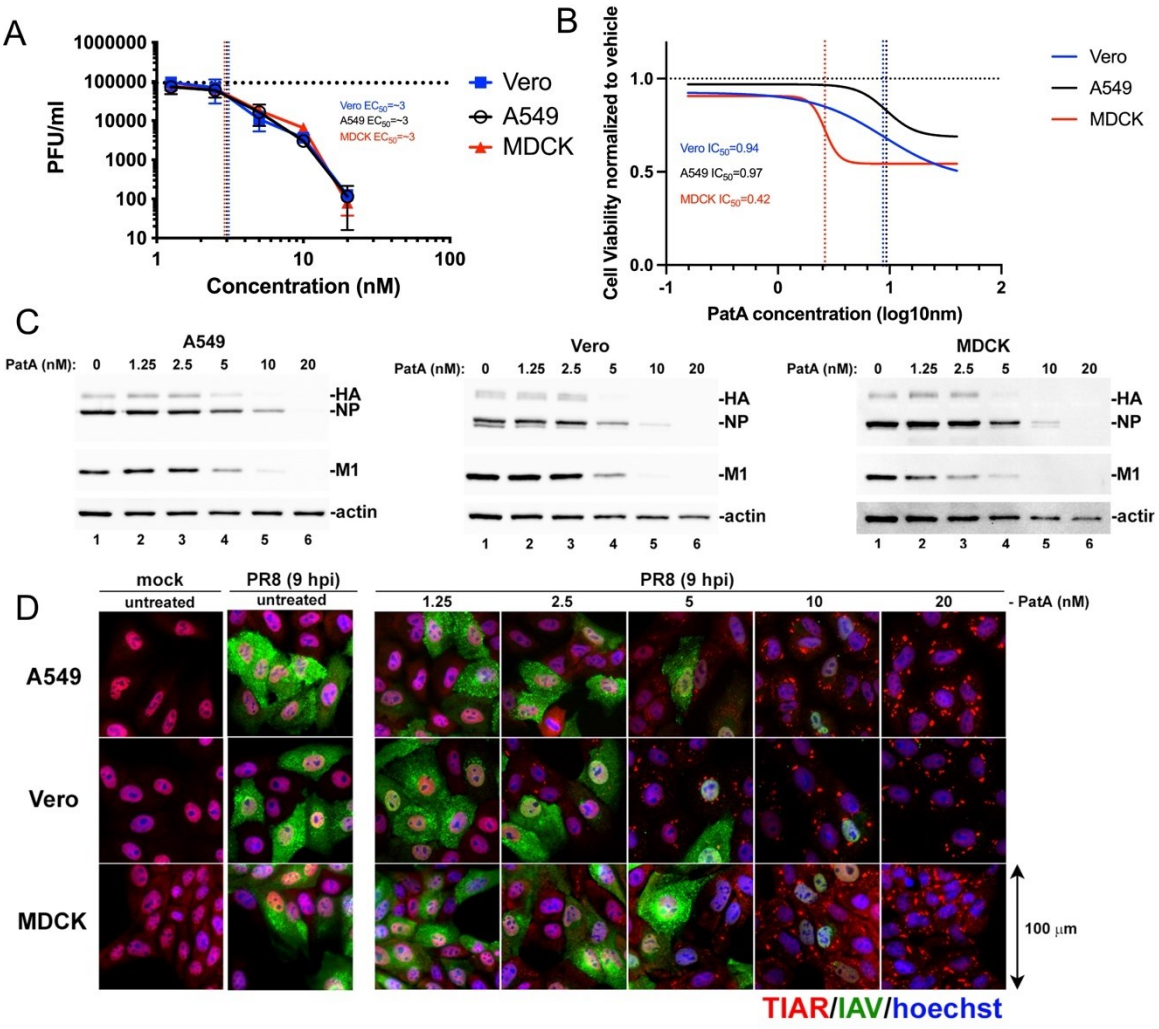
A
PFU/ml
Concentration (nM)
Vero
A549
MDCK
Vero EC50=~3
A549 EC50=~3
MDCK EC50=~3
B
Cell Viability normalized to vehicle
PatA concentration (log10nm)
Vero IC50=0.94
A549 IC50=0.97
MDCK IC50=0.42
C
A549
Vero
MDCK
PatA (nM): 0 1.25 2.5 5 10 20
-HA
-NP
-M1
-actin
1 2 3 4 5 6
D
mock
untreated
PR8 (9 hpi)
untreated
PR8 (9 hpi)
1.25 2.5 5 10 20
- PatA (nM)
A549
Vero
MDCK
100 μm
TIAR/IAV/hoechst

Figure 3.2: Dose-dependent reduction of viral replication, cytotoxicity, and stress-granule formation from treatment with Pateamine A.
A549, MDCK, and Vero cell lines were infected with A/Puerto Rico/08/34 (H1N1) at a MOI of 0.1 for 1 hour. The virus was washed off and the indicated concentration of pateamine A (PatA) was placed on the cells for 23 hours. Infectious progeny was quantified using a plaque assay (A). The dotted horizontal line indicates the average PFU/mL produced by untreated cells. The three model cell lines are indicated with colours: A549 with black, Vero with blue, and MDCK with red. The error bars denote standard deviation of three biological replicates (N=3) (B) Cell viability of A549, MDCK, and Vero cell lines were measured at the indicated concentrations of PatA using an alamarBlue cytotoxicity assay. The relative fluorescent units are normalized to vehicle control (DMSO). The dotted horizontal line indicates the relative fluorescence of untreated cells. The solid lines represent the average of three biological replicates (N=3) that was transformed and analyzed through a non-linear regression analysis. The three model cell lines are indicated with colours: A549 with black, Vero with blue, and MDCK with red. The vertical doted lines denote the IC_{50} values. (C) Indicated cells were infected with PR8 at a MOI of 0.1 for 1 hour and treated with the indicated concentration of PatA for 23 hpi. Viral protein (HA, NA, and M1) accumulation was analyzed from whole cell lysates collected at 24 hpi by western blot. Cellular actin staining was used as a loading control. (D) A549, MDCK, and Vero cell lines were infected with PR8 and treated with the indicated concentration of PatA. Stress granule formation and viral protein accumulation were visualized using immunofluorescence microscopy at 9 hpi by probing the indicated cell line with primary antibodies the stress granule marker TIAR (red), and polyclonal antibody against HA, NA, and M1 proteins(green). Hoechst dye (blue) stained host nuclei. The scale bar on the bottom right indicates 100 μm. Published in Slaine et al., 2017 and was completed with Dr. Khaperskyy and Mariel Kleer.

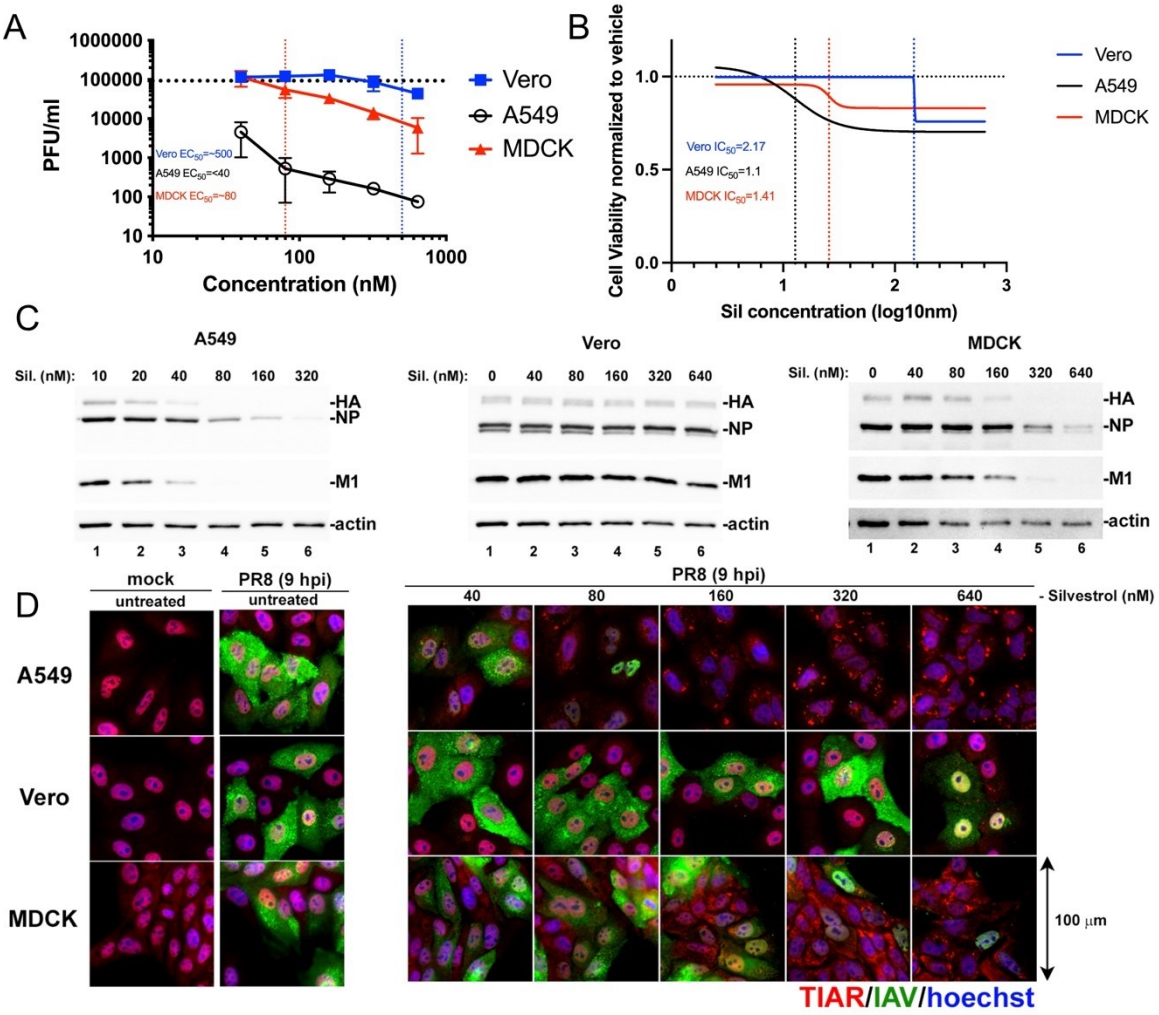
A
PFU/ml
Concentration (nM)
Vero
A549
MDCK
Vero EC50=~500
A549 EC50=<40
MDCK EC50=~80
B
Cell Viability normalized to vehicle
Sil concentration (log10nm)
Vero IC50=2.17
A549 IC50=1.1
MDCK IC50=1.41
C
A549
Vero
MDCK
Sil. (nM): 10 20 40 80 160 320
Sil. (nM): 0 40 80 160 320 640
-HA
-NP
-M1
-actin
D
mock
PR8 (9 hpi)
untreated
PR8 (9 hpi)
40 80 160 320 640
- Silvestrol (nM)
100 μm
TIAR/IAV/hoechst

Figure 3.3: Dose-dependent reduction of viral replication, cytotoxicity, and stress-granule formation from treatment with Silvestrol.
A549, MDCK, and Vero cell lines were infected with A/Puerto Rico/08/34 (H1N1) at a MOI of 0.1 for 1 hour. The virus was washed off and the indicated concentration of silvestrol (Sil.) was placed on the cells for 23 hours. Infectious progeny was quantified using a plaque assay (A). The dotted horizontal line indicates the average PFU/mL produced by untreated cells. The three model cell lines are indicated with colours: A549 with black, Vero with blue, and MDCK with red. The vertical lines denote the EC_{50} values. The error bars denote standard deviation of three biological replicates (N=3) (B) Cell viability of A549, MDCK, and Vero cell lines was measured at the indicated concentrations of Sil. using an alamarBlue cytotoxicity assay. The relative fluorescent units are normalized to vehicle control (DMSO). The dotted horizontal line indicates the relative fluorescence of untreated cells. The solid lines represent the average of three biological replicates (N=3) that was transformed and analyzed through a non-linear regression analysis. The three model cell lines are indicated with colours: A549 with black, Vero with blue, and MDCK with red. The vertical doted lines denote the IC_{50} values. (C) Indicated cells were infected with PR8 at a MOI of 0.1 for 1 hour and treated with the indicated concentration of Sil. for 23 hpi. Viral protein (HA, NA, and M1) accumulation was analyzed from whole cell lysates collected at 24 hpi by western blot. Cellular actin staining was used as a loading control. (D) A549, MDCK, and Vero cell lines were infected with PR8 and treated with the indicated concentration of Sil. Stress granule formation and viral protein accumulation were visualized using immunofluorescence microscopy at 9 hpi by probing the indicated cell line with primary antibodies the stress granule marker TIAR (red), and polyclonal antibody against viral HA, NA, and M1 proteins (green). Hoechst dye (blue) stained host nuclei. The scale bar on the bottom right indicates 100 μm. Published in Slaine et al., 2017 and was completed with Dr. Khaperskyy and Mariel Kleer.

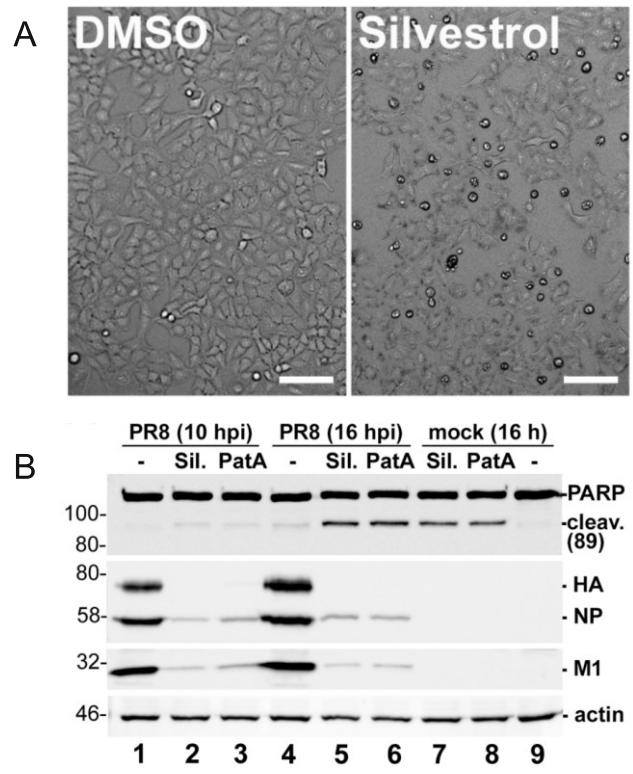

Figure 3.4: Pateamine A and Silvestrol treatment cause cytotoxicity and induce apoptosis in treated cells.
(A) Representative phase contrast images of A549 cell monolayers treated with Silvestrol (320 nM) or vehicle (DMSO) control for 23 h. Scale bars represent 100 µm. (B) A549 cells were infected with A/Puerto Rico/08/34 at a MOI of 0.1. Cells were treated with Silvestrol (Sil), Pateamine A (PatA), or vehicle control (DMSO) at 1 hpi. Total protein was harvested at 10 and 16 hpi and analyzed by western blot. Lysate was probed for full length PARP and its cleaved product (cleav. at ~89 kDa), HA, NP, and M1 proteins. Cellular actin was stained as a loading control. Published in Slaine et al., 2017 and was completed with Dr. Khaperskyy and Mariel Kleer.

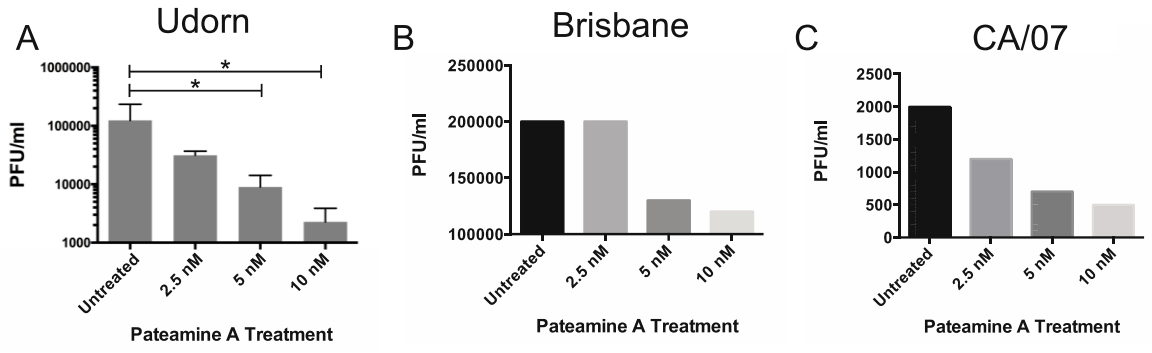

Figure 3.5: Pateamine A treatment reduces Udorn replication and may reduce the proliferation of different IAV subtypes across different IAV subtypes.
(A) A549 cells were infected with A/Udorn/72 (H3N2) at a MOI of 0.1 and treated with the indicated concentrations of PatA at 1hpi. Infectious viral progeny was enumerated at 24 hpi using a plaque assay. Error bars denote standard deviation of 3 biological replicates (N=3). MDCK cells were infected with (B) A/Brisbane/57/07 (H1N1) and (C) A/California/07/09 (H1N1) at a MOI of 0.1. Cells were treated with the indicated concentration of PatA at 1 hpi. Infectious progeny was enumerated at 24 hpi using a plaque assay. Both C and D represent a single replicate (N=1). Published in Slaine et al., 2017.

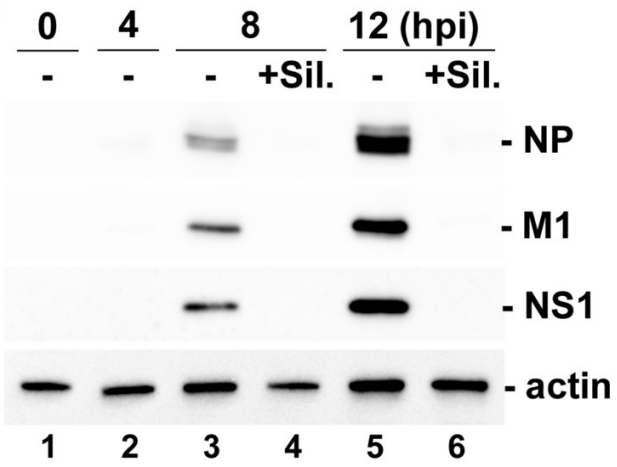

Figure 3.6: Silvestrol treatment reduces accumulation of A/Udorn/72 (H3N2). A549 cells were infected with A/Udorn/72 (H3N2) at a MOI 0.1 for 1 hour, cells were then treated with silvestrol for 8 and 12 hours. Total protein was harvested at 0, 4, 8, and 12 hpi. Accumulation of viral protein was analyzed using western blotting, staining for viral NP, M1, and NS1. Cellular actin staining was used as a loading control. Published in Slaine et al., 2017 and was completed with Dr. Khaperskyy and Mariel Kleer.

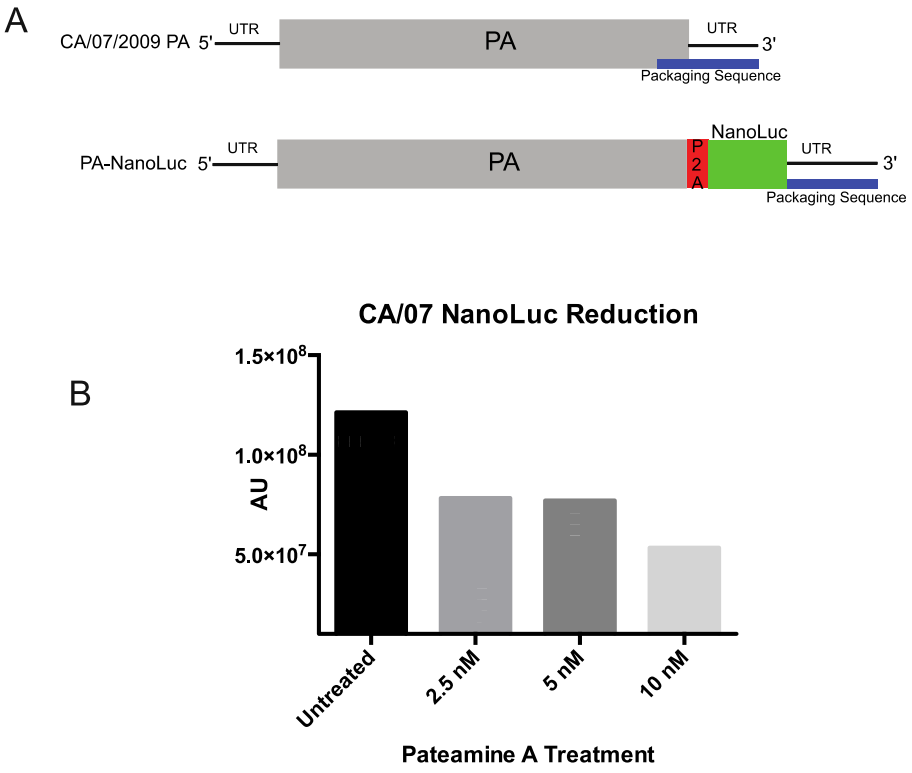

Figure 3.7: Pateamine A treatment may reduce the synthesis of viral encoded Nanoluciferase.
(A) Schematic drawing of the insertion of the Nanoluciferase downstream of the Porcine Teschovirus 2A(P2A) self-cleavage sequence that is inserted downstream of the polymerase acidic ORF. (B) Quantification of Nanoluciferase activity from A549 cells infected with CA/07-NL at a MOI of 0.1. Cells were treated with the indicated concentration of PatA at 1 hpi and cells were harvested at 24 hpi for quantification of fluorescence. Bars represent a single biological replicate (N=1). This work was completed by Patrick Slaine and not published in Slaine et al., 2017.

CHAPTER 4: THE THIOPURINES 6-TG AND 6-TGo ACTIVATE AN ANTIVIRAL UNFOLDED PROTEIN RESPONSE THAT BLOCKS INFLUENZA A VIRUS GLYCOPROTEIN ACCUMULATION

4.1 Introduction

In Chapter 3 I demonstrated the antiviral properties of eIF4A inhibitors against IAV translation and replication. Both Sil and PatA reduced the accumulation of all viral proteins, which subsequently impaired viral genome replication. I also demonstrated the cytotoxicity of eIF4A inhibitors in IAV infection models, which clearly limit the potential implementation of eIF4A inhibitors as antivirals. Chapter 3 laid the groundwork to identify a new HTA that impairs virus replication without cytotoxicity. Here in Chapter 4, I investigated the IAV glycoprotein synthesis and the UPR as a target for a new HTA.

IAV encodes three integral membrane proteins that are synthesized in the ER: HA, NA, and M2 (Hull et al., 1988; Janda et al., 2010). The proper synthesis, folding, modification, and oligomerization of these three proteins is required to support the production of infectious progeny virions.

HA is a canonical type I transmembrane glycoprotein. Like all such glycoproteins, synthesis is initiated on free cytoplasmic ribosomes, followed by redirection to the ER upon synthesis of the nascent signal peptide. The signal peptide is cleaved off by the host protease signal peptidase, removing the first 16 (HA3) or 17 (HA1) amino acids from the protein (Abdul Jabbar & Nayak, 1987). The cleavage of the signal peptide occurs during the translation of the glycoprotein through the translocon. The viral glycoprotein requires proper folding, N-linked glycosylation, disulfide bond

formation, proteolytic cleavage, and trimerization for its proper function (Copeland et al., 1988; Daniels et al., 2003; Gething et al., 1986; P. C. Roberts et al., 1993; Wilson et al., 1981; Yewdell et al., 1988). HA is then transported to the Golgi complex, where the N-linked oligosaccharides are further modified by resident glycosyltransferases and where HA can be proteolytically cleaved by host proteases. Full-length HA (referred to as HA0) is proteolytically cleaved by the host serine protease TMPRSS2 into HA1 and HA2, a step that is essential for HA maturation and function (Limburg et al., 2019). Cleavage liberates a stretch of hydrophobic residues, the fusion peptide in HA2, that is responsible for penetrating the late endosome's membrane of the future host. HA1 contains the RBD that has affinity to host α-2,6 and α-2,3 sialic acid linkages, which initiates receptor-mediated endocytosis (Bertram et al., 2010; Gaymard et al., 2016).

NA is a type II transmembrane protein, and like HA, requires proper folding, N-linked glycosylation, disulfide bonds, and tetramerization for its enzymatic function. The signal peptide is not cleaved off but is imbedded into the ER membrane. The N-terminus of type I transmembrane glycoproteins is in the ER lumen, while the C-terminus is in the cytosol. Type II glycoproteins have the opposite orientation, with the N-terminus in the cytosol while the C-terminus is in the ER lumen (Hogue & Nayak, 1994). NA is an enzyme with sialidase activity that removes terminal sialic acid on glycoproteins, including HA and NA molecules (Kosik & Yewdell, 2019). NA itself contains four known N-linked glycosylation sites. These glycosylations are essential for NA oligomerization, stability, and function (Bao et al., 2021). NA is transported through the Golgi complex to the plasma membrane where it is packaged into budding progeny virions (Bao et al., 2021; Hogue & Nayak, 1992; Saito et al., 1995). Oseltamivir

phosphate (TamiFlu™) is administered orally and is metabolised into the active metabolite Oseltamivir carboxylate, which mimics sialic acid and antagonizes the sialidase domain of NA. Impairing sialidase activity prevents the proper trimming of sialic acid from HA and host glycoproteins, resulting in the aggregation of virions that fail to escape from the infected cell surface (Heneghan et al., 2016).

M2 is the viroporin responsible for the acidification of the virion interior during entry in the late endosome, which dissociates M1 from the vRNP complex. The viroporin is a pH-regulated selective proton channel. M2 is found on the spliced mRNA from segment 7 and is the smallest of the canonical proteins encoded by IAV. Segment 7 produces 3 transcripts, the first is unspliced and encodes M1 and the second is a spliced mRNA that encodes M2. The N-terminal 9 amino acids are identical across M1 and M2, with the reading frame changing after the splice site. The mRNA encoding M2 is not spliced until late time points during infection (Manzoor et al., 2017; Shih et al., 1995). The third mRNA is also spliced and does not encode an ORF and has little effect on viral replication (Chiang et al., 2008). M2 is modified post-translationally with intermolecular disulfide bonds, palmitoylation, and phosphorylation. M2 is involved in both viral entry and egress. The dissociation of M1 from vRNPs is essential for the migration of the vRNPs to the nucleus. During egress, M2 deprotonates the trans-Golgi network, preventing HA activation, and is responsible for the scission of the viral envelope from the host membrane (Manzoor et al., 2017; Schnell & Chou, 2008). Tetrameric M2 is the molecular target of the direct-acting antiviral amantadine, which shows a high degree of antiviral activity against sensitive isolates. The inside of the channel is lined by residues 27, 30, 31, 34, 37, and 41. Amantadine specifically binds to residues Val27, Ala30, Ser

31, and Gly 34 in the ion channel of M2. Resistance to amantadine is generated by substituting these amino acids. Amantadine enters the viroporins ion channel and blocks the translocation of proton ions across the virus membrane (Manzoor et al., 2017). The laboratory adapted virus A/Puerto Rico/08/34 (H1N1) (PR8) is resistant to amantadine. In this chapter, I generated a PR8 that is amantadine-sensitive (PR8-AmantS) using the 8-plasmid recombinant system (E. Hoffmann et al., 2000).

HA, NA, and M2 are required to build infectious viral progeny, and these proteins require the host ER for proper synthesis and maturation through post-translational modification. The secretory pathway originates in the ER, being the site for protein synthesis, initiating glycosylation, oligomerization, disulfide bond formation, sorting, and subsequent delivery to the targeted organelle (Schwarz & Blower, 2016). The ER must maintain homeostasis while serving these cellular functions. The accumulation of unfolded proteins results induces ER stress. The response to ER stress that governs protein synthesis rates and folding capacity is called the UPR. The three sensors that are activated during the UPR are IRE1, PERK, and ATF6. All three arms are controlled by the luminal chaperone BiP (Pobre et al., 2019). BiP detects unfolded proteins by binding to exposed hydrophobic domains (Lewy et al., 2017). If ER stress cannot be resolved, the persistent UPR signaling directs the cell to the apoptotic cascade (B'chir et al., 2013).

IRE1 is the first sensor in the UPR. IRE1 has endoribonuclease and kinase domains. BiP maintains IRE1 in monomeric form until BiP is sequestered away by unfolded proteins, releasing IRE1 and allowing it to dimerize. IRE1 dimerization promotes trans-autophosphorylation, which increases ATP binding and subsequent activation of the endonuclease domain (Lee et al., 2008; Ron & Hubbard, 2008). Active

IRE1 cleaves two sequences found in stem-loop structures on *XBP1*, which removes 26 base pairs. The cleaved *XBP1* mRNA is ligated by the tRNA ligase RctB to create *XBP1s* mRNA (Calfon et al., 2002). The tRNA ligase RctB is responsible for reforming the phosphodiester linkage in the mRNA backbone, resulting in a shift in the reading frame subsequently changing all downstream amino acids (Jurkin et al., 2014; Y. Lu et al., 2014). The spliced mRNA encodes for XBP1s that has a longer C-terminus that contains an activation domain for a bZIP transcription factor. XBP1s upregulates proteins involved in ER associated degradation (ERAD), cellular chaperones involved in protein folding (BiP), and lipid biosynthesis (Cox et al., 1993; Cox & Walter, 1996). Activated IRE1 also reduces the translation burden of the ER by up to 15% through RIDD mediated degradation of a subset of mRNAs that contain a single secondary RNA stem-loop structure (Hollien et al., 2009). Targeted mRNAs are cleaved and degraded by the exonuclease Xrn1 in the 5' to 3' direction. IRE1 activation has also been shown to activate inflammatory responses by recruiting TNF receptor-associated factor 2 (TRAF2) through its kinase activity, which in turn activates the NF-kB pathway to increase expression of IL-6 (Keestra-Gounder et al., 2016).

Among the UPR sensor proteins, PERK is the sentinel kinase that regulates global translation through the ISR (Pakos-Zebrucka et al., 2016). Similar to IRE1, PERK is held as a monomer by the chaperone BiP until it is liberated by the accumulation of unfolded proteins (Lewy et al., 2017). PERK then dimerizes and trans-autophosphorylates, which enables the kinase domain to phosphorylate the α subunit of eIF2, which induces ISR signaling (Cui et al., 2011; Harding et al., 1999; Krishnamoorthy et al., 2001). eIF2α phosphorylation reduces the recycling of eIF2-GDP to eIF2-GTP in the TC. Therefore,

PERK activation reduces global translation. The phosphorylation of eIF2α selectively promotes the translation of uORFs, which contain proteins that are involved in stress responses, such as activating transcription factor 4 (ATF4). Similar to XBP1s, ATF4 is a bZIP transcription factor that specifically transactivates genes downstream of C/EBP-ATF Response Elements (CAREs) that are involved in amino acid biosynthesis, antioxidant responses, and autophagy (B'chir et al., 2013). ATF4 also upregulates CHOP, which in turn upregulates pro-apoptotic factors such as BAX (Oyadomari & Mori, 2004). The ISR utilizes a phosphatase to resolve translation inhibition if the stress is resolved. ATF4 upregulates GADD34, which is a cofactor that recruits PP1 to dephosphorylate Ser51 on eIF2α. If the cell fails to alleviate stress, persistent PERK activation will eventually result in the induction of apoptosis through the accumulation of BAX and BAD proteins (Oyadomari & Mori, 2004).

The last sensor of the UPR is ATF6, which is also bound in its inactive state by BiP and is released following dissociation of BiP. Once liberated, ATF6 is transported to the cis-Golgi by COP II vesicles where it is cleaved by S1P and S2P (Ye et al., 2000). This releases the N-terminal fragment of ATF6, allowing its NLS to recruit the fragment to the nucleus where it functions as a bZIP transcription factor upregulating chaperones, proteins involved in lipid synthesis, and XBP1 (Yoshida et al., 2001). The liberation of the bZIP transcription factor through proteolytic cleavage is known as regulated intramolecular proteolysis. The three arms of the UPR work together to alleviate ER stressors and return the ER to homeostasis (Yoshida et al., 2000). XBP1s can form homo- or heterodimers with ATF6-N to upregulate ERAD associated genes (Newman & Keating, 2003). XBP1s and ATF6-N express genes downstream of the ERSE. Proteins

upregulated from the ERSE increase the size of the ER, its folding capacity, and degradation capacity (Yamamoto et al., 2004).

Several compounds are commonly used to analyze the UPR by inhibiting key ER enzymes. The first is thapsigargin (Tg), which inhibits the sarco/endoplasmic reticulum Ca^{2+} ATPase (SERCA) pump, thereby depleting lumenal Ca^{2+} levels and triggering the UPR (Sehgal et al., 2017). Reducing the Ca^{2+} content reduces ER folding capacity, as Ca^{2+} can bind directly to proteins to aid in their folding (Goulding et al., 2020). Reduced Ca^{2+} also affects the functionality of the ER resident chaperone BiP by modulating its ATPase cycling and altering BiP-substrate stability (Preissler et al., 2020). The expression of SERCA mRNA is upregulated during the UPR, indicating its role in maintaining Ca^{2+} homeostasis during ER stress (Caspersen et al., 2000). The bacterial toxin tunicamycin (TM) inhibits asparagine-linked glycosylation 7 (ALG7), an enzyme that adds the first GlcNAc in N-linked glycosylation (Yamamoto & Ichikawa, 2019). Inhibiting ALG7 globally inhibits N-linked glycosylation, thereby disrupting protein folding and function. Unglycosylated proteins are unable to be transported to their targeted organelle therefore accumulating in the ER lumen and activate the UPR.

Other compounds have been shown to modulate the UPR by artificially alleviating ER stress or blocking signal transduction. 4-phenylbutyric acid (4-PBA) is used to increase the folding capacity of the ER lumen by masking hydrophobic surfaces commonly exposed on unfolded proteins. 4-PBA has been used to blunt ER stress responses and is being investigated as a therapeutic agent for protein aggregation disorders such as urea cycle disorder (Kolb et al., 2015). ISRIB is another compound that directly binds to the GEF eIF2B, promoting the recycling of GDP to GTP even if eIF2α is

phosphorylated (Anand & Walter, 2020). Therefore, ISRIB treatment alleviates any translation repression caused by the ISR. Further work has shown that the presence of phosphorylated eIF2α enhances ISRIB binding to eIF2B, furthering the inhibition of the ISR (Zyryanova et al., 2021).

Previous studies demonstrated limited ER stress from IAV infection. Interestingly, IRE1 has been shown to be activated, while ATF6 and PERK show no activation during infection. Furthermore, chemical inhibition of the IRE1 arm of the UPR impaired viral replication (Hassan et al., 2012, p. 1). Overexpression of HA induced ER stress and led to its degradation via ERAD (Frabutt et al., 2018). Bao and coauthors demonstrated that the proper folding and oligomerization of NA requires successful N-linked glycosylation. They demonstrate that substituting asparagine residues that were N-link glycosylated with alanine in NA induced the UPR (Bao et al., 2021).

The UPR has been targeted in previous studies for HTAs. Previous studies have targeted the ER to create an antiviral environment that effectively impairs coronaviruses, respiratory syncytial virus, influenza virus, Newcastle disease virus (NDV), and Peste des petits ruminants virus (Al-Beltagi et al., 2021; Goulding et al., 2020; Kumar et al., 2019). Treating IAV infected mice with sub-toxic concentrations of Tg impaired virus replication and demonstrated protective effects. Interestingly, Kumar and coauthors discovered resistance to Tg treatment after passaging NDV 70 times at a sub-lethal dose. Tg was found to block NDV entry, and the subsequent resistant mutations were found within the fusion protein (Kumar et al., 2019). One of the original hypotheses of developing an HTA is that the evolutionary barrier to resistance would be too great for the virus to overcome.

Viral mRNAs are almost identical to host mRNAs. They may be sensitive to host translation arrest. The ISR can block cap-dependent translation which can lead to the formation of SGs. These aggregates recruit nucleating proteins, such as G3BP1, that help assemble the mRNP complex. (McCormick & Khaperskyy, 2017). SGs are likely detrimental to viral replication. Numerous viruses dedicate precious coding capacity to thwart the formation of SGs, including IAV (Gao et al., 2021). IAV dedicates three of its proteins to prevent the formation of SGs during infection (Khaperskyy et al., 2014). These proteins are: NS1-that blocks PKR activation and subsequently prevents the phosphorylation of eIF2α, NP-that prevents the aggregation of SGs independent of the ISR, and PA-X-which degrades RNA transcripts synthesized by RNA Polymerase II and thereby reduces the pool of available host mRNAs (Khaperskyy et al., 2012, 2016). SGs can be induced independent of the ISR with hyperosmotic stress and pharmacological inhibition of eIF4A. As previously described in Chapter 3, eIF4A inhibitors displayed antiviral properties against all influenza viruses tested, but also demonstrated a high degree of cytotoxicity (Slaine et al., 2017).

Dr. Denys Khaperskyy performed a small molecule screen in collaboration with Dr. Michel Roberge at the University of British Columbia to identify and repurpose compounds as HTAs against IAV replication. Dr. Khaperskyy screened for small molecules that specifically induce SGs in infected cells. He created an A549 cell line that constitutively expressed the SG constituent protein G3BP1 fused with EGFP to visualize the formation of SGs. G3BP1-EGFP expressing cells were then infected with Udorn (H3N2), treated in parallel with over 50, 000 small molecules and imaged using a Cellomics Arrayscan instrument to rapidly image and quantify EGFP foci. Using this

technology, Dr. Khaperskyy identified 12 compounds that showed some degree of selective SG induction in infected cells. The induction of SGs in infected cells likely impairs viral replication, as viral mRNAs are likely sequestered and potential induction of innate pathways. Two of the identified compounds were almost identical to each other. The two compounds are from the same family of thiopurines, 6-thioguanine (6-TG) and 6-thioguanosine (6-TGo), and only differ by a ribose sugar group. 6-TGo contains both the nitrogenous base and the 5-carbon ribose sugar required to make it a nucleoside, while 6-TG is just the nitrogenous base (Figure 4.1A). 6-TG is an FDA-approved drug used to treat inflammatory bowel disease (IBD) and leukemia. Dr. Khaperskyy discovered that 6-TG and 6-TGo treatment of infected cells induced SGs in the minority of cells, with roughly 5-10% showing G3BP1-EGFP foci (Slaine et al., 2021). These EGFP-G3BP1 foci were confirmed to be SGs that harbour other SG markers such as eIF3 and TIAR.

Thiopurines have been used since 1953 to treat myelogenous leukemia and their safety profiles have been well established (Burchenal et al., 1953). Other members of the thiopurine family that are used in clinical settings are azathioprine (AZA) and 6-mercaptopurine (6-MP). Thiopurines are metabolised by ubiquitously expressed cellular enzymes into their active metabolites 6-thioguanine nucleotides (6-TGN). 6-TGN refers to 6-Thioguanosine mono, di, and triphosphates that mimic guanosine mono, di, and triphosphates respectively. 6-TG is directly metabolised to 6-TGN by cellular hypoxanthine guanine phosphoribosyl transferase (HGPRT), whereas 6-MP and AZA require several steps to become 6-TGN. 6-TG has a serum half-life of 20-60 minutes, whereas 6-TGN has a half-life of up to 5 days (Derijks et al., 2006). Metabolic tracing of

radiolabelled 6-TG indicated that 6-TG is rapidly excreted in the urine, while the remaining drug is circulated systemically before accumulating in the small intestine and spleen (Moore & LePAGE, 1958). The side effects of prolonged 6-TG treatment are hepatotoxicity and mild immune suppression. Specifically, 6-TG therapies can result in nodular regenerative hyperplasia of the liver. At higher doses, 6-TG can induce hypoplasia of the bone marrow, oral lesions, and gastric intestinal symptoms. Thiopurine tolerance is variable across individuals due to polymorphisms found in the metabolic and excretion pathway (Burchenal et al., 1953; R. L. Roberts et al., 2018). 6-TG can also impair immune cell activation and proliferation, resulting in immune suppression. 6-TG causes this suppression by binding and blocking the action of the GTPase Ras-related C3 botulinum toxin substrate 1 (Rac1) (Yin et al., 2018). Rac1 is a member of the Ras superfamily of Rho GTPases. GTP bound Rac1 interacts with numerous cellular processes such as actin organization, gene transcription, and cell migration (Haga & Ridley, 2016). Impairing Rac1 in leukocytes prevents their activation and proliferation which is beneficial during the treatment for IBD. At higher concentrations, 6-TGN are incorporated into DNA and RNA as analogs to guanosine and can cause substitution mutations. 6-TGNs may also block amido phosphoribosyltransferase, preventing de novo purine synthesis (Shi et al., 1998). Despite these effects, 6-TG is generally well-tolerated in patients (Bayoumy et al., 2020).

In this chapter, I characterized the efficacy of the two thiopurines 6-TG and 6-TGo as antivirals against IAV. The work in this chapter is published in the peer reviewed journal “Journal of Virology” and some experiments from that publication were performed by other members of the McCormick lab (Slaine et al., 2021). The work

completed by my co-authors is explored in the discussion of this chapter. I determined the antiviral properties of 6-TG and 6-TGo against different IAV subtypes. I discovered that treating infected cells with 6-TG or 6-TGo dramatically impaired the accumulation of viral glycoproteins, whereas most cytoplasmic proteins are unperturbed. The origin of the glycoprotein impairment is the activation of the unfolded protein response. Further, I characterized the host cell response to thiopurine treatment. I showed for the first time, that 6-TG and 6-TGo, but not the structurally similar thiopurine 6-MP, induced the UPR. The induction of the UPR impaired the synthesis of viral glycoproteins HA and NA, and that the activation of the UPR subsequently reduced virus production. Furthermore, I was able to partially restore viral glycoprotein accumulation, but not viral replication, through chemical and genetic manipulation of the PERK pathway. However, intraperitoneal injection with 6-TG did not provide protection against a lethal dose of mouse adapted CA/07 (CA/07-MA) in a murine infection model but did modulate the immune cell infiltrate and cytokine response.

4.2 Results

4.2.1 6-TG and 6-TGo are Cytostatic

Dr. Khaperskyy identified the thiopurines 6-TG and 6-TGo as candidate HTAs against IAV infection. 6-TG is the nucleobase analog of guanine, while 6-TGo is the nucleoside analog of guanosine (Fig 4.1A). I investigated any potential negative effects of 6-TG, 6-TGo, and the nucleobase 5-fluorouracil (5-FU) on the A549 human lung adenocarcinoma cell line commonly used for IAV infections (Fig 4.1B). 6-TG is an antimetabolite agent that is known to be cytostatic in transformed cells (Rajendran et al.,

2020). Dr. Khaperskyy demonstrated that SGs form in cells treated with 2 μM, 10 μM, and 30 μM concentrations of 6-TG. I wanted to further elucidate the potential cytotoxic effects of 6-TG on treated cells at these concentrations. I quantified A549 cell viability in the presence of drugs using the alamarBlue assay, which quantifies the aerobic metabolism of the treated cells by measuring the conversion of resazurin to resorufin, which is a fluorescent compound that can be detected by a spectrophotometer. Thus, the alamarBlue assay quantifies cellular metabolic activity which could reflect the overall viability of a cell population. A549 cells were treated with the indicated compound for 20 hours, before alamarBlue was added to the media and incubated for an additional 3 hours before fluorescence was quantified. 6-TGo showed the largest reduction in cell viability, with treated cells showing 70% cell viability at 2.5 μM (Fig 4.1B). Cell viability of treated A549 cells with 6-TGo plateaued at 70% viability from 2.5 μM to the highest concentration (40 μM). The cell viability of A549s treated with 6-TG closely mirrored cells treated with 6-TGo, with treated cells also plateauing at 70% up to the highest concentrations. 5-FU, another nucleobase analog, showed minimal cytotoxicity with a maximum of 10% reduction in cell viability at the highest concentration of 40 μM. To determine whether 6-TG and 6-TGo treatment are cytotoxic or cytostatic, I captured brightfield images of an A549 cell monolayer treated for 23 hours with 6-TG (10 μM) or vehicle control (DMSO). Cells showed no remarkable visual differences between vehicle control and 6-TG, with cells from both treatment groups adherent to the dish and both groups lacked cells that displayed atypical morphology (Fig 4.1C). To further analyze potential apoptotic effects on the cell line, I harvested total protein from treated cells and probed lysates for PARP and its cleaved product. PARP is a target of caspase activity.

Accordingly, the identification of PARP cleavage products indicates caspase activity and therefore induction of the apoptotic cascade (Casao et al., 2015). I used the eIF4A inhibitor Sil as a positive control, as I had previously shown that Sil treatment induced apoptosis in Chapter 3 (Slaine et al., 2017). A549 cells were treated with the indicated compound for 23 hours before harvesting protein samples. Cells treated with the thiopurines 6-TG, 6-TGo, and 6-MP showed minimal PARP cleavage, whereas PARP was cleaved in cells treated with Sil (Fig 4.1D). These data agree with the literature that 6-TG and 6-TGo treatment reduce cell proliferation through their antimetabolite activity which results in a cytostatic effect (Fulda et al., 1995; Rajendran et al., 2020). Treatment with these compounds for this length of time at these concentrations did not cause overt cytotoxicity, with no implication that treated cells underwent apoptosis. Using these data, I continued my studies using either 2 μM or 10 μM as the treatment concentrations for the remainder of the study.

4.2.2 Treating Infected Cells with 6-TG and 6-TGo Impaired Virus Production

The thiopurines induced SGs in infected cells, but their potential antiviral effects remained unknown. Here, I tested the antiviral properties of the two thiopurines 6-TG and 6-TGo against genetically diverse influenza viruses *in vitro*. I infected the model A549 cell line with PR8-AmantS (Fig4.2A), CA/07 (Fig 4.2B), and Udorn (Fig 4.2C) for 1 hour and treated them with 6-TG and 6-TGo for 23 hours before harvesting cell supernatants to quantify virus production. I used two sub-cytotoxic concentrations for the candidate antivirals, 2 μM and 10 μM. As a control, infected cells were also treated with

the known UPR-inducing drug TM and the heterocyclic base analog 5-FU. Cells infected with Udorn were also treated with the structurally similar thiopurine 6-MP. Treatment with TM inhibited virus production of all three IAVs, with the laboratory adapted viruses PR8-AmantS and Udorn showing the most sensitivity to TM treatment. By contrast, 5-FU and 6-MP had no effect on virus production. All tested viruses showed a dose-dependent reduction in virus production following treatment with 6-TG and 6-TGo. PR8-AmantS showed the highest sensitivity to 6-TG and 6-TGo out of the viruses tested. Treatment of PR8-AmantS infected cells with 2 μM 6-TG reduced virion production by roughly 10-fold, whereas 2 μM 6-TGo reduced virion production by roughly 100-fold. Furthermore, PR8-AmantS infected cells treated with 10 μM 6-TG or 6-TGo further reduced viral replication, impairing viral production by roughly 500-fold for each treatment (Fig 4.2A). Similar to my results in Chapter 3, CA/07 did not replicate to high titers in A549 cells, possibly because CA/07 is not cell-culture adapted. Treating CA/07 infected cells with 6-TG did not significantly impair virus production. 10 μM treatment with 6-TG and 6-TGo did reduce viral titers by ~10 fold, whereas 2 μM 6-TG and 6-TGo reduced viral production by ~4 fold and ~9 fold respectively (Fig 4.2B). The replication of Udorn was not significantly affected by 2 μM 6-TG treatment, but 2 μM 6-TGo showed ~6-fold reduction of viral titer. Both 10 μM treatment with 6-TG and 6-TGo reduced viral production by ~6-fold and ~11-fold respectively. Interestingly, treating Udorn infected cells with the structurally similar thiopurine 6-MP had no effect on viral replication (Fig 4.2C). These data indicate that all tested influenza viruses share some degree of sensitivity to 6-TG and 6-TGo treatment, with PR8-AmantS being the most sensitive.

These data also indicate that the nucleobase 5-FU and the structurally similar thiopurine 6-MP have minimal antiviral effects against IAV.

To further characterize the antiviral properties of 6-TG, I analyzed CA/07 and PR8-AmantS proliferation over a single round of replication. I infected MDCK cells with CA/07 (Fig 4.3A) and PR8-AmantS (Fig 4.3B) and quantified virus production every 4 hours post infection (hpi). Infected cells were treated with vehicle control (DMSO), Sil, the nucleoside analog ribavirin, or 6-TG. MDCK cells supported CA/07 virus infection to a higher degree than the A549 cell line model. Release of viral progeny was first observed at 8 hpi and continued until the 24 hpi time point. Ribavirin is another purine analog and is a known antiviral against IAV infection and serves as a positive control as a nucleoside antiviral in this experiment. Ribavirin treatment significantly impaired both CA/07 and PR8-AmantS replication in MDCK cells. Treating CA/07 and PR8-AmantS infected cells with 6-TG reduced virus production by roughly 10-fold at all time points beyond 4 hpi. The replication of CA/07 and PR8-AmantS in MDCK cells showed less sensitivity to Sil treatment compared to 6-TG, with Sil treatment reducing virus production by 2-4-fold. Interestingly, both viruses generally showed equal sensitivity to each antiviral. Furthermore, the fold reduction in virus production was consistent across time points for each candidate antiviral.

To further characterize the dose dependent antiviral properties of 6-TG on PR8-AmantS replication, I tested a gradient of different concentrations of 6-TG on infected cells. I treated PR8-AmantS infected cells with 1:2-fold serial dilutions to quantify the antiviral effects of 6-TG (Fig 4.3C). Doses of 6-TG ranged between 5 μM and 0.3125 μM. Cells were infected at an MOI of 0.1 for 1 hour and treated with the indicated

concentration of 6-TG for 23 hours before quantifying virus production using a plaque assay. Infected cells treated with 1.25 μM 6-TG showed ~50% reduction in virus replication, whereas infected cells treated with 5 μM 6-TG produced ~40-fold less virus compared to the untreated group. These data show a dose-dependent antiviral response to 6-TG treatment, with a mean inhibitory concentration 50 value (IC_{50}) roughly equating to 1.25 μM.

Previously, I demonstrated that the structurally similar thiopurine 6-MP had no effect on Udorn replication. I reconfirmed this with PR8-AmantS in A549 cells. I infected A549 cells at an MOI of 0.1 for an hour and incubated the cells with the thiopurines for 23 hours before quantifying virus production using a plaque assay. I used TM as a positive HTA control. Like Udorn, 6-MP did not impair PR8-AmantS replication, whereas 6-TG reduced viral titer by ~150-fold (Fig 4.3D).

Moving forward, I focused my investigation on PR8-AmantS as my favoured IAV infection model in most experiments in this Chapter for four reasons. The first reason is that PR8-AmantS grew to high titers in all model cell lines tested, enabling accurate and statistically significant analysis of candidate antivirals. The high titers of PR8-AmantS enables consistent measurements across different variables, allowing me to confidently make conclusions about virus production. The second reason is PR8-AmantS harbours sensitivity to both clinically available classes of antivirals and the virus is highly lab adapted. PR8-AmantS is the safest virus I could handle in laboratory settings. The third reason is that the study of PR8 is facilitated by an abundance of antibodies, primers, and expression systems. The fourth reason is that I have the recombinant system for PR8, giving me the opportunity to generate mutant viruses.

4.2.3 6-TG And 6-TGo Treatment Impaired the Accumulation of Viral Glycoproteins

To further analyze the antiviral effects of 6-TG and 6-TGo, I characterized viral protein accumulation after treating infected cells. I infected A549 cells with PR8-AmantS at an MOI of 0.1 for one hour and treated cells with the two thiopurines 6-TG and 6-TGo, along with the nucleobase 5-FU for 23 hours prior to harvesting total protein. I used TM as a positive control. Treating infected cells with TM impaired the glycosylation of glycoproteins, including viral glycoproteins. Lysates from infected cells were probed for HA, NP, NA, PA, M1, and NS1, with cellular actin as a loading control (Fig 4.4). Analysis of viral proteins showed that 6-TG and 6-TGo specifically reduced viral glycoprotein accumulation. Analysis also revealed that treatment generated viral glycoproteins with greater electrophoretic mobility. Both HA and NA receive post translational modifications in the ER, allowing for their proper folding and maturation. Importantly, HA and NA are N-linked glycosylated, which increases the molecular weight of the target protein by up to 2.5 kDa per modification. Both NA and HA are modified by intra- and intermolecular disulfide bonds, but these were reduced by the addition of DTT during sample preparation. Meanwhile, the accumulation of NP, PA, and NS1 showed almost no difference between the treatments, with M1 showing a mild reduction in protein accumulation with thiopurine treatment. NP, PA, M1, and NS1 are synthesized independent of the ER on free cytoplasmic ribosomes. Thus, the effects of 6-TG on viral protein synthesis appear to be largely restricted to viral glycoproteins in the ER. I also treated infected cells with the N-linked glycosylation inhibitor TM, which

prevents the development of oligosaccharides in the ER as positive control to induce the UPR. TM treatment similarly impaired the accumulation of the mature viral glycoprotein species only seen with 6-TG and 6-TGo treatment. TM also had little effect on cytoplasmic viral proteins. The nucleobase analog 5-FU had no effect on viral protein accumulation. Taken together, these data indicate that 6-TG and 6-TGo treatment specifically impair viral glycoprotein synthesis and maturation. Accordingly, I investigated the effects of 6-TG and 6-TGo on the ER and the UPR to elucidate mechanism of action of the two antiviral thiopurines.

4.2.4 6-TG And 6-TGo Treatment Induced the UPR in Treated Cells

To further understand the effects of 6-TG and 6-TGo in my infection model, I treated uninfected cells with an array of different nucleobase and nucleoside analogs to ascertain the effects of 6-TG and 6-TGo on the ER. I previously demonstrated that treating infected cells with 6-TG and 6-TGo dramatically impaired viral glycoprotein accumulation. Furthermore, viral glycoproteins from 6-TG treated cells had a higher electrophoretic mobility. Interestingly, treating infected cells with the N-linked glycosylation inhibitor TM reduced the accumulation of viral glycoproteins and dramatically reduced virus production. TM treatment is known to induce the UPR by directly increasing the amount of unfolded proteins in the ER. Glycoproteins require glycosylation for their proper folding, sorting, and export, so impairing N-linked glycosylation leads to the accumulation of unglycosylated and unfolded proteins in the ER lumen. Like TM, 6-TG and 6-TGo treatment reduced the molecular weight and the

abundance of viral glycoproteins in comparison to untreated cells. This similarity between treatments suggests that these thiopurines impair glycoprotein synthesis. Thus, I investigated the status of the UPR in 6-TG and 6-TGo treated cells independent of infection to determine whether the thiopurines affected the ER. I treated A549 cells with 2 μM and 10 μM 6-TG, 6-TGo, 6-MP, 5-FU, and ribavirin for 6 hours before harvesting total protein. I also treated cells with TM as a positive control for UPR induction. TM treatment caused activation of the three UPR sensor proteins PERK, IRE1, and ATF6, along with the accumulation of UPR induced proteins BiP, CHOP, and XBP1s (Fig 4.5A). 6-TG and 6-TGo also activated all three arms of the UPR, as seen with the activation of the sensors PERK, IRE1, and ATF6; and again, the accumulation of BiP, CHOP, and XBP1s. BiP has more than one isoform, which is seen in Fig 4.5A.

The primary function of IRE1 is to splice *XBP1* mRNA to produce the XBP1s protein. I quantified the splicing of the *XBP1* mRNA from treated cells by performing a standard semi-quantitative *XBP1* mRNA splicing assay (Fig 4.5B). I generated cDNA from cells treated with TM, 6-TG, 6-TGo, 6-MP, 5-FU, and ribavirin by reverse transcribing all mRNA using an oligo-dT primer. I then was able to amplify the *XBP1* mRNA from the cDNA library using sequence-specific primers. The unspliced *XBP1* cDNA contained a PstI cleavage site in the 26-nucleotide intron, allowing me to digest unspliced cDNA into *XBP1u1* and *XBP1u2*. Whereas the spliced cDNA remains undigested, due to the restriction digestion site being removed with the 26-nucleotide intron. I was able to visualize the spliced cDNA transcript and digested product on a 2.5% agarose gel following ethidium bromide staining (Fig 4.5B). TM treatment strongly induced IRE1 activity, resulting in the majority of the *XBP1* transcript being spliced. 6-

TG and 6-TGo treatment reduced *XBP1u1, XBP1u2,* and increased *XBP1s*, but not as strongly as TM. The structurally similar thiopurine 6-MP did not cause *XBP1* splicing. Ribavirin and 5-FU did not induce the UPR. These data strongly indicated that the two thiopurines 6-TG and 6-TGo, but not 6-MP, induced the UPR in treated cells independent of viral infection. This strongly correlated with the antiviral effects shown by 6-TG and 6-TGo and provides evidence that UPR induction likely impairs viral glycoprotein synthesis. The failure of 5-FU to induce the UPR also correlated with its failure to impair viral replication at similar concentrations to 6-TG and 6-TGo.

4.2.5 Modulating the UPR Restored Viral Glycoprotein Accumulation but Failed to Restore Virus Production

After discovering that 6-TG and 6-TGo induce the UPR, I next investigated whether the UPR is responsible for the defect in viral glycoprotein accumulation. I specifically analyzed NA from infected cells. Analyzing just HA from infected cells was difficult due to the polyclonal nature of the antibody used in this study, the HA with higher electrophoretic mobility merged into viral NP on a western blot. NA forms dimers/tetramers immediately following glycosylation through intra- and inter-molecular disulfide bond formation. NA homodimers are linked by intermolecular disulfide bonds in the stalk region. Two dimers then oligomerize to form tetramers. Thus, treating protein lysates with DTT reduced disulfide bond formation resulting in monomeric NA. I probed for NA using a western blot with total protein lysate +/- DTT to observe both homodimeric and monomeric structures of NA. Probing for NA without DTT treatment from untreated infected cells show that the majority of NA exists as dimers that migrate

at roughly 120 kDa, with a minority existing as monomeric forms. Tetrameric NA dissociates into dimers during electrophoresis and therefore can only be visualized as homodimers on DTT negative gels (Hogue & Nayak, 1992). To determine the role of PERK in 6-TG treated cells, I co-treated infected cells with 200 nM ISRIB to observe any changes in viral glycoprotein accumulation. ISRIB treatment promotes the GEF eIF2B to recycle GDP to GTP even if eIF2α is phosphorylated, effectively relieving the translation inhibition from ISR activation. Treating infected cells with TM or 6-TG dramatically reduced the accumulation of dimeric and monomeric NA (Fig 4.6A). Monomeric NA from 6-TG treated cells migrated closer to the size of deglycosylated NA monomers from TM treated cells. The migration of monomeric NA from 6-TG treated cells suggested that the molecular weight is slightly greater than deglycosylated NA found in TM treated cells, potentially indicating differential glycosylation or other PTMs between the two treatments. Treating cells with ISRIB alone had no effect on viral glycoprotein accumulation. Cotreating infected cells with TM and ISRIB restored monomeric NA accumulation but failed to rescue the glycosylation of monomeric NA or the accumulation of dimeric NA. Like TM, ISRIB was able to restore the accumulation of the lower molecular weight monomeric NA in 6-TG treated cells, but failed to restore the higher molecular weight monomeric NA and the dimerization of NA. These data provide evidence that 6-TG inhibits viral glycoprotein accumulation via UPR/ISR activation and the subsequent reduction of viral mRNA translation.

Treating infected cells with 6-TG and ISRIB restored the accumulation of the lower molecular weight NA. I then analyzed virus production from cells cotreated with 6-TG and ISRIB to determine whether co-treating with ISRIB recovers virus production. I

again used TM as a UPR specific control. Individually, TM and 6-TG treatment reduced viral replication by ~14,000 and ~150 fold respectively (Fig 4.6B). Interestingly, when I cotreated 6-TG and TM with ISRIB, virus production was further reduced instead of restoring viral replication. Cotreatment of ISRIB and TM reduced viral replication by ~42,000 fold, and co-treatment of 6-TG with ISRIB reduced viral replication by ~2,750 fold. These data indicate that the returning the accumulation of the lower molecular weight viral glycoproteins does not rescue viral replication. The failure to recover mature NA dimers from ISRIB treatment correlated with the low virus production. Together, these data indicate that viral glycoprotein synthesis is dampened by PERK activation following 6-TG treatment.

4.2.6 Knocking Out PERK Increased the Antiviral Effects of 6-TG

To determine PERK's role in the ISR following 6-TG treatment, I utilized an A549 PERK knock out (KO) cell line that was generated by Dr. Khaperskyy and myself to test viral glycoprotein accumulation and virus replication. ISRIB treatment effectively nullifies the effects of eIF2α phosphorylation, which is the center point of the ISR. ISRIB relieves translation arrest from the ISR by directly binding to eIF2B and promoting its GEF activity, effectively resuming GDP to GTP cycling and the return to cap-dependent translation. Treatment with ISRIB restored viral protein accumulation, but not glycosylation and maturation, which indicates that the ISR is responsible for reducing the accumulation of viral glycoproteins. Three different PERK KO clones were generated (Clone B3, C3, and A2) along with a non-targeting (NT) control. I confirmed the functional consequences of knocking out PERK by treating cells with Tg and sodium

arsenite (As). Tg treatment specifically induces PERK through the UPR, wherease As induces the ISR through another sentinel kinase, HRI, that also phosphorylates eIF2α activating the ISR independent of PERK. In my NT control cells, both Tg and As increased P-eIF2α levels slightly. In the clonal PERK KO cells (B3), Tg did not induce P-eIF2α, whereas As strongly induced P-eIF2α (Fig 4.7A).

I infected the three clonal PERK KO cell lines along with their NT controls with PR8 at a MOI of 0.1 for an hour and treated with vehicle control (DMSO), the N-linked glycosylation inhibitor TM, 6-TG, or the structurally similar thiopurine 6-MP for 23 hours. After 24 hpi, virus production was measured by collecting cell supernatants and conducting plaque assays. PERK deficiency had no effect on IAV replication, with replication comparable to the NT control cell line. In agreement with previous results, the structurally similar thiopurine 6-MP had no effect on viral production in PERK KO cell lines and NT control cells. Treating infected PERK KO and NT cells with TM significantly reduced viral titers equally across the different cell lines. Treating NT cells with 6-TG reduced virus production by roughly 77-fold. Interestingly, treating PERK KO cells with 6-TG further reduced virus production another 30-fold over the NT cells, representing a ~2,300-fold reduction over untreated cells (Fig 4.7B). PERK KO cells may have increased sensitivity to 6-TG treatment, which would explain the significant reduction of virus production in PERK KO cells. I treated both the NT control and PERK KO clone B3 with 6-TG and 6-TGo and quantified cell viability using the alamarBlue assay. PERK KO cells did not show an increased sensitivity to 6-TG treatment (Fig 4.7C). However, PERK KO cells showed more resistance to the cytostatic effects from 6-TGo treatment compared to the NT control cells. These data indicate that the reduction in

virus production in thiopurine treated PERK KO cells was not from an increased sensitivity to 6-TG treatment. PERK activation reduced the accumulation of viral glycoproteins and that the removal of PERK from the system increased the antiviral effects of 6-TG on viral replication. It remains unknown why PERK KO cells are more sensitive to the antiviral effects of 6-TG.

I further analyzed the UPR and the effect of 6-TG on viral glycoprotein accumulation using 4-PBA. 4-PBA is a chemical chaperone that assists in protein folding, which can mitigate ER stress (H. Zhang et al., 2013). I infected PERK KO clone B3 and the NT control cells with PR8-AmantS for one hour and treated the infected cells with 6-TG and 4-PBA for 23 hours. I analyzed viral glycoprotein accumulation in response to the chemical chaperone. I further analyzed the accumulation of BiP, as it is upregulated during the induction of the UPR (Fig 4.7D). As previously shown, wild-type cells with an intact PERK response accumulated BiP from 6-TG treatment (Fig 4.5A). 6-TG and 4-PBA cotreatment dramatically reduced BiP expression in NT control cells. Co-treating 4-PBA with 6-TG decreased the electrophoretic mobility of NA compared to 6-TG alone (lane 4 vs lane 2), whereas protein accumulation was still less than that of untreated cells (lane 4 vs lane 1) (Fig 4.7D). Treating infected PERK KO cells with 6-TG strongly induced BiP expression, more than in the NT control cells. These data are consistent with previous findings in PERK KO cells. It has been shown that knocking out PERK expression increased the activity of IRE1 (Harding et al., 2000). Like treating infected cells with ISRIB and 6-TG, treating PERK KO clone B3 cells with 6-TG did not reduce viral glycoprotein accumulation. This is consistent with the literature, mammalian cells that lack PERK have been shown to maintain protein synthesis during ER stress (Harding

et al., 2000). Again, 6-TG treatment led to the accumulation of a lower molecular weight species of NA, likely due to the incomplete glycosylation of NA (lane 6 vs lane 2) (Fig 4.7D). Co-treating PERK KO cells with 4-PBA and 6-TG did not significantly reduce BiP accumulation, nor did it rescue NA glycosylation (lane 8 vs lane 4). Knocking out PERK resulted in similar results as treating infected cells with ISRIB, highlighting the role of PERK in dampening viral translation during 6-TG treatment. Taken together, these data indicated that PERK activation through the UPR reduces viral glycoprotein translation after 6-TG treatment. Furthermore, 6-TG treatment impaired the proper glycosylation of the viral glycoproteins that reduced virus production. 4-PBA partially alleviated 6-TG's induction of the UPR in NT cells, but not enough to return translation to normal levels. Treating PERK KO cells with 4-PBA and 6-TG did not reduce the accumulation of BiP and did not rescue the glycosylation of NA. These data indicate that PERK KO cells are more susceptible to 6-TG-mediated UPR induction, which lead to significant reduction in virus production. The KO of PERK likely increased the protein burden in the ER, which may increase the basal level of UPR signaling.

4.2.7 6-TG Is More Effective Than the Rac1 Inhibitor V

My previous results indicated that the other nucleoside and nucleobase analogs do not induce a UPR in treated cells, and that this phenotype is found only in 6-TG and 6-TGo. This suggests that the incorporation of these nucleobases into DNA or RNA may not be involved in UPR regulation. 6-TG is known to inhibit the Rac1 GTPase (Shin et al., 2016). 6-thioguanosine triphosphate (6-TGTP) forms a disulfide adduct with the redox sensitive GTP binding domain of Rac1. 6-TGTP is converted to 6-TG diphosphate

(6-TGDP) + (P_i) by Rac1. 6-TGDP is unable to be exchanged for a free GTP or 6-TGTP. The failure to recycle 6-TGDP to another GTP or 6-TGTP prevents the reactivation of Rac1 leading to the accumulation of 6-TGDP loaded inactive Rac1 (D et al., 2006; Shin et al., 2016). 6-TGTP may also inhibit RhoA or Cdc42, since they have identical GTP binding domains. To further understand the role of Rac1 during IAV infection, I treated infected A549 cells with a Rac1 inhibitor (Rac1 inhibitor V). The Rac1 inhibitor V is a cell-permeable selective inhibitor of Rac1 and reversibly prevents its activation. A549 cells were infected with PR8-AmantS at an MOI of 0.1 for 1 hour and incubated with 6-TG or Rac1 inhibitor V for 23 hours before quantifying virus production (Fig 4.8). 6-TG, at a lower dose than the Rac1 inhibitor V, reduced the viral replication more than the Rac1 inhibitor did, but this conclusion remains uncertain because it was derived from a single biological replicate. These data represent a single biological replicate. These data suggested that 6-TG was more antiviral than the Rac1 inhibitor V.

4.2.8 Calculating the MLD_{50} of CA/07-MA

After demonstrating the antiviral properties of 6-TG and 6-TGo in our cell models, I expanded my investigation into an *in vivo* model. The murine model is well established for studying IAV infection. Mice are not naturally infected with IAV due to their inability to transmit the virus from mouse-to-mouse. Clinical isolates of IAV do not replicate efficiently in the mouse and must be adapted to the new host to efficiently replicate. Most inbred mice lack the antiviral Mx1 proteins, and therefore are more susceptible to viral infection. Mx1 proteins are well-studied host antiviral factors that are upregulated by IFN during infection. Working with the mouse model yields numerous

advantages: they are small and easy to handle, they have numerous genetic knockouts to study, inbred colonies ensure similar genetics in experiments, mice fail to aerosolize the virus, and there is a plethora of tools available to analyze samples to quantify immune responses. Importantly, mice have been used for decades as a platform to study antiviral therapies and vaccine strategies (Matsuoka et al., 2009).

I generated a working stock of A/California/07/2009 (H1N1) mouse adapted (CA/07-MA) from the allantoic fluid from fertilized chicken eggs. The properties of this virus are discussed in detail in Chapter 5. I calculated the mean lethal dose 50 (MLD_{50}) units of the stock to establish a benchmark for all future *in vivo* experiments. To calculate the MLD_{50}, nine groups of five mice were infected with stock virus serially diluted 10-fold in sterile 1xPBS. One cohort of mice were mock infected with vehicle control (PBS). Mice were humanely euthanized if their body weight dropped below 80% of their original weight or if they scored ≥ 12 on our clinical scoring. Mice infected with 10^{-4} dilution all hit ethical end points, whereas mice infected with 10^{-5} dilution showed >50% mortality, and mice infected with 10^{-6} dilution had 0% mortality (Fig 4.9). Using ethical endpoints as mortality, I used the Reed-Muench method to calculate the MLD_{50} of the CA/07-MA stock to be 162 181 MLD_{50}/50 µL, with 1x MLD_{50} equated to ~3 PFU/50 µL. For the remaining experiments, I consistently used 5x MLD_{50}/50 µL (15 PFU/50 µL) to infect mice to characterize the effectiveness of 6-TG treatment in this model.

4.2.9 Drug Delivery and 6-TG Tolerance in Mice

6-TG administration via gavage leads to the majority of the compound being absorbed and metabolised by the gastrointestinal tract before being absorbed into the

bloodstream (Bronk et al., 1988; Jharap et al., 2011). To avoid this dramatic reduction of potency, I first investigated intranasal (I.N.) administration of sterile PBS during infection. Here, I infected two groups of five mice each with 5xMLD_{50}/50 µL, one group with I.N. administration of 50 µL PBS and the other untreated, with one group of five that was mock infected. The mice that received 1xPBS administered I.N. lost weight and subsequently their ethical end points faster than the non-treated cohort (Fig 4.10A). I discovered administering I.N. PBS significantly decreased the life expectancy of infected mice (Fig 4.10B). For this reason, I switched to interparental (I.P.) injections for future experiments, which ensured efficient drug administration while avoiding the health risks associated with gavage.

Using I.P. injections to administer 6-TG to infected mice, I calculated the best dosage to get 6-TG to the lungs without causing immune dysregulation. Here, being wary of the immunosuppressive side effects of 6-TG, I calculated that administering 0.3mg/Kg/day would be the highest amount I could inject into the mice without causing immune dysregulation. I calculated this by referring to the published literature; Nelson and Vidale demonstrated that 0.3mg/kg/day administered I.P. is well below lethal concentrations (Nelson & Vidale, 1986). Moore and LePage showed that up to 10% of administered 6-TG can be found in the lung within a minute of administration (Moore & LePAGE, 1958). In clinical settings, humans are routinely treated with 0.3 mg/kg/day delivered orally, with favourable concentrations being reached and maintained (Jharap et al., 2011). Injecting I.P. increases absorption and distribution. Furthermore, gavage administration of 0.5 mg/kg/day showed no systemic toxicity, while 1 mg/kg/day resulted in weight loss in mice over an extended period of time (Oancea et al., 2013). In the same

study, the authors demonstrated haematopoietic toxicity at 0.5 mg/kg/day, but not 0.2 mg/kg/day. Considering this evidence from the literature, I decided that 0.3 mg/kg/day of 6-TG delivered I.P. is the maximum concentration I could use without causing immune suppression and systemic cytotoxicity.

I tested several concentrations of 6-TG in BALB/c mice line to further establish the dosing for the challenge study. I treated mice with vehicle control (PBS), 1, 0.3, and 0.1 mg/Kg/day through I.P. injection and observed for weight loss over ten days (Fig 4.10C). All groups were healthy with no weight loss, indicating no overt cytotoxicity. Although, the body weight of mice does not directly represent the immune status of treated mice. Mice treated with 1mg/kg/day likely experienced mild immune suppression which did not manifest in weight loss. From these data and previously published work by other groups, I determined that 6-TG is best administered through I.P. injections at 0.3 mg/kg/day.

4.2.10 6-TG Did Not Protect Against Lethal Infection

To test the effectiveness of 6-TG as an antiviral against influenza infection in a murine model, I treated infected mice in a IAV challenge study. I injected a group of mice prophylactically 2 days prior to infection (Day -2), with 0.3mg/kg/day I.P. and continued treatment daily until Day 10. I mock-infected or infected mice on Day 0 with 5xMLD_{50}/50 µL and monitored for symptoms until day 10, euthanizing mice that reached their ethical end points (Fig 4.11A). I treated one group of infected mice with ribavirin, a nucleoside analog with antiviral properties against influenza, as a positive control and treated another group with vehicle control (PBS) as a negative control. Previous work

demonstrated that ribavirin protected mice from lethal CA/04 infection (Rowe et al., 2010). The challenge study was completed three independent times to generate three biological replicates.

Treating infected mice with 6-TG did not protect against a lethal challenge of IAV. Treated mice with I.P. 6-TG did not improve the survival rate of infected mice over the untreated group (Fig 4.11B). 6-TG treated mice lost weight at the same rate as the untreated mice, whereas mice treated with ribavirin showed no morbidity or mortality (Fig 4.11C). I harvested Bronchoalveolar Lavage Fluid (BALF) from both 6-TG treated and vehicle (PBS)-treated mice to quantify virus production in the lung. 6-TG treatment did not reduce viral replication compared to the untreated group (Fig 4.11D). These results indicated that the 6-TG treatment had little to no effect on viral replication, disease manifestation, and survival against a lethal dose of IAV. Anecdotally, 6-TG treated mice showed a mild improvement in activity and coat appearance. This slight difference may arise from the immune modulatory effects of 6-TG.

4.2.11 6-TG Treatment Altered the Immune Response of Infected Mice

I further analyzed the effect of 6-TG treatment on the cytokine responses of infected mice through a multiplex ELISA. BALF was sterile-filtered and UV-sterilized before analysis. Samples were harvested on 3 dpi. Samples were analyzed on Day 3 because there was no survivor bias, while day 7 saw a significant number of mice lost to their ethical end points. In total, 23 targets were analyzed by the multiplex assay, the majority of which showed no differences between treated and untreated or were

unquantifiable (out of range=OOR) (Table 4.1). The chemokines CXCL2 (Fig 4.12A), CXCL1 (Fig 4.12B), and CXCL10 (Fig 4.12C) were found to be markedly reduced in 6-TG treated mice at 3 dpi. IAV infection is known to promote CXCL2 release from recruited neutrophils, which in turn recruit more neutrophils (Short et al., 2014). CXCL10 is also produced by activated neutrophils and is correlated with a poor prognosis (Ichikawa et al., 2013). CXCL2 and CXCL10 is thought to aid in neutrophil mediated damage to lung tissue. Neutrophils further damage endothelial and epithelial cells of the lung during infection through the formation of extracellular traps (Narasaraju et al., 2011). However, these results are from two mice per group, and therefore do not have the power to test for statistical significance. Results from 7 dpi were highly variable, with no cytokine or chemokine showing any trend in between treatment groups. The filtered BALF from infected mice collected 7 dpi also had a reddish colour, possibly indicating extensive lung damage.

To further analyze the immune response to IAV infection and subsequent 6-TG treatment, I investigated the immune cell infiltrate in the BALF. Cells were obtained from BALF 3 dpi and stained for immune markers to allow differentiation and quantification through flow cytometry. Samples from 7 dpi were unusable due to excessive lung damage that resulted in a dramatic reduction in viable cell counts. Cells from 3 dpi were gated first on forward and side scatter, then for CD45+ and side scatter, then CD11c and SigLig F, and lastly on Ly6G and CD11b. Alveolar macrophages (AM), high in both SigLig F and CD11c, comprise the majority of immune cells found in a healthy lung and are responsible for clearing particulates along with remodeling the alveolar space. Influenza virus infection has been shown to reduce AM populations by up

to 90% in the murine lung (Ghoneim et al., 2013). In agreement with the literature, infection dramatically reduced the AM populations in the lung of vehicle treated-infected mice. Treating infected mice with 0.3 mg/kg/day 6-TG increased the survival of alveolar macrophages by almost two-fold over the untreated infected group (Fig 4.13). In the healthy-uninfected control group, neutrophils were not present in the BALF. The untreated-infected mice had a high degree of neutrophil infiltration. 6-TG treatment reduced neutrophil infiltration into the mouse lung. Higher levels of neutrophil infiltration is negatively correlated with disease outcomes (Weiland et al., 1986). 6-TG treatment reduced CXCL2 levels in infected mice, which complements the reduction in neutrophil infiltration. Taken together, these data suggest that treating infected mice with 0.3 mg/kg/day 6-TG I.P. did not reduce viral replication, but slightly modulated the immune response. Accordingly, the virus replicated unperturbed and treated mice experienced similar mortality rates to the vehicle control group.

4.2.12 6-TG Failed to Induce the UPR in Mouse Cell Lines

My previous results indicated that treating cells with 6-TG induced the UPR and this prevented the accumulation of viral glycoproteins and ultimately impaired viral production. After discovering that 6-TG did not improve the survival of IAV infected mice, I investigated whether 6-TG could activate the UPR in murine cells. Here, I treated A549, mouse embryo fibroblasts (MEF), and murine L929 cells with 5-fold dilutions of 6-TG for 4 and 8 hours before harvesting total protein lysate. I also treated cells with TM or Tg controls to induce the UPR. I probed lysates for XBP1s, as I previously demonstrated that 6-TG treatment activates IRE1. A549 cells accumulated XBP1s at 4-

and 8-hours post-6-TG treatment (Fig 4.14A). These data are consistent with my previous findings. The accumulation of XBP1s plateaued after treating A549 cells with 10 μM 6-TG. XBP1s did not accumulate in 6-TG treated MEFs (Fig 4.14B) or L929 cells (Fig 4.14C), even at the highest concentrations and longest time points. I confirmed that XBP1s accumulated during the UPR. TM and Tg treated murine cells accumulated XBP1s to high levels.

4.2.13 Treating Infected MEFs with 6-TG did not Impair Virus Production

I further analyzed the potential antiviral effects of 6-TG in murine cells. I infected MEFs with PR8-AmantS at an MOI of 0.1 for 1 hour and treated infected cells with TM, 6-TG, 6-TGo, and 5-FU (Fig 4.14D). TM treatment dramatically reduced virus production from treated MEF cells, which is consistent with my previous findings in A549 cells. Both 6-TG and 6-TGo failed to reduce virus production from treated cells, even at the highest concentration of 10 μM. However, these data only represented one biological replicate, and therefore were not statistically significant. The nucleobase 5-FU had no effect on virus production, which is also consistent with my previous results in A549 cells. These data indicate that 6-TG and 6-TGo failed to induce the UPR in murine cells. The induction of the UPR likely created an antiviral environment that impaired viral glycoprotein synthesis and subsequent virus production. These data indicated that the murine model is not appropriate to test the efficacy of 6-TG due to murine resistance to 6-TG mediated UPR induction. Further research is required to fully characterize

murine cell's resistance to 6-TG treatment and the correlation between UPR induction and impairing viral replication.

4.3 Discussion

HTAs may provide a higher barrier to the emergence of antiviral resistant viruses, while direct-acting antivirals quickly select for resistance. It remains challenging to identify cellular pathways that can be targeted to impair virus replication without causing overt cytotoxicity in uninfected cells. In this Chapter, I report the antiviral effects of the FDA-approved thiopurine analogs 6-TG and structurally similar 6-TGo against IAV infection. 6-TG is currently used in clinical settings to treat leukemia and IBD, with 6-TGN metabolites impairing the small GTPase Rac1 (de Boer et al., 2006; Moore & LePAGE, 1958; Shin et al., 2016, p. 1). My results indicate that targeting the ER significantly impairs virus production. Furthermore, I demonstrated that 6-TG is an effective antiviral against several influenza viruses. I characterized a cellular pathway that can be targeted that did not cause overt cytotoxicity in bystander cells, while impairing the accumulation of viral glycoproteins. These findings indicate, for the first time, that the thiopurines 6-TG and 6-TGo induce the UPR in human cell lines. Furthermore, I demonstrated for the first time, that 6-TG and 6-TGo are effective antivirals against IAV infection in human cell lines. 6-TG and 6-TGo treatment significantly reduced the accumulation of viral glycoproteins in human cells. Other nucleoside and nucleobase analogs 5-FU, ribavirin, and the structurally similar thiopurine 6-MP did not induce the UPR. Accordingly, these analogs did not significantly impair virus production. The selective disruption of viral glycoprotein accumulation with

minimal effects on other viral proteins suggests that UPR induction by 6-TG and 6-TGo treatment is the main antiviral mechanism. I confirmed the involvement of the UPR in the reduction of viral glycoproteins by treating infected cells with chemical chaperones and the ISR inhibitor ISRIB, which partially restored the accumulation of viral glycoproteins. Furthermore, genetic manipulation using the CRISPR Cas9 system to destroy the expression of PERK partially restored viral glycoprotein synthesis.

In Chapter 3, I demonstrated that silvestrol and pateamine A have a high degree of cytotoxicity in both mock infected and IAV infected cells. Both eIF4A inhibitors reduced cell viability and induced apoptosis at effective antiviral concentrations. Here, 6-TG and 6-TGo moderately reduced cell viability but did not induce the apoptotic cascade at the concentrations and time points used in this study. Therefore 6-TG and 6-TGo likely reduced the cell cycle, displaying their known cytostatic effects (Fulda et al., 1995). 6-TG is a more favourable HTA over eIF4A inhibitors due to its higher threshold of tolerance in treated cells with no overt cytotoxicity. Furthermore, 6-TG is an FDA-approved compound and used in clinical settings.

Dr. Denys Khaperskyy identified 6-TG and 6-TGo in a small molecule screen for compounds that specifically induce SGs in infected cells. IAV encodes three proteins to thwart the formation of SGs but treating infected cells with the thiopurines induced SGs in 5%-10% of infected cells. Furthermore, 6-TG did not induce SG formation in uninfected cells. However, 6-TG induced the UPR in both infected and uninfected cells, suggesting that the activation of PERK may not be solely responsible for the formation of SGs. Furthermore, SGs only formed in a fraction of 6-TG treated infected cells, while the accumulation of HA and NA was almost completely blocked by 6-TG. Is the

phosphorylation of eIF2α responsible for the formation of 6-TG induced SGs? To answer this question, I would perform immunofluorescence on Udorn-infected A549 PERK KO cell lines to visualize and quantify SG formation. Alternatively, I would perform immunofluorescence on infected A549 cells co-treated with 6-TG and ISRIB to visualize SGs. If SGs fail to form in the PERK KO cell lines or in cells co-treated with ISRIB, then that would give evidence that SG formation is PERK and ISR dependent.

Both HA and NA are modified by N-linked glycans in the ER. This PTM is essential for the oligomerization, stability, and function of HA and NA (Ohuchi et al., 1997; P. C. Roberts et al., 1993). I demonstrated that 6-TG and 6-TGo treatment reduced the accumulation of viral glycoproteins HA and NA. Furthermore, 6-TG and 6-TGo treatment resulted in the generation of lower molecular weight HA and NA, as seen through their increased electrophoretic mobility. The failure to properly glycosylate the viral glycoproteins likely is the reason for the accumulation of the lower molecular weight glycoproteins, although the exact mechanism remains unknown.

In this chapter, I analyzed PERK's response to 6-TG treatment on the accumulation of viral glycoproteins. Both PERK KO cells and the NT control cell lines produced equal amounts of virus, suggesting that functional PERK is not required to sustain virus replication. Previous work had indicated that PERK activation during IAV replication is detrimental to the accumulation of viral protein (Landeras-Bueno et al., 2016). Treating infected PERK KO cells with 6-TG rescued the accumulation, but not the molecular weight, of viral glycoproteins. Furthermore, treating infected cells with ISRIB similarly restored the accumulation, but did not restore its electrophoretic mobility. Taken together, these data indicate that PERK is responsible for repressing viral

glycoprotein synthesis through the ISR. Interestingly, treating infected PERK KO cells with 6-TG dramatically reduced virus production, a further ~1.5 log more than the 6-TG treated NT control cell line. An alamarBlue assay determined that PERK KO cells had similar, if not stronger, resistance to potential 6-TG cytostatic effects. It remains unknown why 6-TG treated PERK KO cells further fail to produce virus over the NT control cell line. The phosphorylation of eIF2α by PERK reduces the translation burden within the ER. Knocking out PERK may result in the ER being overwhelmed during 6-TG treatment. Furthermore, co-treating PERK KO cells with 6-TG and 4-PBA did not alleviate the stress completely, as seen with a higher accumulation of BiP and the failure to restore glycosylated NA. However, an analog to 4-PBA, 2,4-dioxo-4-phenylbutanoic acid, is a known inhibitor of the endonuclease domain of PA (Dias et al., 2009). It is unknown if 4-PBA contains the same inhibitory effects as 2,4-dioxo-4-phenylbutanoic acid on PA, but it may explain the reduction of viral protein accumulation in 4-PBA treated cells. Mariel Kleer quantified virus production from 4-PBA treated infected cells and discovered that 4-PBA treatment alone reduced virus production.

The exact mechanism of UPR induction by 6-TG and 6-TGo remains unknown. My data indicates that the effects are unlikely mediated through DNA or RNA incorporation of 6-TGN because: 1) the UPR was rapidly induced following 6-TG and 6-TGo treatment, 2) only viral glycoproteins were significantly affected by 6-TG treatment, 3) work completed by Dr. Khaperskyy and Eileigh Kadijk indicated that mRNA and vRNA levels were unaffected by 6-TG treatment, 4) other nucleoside and nucleobase analogs failed to induce the UPR and failed to impair virus production (Slaine et al., 2021). The structurally similar thiopurine 6-MP is missing the H_2N-amine found on the

nitrogenous base of 6-TG or 6-TGo. Because of this, 6-MP mimics guanine less well compared to 6-TG and 6-TGo.

The mechanism of 6-TG mediated UPR activation may involve the inhibition of a small GTPase involved in ER homeostasis. Numerous GTPases are involved in regulating the ER, such as Rab GTPases that are responsible for vesicular trafficking, dynamin-like GTPases that maintain tubular networks and vesicle formation, and the localization of nascent polypeptides to the ER membrane (Accola et al., 2002; Hu & Rapoport, 2016). 6-TG is known to bind and impair the small GTPase Rac1 through mimicking guanosine and preventing the cycling of GDP to GTP (Yin et al., 2018). Impairing Rac1 is thought to contribute to its mechanism of action as a chemotherapeutic and treatment of IBD (Shin et al., 2016, p. 1). Preliminary results indicated that impairing Rac1 was not as effective as 6-TG as an antiviral. Future work will analyze the accumulation of viral glycoproteins from infected cells treated with the Rac1 inhibitor V.

Studies completed by other McCormick lab members demonstrated that 6-TG treatment induced the UPR in most cell lines tested, including Vero, U2OS, and MDCK cells. Interestingly, high concentrations of 6-TG failed to induce the UPR in treated murine cells, while the same concentrations of 6-TG strongly induced the UPR in human cell lines. Preliminary data indicates that treating infected murine cells with 6-TG has no antiviral effect on virus production, which correlated strongly with the failure to induce the UPR. These data further support the idea that 6-TG antiviral effects are independent of 6-TGN incorporation. Furthermore, treating infected mice with 6-TG did not protect against a lethal infection nor did 6-TG treatment reduce virus production in the mouse

lung. These data give evidence that murine cells are resistant to 6-TG mediated UPR induction, resulting in the failure to protect the model organism against viral replication.

My work demonstrates that not all species are equally sensitive to 6-TG mediated UPR induction, with murine cells showing complete resistance to 6-TG. Moving forward with 6-TG as an HTA, the optimal model organism would closely resemble human cell lines with clear and marked induction of the UPR. The ferret is another well-established model for influenza infection, commonly used to study transmission with their ability to aerosolize the virus and similar clinical manifestation to that of a human (Belser, Katz, et al., 2011; Belser et al., 2020). The efficacy of 6-TG in ferrets can be tested *in vitro* first, since ferrets have their own available cell lines. This will allow us to test ferret cell lines for 6-TG mediated UPR induction prior to a challenge study.

Why are murine cells resistant to 6-TG mediated UPR induction? I hypothesize that 6-TG targets a GTPase in human cell lines that perturbs the ER, while murine cells either do not encode the GTPase, or the GTPase is divergent from human sequences. I aligned the primary amino acid sequence of Rac1 from mice and humans to identify whether there is significant divergence between the two species. Rac1 is 100% identical in amino acid sequence between mice and humans, further indicating that Rac1 is not the target of 6-TG or 6-TGo. Further analysis of GTPases involved in localizing glycoproteins to the ER and the Golgi apparatus highlights several differences in key GTPases between murine and human. The most significant difference is the absence of the dynamin-like GTPase myxovirus resistance protein 1 (MxA) in the model mouse BALB/c. MxA is the human ortholog to murine Mx1. In Chapter 5, I confirm the absence of Mx1 in both the MEF cell lines and the inbred BALB/c mice. The dynamin-like

GTPase MxA is known to tubulate the ER, form cytoplasmic structures even in uninfected cells, and can amplify apoptosis through the UPR (Accola et al., 2002; D. Davis et al., 2019; Numajiri Haruki et al., 2011). Inhibiting MxA may impair the tubulation of the ER and induce ER stress, resulting in the activation of the UPR.

The cell relies on three GTPases to localize growing polypeptides to the ER to be translated into the ER lumen. The first is the signal recognition particle (SRP) 54 kDa subunit (SRP54), the second is the 70 kDa α-subunit of the SRP receptor (SR), and the third is the 20 kDa β-subunit of SR. All three GTPases work in concert with each other to identify, translocate, and release nascent polypeptides into the translocon. SRP54 and SRα reside in a unique subfamily of GTPases, while SRβ is a member of the Ras family of small GTPases (Legate & Andrews, 2003). SRα and SRβ have been shown to bind GTP, with SRβ showing rapid binding of fresh GTP with binding efficiency at ~1μM (Miller et al., 1995). Recognition of the signal peptide and targeting of the nascent protein to the ER is independent of GTP hydrolysis. The insertion of the nascent polypeptide into the translocon and dissociation of SRP from the SR is GTP-dependent (Bacher et al., 1999; Rapiejko & Gilmore, 1994). I aligned the primary amino acid sequences of the three GTPases from murine and human origins, with SRP54 showing 99.8% identity, SRα showing 97.2% identity, and SRβ showing 90.4% amino acid identity. Some amino acid differences between SRβ from the mouse and human sequences flanked the GTP binding domain, but not within the GTPase domain itself. Furthermore, within SRβ there are numerous substitutions between mice and human in the switch domains. Switch domains are responsible for changing confirmation of the protein during GTP hydrolysis to increase its affinity to its target proteins (Wennerberg et

al., 2005). SRβ contains two switch domains, the first contains 60% amino acid identity between human and mice sequences, while the second domain shows 80% amino acid identity. These switch domains may alter the GTPases ability to bind 6-TG. Interestingly, it has been demonstrated that impairing the SRP and SR pathway induce the UPR (Bacher et al., 1999; Prevo et al., 2017). Further research is required to identify the molecular target of 6-TG and 6-TGo.

HTAs are becoming more widely researched and show potential against numerous viruses. In this chapter, I demonstrated the applicability of 6-TG as an HTA against several influenza viruses. In 2019, a member of the betacoronavirus genus, severe acute respiratory syndrome coronavirus-2 (SARS COV-2), entered the human population initiating the deadliest pandemic of the 21st century thus far. The McCormick lab has tested the antiviral properties of 6-TG on the biosafety level-2 (BSL-2) betacoronavirus OC43, which also infects the human population but is generally limited to mild symptoms. Work completed by the McCormick lab has indicated that 6-TG is antiviral against OC43, with treatment significantly impairing the accumulation of the viral spike (S) glycoprotein. Unlike IAV, coronaviruses replicate their genome in the cytoplasm in replication compartments derived from the ER and secretory pathway (Cortese et al., 2020). These replication compartments are double membrane vesicles that are captured lipids from the ER (Knoops et al., 2008). Perturbing the ER through UPR induction with 6-TG may prove to not only impair viral glycoprotein accumulation, but directly limit viral transcription and replication by blocking the formation and function of coronavirus replication organelles.

Table 4.1: Average concentrations of chemokine/cytokine from the BALF of infected mice at 3 dpi. The average values of immune signaling molecules were quantified from mice that were infected and treated with PBS vehicle, infected and treated with 6-TG, and healthy uninfected controls. 23 molecules were quantified using Luminex that was quantified on the Bio-Plex 200 from Bio-Rad. OOR< =Out of Range below. This work was completed by Patrick Slaine and is not published.

Molecule	Infected untreated(pg/mL)	Infected 6-TG(pg/mL)	Uninfected(pg/mL)
GM-CSF	6.8	6.8	6.38
TNF-α	1.12	7.74	6.97
MCP-1/JE/CCL2	23.42	1421.96	1153.615
MIP-2/CXCL2	0.1	55.605	39.855
IL-5	OOR <	OOR <	OOR <
IL-10	OOR <	OOR <	OOR <
IL-17A	OOR <	OOR <	OOR <
RANTES/CCL5	37	444.535	369.475
MIP-1a/CCL3	0.87	16.045	12.97
KC/CXCL1	24.1	479.79	389.21
IL-12p70	7.7	10.74	11.42
IL-1 β	OOR <	OOR <	OOR <
IL-4	OOR <	OOR <	OOR <
IL-6	18	298.965	344.3
IL-13	OOR <	OOR <	OOR <
IP-10/CXCL10	50	1444.45	887.835
IL-23p19	OOR <	OOR <	OOR <
IL-18	OOR <	OOR <	OOR <
IL-15/IL-15R	OOR <	OOR <	OOR <
ST2/IL-33R	OOR <	OOR <	OOR <
TSLP	OOR <	OOR <	OOR <
IL-25/IL-17E	OOR <	OOR <	OOR <
IL-22	OOR <	OOR <	OOR <

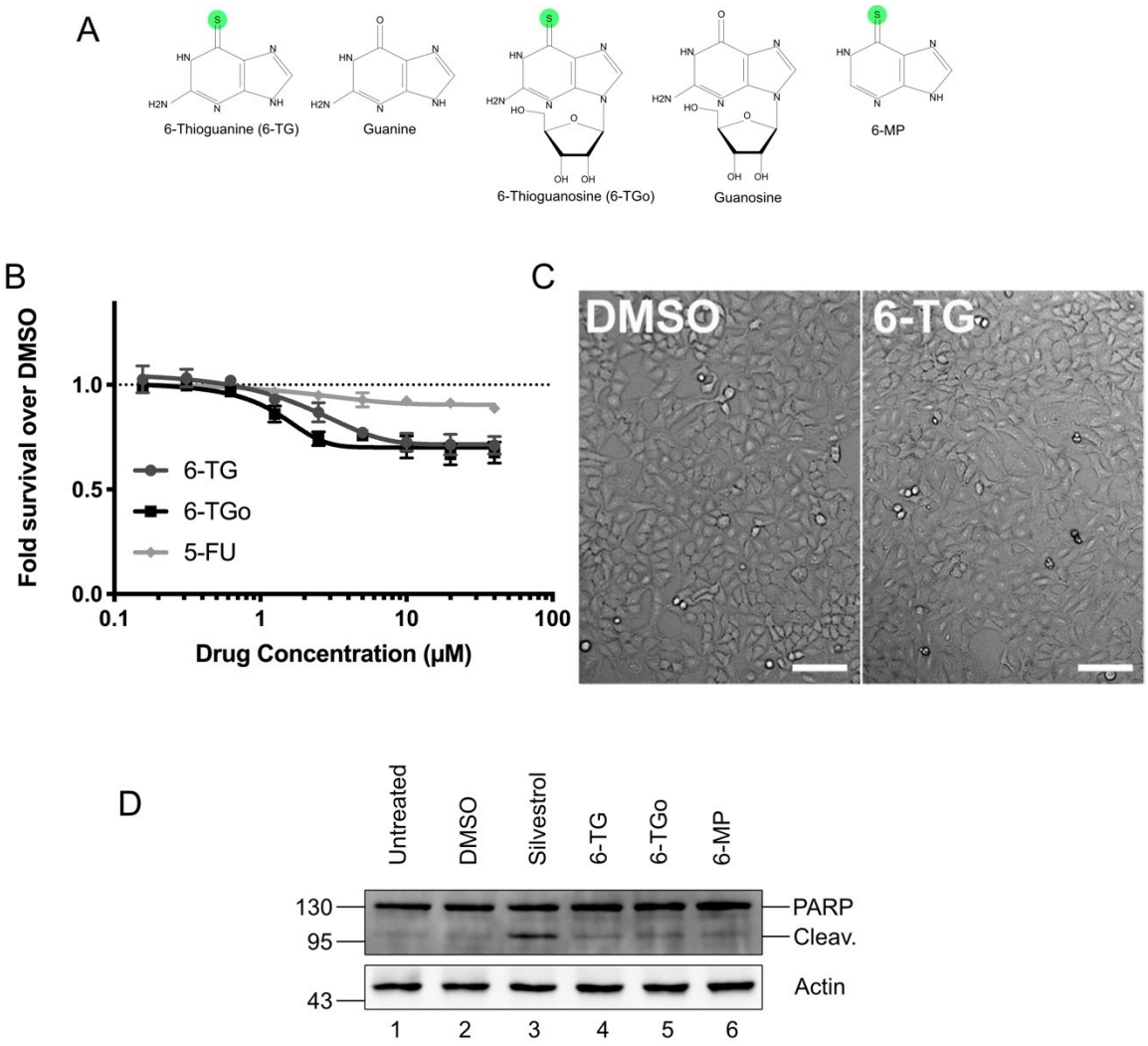

Figure 4.1: 6-Thioguanine and 6-Thioguanosine demonstrate cytostatic effects on treated cells.

(A) Structures of 6-thioguanine (6-TG) and 6-thioguanosine (6-TGo) and structurally similar nucleobases and nucleosides. Thiol groups present in 6-TG, 6-TGo, and 6-mercaptopurine (6-MP) are highlighted in green. (B) A549 cells were treated with increasing doses of 6-TG, 6-TGo, 5-FU, or vehicle control (DMSO) for 23 hours and cell viability was measured using an alamarBlue assay. Relative fluorescence units were normalized to vehicle control. Error bars represent standard deviation (N=3). Horizontal dotted line represents the relative fluorescence of untreated cells. (C) Representative phase contrast images of A549 cell monolayers treated with 6-TG (10 μM) or vehicle (DMSO) control for 23 h. White scale bars in the bottom right corner of images represent 100 μm. (D) Lysates of A549 cells treated with the Silvestrol (320 nM), thiopurines (10 μM), and vehicle DMSO control were analysed by western blotting for total PARP (full length and cleaved). Cellular actin is used as a loading control. This work is published in Slaine et al., 2021 and completed by Patrick Slaine.

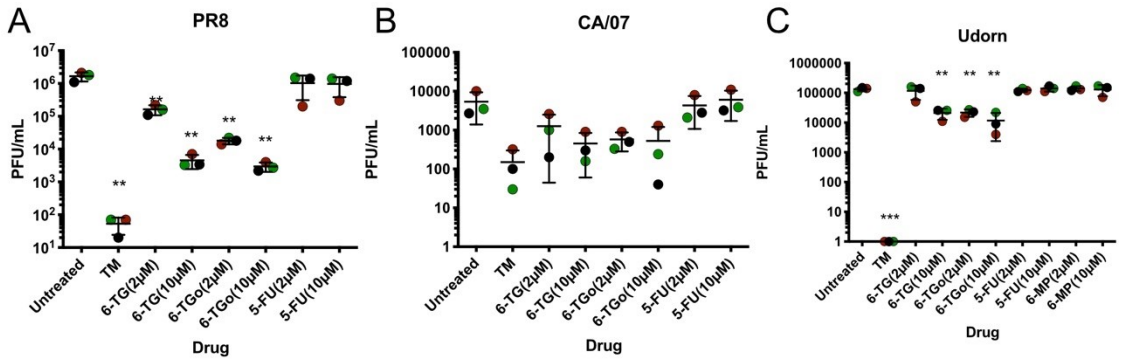

Figure 4.2: 6-TG and 6-TGo treatment impairs replication of genetically diverse influenza subtypes.
A549 cells were infected with (A) A/Puerto Rico/08/34 (H1N1) (PR8), (B) A/California/07/2009 (H1N1) (CA/07), and (C) A/Udorn/73 (H3N2) (Udorn) at a MOI of 0.1 for 1hpi. Cell monolayers were washed and treated with the compounds at the indicated concentrations for 23 hpi. Infectious progeny in the cellular supernatant was enumerated by plaque assay. Error bars denote the standard deviation of three biological replicates (N=3). Dots are coloured for their representative replicate. This work is published in Slaine et al., 2021 and completed by Patrick Slaine.

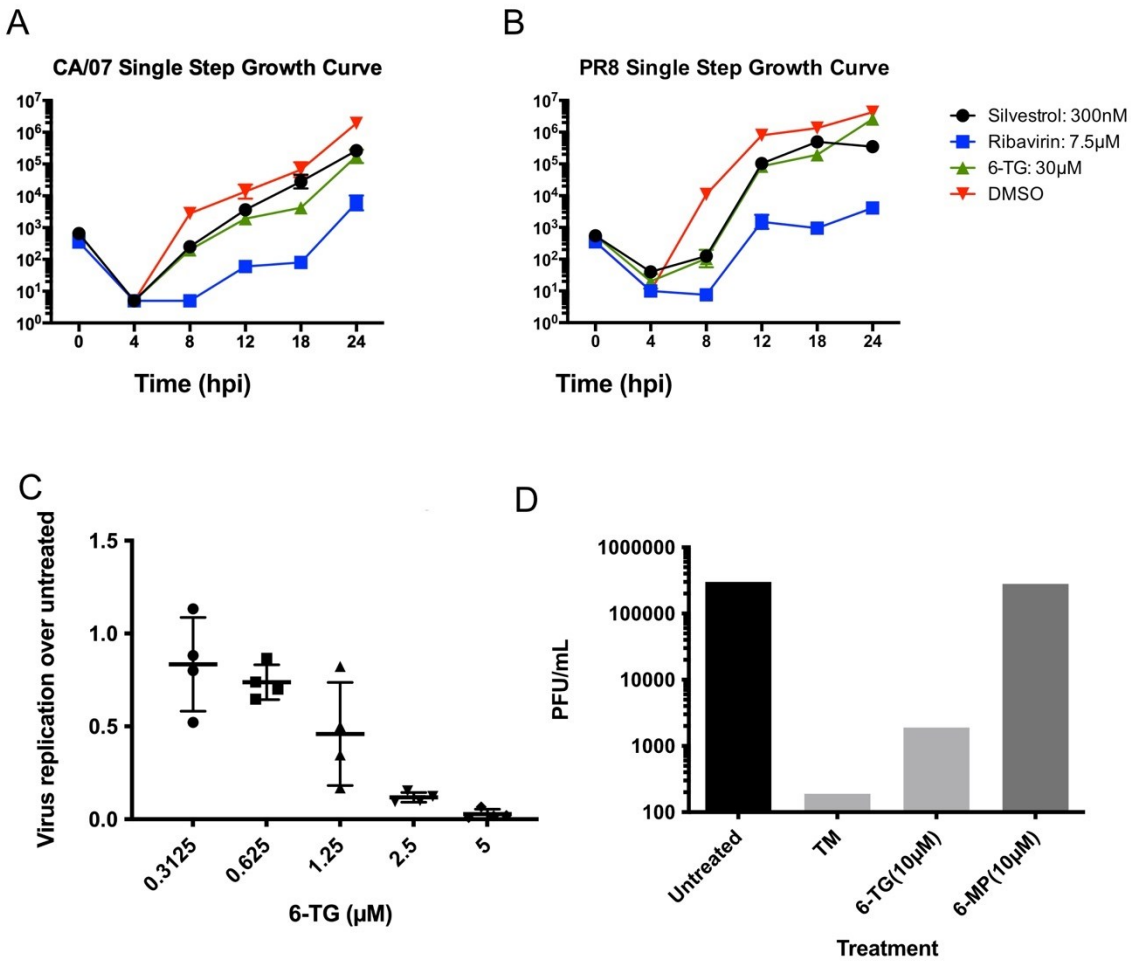

Figure 4.3: Characterization of 6-TG and 6-TGo antiviral effects over time and at different concentrations.
MDCK cells were infected with (A) CA/07 and (B) PR8 at a MOI of 0.1 for one hour, before treating with vehicle control (DMSO), Silvestrol, Ribavirin, or 6-TG. Supernatant was collected from infected cells at the indicated hours post infection (hpi). Infectious viral progeny were enumerated by a plaque assay using confluent MDCK cells. (C) A549 cells were infected with PR8 at a MOI of 0.1 for 1 hour and incubated with 2-fold diluted 6-TG or vehicle control (DMSO) for 23 hours. Virions released into the cell supernatant at 24 hpi were enumerated by plaque assay. Treated samples were normalized to DMSO treated cells to calculate fold reduction. Error bars denote the standard deviation of four biological replicates (N=4). (D) A549 cells were infected with PR8 at a MOI of 0.1 for 1 hour before incubating infected cells with Tunicamycin, 6-TG (10μM), and 6-MP (10μM). Infectious progeny was enumerated at 24 hpi using a plaque assay. Bars represent a single biological replicate (N=1). This work was completed by Patrick Slaine and not published.

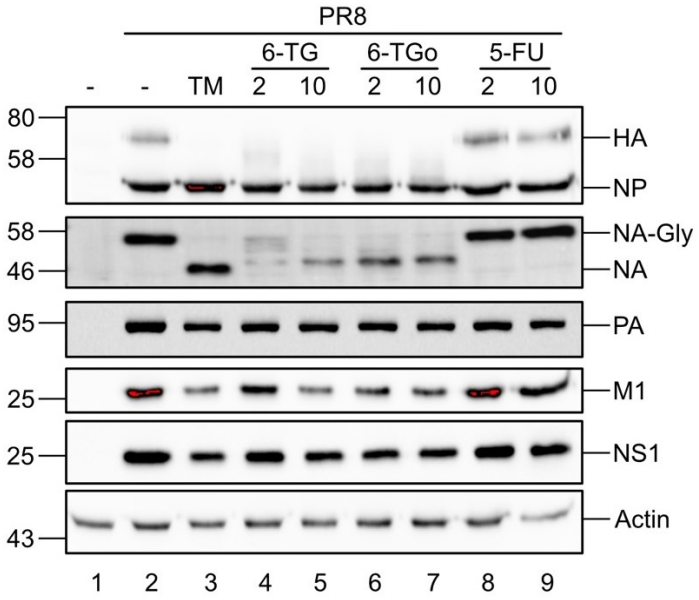

Figure 4.4: 6-TG and 6-TGo impair viral glycoprotein synthesis.
A549 cells were mock infected or infected with A/Puerto Rico/08/34 (H1N1) (A) or CA/07 (B) at a MOI of 0.1 for 1hpi. Cells were washed and treated with compounds at the indicated concentration or vehicle control (DMSO) for 23 hours before total protein was harvested. Cell lysates were collected and analyzed by western blot, using a polyclonal IAV antibody that detects HA, NP and M1 as well as antibodies that detect IAV PA, NA, NS1, or cellular actin. The representative of 3 independent experiments is shown. This work is published in Slaine et al., 2021 and completed by Patrick Slaine.

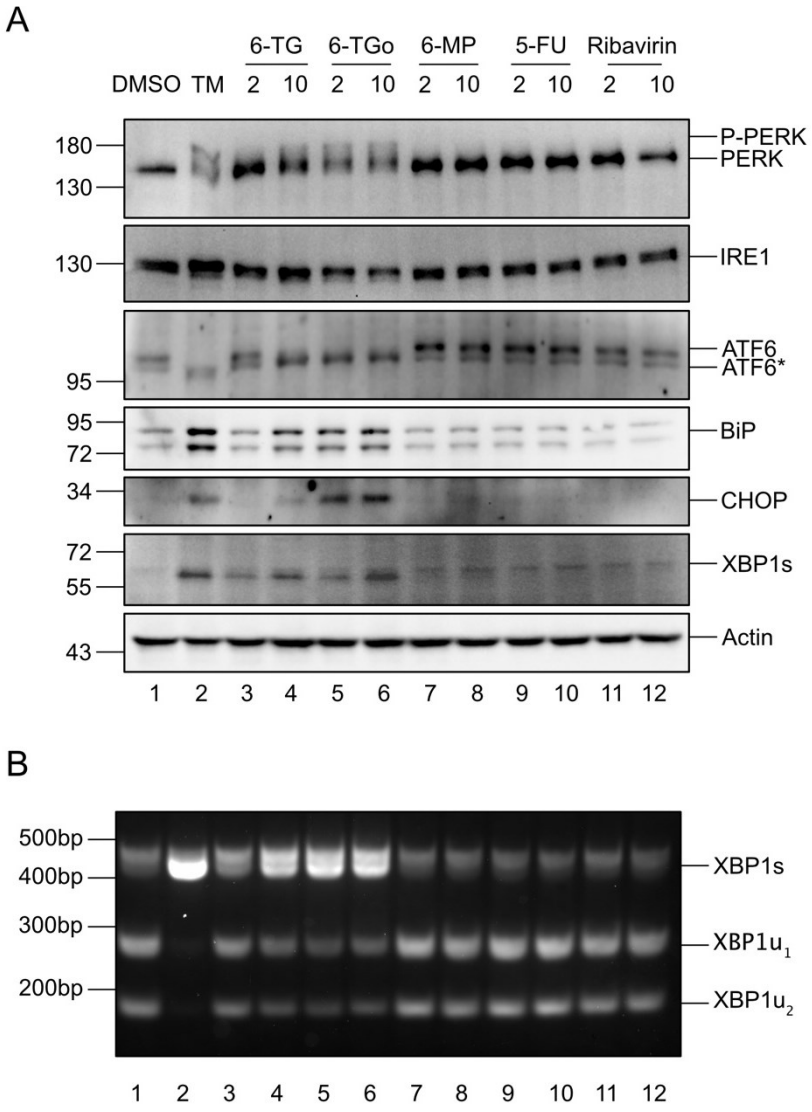

Figure 4.5: 6-TG and 6-TGo activate the UPR.
(A) A549 cells were treated with 6-thioguanine (6-TG), 6-thioguanosine (6-TGo), 6-mercaptopurine (6-MP), 5-fluorouracil (5-FU) or ribavirin at the indicated concentrations for 6 hours prior to harvesting lysates for immunoblotting for the indicated cellular proteins. 5 µg/ml tunicamycin (TM) served as positive control for UPR activation. ATF6* indicates a lower molecular weight species that is presumably not glycosylated and not cleaved to its active form. (B) cDNA was generated from total RNA that was isolated from treated cells. XBP1 mRNA splicing was determined by the semi-quantitative RT-PCR splicing assay. XBP1u1 and XBP1u2 indicate the cleaved produces from digesting the unspliced XBP1 cDNA with PstI-HF. This work is published in Slaine et al., 2021 and completed by Patrick Slaine.

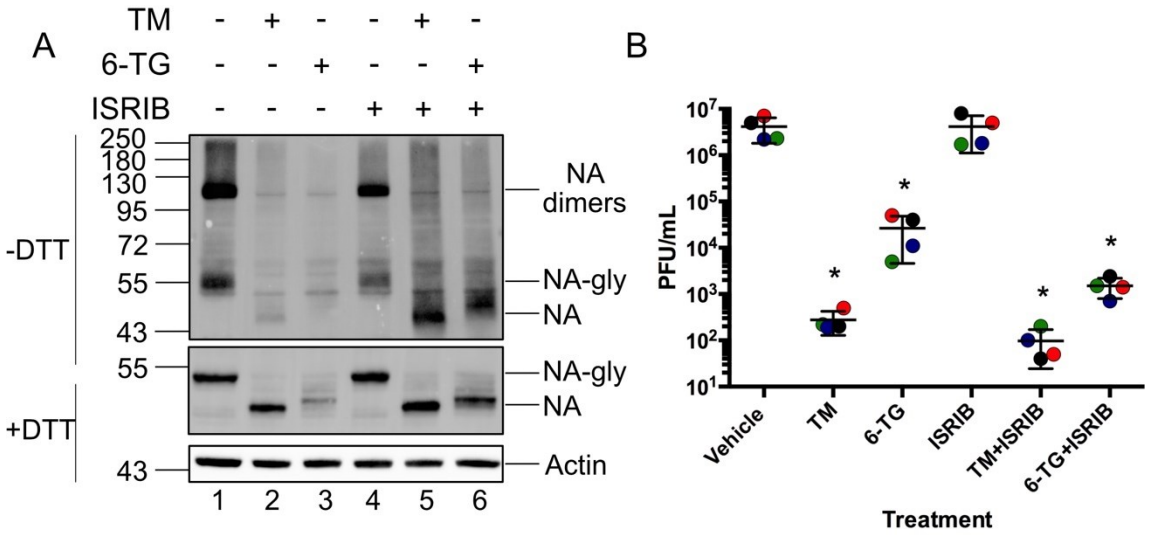

Figure 4.6: ISR inhibition restores NA synthesis in the presence of 6-TG, but NA processing and virion production remain impaired.
A549 cells were infected with PR8 at a MOI of 1. After 1 h, cells were washed and treated with tunicamycin (TM, 5 µg/ml), 6-thioguanine (6-TG, 10 µM) and/or 500 ng/ml ISRIB. (A) At 24 hpi, cell lysates were collected and processed for native SDS-PAGE and immunoblotting using an anti-NA antibody. N-glycosylated forms of NA are indicated as NA-glyco, whereas glycosylated NA dimers are indicated as dimers. Cellular actin was used as a loading control. (B) At 24 hpi, cell supernatants were collected and infectious IAV-PR8 virions were enumerated by plaque assay. Error bars represent the standard deviation between biological replicates (N=4); circles represent biological replicates. This work is published in Slaine et al., 2021 and completed by Patrick Slaine.

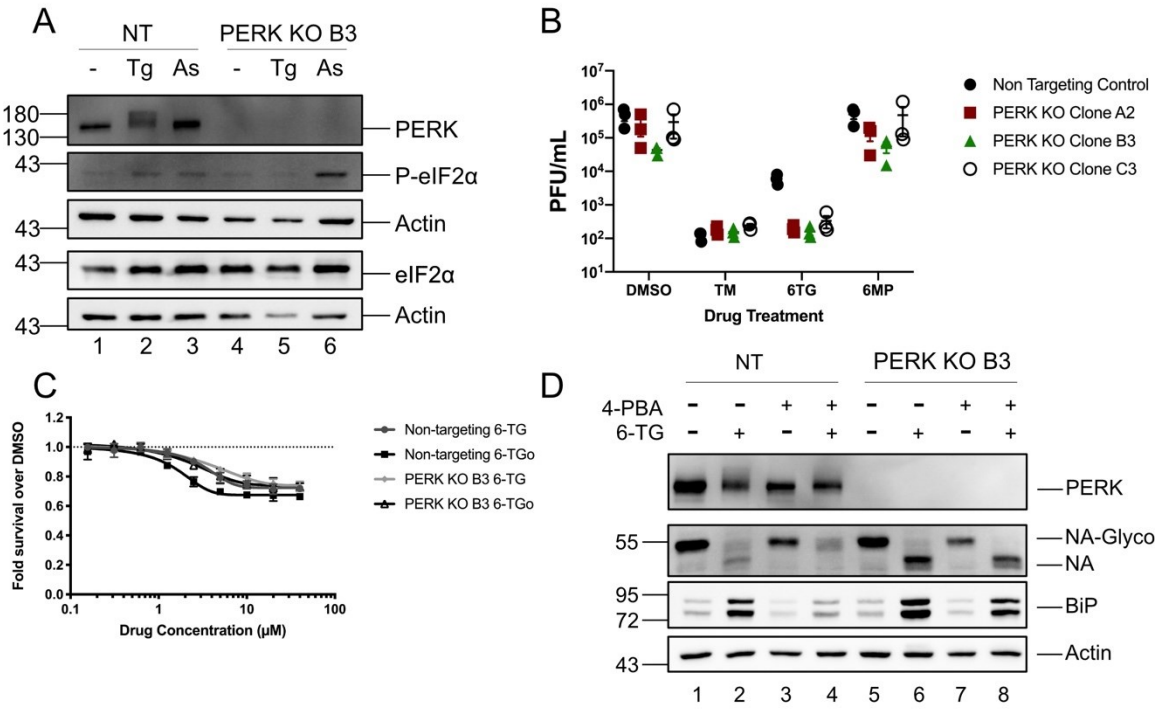

Figure 4.7: Knocking out of PERK enhances inhibition of viral replication by 6-TG. (A) Western blotting analysis of PERK KO cells (clone B3) and non-targeting control gRNA lentivirus-transduced cells (NT) treated with thapsigargin (Tg, 250nM) or sodium arsenite (As, 500μM). Lysates were collected 1 h post-treatment and analysed for PERK expression and activation, total and phosphorylated eIF2α. (B) A549 PERK KO cells (clones A2, B3, and C3) and the non-targeting control cell line were infected with PR8 at a MOI of 0.1 and were treated with the indicated compounds for 23 hours. Supernatant was collected at 24 hpi and viral progeny were quantified using a plaque assay. (C) A549 PERK KO clone B3 and the non-targeting control cells were treated with escalating doses of 6-TG, 6-TGo, or vehicle control for 23 hours and cell viability was measured using an alamarBlue assay. Relative fluorescence units were normalized to vehicle control. Error bars represent standard deviation (N=3). (D) Western blot analysis of PERK KO cells (Clone B3) and non-targeting control gRNA lentivirus-transduced cells (NT) infected PR8 at a MOI of 0.1 for 1 hour. Cells were washed and incubated with media containing 6-TG (10μM) and the chemical chaperone 4-PBA (10mM). Total protein was harvested at 24 hpi. Lysates were probed for PERK, viral NA, and BiP. Cellular actin was used as a loading control. This work is published in Slaine et al., 2021 and completed by Patrick Slaine and Dr. Khaperskyy

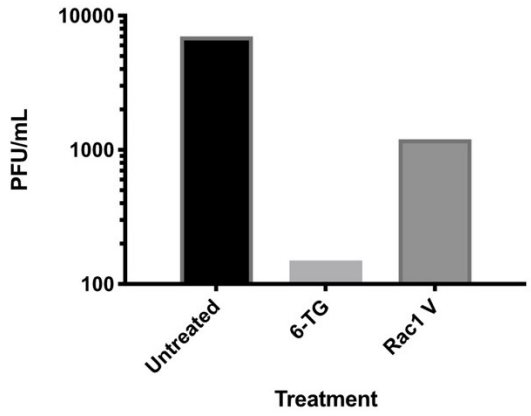

Figure 4.8: Rac1 inhibitor V may not be as effective as 6-TG at reducing viral titers. A549 cells were infected with PR8 at a MOI of 0.1 for 1 hour and infection media was replaced with media containing 6-TG (10μM) and Rac1 inhibitor V (25μM). Infectious progeny was enumerated using a plaque assay. Graphical data represents one biological replicate (N=1). This work was completed by Patrick Slaine and not published.

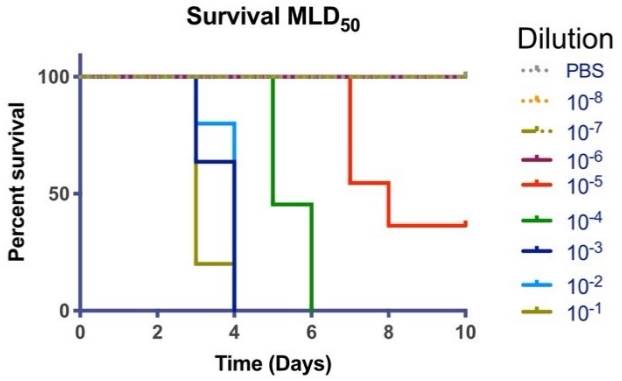

Figure 4.9: Determining the MLD_{50} of CA/07-MA.
(A) 5-week-old BALB/c mice were infected with serially diluted stock of CA/07-MA to determine the mean lethal dose 50 unit (MLD_{50}) of the stock virus. Mice were anesthetized with 5% isoflurane and infected with indicated serially diluted virus in 50µL 1xPBS. Mice were monitored for clinical manifestation of disease and euthanized if they crossed ethical endpoints, such as 20% reduction in body weight. Mice were monitored for 10 days before ending the experiment. Survival curves were graphed for each dilution. This work was completed by Patrick Slaine and not published.

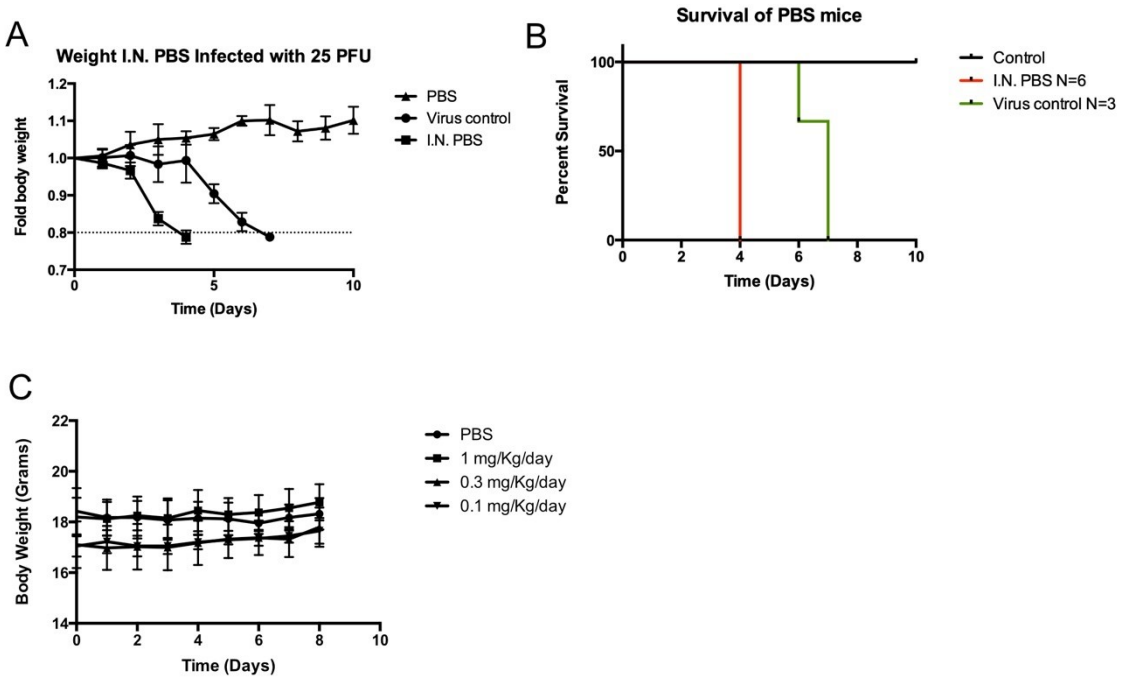

Figure 4.10: Testing the intranasal route of administration in infected mice and testing different concentrations of 6-TG intraperitoneal.
5-week-old BALB/c mice were infected with 5xMLD50 of CA/07-MA or mock infected with PBS and treated with intranasal (I.N.) PBS or not. Mice were monitored for clinical manifestation of disease and euthanized if they crossed ethical endpoints, such as 20% reduction in body weight. Mice were monitored for 10 days before ending the experiment. (A) Body weight was plotted as fold reduction over Day 0 weight. (B) The survival curve for each treatment group is plotted. (C) 5-week-old BALB/c mice were injected intraperitoneally (IP) with increasing doses of 6-TG or vehicle (PBS) and monitored for weight loss. Injections were made once daily on alternating sides. This work was completed by Patrick Slaine and not published.

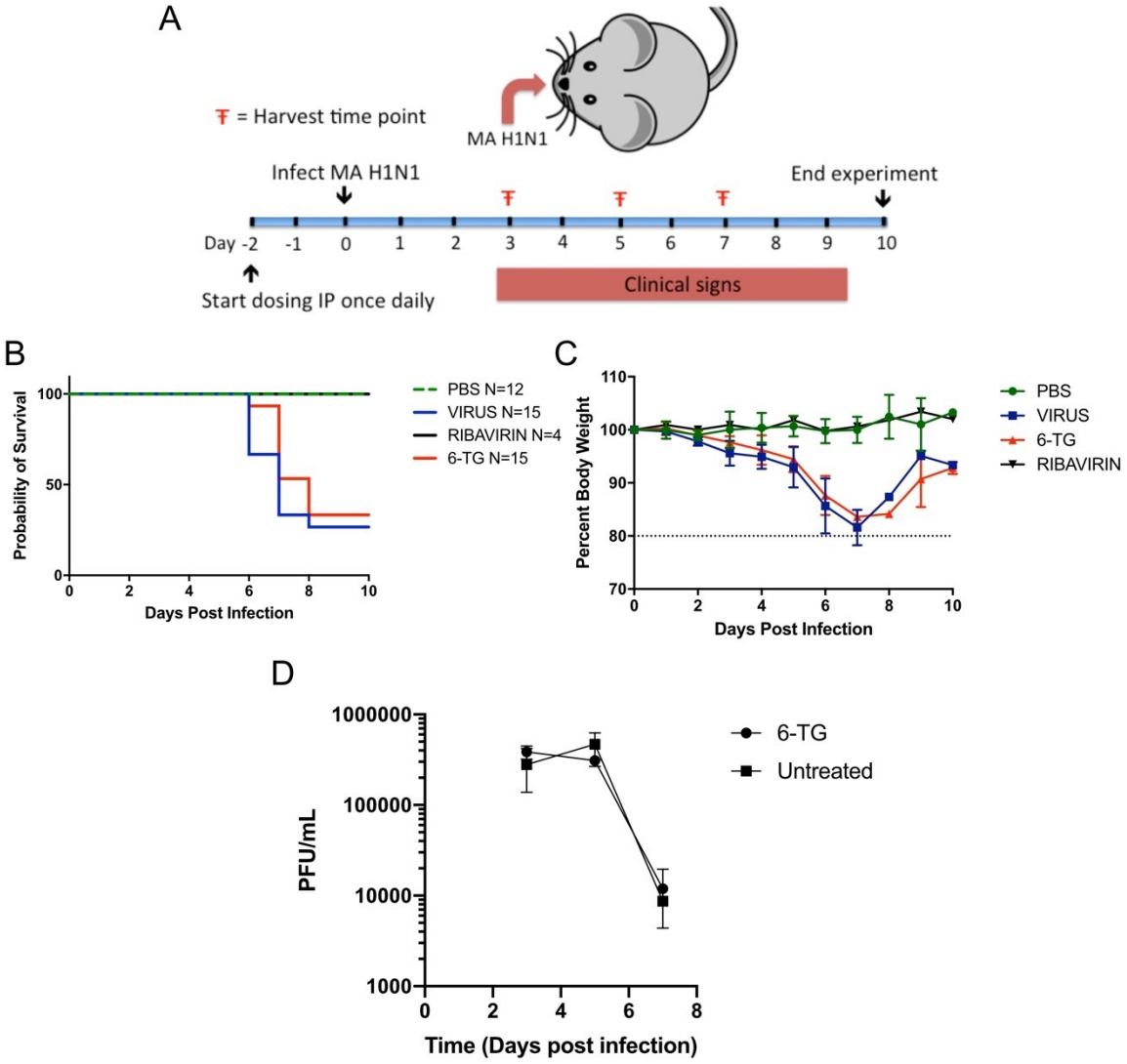

Figure 4.11: IP injection of 0.3 mg/kg 6-TG does not protect against a lethal dose of CA/07-MA.

(A) Illustration of the timeline the influenza challenge study. Dosing started 2 days prior to infection to mimic a prophylactic therapy, where they were dosed once daily until the end of the experiment. Mice were intranasally infected with 5xMLD50 units of CA/07-MA on day 0 and monitored for clinical signs until day 10. Samples were collected on day 3, 5, and 7 for analysis. (B) Survival curves of treated mice were plotted, graph shows sham infected (PBS) mice (N=12), infected mice treated with vehicle (PBS, N=15), infected mice treated with ribavirin (N=4), and infected mice treated with 6-TG (N=15). (C) Fold body weight was graphed over time of the infected mice indicated in (B). Horizontal dotted line indicated 20% body loss, the ethical end point for the infected mice. (D) Bronchoalveolar lavage fluid (BALF) was collected from two mice on day 3, 5, and 7 post euthanasia from each treatment group. Infectious viral progeny was enumerated from sterile filtered BALF with a plaque assay on MDCK cells. This work was completed by Patrick Slaine and not published.

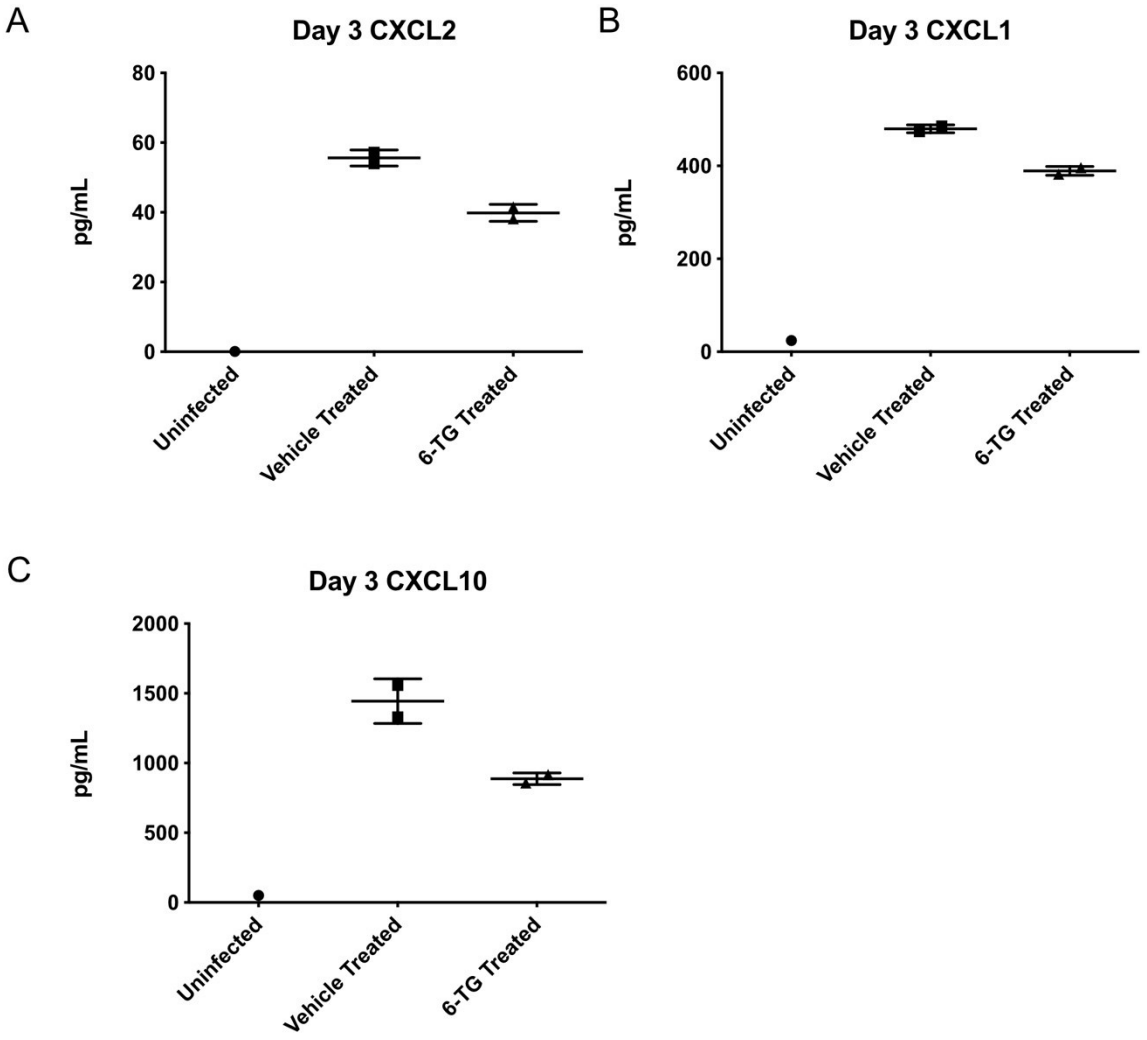

Figure 4.12: Multiplex ELISA from mouse BALF showed changes in 6-TG treated mice.

BALF was taken from 2 treated mice on day 3 and multiplexed for 36 different immune signalling molecules. Three signaling molecules were selected and graphed; (A) CXCL2, (B) CXCL1, and (C) CXCL10. Graphs represent two mice (N=2). This work was completed by Patrick Slaine and not published.

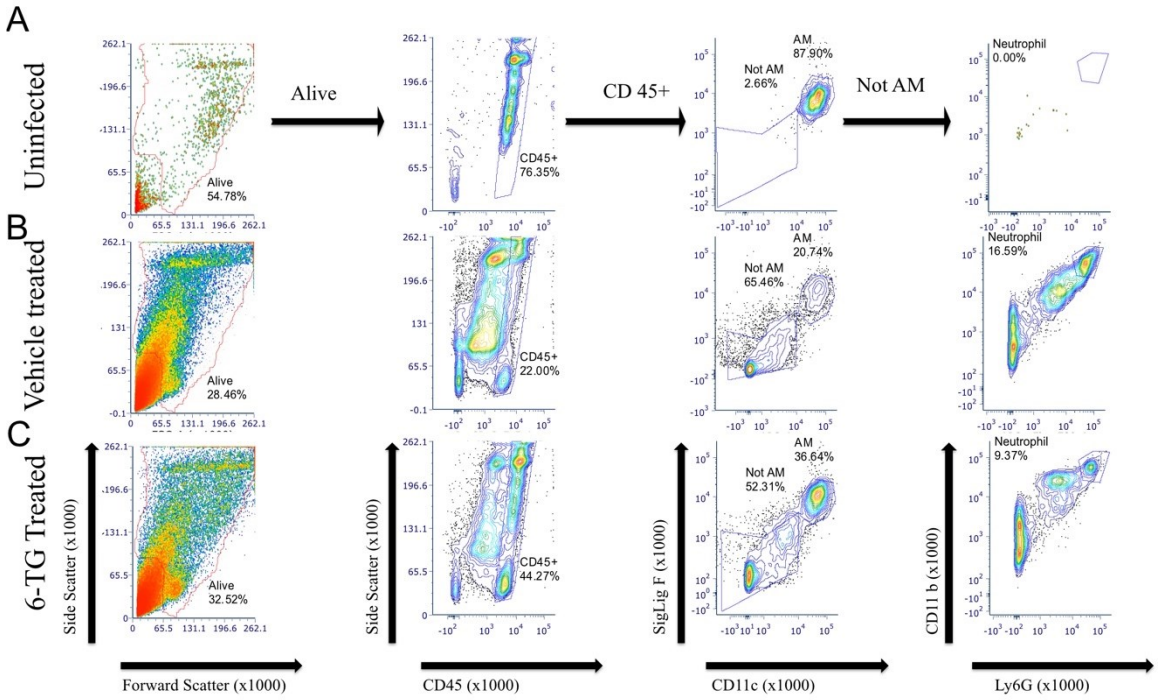

Figure 4.13: Representative flow cytometric analysis of immune cells found in the BALF of treated mice.

BALF was harvested from two mice in the (A) uninfected, (B) infected and vehicle treated, and (C) infected and treated with 6-TG on day 3. Lungs were washed postmortem on day 3 post-infection with PBS containing 0.5% Bovine Serum Albumin (BSA) to obtain infiltrating immune cells. Cells were stained and analyzed using FCS Express 6™. Cells were stained for CD45 (PerCP Cy5-5-A), CD11c (APC A), CD11b (FITC A), SigLig F (PE A), and Ly6G (APC eFluor 780) and data collected using a BD LSR Fortessa instrument. Cells were gated left to right on alive, CD45+ cells, and not alveolar macrophages (not AM). Percentages are shown as total hits within the gate. This work was completed by Patrick Slaine and not published.

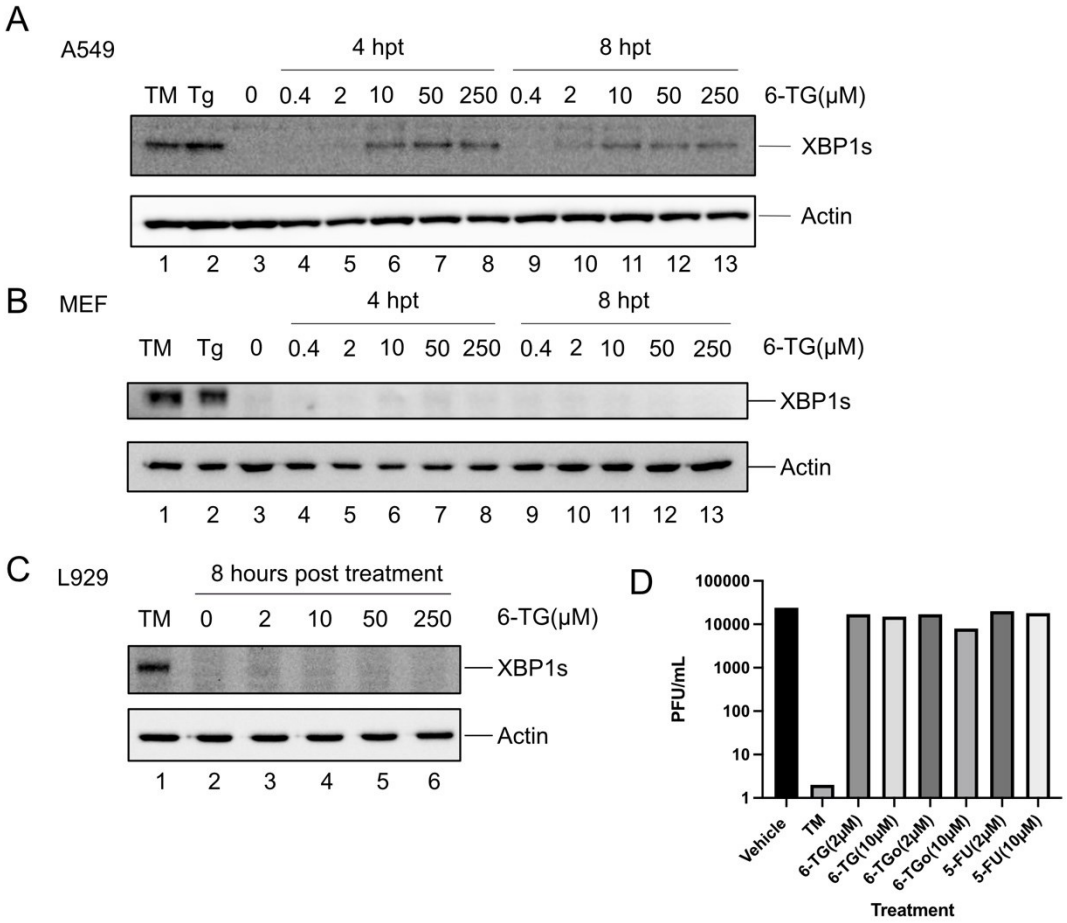

Figure 4.14: 6-TG fails to induce the UPR in murine cells and fails to reduce virus production from infected mouse cells.
(A) Human lung adenocarcinoma (A549), (B) Mouse embryo fibroblast (MEF), and (C) mouse L929 cells were treated with increasing concentrations of 6-TG and harvested at 4 and 8 hours post treatment. Cells were also treated with tunicamycin (TM) and thapsigargin (Tg) to induce the UPR. After incubating for the indicated amount of time, total protein was harvested and probed for XBP1s. Cellular actin was used as a loading control. (D) MEF cells were infected with PR8 for 1 hour at a MOI of 0.1 and treated with the indicated compounds for 23 hours. Supernatant was harvested at 24 hpi to enumerate infectious progeny with a plaque assay. This work was completed by Patrick Slaine and not published.

CHAPTER 5: ANALYSIS OF ADAPTIVE MUTATIONS FOUND IN THE INFLUENZA A VIRUS POLYMERASE SUBUNITS

5.1 Introduction

The 1918 H1N1 pandemic is one of the most impactful events in human history. The outbreak caused millions of deaths worldwide and was a significant catalyst that initiated intense scientific investigation into pathogens. This pandemic was marked by three waves with high infection rates and mortality. The first wave occurred in the summer of 1918, the second in the autumn, and the third in the middle of the winter. The second wave showed the highest rates of infection and the highest mortality. Numerous factors might have been responsible for the severity of the second wave, including the potential adaptation of the virus to humans. Retrospective studies have confirmed that the second wave had the highest absolute mortality when controlling for other variables (Pearce et al., 2011). Interestingly, the third wave was less deadly than the second. It is thought that the virus became less virulent over the course of the pandemic. A decrease of virulence explains the reduced mortality seen in areas that were affected significantly later in the pandemic (Pearce et al., 2011). The virus continued to circulate worldwide after the pandemic with significantly decreased mortality rates. Although the exact details of the origin of the 1918 virus remain unknown, it is widely accepted that H1N1 entered the human population through a zoonotic event from an avian origin (Barry, 2004; Reid et al., 1999).

Understanding the barriers that limit zoonotic transmission of IAV is critical for the implementation of appropriate pandemic prevention strategies. Currently, the mouse

infection model provides a platform to investigate the adaptations of IAV to a new host in a controlled setting. Initial adaptation to a new host typically improves viral replication, increasing viral load and virulence. Host adaptation in controlled laboratory settings promotes the accumulation of mutations that increase the replicative fitness of the virus. By contrast, natural infections are more restricted by transmission. Accordingly, in natural setting the virus is both selected for replicative fitness and transmissibility. This may result in viruses that are less virulent but more transmissible (Ghafari et al., 2020).

IAV genomes exist in a constant state of flux, accumulating a cloud of genotypes known as quasispecies (Bull et al., 2005). There are several factors that increase IAV genomic diversity. The first variable is the segmented nature of the IAV genome, which enables reassortment of genome segments between genetically distinct viruses. Genetic reassortment requires one cell to be infected with the two distinct viruses to enable the production of viruses with distinct hybrid genomes. However, reassortment is limited by intersegment RNA-RNA interactions during packaging and within the virion (Dadonaite et al., 2019; Phipps et al., 2017). The creation of new viruses with hybrid genomes is termed antigenic shift. The second origin of IAV genomic diversity is the high error rate of the viral polymerase, which has a mutation rate of $1.8x10^{-4}$ s/s/r, leading to 2-3 nucleotide mutations each time the genome is copied (Pauly et al., 2017). The accumulation of mutations over time that changes the antigenic properties of viral proteins is termed antigenic drift. Most mutations are detrimental to viral replication. Some of these mutations destroy critical functions of viral proteins, rendering the mutant virus unfit. By contrast, some mutations provide an advantage that allows them to outcompete other genotypes and become fixed in the population (Belshaw et al., 2011;

Visher et al., 2016). The high error rate of the polymerase aids viral replication, with higher fidelity polymerase mutants showing a marked reduction in viral fitness in cell culture (Cheung et al., 2014). Beneficial mutations may increase viral polymerase activity, confer resistance to antiviral drugs, improve transmission between hosts, expand host tropism, evade adaptive and innate immune responses, evade host restriction factors, or improve utilization of host factors (Forbes et al., 2012; Gu et al., 2019; Koelle et al., 2006; Rambaut et al., 2008).

Mice are inexpensive models for IAV adaptation studies with a large diversity of available reagents and tools available to study the virus in this model. Decades of mouse model research has yielded countless antibodies against mouse target proteins, numerous gene knockout mouse lines, extensive anatomical knowledge, and well-established protocols in mouse husbandry. Mice are not a natural reservoir species for IAV and are not readily infected by this virus. When mice are infected with clinical isolates of IAV, they typically are asymptomatic during the course of viral replication (Hirst, 1947). The virus still replicates in the upper and lower respiratory tracts of the mice in asymptomatic infections. Meanwhile, mice infected with an adapted virus display morbidity with similar pathological consequences seen in human infection (Sweet & Smith, 1980).

There are numerous adaptation mutations required for the virus to replicate efficiently in the mouse lung. Mouse adaptation mutations have been identified in many viral proteins, and most frequently in HA (Brown, 1990; L. Xu et al., 2011; Zheng et al., 2010). HA binds to sialic acid (N-acetyl neuraminic acid) receptor on the cell surface to initiate receptor-mediated endocytosis. Sialic acid is linked to galactose through an α-2,3 or α-2,6 bond, which is found on oligosaccharide modifications on glycoproteins (L. Xu

et al., 2011). Human IAV preferentially binds to terminal α-2,6-linked sialic acid residues found on mature glycoproteins on the plasma membrane, whereas avian IAV preferentially binds α-2,3-linked sialic acid linkages. α-2,6 sialic acid is predominantly found in the upper respiratory tract (nasopharyngeal cavity) of humans, while α-2,3 sialic acid is primarily in the lower respiratory tract (bronchi, alveoli). Infection of the upper respiratory tract enables transmission of virus between individuals through contact and respiratory secretions. As IAV only infects individuals for a short period of time, IAV must maintain transmission between infected individuals and therefore maintains α-2,6 sialic acid tropism. For the virus to infect and maintain transmission in an organism, IAV receptor affinity must be compatible with the host. The mouse lung does not contain α-2,6-linked sialic acid modifications; therefore most adaptations in HA change the receptor preference to the highly abundant α-2,3 sialic acid linkage (Ibricevic et al., 2006). Several mouse adaptation studies have identified the D222G substitution in the receptor binding domain (RBD) of HA (L. Xu et al., 2011; Zheng et al., 2010). Avian IAVs occasionally enter the human population where they can cause severe disease. These avian viruses fail to establish human-to-human transmission because they do not replicate to high levels in the upper respiratory tract and subsequent release and transmission. Avian IAVs must acquire mutations to adapt to the human α-2,6 sialic acid linkages to establish human-to-human transmission (Herfst et al., 2012).

Further host adaptation mutations are required in the viral polymerase to overcome barriers between hosts. Polymerases from avian IAVs struggle to synthesize RNA in mammalian cells because of species differences in acidic nuclear phosphoprotein 32A (ANP32A). ANP32A is an essential host factor for viral polymerase function. Avian

IAVs generally harbor a glutamic acid at the 627th amino acid of PB2 (PB2 E627) that restricts polymerase activity in human cell lines, with the E627K mutation conferring high rates of polymerase activity in human cells (C. W. Davis et al., 2020; Ek et al., 1993; J. Li et al., 2009). ANP32A has been identified in recent crystal structures of influenza polymerase heterodimers, identifying it as a scaffold for the formation of heterodimeric polymerase complexes (Carrique et al., 2020). PB2 K627 is able to utilize mammalian ANP32A during viral replication, whereas PB2 E627 utilizes avian ANP32A. Therefore, the E627K substitution is critical for the adaptation of avian IAV to mammals (Mehle & Doudna, 2009). The E627K mutation has been recently identified in human H5N1 isolates, indicating rapid adaptation to the human lung (Welkers et al., 2019). These studies show that the viral polymerase as an adaptation hotspot, harbouring mutations involved in the zoonosis of influenza viruses.

Cara MacRae, an honours student from Dr. Todd Hatchette's lab (Dalhousie University), passaged a clinical isolate from the H1N1 swine flu outbreak in 2009, A/California/07/2009 (H1N1) (CA/07), in Swiss-Webster mice 10 times to adapt the virus to optimally infect the mouse (Slaine et al., 2018). The initial cohort of mice were infected with $2x10^3$ $TCID_{50}$ units of CA/07 in 50 µL of PBS. The lungs were harvested from infected mice on 3 dpi, homogenized, and used to infect a new cohort of mice. This was repeated 10 times before the virus was analyzed for adaptation mutations. Serial passaging is a well-established technique for adapting viruses to a new host (Herfst et al., 2012; Sutton et al., 2014). Serial passaging IAV in mice is required for adaptation, and experiments typically range between 5 and 10 passages (Guo et al., 2020, p. 2; Ilyushina et al., 2010; Matsuoka et al., 2009). During passaging, virus is harvested from the mouse

lung at 3 dpi and used to intranasally infect the next cohort of mice. This artificially selects for the most replication fit virus bypassing transmission. Mice lost significantly more weight by passage 10 compared to the first passage (Fig 5.1A) (Slaine et al., 2018). Cara analyzed the $TCID_{50}$ from lung homogenates over the ten passages and saw a marked increase in viral replication at passage 7 and furthermore another spike in viral replication at passage 9 (Fig 1B). The adaptation of IAV to mice can also change its tissue tropism, which can contribute to pathogenesis. For example, viral antigens were previously identified in the olfactory bulb in the central nervous system (CNS) in mice infected with mouse-adapted virus (Leyva-Grado et al., 2009). In these experiments, IAV likely entered the CNS through retrograde transport through olfactory neurons found in the nasal passage (Reinacher et al., 1983; Sun et al., 2010). Accordingly, Cara harvested infectious virus from brain homogenates (Fig 1C), which indicated that CA/07-MA disseminated into the mouse brain. In Chapter 4, I calculated the MLD_{50} of CA/07-MA to be ~3 infectious virions to lethally infect a mouse. Previous work showed that the parental CA/07 virus had an MLD_{50} of ~$2x10^6$ PFU (Zheng et al., 2010). This indicates that the CA/07-MA virus is ~$6x10^5$ times more lethal in mice than its parental virus, which is consistent with the idea that laboratory adaptation increases virulence in model organisms.

In this chapter, I characterized the A/California/07/2009 (H1N1)-mouse adapted (CA/07-MA) genome to identify adaptive mutations and determine their molecular contribution to adaptation. The work in this chapter was published in the peer reviewed journal "Viruses" and some experiments from that publication were performed by other members of the McCormick lab (Slaine et al., 2018). Dr. Denys Khaperskyy and Mariel

Kleer performed several experiments, and their experiments will be examined in the discussion. I identified all mutations present in CA/07-MA using the Illumina sequencing platform. Deep sequencing the virus allowed unbiased characterization of viral quasispecies. I then further analyzed the location and effects of the mutations on viral proteins. I identified novel host adaptation mutations in the viral polymerase and described their effects on viral replication. Identification of host adaptation mutations may lay the groundwork to identify new host-pathogen interactions.

5.2 Results

5.2.1 Swiss-Webster Mice Lack Functional Mx1

Inbred mice often have deletions in the Mx1 gene, which is a potent antiviral restriction factor that is upregulated by interferon. The deletions typically remove large sections of the Mx1 ORF rendering the protein non-functional. Mx1 is a large GTPase that protects the host against numerous infections including IAV (Haller & Kochs, 2020). Mice harbouring Mx1 survive viral infections that would otherwise be lethal to mice lacking Mx1 (Grimm et al., 2007). I characterized the Mx1 allele of Swiss-Webster mice by sequencing the Mx1 transcript. Total RNA was isolated from lung homogenates on day 3 that were infected with passage 10 CA/07-MA and from MEFs. cDNA libraries were generated using an oligo(dT) primer, which converts all mRNA to cDNA. Mx1 mRNA was amplified using a PCR with gene specific primers using the MEF cDNA library as a template. PCR products from the lung homogenate and MEFs were resolved on an agarose gel (Fig 5.2A). The PCR product was then submitted for Sanger sequencing to determine the nucleotide sequence. Sequence alignment shows that Swiss-

Webster mice have a ~500 bp deletion in the middle of the Mx1 ORF on one chromosome, while the second chromosome contains a ~440 bp deletion in a similar location (Fig 5.2A). Both deletions change the reading frame after the junction. The new reading frame changes all downstream amino acids and results in a stop codon just a few amino acids away from the junction, effectively destroying Mx1 function. These data indicate that Swiss-Webster mice are deficient in the restriction factor Mx1.

5.2.2 Utilizing the Illumina MiSeq Platform for Deep Sequencing

I used Illumina MiSeq to analyze CA/07 and CA/07-MA quasispecies. MiSeq can generate up to 25 million reads that range in 150-300 bp. The advantage of deep sequencing is the extensive coverage of the genome by sequencing the cDNA library numerous times. Because of this, next-generation sequencing captures the entire genetic cloud of IAV quasispecies. However, deep sequencing struggles to obtain high coverage of the very 5' and 3' ends of the amplicon. To combat this, I developed primers to amplify all eight genomic segments of IAV that also contain the P5 and P7 Illumina adaptors. Since the IAV genome is negative sense RNA, it must be converted to cDNA before I can analyze or manipulate the sequence.

My forward primer contained the P5 Illumina adaptor and Uni12 sequences whereas the reverse primer harboured the P7 Illumina adaptor and Uni13 sequences (table 5.1).

Viral cDNA was synthesized using the Uni12 primer from total RNA from infected cells. cDNA was then amplified with the unique forward and reverse primers to amplify all 8 segments at once, while the primers attached the P5 and P7 adaptors on the

5’ and 3’ ends respectively. PCR can preferentially amplify shorter strands of DNA during the reaction. The PCR was only run for 10 cycles to prevent the shorter segments and potential artefacts from being amplified during the extension period of the PCR. PCR products were then purified using the Qiagen PCR purification kit, quantified, and submitted to the Integrated Microbiome Resource (IMR) for Illumina MiSeq analysis. I visualized the multi-segment amplification PCR product from CA/07-MA on an agarose gel to analyze the products of the different segments (Fig 5.3). cDNA copies of all 8 genome segments were amplified, but some were amplified poorly. Interestingly, numerous cDNA species were amplified that were smaller than any genomic segment (<890 bp).

5.2.3 Deep Sequencing of the Mouse Adapted Viruses Identified Unique Mutations

I used the Illumina MiSeq platform (San Diego, CA, USA) to deep sequence CA/07 and CA/07-MA to identify and quantify adaptive mutations. My sequencing pipeline used modified primers to cover the 5’ and 3’ ends of the genome which contains the untranslated regions (UTRs) and packaging sequences. Similar to Sanger sequencing, the very 5’ and 3’ ends of an Illumina read have a low degree of confidence when calling a specific nucleotide. Current bioinformatic programs automatically trim back the 5’ and 3’ ends until the chromatogram yields a high degree of confidence identifying the nucleotide. The Illumina reads were trimmed for quality control with a Q score of 30, meaning that any read below a 99.9% confidence interval was removed from the analysis. After trimming, forward and reverse sequences were paired and aligned to each segment

of the reference genome individually. Illumina reads from the parental virus was aligned to the reference sequences available for CA/07 from GenBank. The parental virus had in total 1,125,945 reads aligned across the 8 different genomic segments. CA/07 genome is 13,635 bp in total, which gave an average coverage of 10,194 reads/base. Numerous nucleotides were different in my parental CA/07 compared to GenBank's reference sequence. The MA virus had in total 926,042 reads aligned across the 8 different segments, for an average coverage of 9,680 reads/base. A fraction of reads could not be aligned from both viruses due to low/no sequence homology. I compiled the sequences from CA/07 to generate new consensus sequences which served as a reference for the CA/07-MA virus. Several segments were not equally amplified during the PCR step, resulting in them having lower read coverage than other segments such as the PA segment. These data complement the agarose gel analyzing the PCR products. Even with the under representation of PA within the viral population, the average coverage is well over 1,000 reads providing high-confidence assessment of the identity and frequency of each adaptive mutation (Table 5.2).

5.2.4 CA/07-MA Virus Displayed Differential Junction Sites and Read Coverage Compared to Parental CA/07

During viral replication, only 2-30% of viral progeny are replication competent, whereas the majority of new viral particles are semi-infectious particles (SIP) or defective interfering (DI) particles (Brooke, 2017). SIPs are created from the failure to fully package all 8 genome segments; SIPs are only replication competent if they are complemented by another viral particle that is fully infectious or provides the missing

genome segments *in trans* to support viral replication. Approximately 90% of viral particles are unable to initiate multi-cycle infections (Brooke et al., 2013). SIP production is thought to be universal across all IAV infections and is minimally affected by host factors. Accordingly, SIPs are observed across different cell lines, animal models, and their creation is independent of MOI.

DI particles were first discovered 60 years ago as a product of passaging virus at a high MOI. Like SIPs, DI particles require coinfection with fully infectious particles to propagate themselves. DI particle coinfections interfere with the replication cycle of the fully infectious virion, essentially parasitizing the replication of the fully infectious virus. DI particles contain defective viral genomes (DVGs) that have large internal deletions in one or more of the viral segments but retain 5' and 3' packaging sequences (A. R. Davis et al., 1980). The internally deleted genome segments can outcompete their full-length genomic segment counterparts during cRNA and vRNA synthesis. The rapid production of the shorter genome segments can produce higher number of DVGs, which can overcome the number of full-length segments. DVGs also interfere with segment packaging during budding (Odagiri & Tashiro, 1997). DI particles are generated during both *in vitro* and *in vivo* infection (Saira et al., 2013). Illumina sequencing identifies the location and frequency of deletions in genome segments, allowing me to enumerate DVGs in prepared cDNA libraries.

I quantified the DI particles present in both virus stocks. Numerous Illumina sequencing reads spanned junctions of DVGs, which generate DI particles if they are incorporated into a budding virion (Brooke, 2017; Nj et al., 2008). DI particles can be quantified through deep-sequencing viral stocks or total RNA from infected cells. I

aligned Illumina reads to the consensus sequence to identify and quantify DI particles in the viral population. The reads covered the 5' and 3' sequences, spanning the junctions where the internal sequences were deleted. I quantified the DI particle population in both the parental CA/07 and CA/07-MA virus populations. I enumerated the number of reads that spanned these deletion junctions, with reads aligning to 5' and 3' sequences (Table 5.3). Interestingly, CA/07-MA had more reads span the DVG junctions than the parental CA/07 virus. The majority of DVGs for both viruses were identified in the first three segments, with PB2 having the highest number of DVG junction-spanning reads. I mapped all the detected deletions on the 5' and 3' junctions are for both CA/07 and CA/07-MA on the viral polymerase segments (Fig 5.4). I selected the polymerase segments since the majority of DVGs originate from the first three segments. Interestingly, The CA/07-MA virus showed unique junctions compared to parental CA/07.

5.2.5 Identification and Quantification of Adaptive Mutations in CA/07-MA

Numerous mutations were identified and quantified that were above 1% abundant in CA/07-MA when compared to parental CA/07 consensus sequence (Table 5.4). Several mutations were also identified between the parental virus and the reference sequence, this is likely from genetic drift and the adaptation to cell culture conditions. No mutations were identified in the 5' and 3' UTRs or in the packaging sequences of either viruses. I found a significant number of mutations when I compared CA/07-MA to CA/07, almost all of which were roughly 1% abundant. I found four synonymous

mutations in CA/07-MA that did not alter the predicted primary amino acid sequence that were above 50% abundance in the population. Two were found in PB1, one in M, and one in NS. By definition, these synonymous mutations do not change the sequence of the protein. The effect of these mutations on viral adaptation is difficult to assess due to their subtle effects. Hypothetically, these synonymous mutations may have arisen through codon optimization to the murine tRNA pool. The adaptation to the new host's tRNA pool has been demonstrated previously (Luo et al., 2020; Wong et al., 2010). These synonymous mutations may also have effects on viral RNA secondary structure, metabolism, and innate sensing.

I identified 11 non-synonymous mutations that were greater than 25% abundant in the population. Illumina MiSeq, unlike Sanger sequencing, allowed me to quantify mutations that were less prevalent, allowing me to confidently identify mutations that were at 1% or greater abundance. I identified mutations in PB1, HA, NA, and M segments that were less than 50% abundant in the population. Mutations that exist at lower frequencies contribute to the quasispecies of the virus and may have a functional role during replication. However, the drawback of using Illumina MiSeq is that reads are on average 150 bp in length, preventing me from determining whether these mutations exist together on the same RNA species, or exist independently.

Five mutations existed at 50% or greater abundance in the viral population. Of these five non-synonymous mutations, three resided in HA (N156D, S183P, and D222G) while the other two were found in PA (E18G and E349G). The amino acid sequence of HA is annotated without the signal peptide, which is 17 amino acids long. The D222G substitution resided in the RBD, which was previously identified in other mouse-adapted

viruses (Belser, Jayaraman, et al., 2011; Ilyushina et al., 2010; L. Xu et al., 2010; Zheng et al., 2010). Here, the authors note that the parental strain had an MLD_{50}=$2x10^6$ PFU, while the virus harbouring just the D222G substitution had an MLD_{50}=150 PFU (Zheng et al., 2010). The authors of this study demonstrated that D222 showed preference for α-2,6 sialic acid, while G222 showed similar preference for α-2,3 and α-2,6 sialic acid linkages (Belser, Jayaraman, et al., 2011). The mouse lung only contains α-2,3 sialic acid linkages, providing strong selection on the D222G substitution.

The other two substitutions that I identified in HA were not as well studied, and their consequence on receptor binding and fusogenic properties remain unknown. The S183P substitution was identified in a previous study with mouse-adapted CA/04 (Ilyushina et al., 2010). Ilyushina and coauthors noted an increased affinity for α-2,3 sialic acid linkages and a decreased affinity for α-2,6 sialic acid linkages in the mouse-adapted HA. However, the HA also harboured the D222G substitution, and the authors did not investigate S183P alone. Because of this, it is difficult to ascertain the exact role of S183P has on receptor affinity and subsequent host adaptation.

The HA N156D substitution identified in this experiment is unique to this study, and its effect on receptor binding or fusion is unknown. The rapid fixation of these mutations over the 10 passages indicates an evolutionary advantage compared to wild-type sequences. Because the HA substitutions that arose during mouse adaptation have been intensively studied, I decided to focus on the substitutions in the polymerase subunits.

I identified four mutations in viral polymerase subunits PA and PB1 that had higher than 25% frequency in the mouse adapted virus population. The PA segment had

two mutations that resulted in E18G and E349G amino acid substitutions. Both mutations reached over 99% abundance in read frequency, showing complete fixation of the mutation in 10 passages, which indicated a strong evolutionary pressure on these sites. Interestingly, the parental virus also had the E18G substitution, but at ~10% abundance in the population. The PB1 segment had two mutations that resulted in T156A and F740L amino acid substitutions that were 36% and 49.9% prevalent, respectively (Fig 5.5). The E349G substitution has previously been identified in both A/Puerto Rico/8/1934 (H1N1) and A/chicken/Hubei/01/1999 (H9N2) (Rolling et al., 2009; Z. Zhang et al., 2011). In both viruses, the polymerase mutation enhanced virulence in mice.

5.2.6 All Identified Adaptation Mutations on the RdRp are Surface Exposed in Viral RdRp

To further investigate the mutations identified in the viral polymerase complex, I mapped all four substitutions to, at the time, the only available 3D crystal structure of the IAV ternary complex (Pflug et al., 2014). Mapping the substitutions identified in this study onto the bat influenza A/little yellow-shouldered bat/Guatemala/060/2010 (H17N10) bound to an RNA primer (Protein accession number: 4WSB) allowed me to visualize whether the amino acids were found on the surface of the protein, interacting with another subunit of the viral polymerase, or if they were buried in the ternary complex. All four mutations were exposed at the surface of the protein complex. The two PB1 substitutions were distant in primary amino acid sequence, but close in proximity in the 3D crystal structure and close to the PA interface. The F740L mutation was in the C-terminal PB2 interacting domain of PB1. The F740L mutation made direct contact with

the PA endoribonuclease domain in the crystal structure. Illumina MiSeq generates short reads that prevented me from identifying whether the T156A and F740L mutation exist together *in cis*, or if the mutations are independent of each other. The two mutations may work in concert with each other on one molecule of PB1 but determining this would require longer sequencing reads. The two mutations identified in PA were fixed in the population at 99% abundance, ensuring that both mutations are present on each molecule. The PA E18G substitution was located in the N-terminus of the protein and is close to the PB1 T156A substitution in the 3D crystal structure. The E349G substitution in PA is surface-exposed and is not close to interacting with the other subunits of the viral polymerase (Fig 5.6). Further crystal structures have been generated recently for A/NT/60/1968 (H3N2) (Fan et al., 2019). I analyzed the localization of the four substitutions identified in this study and all show identical localization as the bat influenza trimeric complex analyzed in Figure 6.

5.2.7 Generation the Infectious Clone of CA/07

I generated the infectious clone of CA/07 using the pHW2000 reverse genetics system. IAV has a negative sense RNA genome, which cannot directly generate infectious progeny from a DNA vector. I generated cDNA libraries of all eight segments using the Uni12 primer for the reverse transcription reaction. Each segment was individually PCR-amplified from the cDNA library using segment specific primers that contained BsmBI or BsaI restriction sites. BsmBI and BsaI restriction enzymes are used in a scar-free cloning technique commonly referred to as “Golden Gate” cloning (Engler et al., 2009). Both BsmBI and BsaI are type IIS restriction enzymes that recognize non-

palindromic DNA sequences and cleave several nucleotides beyond the recognition sequence, enabling directional cutting outside of the restriction site that allows scar-free cleavage and directional insertion into the pHW2000 vector (E. Hoffmann et al., 2000). The inserted viral cDNA is flanked by an RNA polymerase I (Pol I) promoter that generates the negative sense genome segment of IAV that contains a 5' triphosphate. The pHW2000 plasmid also contains RNA polymerase II (Pol II) promoter on the opposite flank of the viral cDNA to create positive sense viral mRNA, encoding the protein on that segment. Viral ribonucleoproteins NP, PA, PB1, and PB2 are then translated from the mRNA, which translocate to the nucleus and complex with the negative sense RNA generated by the Pol I promoter (E. Hoffmann et al., 2000). The vRNP then further initiates transcription from the negative segments. The genome then undergoes replication and the genomic segments along with viral proteins are packaged into budding virions, resulting in the creation of recombinant infectious progeny.

5.2.8 Generation of Mouse Adaptation Mutations in PA and PB1 Using Site Directed Mutagenesis

The construction of the infectious clone of the parental CA/07 virus allowed me to study specific amino acid substitutions in the viral polymerase complex. I was able to introduce each individual substitution, or paired substitutions, into the coding sequence. This allowed me to assay the polymerase activity through a minigenome replicon, or rescue virus harbouring the specific mutations for further testing. The parental CA/07 virus had the E18G mutation present at 9.9% abundance in its population. Interestingly, GenBank's reference sequence (NC_026437) for the PA segment had this amino acid

annotated as X, indicating that this site was likely variable during the initial sequencing of the viral isolate. This could be due to the adaptation of the reference strain to cell culture or egg adaptation. When I cloned the PA segment from cDNA generated from parental CA/07, the PA segment contained the E18G substitution. Since the parental strain was heterogeneous at this site, I decided to use the G18 variant for all future experiments. The E349G mutation was substituted into PA, and each PB1 mutation was introduced into individual constructs and one construct was generated that harboured both the PB1 T156A and F740L mutations.

5.2.9 PA E349G Enhanced Viral Polymerase Activity in the Minigenome Replicon Assay

I used the firefly luciferase minireplicon assay in human HEK 293T and mouse L929 cells to determine the effects of adaptation substitutions on polymerase activity. This assay quantifies the amplification and expression of a reporter by the polymerase proteins in a model cell line. The assay required transfection of 6 plasmids into one cell. The first four plasmids expressed the mRNA for the three viral polymerase subunits and NP. The fifth generated a negative sense RNA that encodes the luciferase enzyme on its positive sense mRNA. The reporter, pPol I-WSN-NA-*firefly*-luciferase, contained the 3' and 5' sequences from the NA segment originating from A/WSN/34 (H1N1), which is expressed from the plasmid using host RNA polymerase I. The RNA Pol I promoter generated a viral-like RNA that mimics the 5' end a viral genome segment, while the 3' end is generated by a Pol I terminator sequence (Te Velthuis et al., 2018). The NA ORF has been replaced by an ORF encoding luciferase. This transcript is negative sense to the

mRNA and contained a 5’ triphosphate (Pleschka et al., 1996). The viral polymerase recognized this negative sense transcript and synthesized the positive sense mRNA that harbours a 5’ cap. This mRNA is then translated by host ribosomes and produces luciferase. Luciferase then catalyzed a light producing reaction using luciferin substrate. The release of light was quantified by a spectrophotometer. The last plasmid encoded the Renilla luciferase that acted as a transfection control that is expressed independent of viral polymerase activity (Te Velthuis et al., 2018).

I first tested the minigenome replicon in human HEK 293T cells. The minigenome replicon creates the negative sense RNA of the luciferase reporter that complexes with viral polymerase subunits to form vRNPs. The polymerase replicates the luciferase RNA as it directly mimics vRNA and expresses luciferase as an mRNA. Adaptation substitutions in the polymerase complex can increase the polymerase activity, which directly correlates with higher expression of luciferase, which in turn can be quantified. Constructs harbouring the mouse adaptation mutations were normalized to the parental wild-type constructs. The PB1 T156A and F740L substitutions had no effect on viral polymerase activity when introduced alone, or together when compared to the parental polymerase. Interestingly, all reactions harbouring the PA E349G mutation showed an increase of viral polymerase activity by 2 to 3-fold (Fig 7B). I then tested the effect of polymerase mutations in the murine L929 (L) cell line to determine whether the polymerase substitutions have species-specific effects on RdRp activity. The mouse RNA Pol I promoter for murine species is significantly different to the human Pol I promoter, accordingly I used the pHL-NS-FF-Luc reporter construct to quantify viral polymerase in the murine cells. Here, firefly luciferase is flanked by the 5’ and 3’ sequences from the

NS segment from WSN and its expression is driven by a murine Pol I promoter. Like human HEK 293T cells, the PB1 T156A and F740L substitutions did not increase viral polymerase activity in the murine cell line. In the mouse cells, the E349G constructs increased viral polymerase function by 4 to 10-fold (Fig 5.7C).

I then harvested total protein from transfected cells to analyze viral proteins to ensure that the adaptation mutations did not affect the translation of viral proteins. All constructs analyzed in this experiment did not significantly increase viral protein accumulation in 293T cells (Fig 5.7D).

The PA E349G substitution significantly enhanced viral polymerase activity in both mammalian and murine cell lines, while the PB1 mutations had little effect. Thus, the true effects of the PB1 substitutions remain unknown, with potential effects being missed by the minigenome assay. The PB1 mutations may still modulate polymerase function or viral replication *in vivo*.

5.2.10 Recombinant Virus Harbouring the Polymerase Adaptation Mutations in PB1 and PA Replicated Efficiently in Mouse Cells

There are numerous limitations of the minigenome replicon assay, the most impactful of which is that it does not perfectly mimic infection. Reconstituting the virus harbouring the mutations is the best way to fully characterize the mutations on viral replication. I created a recombinant CA/07 virus that contained the three polymerase mutations; PA E349G, PB1 T156A and PB1 F740L. The parental CA/07 virus was also generated in parallel as a control virus. The virus harbouring the three amino acid

mutations is hereafter referred to as CA/07-PA, PB1-MA. Both rescued viruses were used to infect MEF cells at a low MOI of 0.1. I measured virus production and viral protein accumulation from infected cells from both the parental CA/07 and CA/07-PA, PB1-MA. The CA/07-PA, PB1-MA virus grew to significantly higher levels in MEF cells compared to the parental CA/07 virus. The one-step replication kinetics of the virus showed 7-21 times higher virus production at 18 hpi (Fig 5.8A). Interestingly, the virus yield was only 2-6 times higher at the 12 and 24 hpi time points. Infection was quantified using immunofluorescence to ensure equal rates of infection (Fig 5.8B). Taken together, these data indicate PA E349G mutation increases the CA/07 replication in mouse cell lines, independent of viral attachment.

5.2.11 Bioinformatic Analysis of Clinical Isolates of H1N1 Shows Low Abundance of PA E349G

The PA E349G adaptation mutation showed a modest increase in polymerase activity in human cell lines. Advantageous mutations that increase fitness typically become fixed in circulating strains of the virus. I analyzed H1N1 PA sequences from human isolates from 2009 to 2017 to determine the prevalence of the E349G mutation in circulating strains. Out of 8,453 sequences analyzed, only 3 isolates (0.03%) harboured the E349G mutation (A/Netherlands/602/2009(H1N1), A/Chita/CRIE-8/2009(H1N1), and A/Singapore/GP3667/2010(H1N1)). The three identified isolates were geographically distinct (Russia, Netherlands, and Singapore), and were isolated in 2009 and 2010. No clinical outcomes were publicly available for the infected individuals. Hypothetically, if this mutation was beneficial for viruses in the human population, the

mutation would have become fixed in the genome and show a significantly higher abundance worldwide. These data suggest that the PA E349G mutation provides an advantage to the IAV polymerase in murine cells *in vitro*, but not in the human population.

5.3 Discussion

IAV must overcome several host barriers during zoonotic events while replicating efficiently and successfully spreading to a new host. In this chapter, CA/07 was experimentally adapted to replicate in Swiss-Webster mice. This adaptation process was controlled in a laboratory setting under the appropriate biosafety protocols in a host that cannot maintain transmission. The mechanical isolation and subsequent infection bypassed the bottleneck of transmission, actively selecting viruses that are most fit for replication (Ghafari et al., 2020). Swiss-Webster mice are considered outbred and are less well characterized than other murine models. I demonstrated that the Swiss-Webster lack proper expression of the restriction factor Mx1 protein. Passaging the virus from lung-to-lung allowed the accumulation of mutations required to adapt the virus to optimally replicate in the mouse lung. Serial-passaging of virus from mouse lung to mouse lung bypasses the selective nature of transmission through direct intranasal infection with virus harvested from infected lungs. The advantage of passaging virus in the *in vivo* model is the more faithful representation of human tissue architecture and innate immune responses that maintain evolutionary pressure, while passaging virus in murine cell lines or eggs does not present the same evolutionary bottlenecks. Passaging the virus resulted

in an increase in viral replication, pathogenesis, and dissemination into the brain of infected mice.

I used Illumina MiSeq to deep-sequence parental and mouse-adapted viruses and identified all mutations present in both genomes. I was able to sequence all eight genome segments of IAV simultaneously and quantified the abundance of all mutations at and above 1% abundance. Furthermore, I quantified the presence of DVGs in the population and identified where the junctions are on the segments and the number of reads at each site. By adding the Illumina P5 and P7 adapter sequences onto the forward and reverse primers to amplify the viral segments, I was able to capture the 5' and 3' most sequences in the viral genome that encompass the UTRs. I found several mutations in HA, most of which had previously been identified in other mouse adaptation studies. I identified the viral RdRp as the site for several adaptation mutations, some of which were unique to this study. One mutation, PA E349G, displayed significantly increased polymerase function in the mini-replicon assay. This study highlights key biological functions in the viral RdRp that are essential for host adaptation.

One limitation in my analysis that restricted my ability to detect all viral genotypes was deep sequencing the egg-grown stock of CA/07-MA. This single passage in eggs could have reduced the genetic diversity of CA/07-MA by selecting progeny that replicate favourably in the egg instead of the mouse. Previous studies have demonstrated rapid egg adaptation by H3N2 during propagation for vaccine production (Zost et al., 2017). To capture the true cloud of genotypes generated by adaptation to the mouse, I could have bypassed the egg inoculation step and generated my cDNA library directly from the lung homogenate from passage 10. Furthermore, generating cDNA libraries

from purified viral particles from the supernatant would enable me to determine the DI-fully infectious particle ratio. However, recent work demonstrated that DVGs are poorly packaged into budding virions (Alnaji et al., 2021, preprint *BioRxiv*). DVGs are thought to inhibit virus replication by impairing synthesis of new viral genomes and the packaging of genomic segments into budding virions. Interestingly, deep sequencing of parental CA/07 and CA/07-MA stocks showed that the CA/07-MA virus had more DVGs present in the population, whereas later experiments completed by Dr. Khaperskyy indicated that CA/07-MA produces less DVGs.

IAV requires host translation machinery to synthesize viral proteins. Viruses often optimize codon usage to match available host tRNA pools (Luo et al., 2020). I identified several synonymous mutations that arose to ~99% abundance in CA/07-MA. Synonymous mutations do not alter the primary amino acid sequence. Previous reports have indicated optimal codon usage as a means of adaptation to a new host (Goñi et al., 2012). There is strong negative selection against CpG islands as they are immunostimulatory in mammalian species, with significant synonymous mutations found in mammalian adapted avian IAVs. CpG islands are recognized by the innate sensors Toll-Like-Receptor 7 (TLR7) (Greenbaum et al., 2009; Luo et al., 2020; Wong et al., 2010). All synonymous mutations identified above 70% prevalence reduced the C/G content of CA/07-MA. With this information, I hypothesize that these mutations allow optimal utilization of tRNA pools in the new host and reduce CpG content of viral RNA.

I identified several nonsynonymous mutations in the HA glycoprotein. These mutations were expected, as the sialic acid preference of the virus must switch from α-2,6 sialic acid to α-2,3 sialic acid during adaptation. Mice do not express α-2,6 sialic acid in

their respiratory tract, creating a strong selective pressure for the virus to change its preference to α-2,3 sialic acid. I identified the previously studied D222G substitution in HA, which had been demonstrated to increase α-2,3 sialic acid preference. Interestingly, the parental CA/07 virus harbored the D222G substitution at ~53% abundance and was fixed at 99.5% during the passaging of the virus in the lung. The D222G substitution was identified in two similar CA/04 mouse adaptation studies. The 222nd amino acid of HA has also been investigated during the adaptation of zoonotic viruses entering the human population. Retrospective investigation into the 1918 pandemic highlighted a G222D substitution in clinical isolates from infected individuals over time, to switch its specificity to the human α-2,6 sialic acid linkages (Stevens et al., 2006). These data indicate that CA/07-MA adapted to the sialic acid linkages prevalent in the mouse lung.

I identified three mutations in the viral polymerase, with the PA E349G substitution being previously reported to increase virulence in mice (Ilyushina et al., 2010; Z. Zhang et al., 2011, p. 2). Two of the identified mutations in PB1 were less than 50% abundant in the population. Illumina MiSeq technology generates reads that are on average 150 bp in length, which restricts my ability to confirm whether these mutations exist on the same RNA strand. Future research could utilize the PacBio sequencing platform that generates long sequencing reads from a single strand. PacBio reads would allow me to identify whether the two mutations are found on *in cis* or *in trans.* If the mutations arise in parallel with each other, then they interact with each other.

I have shown that the PA E349G substitution significantly improved both viral polymerase activity and replication *in vitro*. The PA E349G substitution showed a significant increase in viral polymerase activity in the minigenome assay. This assay

effectively quantifies the expression of a reporter construct by the viral polymerase. The limitations of the minigenome assay is that it does not include other viral proteins that may affect polymerase activity or translation, such as NS1 or NEP. Previous work has also indicated that polymerase substitutions that result in increased polymerase activity in the assay do not always equate to increased virulence in mice (Bussey et al., 2011). Further investigation of the E349G substitution in the minigenome assay should include analysis of polymerase activity in avian cell lines. This substitution may increase viral polymerase function in avian hosts. I demonstrated that recovered virus harbouring the PA E349G substitution replicates to a significantly higher degree than the parental virus in model murine cell lines. The recombinant CA/07-PA, PB1-MA virus harboured the PB1 substitutions as well, making it difficult to confirm that the PA E349G substitution is solely responsible for the increased replication of the virus. Even with this, the data supports enhanced viral polymerase activity in murine cell lines from the mutations identified in this study. Thus, I have identified PA as a hotspot for virus adaptation.

My investigation into E349G as a virulence factor was restricted to *in vitro* cell lines. To further analyze the effects of PA E349G on virulence, two cohorts of mice could be inoculated with equal number of infectious parental CA/07 or CA/07-PA E349G. Monitoring mice for disease manifestation through weight loss and other morbidities would show whether CA/07-PA E349G virus displays increased virulence *in vivo*. Furthermore, BALF could be harvested 3, 5, and 7 dpi to be prepared for plaque assays. I showed that E349G mutation dramatically increases viral polymerase activity in murine cells, while the mutation modestly increases polymerase activity in human cell lines. Analyzing the growth kinetics in the murine lung would demonstrate an increase in

replication from the E349G substitution. I hypothesize that recombinant virus harbouring the PA E349G substitution would replicate to a higher degree than the parental virus.

Work completed by Dr. Denys Khaperskyy showed that CA/07-MA viral genomic vRNA accumulated faster than the parental CA/07 virus. This further supports that the PA E349G substitution enhanced polymerase output. The PA segment is also thought to be involved with DVG production, however the underlying mechanism of this remains unknown. For instance, the PA A638R substitution has been demonstrated to increase DVG production, while the PA D529N mutation has been shown to reduce the accumulation of DVGs (Fodor et al., 2003; Vasilijevic et al., 2017). Interestingly, the D529N mutation has been correlated with a negative prognosis in clinical settings, indicating that DVG accumulation may have a protective effect *in vivo* (Vasilijevic et al., 2017). Dr. Khaperskyy also demonstrated that the recombinant CA/07-PA, PB1-MA virus generated significantly less DVGs than the parental virus from infected MEFs. Interestingly, this data complements the dramatic increase in proliferation of CA/07-PA, PB1-MA in murine cells, with the rescued recombinant virus showing a ~10-fold increase in virus production in MEF cells. The presence of DVGs in clinical isolates correlate positively with better clinical outcomes (Vasilijevic et al., 2017). Furthermore, DVGs have been shown to impair viral transcription from most IAV genome segments (Meng et al., 2017). These data indicate that the PA E349G mutation may reduce DVG production in murine cell lines, which may have decreased the parasitic DI particle population. As mentioned previously, the number of DVGs was higher in the CA/07-MA stock compared to parental CA/07. Direct comparison of DVG production and accumulation across two different stocks with different passage history does not

accurately portray DVG production. The creation of recombinant viruses harbouring the PA/PB1 mutations, along with the parental virus in parallel, allowed us to more effectively control for DVG production and accumulation. The experiment completed by Dr. Khaperskyy and I was properly controlled allowing the analysis of DVG produced by two different viruses. The original stocks of CA/07 and CA/07-MA were generated using dramatically different methods, making direct comparisons between the two difficult.

Recent studies show that the C-terminal domain of PA contains a homo-oligomerization site responsible for binding a second trimeric polymerase complex (Be et al., 2017; Carrique et al., 2020; Dadonaite et al., 2019). Here, two trimeric polymerases bind to each other to form higher order heterodimer complexes through a key loop structure in PA. This loop structure was found at 352-356 in PA and interacts with the same domain on the second trimeric polymerase complex. Other key residues involved in dimerization and the formation of the polymerase complexes is amino acid 347, 348 and 351. Disrupting this domain through genetic modification did not affect the synthesis of viral mRNA or the creation of complementary genomic RNA (cRNA), but did significantly alter the synthesis of new viral genomic RNA (vRNA) from the cRNA template (Fan et al., 2019). Interestingly, the 349th amino acid directly flanks this dimerization domain, potentially affecting polymerase binding and function in mouse cells, resulting in enhanced replication. Dr. Khaperskyy discovered that the E349G mutant virus generated less DVGs compared to the parental virus (Slaine et al., 2018). I hypothesize that the E349G mutation stabilized the dimeric interaction between two polymerase complexes and aids in the generation of full-length genome segments. Further work should address the effects of the E349 mutation in regulating RdRp

oligomerization and the subsequent consequences on viral genome replication. ANP32A has also been shown to interact with PA during the formation of higher order RdRp complexes during cRNA and vRNA synthesis. ANP32A is thought to assist in the scaffolding during oligomerization. The failure to utilize ANP32A as a scaffold and has been directly correlated with the failure to synthesize new vRNA (Carrique et al., 2020). Accordingly, RdRp oligomerization could also be analyzed across different hosts to determine if there are host-specific factors responsible for DVG production and subsequently viral replication. Future research could also investigate the binding affinity of ANP32A towards PA E349 and PA G349 in higher order duplexes of trimeric RdRp complexes.

Using any molecular techniques to modify a pathogenic virus comes with the ethical responsibility to safely investigate adaptation mutations. Several studies in the past have adapted HPAI to ferrets to identify the mutations required for human-to-human transmission, or the reconstruction of the 1918 pandemic virus (Imai et al., 2012; Sutton et al., 2014). These studies have received negative criticism from the public and authorities, for the mutations identified in these studies could hypothetically be used for nefarious purposes by bad actors or result in a lab leak (Lipsitch, 2018). Other projects have recreated the 1918 Spanish flu IAV to ascertain the virulent origins of the worst IAV pandemic in history (Tumpey et al., 2005). I think that these projects are essential because understanding the molecular mechanisms behind adaptation allows enhanced surveillance for newly emerging IAV viruses with pandemic potential. These experiments must follow essential biological containment protocols so this work can be done safely. I also believe in scientific transparency and open collaboration between

groups. Here, in this chapter, we adapted a human isolate of H1N1 to the well-established murine infection model and identified several mutations that likely enhanced pathogenesis in the new model. These mouse adaptation mutations likely reduced the potential for human-to-human transmission of IAV (D222G) and increased polymerase activity in murine cells. Furthermore, there is no evidence that the identified polymerase mutations are naturally selected for in circulating H1N1 virus. Mice are not naturally infected by IAV and they do support transmission of the virus, highlighting that the virus generated in this study poses no risk to natural rodent populations. My thesis research followed all biosafety protocols for handling a BSL-2 pathogen. IAV is extensively studied, with several vaccine platforms available to generate active immunity against the virus.

Table 5.1: Primers used for deep sequencing IAV. The Illumina adaptors P5 and P7 sequences were generated with the Uni12 degenerate and Uni13 sequences respectively. Uni12 and Uni13 sequences are in bold in the fusion primer. Sequences are in the 5' to 3' orientation. This work was published in Slaine et al., 2018 and completed by Patrick Slaine.

Primer name	**Primer sequence**
Uni12	AGCRAAAGCAGG
ForwardP5Uni12	TCGTCGGCAGCGTCAGATGTGTATAAGAGACAG**AGCRAAAGCAGG**
ReverseP7Uni13	GTCTCGTGGGCTCGGAGATGTGTATAAGAGACAG**AGTAGAAACAAGG**

Table 5.2: Deep sequencing overview for parental CA/07 and CA/07-MA. Reads generated from Illumina MiSeq were trimmed, paired, and aligned to the reference sequence for the parental CA/07, and the consensus sequence of the parental CA/07 for CA/07-MA. Alignments were performed using Geneious R 8.0.8. This work was published in Slaine et al., 2018 and completed by Patrick Slaine.

Segment	Length (nt)	CA/07 (Parental)		CA/07-MA	
		Reads	Average Coverage	Reads	Average Coverage
PB2	2,341	164,128	9,083	238,586	14,561
PB1	2,341	246,811	11,777	231,591	16,572
PA	2,236	36,512	1,615	19,202	1,047
HA	1,777	144,547	8,653	82,826	6,377
NP	1,565	123,227	7,974	81,618	6,310
NA	1,458	57,397	4,654	33,070	2,746
M	1,027	118,520	11,089	90,245	9,089
NS	890	234,803	26,704	148,904	20,738
Total	13,635	1,125,945	10,194	926,042	9,680

Table 5.3: Hierarchical indexing for spliced alignment of transcripts 2 (HISAT2) analysis of junction reads. Paired reads were trimmed and aligned to reference sequences using HiSat2 to quantify DVG junction-spanning reads. The relative abundance of junction reads was expressed as number of reads per million reads aligned to each segment (RPM). HiSat2 program reference: Bolger, A. M., Lohse, M., & Usadel, B. (2014). Trimmomatic: A flexible trimmer for Illumina Sequence Data. Bioinformatics, btu170. This work was published in Slaine et al., 2018 and completed by Patrick Slaine.

Segment	Length (nt)	CA/07 (parental)			CA/07-MA		
		Total Reads	Junction reads		Total Reads	Junction reads	
			Reads	RPM		Reads	RPM
PB2	2,341	54,846	1,488	27,131	101,081	10,992	108,744
PB1	2,341	78,165	329	4,209	68,778	1,069	15,543
PA	2,236	9,237	36	3,897	4,079	0	0
HA	1,777	41,576	406	9,765	24,717	96	3,884
NP	1,565	42,013	2	48	27,609	0	0
NA	1,458	17,215	0	0	10,275	0	0
M	1,027	40,315	1	25	31,803	0	0
NS	890	86,919	169	1,944	57,800	25	433
Total	13,625	370,286	2,431	47,019	326,142	12,182	128,604

Table 5.4: Nucleotide substitutions identified by deep sequencing. Sequencing reads were aligned to reference genomes for each segment as described in materials and methods section. Differences between the mouse-adapted CA/07-MA sequence and parental CA/07 sequence (MA vs Parental), the mouse-adapted CA/07-MA and reference sequence (MA vs Reference), and the parental CA/07 and reference sequence (Parental vs Reference) found at frequencies above 0.01 are presented in the table. HA sequence includes the 17 amino acid signal sequence. This work was published in Slaine et al., 2018 and completed by Patrick Slaine.

MA vs Parental

Segment	Nucleotide #	Frequency	ORF	Codon #	Codon	Substitution
1	162	0.013	PB2	54	AGA -> AGG	none
1	196	0.012	PB2	66	AUG -> GUG	M -> V
1	217	0.032	PB2	73	CAA -> AAA	Q -> K
1	242	0.014	PB2	81	ACA -> AAA	U -> K
1	244	0.013	PB2	82	AAC -> CAC	N -> H
1	275	0.019	PB2	92	UCA -> UGA*	S -> Stop
1	282	0.013	PB2	94	CUG -> CUU	none
1	309	0.019	PB2	103	GGC -> GGU	none
1	338	0.016	PB2	113	AAG -> AGG	K -> R
1	340	0.013	PB2	114	GUA -> CUA	V -> L
1	353	0.012	PB2	118	UAU -> UUU	Y -> F
1	575	0.012	PB2	192	GAG -> GGG	E -> G
1	664	0.012	PB2	222	GGC -> AGC	G -> S
1	807	0.013	PB2	269	AGA -> AGG	none
1	1543	0.01	PB2	515	CCC -> ACC	P -> U
1	1928	0.015	PB2	643	UCA -> UAA*	S -> Stop
1	2021	0.019	PB2	674	GCA -> GAA	A -> E
1	2026	0.011	PB2	676	ACU -> UCU	U -> S
1	2142	0.014	PB2	714	AGC -> AGA	S -> R
1	2187	0.038	PB2	729	GGG -> GGA	none
2	78	0.01	PB1	26	GGA -> GGG	none
2	200	0.013	PB1	67	AAC -> AGC	N -> S
2	237	0.015	PB1	79	CCA -> CCC	none
2	279	0.014	PB1	93	GCU -> GCC	none
2	466	0.363	PB1	156	ACA -> GCA	U -> A
2	1023	0.996	PB1	341	CCC -> CCU	none
2	1047	0.017	PB1	349	GCA -> GCU	none
2	1323	0.999	PB1	441	CUC -> CUA	none
2	1891	0.034	PB1	631	UUU -> CUU	F -> L
2	1934	0.011	PB1	645	GUA -> GAA	V -> E

2	2218	0.498	PB1	740	UUC -> CUC	F -> L

MA vs Parental

Segment	Nucleotide #	Frequency	ORF	Codon #	Codon	Substitution
3	7	0.029	PA	3	GAC -> AAC	D -> N
3	9	0.023	PA	3	GAC -> GAA	D -> E
3	53	0.992	PA	18	GRA -> GGA	X -> G
3	234	0.011	PA	78	AUA -> AUU	none
3	246	0.011	PA	82	AGA -> AGG	none
3	622	0.033	PA	208	ACA -> GCA	U -> A
3	841	0.015	PA	281	AAG -> UAG*	K -> Stop
3	1046	1	PA	349	GAA -> GGA	E -> G
3	1313	0.014	PA	438	AUC -> AGC	I -> S
3	1322	0.017	PA	441	AUG -> AGG	M -> R
4	302	0.445	HA	101	AGU -> AAU	S -> N
4	517	0.997	HA	173	AAU -> GAU	N -> D
4	598	0.996	HA	200	UCU -> CCU	S -> P
4	1218	0.406	HA	406	CAG -> CAU	Q -> H
4	1355	0.015	HA	452	UUG -> UAG	none
4	1454	0.012	HA	485	UAC -> UUC	Y -> F
4	1460	0.014	HA	487	AAA -> AGA	K -> R
4	1472	0.014	HA	491	ACG -> AAG	U -> K
4	1542	0.01	HA	514	AGA -> AGG	none
5	215	0.029	NP	72	GAU -> GCU	D -> A
5	748	0.013	NP	250	AAC -> UAC	N -> Y
6	109	0.021	NA	37	UCA -> CCA	S->P
6	164	0.458	NA	55	ACU -> AAU	U -> N
6	256	0.029	NA	86	GCG -> ACG	A -> U
6	1120	0.027	NA	374	AUU -> GUU	I -> V
6	1173	0.026	NA	391	CAA -> CAG	none
7	324	0.705	M1	108	ACG -> ACA	none
7	479	0.01	M1	160	CGG -> CUG	R -> L
7	773	0.314	M2	29	GCA -> ACA	A -> U
7	832	0.022	M2	48	FS**	FS**
8	474	0.548	NS1	158	GGA -> GGG	none
8	663	0.01	NEP	64	AAG -> AGG	K -> R

MA vs Reference

Segment	Nucleotide #	Frequency	ORF	Codon #	Codon change	Substitution
1	162	0.013	PB2	54	AGA -> AGG	none
1	196	0.012	PB2	66	AUG -> GUG	M -> V
1	217	0.032	PB2	73	CAA -> AAA	Q -> K
1	242	0.014	PB2	81	ACA -> AAA	U -> K
1	244	0.013	PB2	82	AAC -> CAC	N -> H
1	275	0.019	PB2	92	UCA -> UGA*	S -> Stop
1	282	0.013	PB2	94	CUG -> CUU	none
1	309	0.019	PB2	103	GGC -> GGU	none
1	338	0.016	PB2	113	AAG -> AGG	K -> R
1	340	0.013	PB2	114	GUA -> CUA	V -> L
1	353	0.012	PB2	118	UAU -> UUU	Y -> F
1	575	0.012	PB2	192	GAG -> GGG	E -> G
1	664	0.012	PB2	222	GGC -> AGC	G -> S
1	807	0.013	PB2	269	AGA -> AGG	none
1	1543	0.01	PB2	515	CCC -> ACC	P -> U
1	1928	0.015	PB2	643	UCA -> UAA*	S -> Stop
1	2021	0.019	PB2	674	GCA -> GAA	A -> E
1	2026	0.011	PB2	676	ACU -> UCU	U -> S
1	2142	0.014	PB2	714	AGC -> AGA	S -> R
1	2187	0.038	PB2	729	GGG -> GGA	none
2	78	0.01	PB1	26	GGA -> GGG	none
2	200	0.013	PB1	67	AAC -> AGC	N -> S
2	237	0.015	PB1	79	CCA -> CCC	none
2	279	0.014	PB1	93	GCU -> GCC	none
2	466	0.363	PB1	156	ACA -> GCA	U -> A
2	1023	0.996	PB1	341	CCC -> CCU	none
2	1047	0.017	PB1	349	GCA -> GCU	none
2	1323	0.999	PB1	441	CUC -> CUA	none
2	1891	0.034	PB1	631	UUU -> CUU	F -> L
2	1934	0.011	PB1	645	GUA -> GAA	V -> E
2	2218	0.498	PB1	740	UUC -> CUC	F -> L
3	7	0.029	PA	3	GAC -> AAC	D -> N
3	9	0.023	PA	3	GAC -> GAA	D -> E
3	53	0.992	PA	18	GRA -> GGA	X -> G
3	234	0.011	PA	78	AUA -> AUU	none
3	246	0.011	PA	82	AGA -> AGG	none
3	622	0.033	PA	208	ACA -> GCA	U -> A

MA vs Reference

Segment	Nucleotide #	Frequency	ORF	Codon #	Codon change	Substitution
3	841	0.015	PA	281	AAG -> UAG*	K -> Stop
3	1046	1	PA	349	GAA -> GGA	E -> G
3	1313	0.014	PA	438	AUC -> AGC	I -> S
3	1322	0.017	PA	441	AUG -> AGG	M -> R
4	302	0.445	HA	101	AGU -> AAU	S -> N
4	517	0.997	HA	173	AAU -> GAU	N -> D
4	598	0.996	HA	200	UCU -> CCU	S -> P
4	716	0.995	HA	239	GAU -> GGU	D -> G
4	1218	0.406	HA	406	CAG -> CAU	Q -> H
4	1355	0.015	HA	452	UUG -> UAG	none
4	1454	0.012	HA	485	UAC -> UUC	Y -> F
4	1460	0.014	HA	487	AAA -> AGA	K -> R
4	1472	0.014	HA	491	ACG -> AAG	U -> K
4	1542	0.01	HA	514	AGA -> AGG	none
5	159	0.996	NP	53	GAU -> GAG	D -> E
5	215	0.029	NP	72	GAU -> GCU	D -> A
5	341	0.998	NP	114	GRA -> GAA	X -> E
5	365	0.999	NP	122	CUA -> CAA	L -> Q
5	748	0.013	NP	250	AAC -> UAC	N -> Y
6	109	0.021	NA	37	UCA -> CCA	S->P
6	164	0.458	NA	55	ACU -> AAU	U -> N
6	256	0.029	NA	86	GCG -> ACG	A -> U
6	1052	0.998	NA	351	UAC -> UUC	Y -> F
6	1059	0.996	NA	353	UAU -> UAC	none
6	1120	0.027	NA	374	AUU -> GUU	I -> V
6	1173	0.026	NA	391	CAA -> CAG	none
7	324	0.705	M1	108	ACG -> ACA	none
7	479	0.01	M1	160	CGG -> CUG	R -> L
7	773	0.314	M2	29	GCA -> ACA	A -> U
7	832	0.022	M2	48	FS**	FS**
8	474	0.548	NS1	158	GGA -> GGG	none
8	663	0.01	NEP	64	AAG -> AGG	K -> R

Parental vs Reference

Segment	Nucleotide #	Frequency	ORF	Codon #	Codon change	Substitution
1	207	0.018	PB2	69	GAG -> GAC	E -> D
1	265	0.011	PB2	89	GUG -> CUG	V -> L

Parental vs Reference

Segment	Nucleotide #	Frequency	ORF	Codon #	Codon change	Substitution
1	462	0.022	PB2	154	CUC -> CUU	none
1	696	0.015	PB2	232	UUG -> UUA	none
1	1073	0.015	PB2	358	GAA -> GCA	E -> A
1	1311	0.013	PB2	437	CAU -> CAC	none
1	1445	0.014	PB2	482	AAA -> AGA	K -> R
1	1711	0.163	PB2	571	UUA -> CUA	none
1	2052	0.017	PB2	684	UCU -> UCC	none
2	760	0.016	PB1	254	UUU -> CUU	F -> L
2	1023	0.297	PB1	341	CCC -> CCU	none
2	1464	0.067	PB1	488	GGG -> GGA	none
3	53	0.898	PA	18	GRA -> GAA	X -> E
3	53	0.099	PA	18	GRA -> GGA	X -> G
3	183	0.011	PA	61	AUA -> AUU	none
3	228	0.014	PA	76	UUU -> UUC	none
3	1848	0.011	PA	616	UCG -> UCA	none
4	165	0.019	HA	55	AAC -> AAA	N -> K
4	166	0.012	HA	56	GGG -> AGG	G -> R
4	171	0.018	HA	57	AAA -> AAU	K -> N
4	172	0.013	HA	58	CUA -> AUA	L -> I
4	424	0.473	HA	142	AAU -> GAU	N -> D
4	432	0.052	HA	144	GAC -> GAA	D -> E
4	437	0.068	HA	146	AAC -> AGC	N -> S
4	511	0.039	HA	171	AAA -> GAA	K -> E
4	598	0.228	HA	200	UCU -> CCU	S -> P
4	622	0.101	HA	208	CUC -> AUC	L -> I
4	716	0.539	HA	239	GAU -> GGU	D -> G
4	719	0.018	HA	240	CAA -> CGA	Q -> R
4	1433	0.022	HA	478	GGA -> GAA	G -> E
5	159	0.676	NP	53	GAU -> GAG	D -> E
5	302	0.031	NP	101	GAC -> GGC	D -> G
5	304	0.265	NP	102	GGA -> AGA	G -> R
5	324	0.27	NP	108	CUC -> CUU	none
5	341	0.993	NP	114	GRA -> GAA	X -> E
5	365	0.998	NP	122	CUA -> CAA	L -> Q
6	17	0.011	NA	6	AAG -> AGG	K -> R
6	258	0.019	NA	86	GCG -> GCA	none
6	1052	0.996	NA	351	UAC -> UUC	Y -> F

Parental vs Reference

Segment	Nucleotide #	Frequency	ORF	Codon #	Codon change	Substitution
6	1059	0.996	NA	353	UAU -> UAC	none
7	177	0.012	M1	59	AUU -> AUC	none
8	42	0.019	NS1	14	UUC -> UUU	none
8	214	0.026	NS1	72	GAA -> AAA	E -> K
8	355	0.018	NS1	119	UUG -> CUG	none
8	817	0.01	NEP	115	GCU -> GCC	none

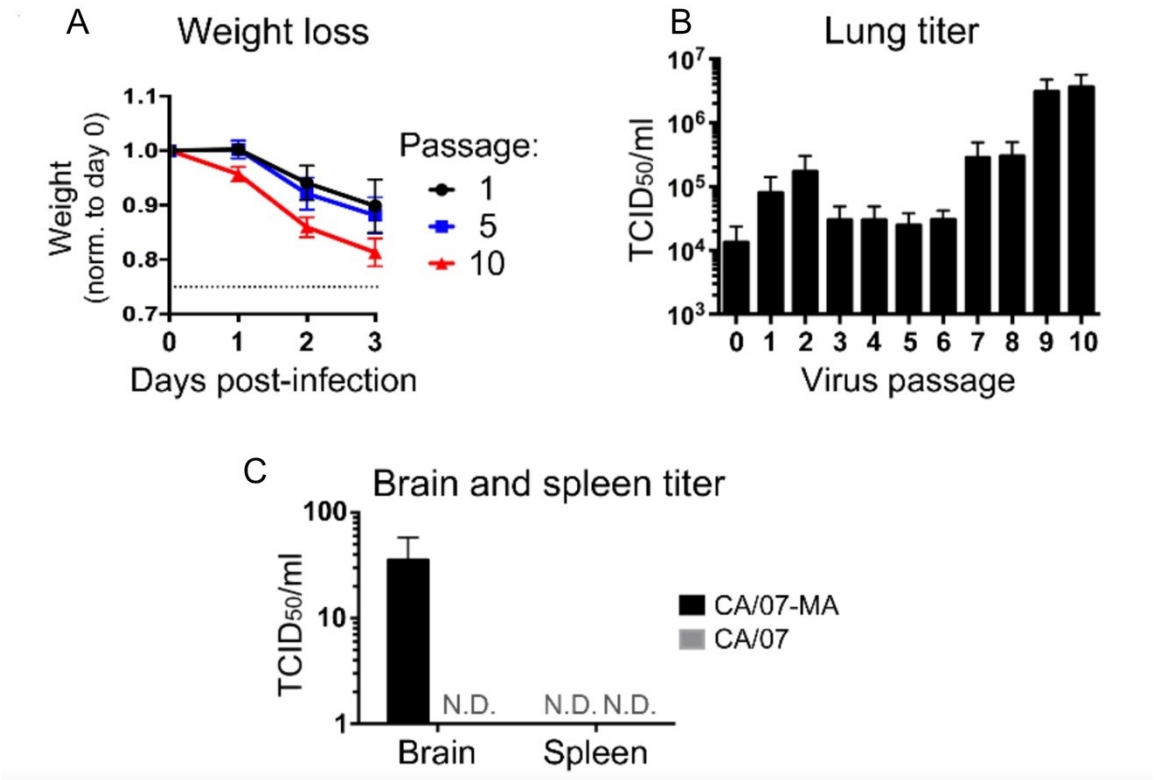

Figure 5.1: Murine adaptation of CA/07 increases virus replication in lungs and spread to brain.
(A,B) Swiss Webster mice were infected with CA/07, and recovered virus was passaged lung-to-lung nine more times, for a total of ten passages. Morbidity was determined by monitoring weight loss over time ((A), passages 1, 5 and 10), and virus titers in the lung were measured by the 50% tissue culture infectious dose (TCID50) assay (B). (C) Dissemination of parental CA/07 and passage 10 (CA/07-MA (mouse adapted)) virus was analyzed by performing TCID50 assays on brain and spleen homogenates. N.D. = not detected. In (A–C), error bars represent the standard deviation (n = 4 mice). This work was published in Slaine et al., 2018 and completed by Cara MacRae.

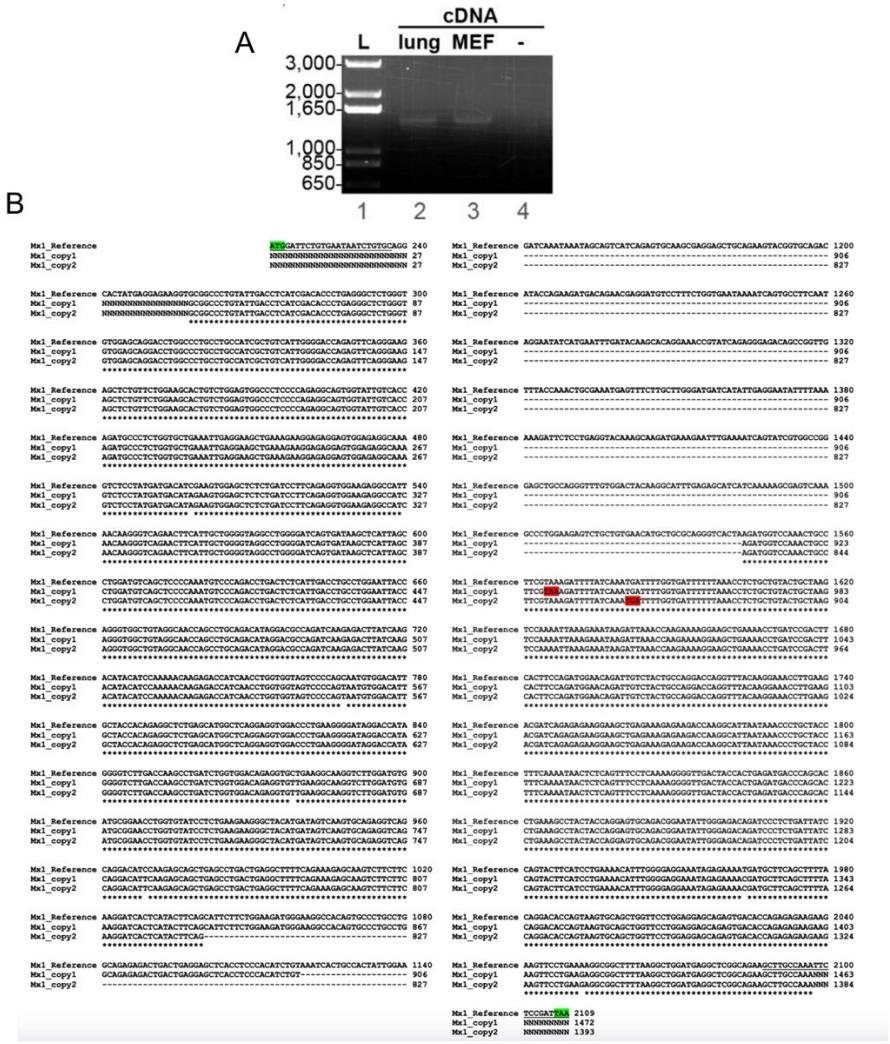

Figure 5.2: Outbred Swiss Webster mice have non-functional Mx1.
Total RNA was extracted from a Swiss Webster mouse lung homogenate collected at 3 days post-infection with passage 10 CA/07-MA virus (lung) and from mouse embryonic fibroblasts from C57BL/6 strain (MEF). (A) Following reverse transcription using Maxima H Minus reverse transcriptase (Thermo) and oligo(dT) priming the coding sequences of Mx1 cDNA were amplified and the products were resolved on 1% agarose gel stained with ethidium bromide (expected product size for the full-length Mx1 coding region is 1896 bp). PCR product from lane 2 (lung) was gel-extracted and sequenced. Sequencing revealed that the gel-extracted band contained two Mx1 amplicons: 1472 bp and 1393 bp that were not resolved by electrophoresis. Both sequences were aligned to the reference Mx1 sequence (NM_010846) using Clustal Omega (https://www.ebi.ac.uk/Tools/msa/clustalo/) and the portions of the alignment corresponding to the full-length Mx1 coding sequence are presented in (B). Sequences that correspond to primers used for amplification are underlined. The start and stop codons for the full-length Mx1 are highlighted green. Premature stop codons that resulted from deletions in both copies of Mx1 amplified from Swiss Webster mouse lung cDNA are highlighted red. This work was published in Slaine et al., 2018 and completed by Patrick Slaine and Dr. Khaperskyy.

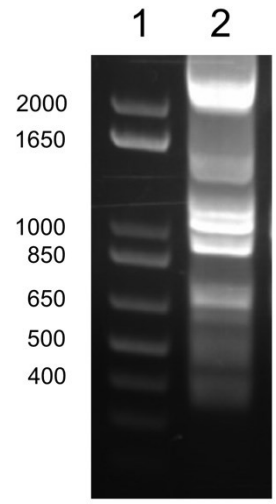

Figure 5.3: Successful multi-segment amplification of the IAV genome.
Total RNA was extracted from MDCK cells infected with CA/07-MA 24 hpi. Following reverse transcription using Maxima H Minus reverse transcriptase (Thermo) and the Uni12 degenerate primer, the genomic segments were amplified with the P5-Uni12 and P7-Uni13 primers. The PCR product was resolved on a 1% agarose gel stained with ethidium bromide. Lane 1 contains the 1 Kb plus ladder (NEB N3200S), with the marked molecular weights annotated to the left of the lane. Lane 2 contains the product from the multi-segment amplification PCR from the cDNA library of CA/07-MA. This work is unpublished and completed by Patrick Slaine.

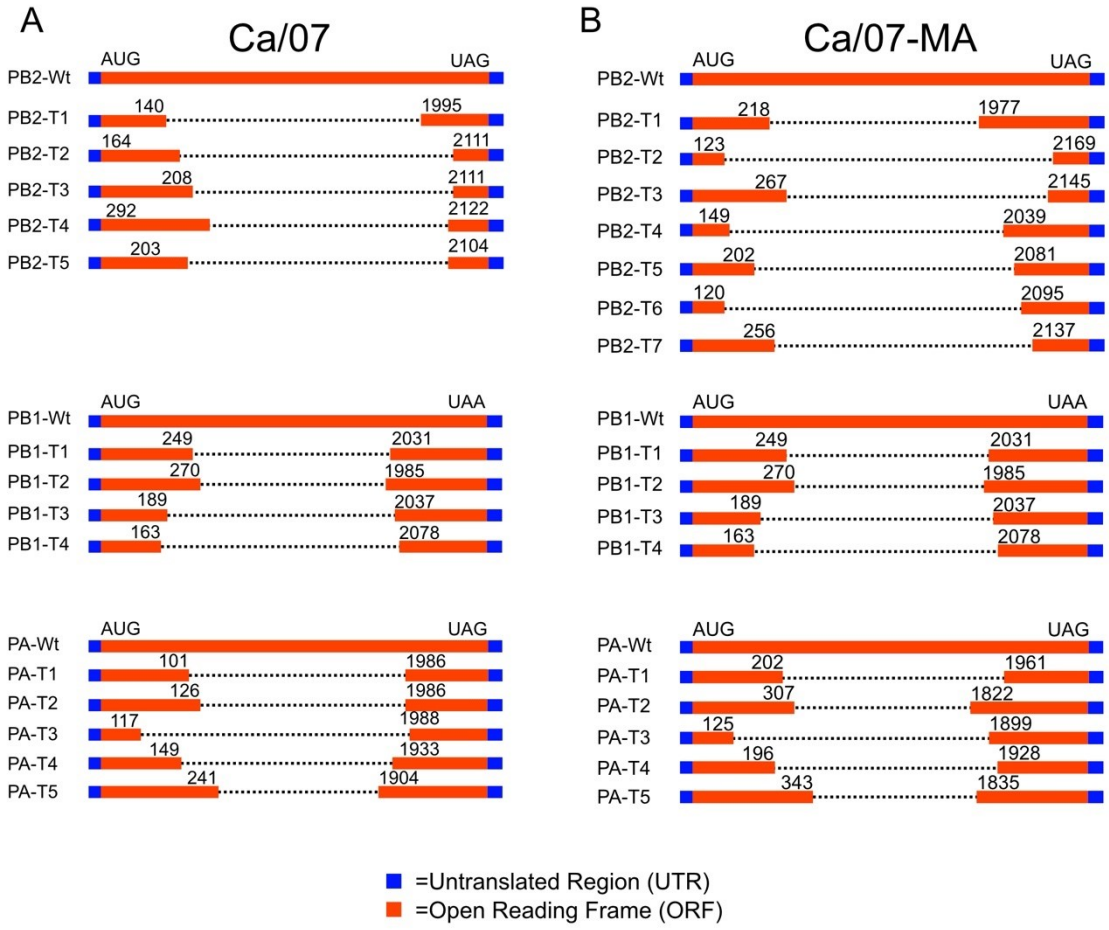

Figure 5.4: Differential generation of defective viral genomes between parental CA/07 and CA/07-MA.

Illumina MiSeq reads for both parental CA/07 (A) and CA/07-MA (B) were aligned to the reference sequence for CA/07. Reads that span the 5' and 3' sequences were identified, and the junctions were determined. Junction sites are annotated with the nucleotide in which the sequencing read spans the internal deletion. The start and stop codon are annotated for the primary protein product of each genomic segment. The 5' and 3' UTRs are coloured blue, while the coding sequences are coloured red. This work is unpublished and completed by Patrick Slaine.

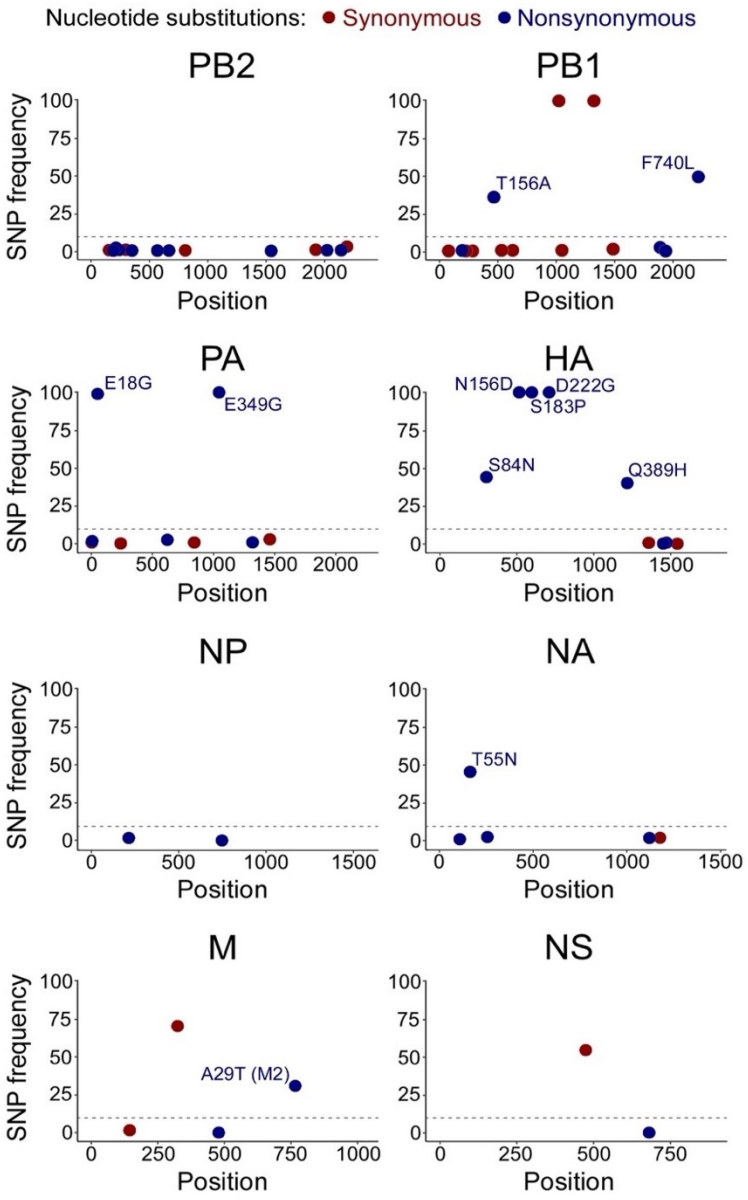

Figure 5.5: Identification of adaptive mutations in CA/07-MA by MiSeq Illumina deep sequencing.
Both parental CA/07 and CA/07-MA were deep sequenced. The parental CA/07 genome was aligned to the reference sequence to generate a consensus sequence for the parental isolate. CA/07-MA reads were then mapped onto the parental CA/07 consensus sequence. All substitutions that identified with a frequency above 1% were plotted. X-axis: nucleotide position relative to the adenine of the first AUG start codon in the largest open reading frame. Y-axis: precent frequency of the substitution. The corresponding amino acid change is indicated for non-synonymous mutations(blue) over 10% frequent. SNP: single nucleotide polymorphism, PB1/2: polymerase basic 1/2, PA: polymerase acidic, HA: hemagglutinin, NP: nucleoprotein, NA: neuraminidase, M: matrix, NA: non-structural. This work was published in Slaine et al., 2018 and completed by Patrick Slaine.

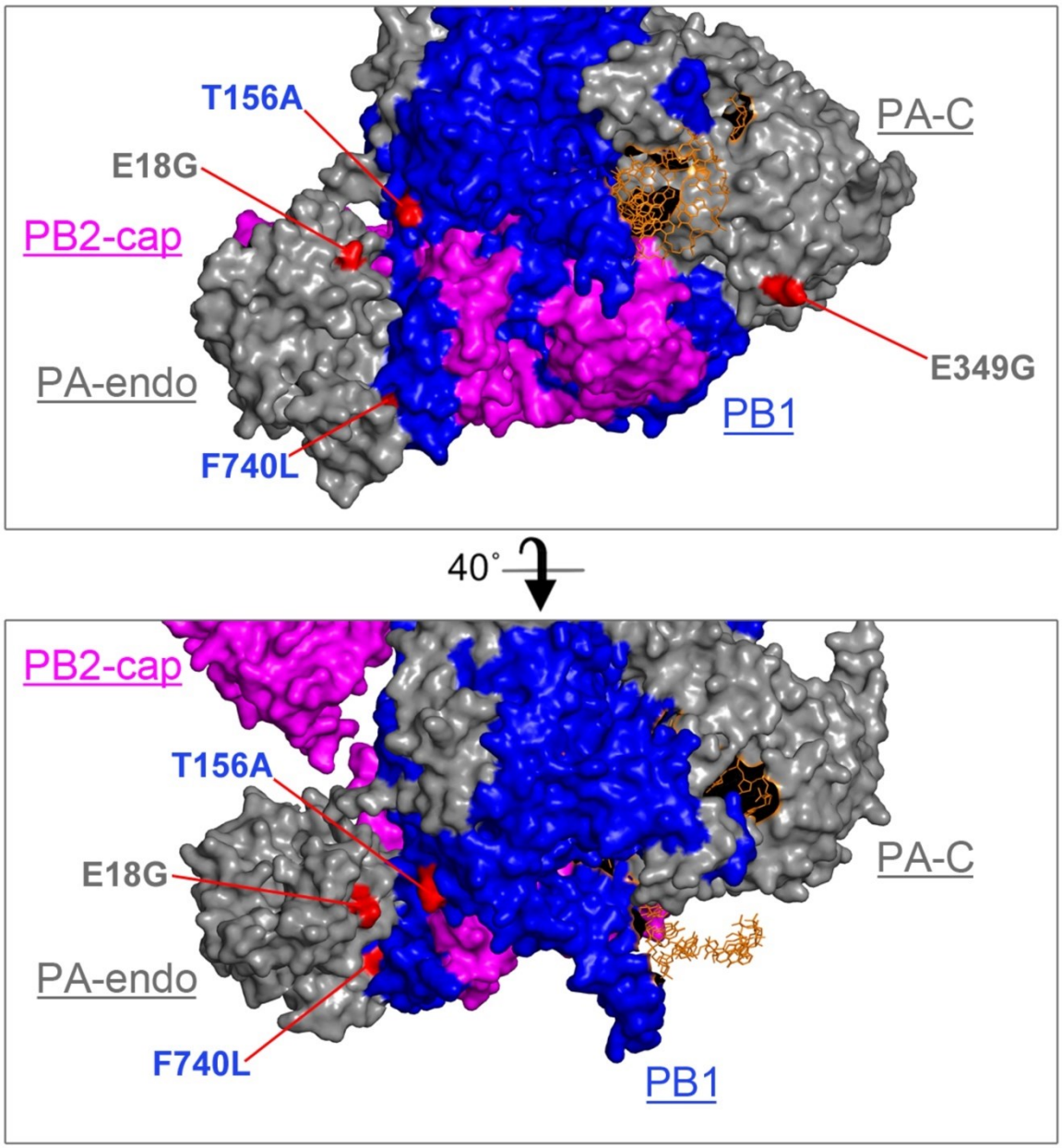

Figure 5.6: CA/07 mouse adaptation mutations are surface exposed in the ternary RdRp complex.
CA/07-MA amino acid substitutions were mapped onto the 3D structure of bat influenza A/little yellow-shouldered bat/Guatemala/060/2010 (H17N10) IAV polymerase bound to an RNA primer (orange) (Protein accession number: 4WSB). PA is grey, PB1 is blue, PB2 is magenta, and the RNA strand is orange. Relative positions of the C-terminal cap binding domain of PB2 (PB2-cap), the N-terminal endonuclease domain of PA (PA-endo), and the C-terminal domain of PA (PA-C) are indicated for reference. The mouse adaptation mutations identified by deep sequencing are highlighted in red. The image was generated in PyMOL Version 2.0.4 Images were rendered at Ray 2400 with 1000 dpi. This work was published in Slaine et al., 2018 and completed by Patrick Slaine.

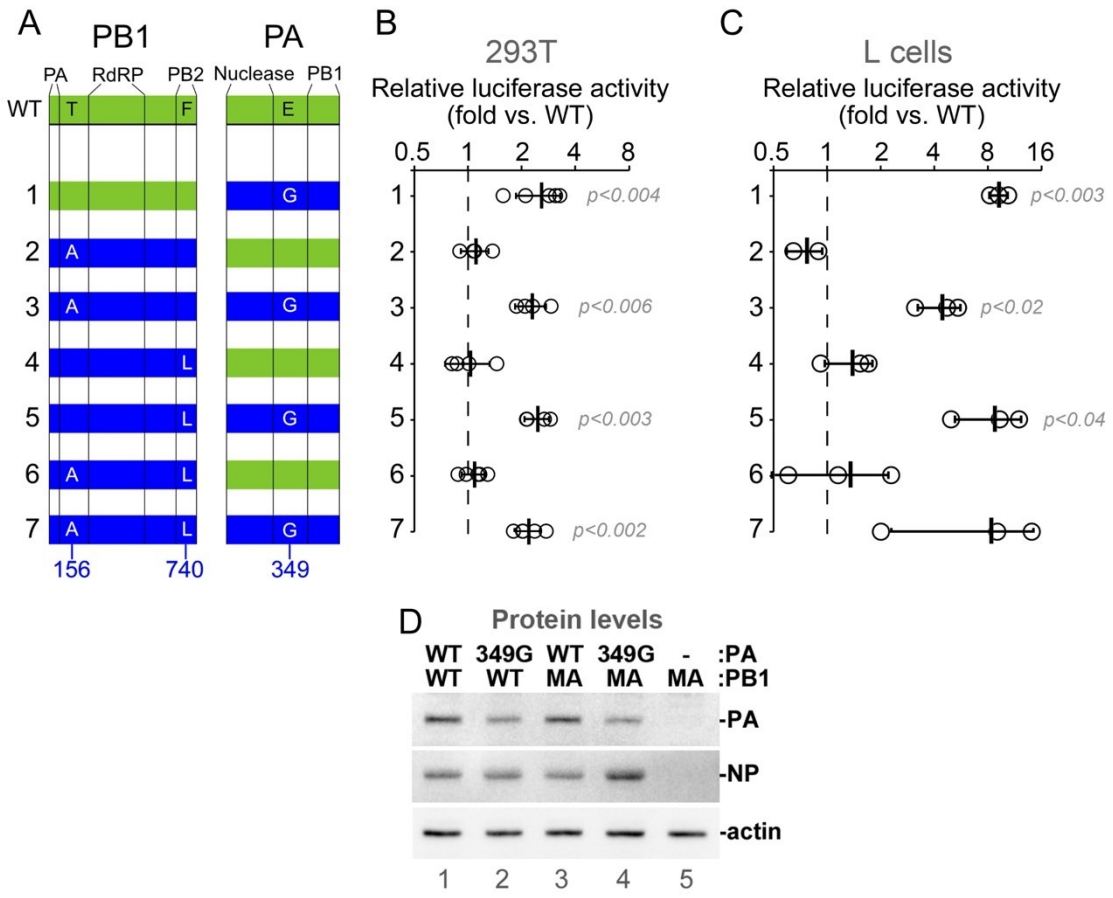

Figure 5.7: PA E349G substitution enhances viral RNA polymerase activity.
(A) Schematic representation of PB1 and PA proteins showing approximate boundaries of major domains in the primary amino acid sequence (vertical lines) and positions of amino acids mutated in this study. Green and blue shading indicated wild-type and mutant proteins respectively. (B) Relative luciferase activity was measured in the replicon assay in 293T cells using constructs derived from wild-type CA/07 PB2 and NP in combination with PB1 and PA constructs that correspond to the numbered combinations depicted in (A). Open circles indicated values for each independent replicate normalized to the wild-type replicon values obtained in parallel (dotted vertical line). p-values were calculated using a paired Student's t test across four biological replicates (N=4). (C) The assay described in (B) was performed in murine L929 cells using a firefly luciferase reporter driven by mouse POL1 promoter. p-values were calculated using a paired Student's t test across three biological replicates (N=3). (D) Western blot analysis of the whole cell lysates of 293T cells transfected with the selected replicon assays shown in (B). This work was published in Slaine et al., 2018 and completed by Patrick Slaine, Mariel Kleer, and Dr. Khaperskyy.

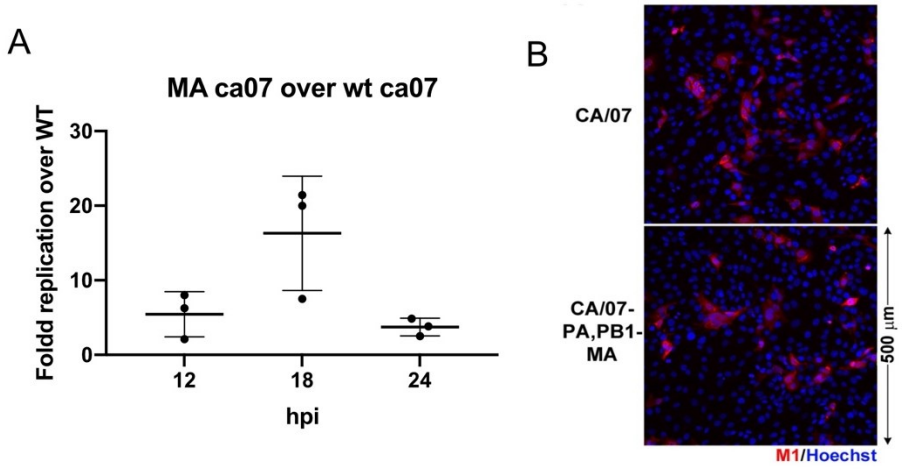

Figure 5.8: Rescued virus harbouring the mouse adapted PA and PB1 increase replication in mouse cells.
Mouse embryo fibroblasts were infected with parental CA/07 or recombinant CA/07-PA, PB1-MA at a MOI of 0.1. (A) Virion production was measured at 12, 18, and 24 hpi using a plaque assay in MDCK cells. Error bars denote the standard deviation of three biological replicates (N=3). Statistics was performed using a paired Student's t test. (B) Cells were fixed at 18 hpi and analyzed by immunofluorescence microscopy staining with anti-M1 (red) and nuclei were labelled with Hoechst (blue). This work was published in Slaine et al., 2018 and completed by Patrick Slaine and Dr. Khaperskyy.

CHAPTER 6: CONCLUSIONS

6.1 Conclusions and Limitations

Although the work presented in my thesis provides insight into the interactions between IAV and its host and the potential antiviral therapies against infection, my work still leaves many questions unanswered. In Chapter 3, I reasoned that IAV may be so reliant on canonical host protein synthesis machinery that disruption of the eIF4A helicase will inhibit IAV replication. IAV mRNAs contain complex 5' structures that may require eIF4A helicase activity. My work demonstrated that IAV is highly sensitive to eIF4A inhibitor mediated-translation arrest. Treating infected cells with Sil or PatA dramatically reduced the accumulation of all viral proteins. However, this work was limited to several *in vitro* cell lines. The cell lines used in this study are transformed and therefore require a high degree of translation to maintain their rapid cell division. Many oncogenes require the eIF4A helicase to melt complex 5' structures in their mRNAs for efficient protein synthesis (Wolfe et al., 2014). I demonstrated that treating the model cells induced apoptosis-mediated cell death. Despite these limitations, I demonstrate that IAV is sensitive to pharmacological agents that impair host cap-dependent translation. The work completed here indicates that targeting global translation in infected cells significantly disrupts the homeostasis of both infected and non-infected cells and is not feasible as an antiviral.

In Chapter 4, I demonstrated that perturbing the host ER selectively impaired viral glycoprotein synthesis, which subsequently reduced virus production. 6-TG has been used in the clinical setting for roughly 70 years and we are the first lab to show that 6-TG

and 6-TGo induce the UPR. This finding has clinical relevance, with thousands of individuals currently taking this drug to treat leukemia and IBD (Bayoumy et al., 2020). My work demonstrated that the rapid induction of the UPR in infected cells is antiviral against IAV, as treatment significantly impaired viral glycoprotein synthesis and virus production. I demonstrated that the activation of the UPR was antiviral across several IAVs. My data indicated that other nucleoside and nucleobase analogs did not induce the UPR. These data indicate that the incorporation of nucleoside analogs into viral and host RNAs is not the mechanism in which 6-TG and 6-TGo induce the UPR. For example, 5-FU, a known nucleoside analog, failed to induce the UPR and did not affect virus production from infected cells (Pauly & Lauring, 2015). I also discovered that murine cells showed resistance to 6-TG mediated UPR induction, and that 6-TG treatment did not provide protection against a lethal infection in the murine model. These data indicate that IAV is sensitive to UPR induction as an antiviral therapeutic and the molecular target of 6-TG may be missing in murine cells.

6-TG has been previously demonstrated to bind and impair the small GTPase Rac1, which has physiological effects in treated patients. I proposed that 6-TG is responsible for binding and impairing another GTPase that is involved in ER homeostasis. There are several candidate GTPases that may be targeted by 6-TG, such as SRP, SR, or Mx1 (Fig 6.1).

The major limitation to this chapter is that the molecular target of 6-TG remains unknown. I was unable to determine the targeted host factor that was responsible for the UPR specific phenotype that I observed. Accordingly, I do not know what is the host factor that is missing or resistant in murine cells to make them unaffected by 6-TG. This

limitation was most notable during the challenge study in the murine infection model. Treating infected mice did not reduce virus production and did not improve survival. A limitation of the murine infection model is that the concentration of 6-TG in the mouse lung was unknown. The failure to protect the model organism could be due to the inability to deliver the compound to the lung in high enough concentrations to be effective against viral replication.

Lastly, In Chapter 5, I hypothesized that the mouse adapted CA/07 virus harboured numerous mutations responsible for its increased virulence in mice, some of which would be found in other viral proteins besides HA. I identified several non-synonymous mutations in the mouse adapted virus, some of which were known mouse adaptation mutations associated with receptor tropism. I identified one substitution in a viral polymerase subunit that increased viral polymerase activity in the minigenome replicon assay and in rescued recombinant virus. I was limited in identifying every mutation present in the last passage from the mouse lung, because I passaged the virus in fertilized eggs and infecting MDCK cells before generating the cDNA library. There may have been some genotypes that were missed because of this. I was also limited in testing the mutations identified in PB1. The minigenome replicon assay did not indicate that these substitutions altered virus polymerase activity, and I did not generate recombinant virus harbouring just the single substitutions. This prevented me from specifically analyze the PB1 mutations in the context of viral replication. Accordingly, whether the PB1 substitutions contribute to viral replication remains unclear. Furthermore, the minigenome replicon assay is limited in accurately depicting viral polymerase function since it only contains the viral polymerase subunits, NP, and an RNA template. It has

been demonstrated that NS1 and NEP can affect translation and polymerase function (Arias-Mireles et al., 2018, p. 1; Robb et al., 2009). The work completed here confirms the viral polymerase as a hot spot for viral adaptation mutations that could be screened for in zoonotic IAVs.

6.2 Testing Sil, PatA, and 6-TG on Primary Cell Lines that Faithfully Represent the Human Respiratory Tract

My work demonstrated that the transformed cancer cells used as IAV *in vitro* infection models were highly sensitive to eIF4A inhibitors. Are primary cells of the lung equally as sensitive to translation arrest? Will 6-TG have detrimental effects on non-dividing cells? To answer these questions, I would analyze virus production in standardized air-liquid interface 3D airway epithelial culture and quantify the cytotoxic and cytostatic effects of treatment. I used transformed cells that did not faithfully represent the environment of the human respiratory tract. My results agree with the study performed by Kuznetsov and coauthors that PatA is cytotoxic in highly proliferative cells (Kuznetsov et al., 2009). The standardized 3-D air-liquid airway model faithfully represents the environment of the human respiratory tract, with cells that are not transformed, polarize apical and basal membranes, form tight cellular junctions, and secrete mucus (Pharo et al., 2020). For instance, this model has been utilized in the past to test the efficacy of oseltamivir carboxylate (Boda et al., 2018). I would treat infected cells with a range of different concentrations of Sil and PatA and quantify virus production (Fig 6.2). Using this model would also allow me to quantify and compare virus production, viral glycoprotein accumulation, host antiviral responses, cell-to-cell

junctions, and any negative side effects from antiviral treatment (Boda et al., 2018). I expect that both eIF4A inhibitors and 6-TG would show greater efficacy at reducing virus production and demonstrate more favourable cell viability. Primary cells have shown significantly higher tolerance to PatA and Sil treatment than transformed cell lines, likely indicating that the viability of treated cells would be more favourable in this model. I would confirm that 6-TG triggers the UPR in the new model cell line and analyze the synthesis of viral glycoproteins. I would track the production of viral glycoproteins to the apical membrane and analyze for defective glycoprotein migration by probing polarised cells for NA and HA. These data would allow me to confirm the antiviral effects of Sil, PatA, and 6-TG in a model that faithfully represents the human lung.

6.3 Further Investigation into the Effects of 6-TG Treatment on the UPR and Cell Fate

In Chapter 4, I demonstrated that 6-TG induced the UPR in both mock-infected and IAV infected cells. The molecular target of 6-TG that is responsible for the UPR phenotype still evades us. 6-TGo, an analog of guanosine, induced all three arms of the UPR, as seen with the activation of PERK, IRE1, and cleavage of ATF6. The activation of PERK and ultimately the ISR is likely the origin of the SGs identified in the original small molecule screen. Future research should confirm the role of PERK on the formation of SGs in 6-TG treated cells. This research can be completed by co-treating infected cells with ISRIB And 6-TG, or by treating A549-PERK KO cells with 6-TG. Analyzing these cells for the formation of SGs will confirm that 6-TG mediated SG formation is PERK and ISR dependent.

The activation of the UPR resulted in the accumulation of proteins that are downstream of the three effector molecules, such as BiP, CHOP, and XBP1s. 6-MP, another thiopurine member that shares a high degree of similarity to 6-TG, failed to induce the UPR. There are numerous GTPases involved in the translation and transportation of glycoproteins in the ER, all of which could be targeted by 6-TG. The effect of 6-TG on the UPR could further be analyzed by probing for caspase-12 activation, which is known to induce the apoptotic cascade during times of ER stress (Hitomi et al., 2004, p. 12). The absence of PARP cleavage in 6-TG treated cells indicated that the apoptotic cascade was not activated. Lastly, cytoplasmic concentrations of Ca^{2+} should be analyzed in 6-TG treated cells. Low Ca^{2+} concentrations within the ER lumen are known to induce the UPR, along with activation of the cytoplasmic calpain proteases (Tabas & Ron, 2011).

Are viral glycoproteins targeted by ERAD in 6-TG treated cells? Treating infected cells with 6-TG reduced the accumulation of viral glycoproteins. I generated evidence that PERK activation reduced the translation of viral glycoproteins, but I did not investigate the degradation of glycoproteins through the ERAD pathway. There are specific pharmacological inhibitors available to impair the ERAD pathway, such as DBeQ that blocks the function of the AAA p97 protein. p97 is an ER residential protein that is responsible for a variety of functions, one of which is responsible for the retrotranslocation of polyubiquitinated proteins into the cytoplasm (Q. Wang et al., 2006). In future studies, I would co-treat infected cells with 6-TG and DBeQ and analyze the accumulation of viral glycoproteins. If inhibiting p97 restored the accumulation of viral glycoproteins, then ERAD may have a role in limiting the synthesis of HA and NA

in 6-TG treated cells. I would expect that inhibiting p97 will partly restore the accumulation of viral glycoproteins.

6.4 Identification of the GTPase Responsible for 6-TG Mediated UPR Activation

Murine cell lines showed complete resistance to 6-TG induced UPR activation, indicating the molecular target of 6-TG is different between the two species. Further investigation is required to characterize the molecular target of 6-TG. I hypothesize that the molecular target of 6-TG is a GTPase involved in the homeostasis of the ER (Fig 6.1). One GTPase that is missing in mouse cell lines is the dynamin like GTPase Mx1, which has been shown to aid in vesicle formation in the ER (Accola et al., 2002). Impairing the formation of vesicles budding off the ER membrane may induce the UPR. Other GTPases that significantly differ in amino acid sequence is the signal recognition particle receptor (SR) found embedded on the ER, showing 90% homology across the two species. I observed a reduction in virus production in infected cells treated with the Rac1 inhibitor V, but not as significant as infected cells treated with 6-TG. Further work should investigate whether the UPR is activated by the Rac1 inhibitor V. If 6-TG is inhibiting a GTPase, using a broad spectrum GTPase agonist in 6-TG treated cells may revert the glycoprotein specific phenotype. ML099 is a broad Ras-related GTPase agonist (Surviladze et al., 2010). Recent experiments completed by the McCormick lab demonstrated that co-treating infected cells with 6-TG and the GTPase agonist ML099 restored the accumulation and processing of the coronavirus spike (S) glycoprotein. These data suggests that 6-TG does inhibit a GTPase involved in the synthesis of viral

glycoproteins. To identify the unknown GTPase that 6-TG forms an adduct with, I would take a protein library of human GTPases and incubate them with 6-TG *in vitro*. I would then add fluorescent (Iwata et al., 2016) or radio-labeled GTP (Miller et al., 1995) in increasing concentrations to displace 6-TG from the GTPase. The GTPase would then be purified and crosslinked to the bound GTP/6-TG by UV radiation. GTPases that tightly bound 6-TG would require significantly higher concentrations of fluorescent/radio-labeled GTP to dissociate the 6-TG from the GTPase. Rac1 is a known target of 6-TG, and therefore would be a positive control in this experiment. Another method to identify the molecular target of 6-TG would be to transduce a human GTPase vector library into the 6-TG resistant MEF or L929 cell line and observe for the UPR phenotype post 6-TG treatment. I would also knock out the expression of MxA in the A549 cell line and observe for any glycoprotein specific phenotype. I would infect the knockout cell line and treat with 6-TG and analyze the accumulation of viral glycoproteins. Conversely, I could introduce human MxA into the Mx1 deficient MEF cell line and observe potential glycoprotein specific phenotypes that may arise.

Future work should further characterize progeny virions from 6-TG treated cells. Do the viral particles still have the same ratios of HA, NA, and M2? Are the HA and NA glycoproteins that are incorporated into viral particles lacking key glycosylations? Future work is required to determine the glycosylation status of HA and NA during 6-TG treatment. The glycoproteins showed increased gel electrophoretic mobility during gel electrophoresis when compared to untreated cells. Un-glycosylated HA has been shown to bind BiP, which may play a role in UPR induction (Gething et al., 1986). Interestingly, NA and HA harvested from TM treated cells displayed a lower molecular weight than

HA or NA from 6-TG treated cells. TM impairs the addition of the first saccharide in the oligosaccharide complex, allowing the synthesis of HA and NA with no glycan modifications. HA and NA from 6-TG treated cells run at a different molecular weight than TM treated proteins, potentially indicating partial glycosylation. Viral glycoproteins could be extracted from purified virions that were produced from 6-TG-treated cells and analyzed through a combination of nano-liquid chromatography/mass spectrometry and MALDI-TOF mass spectrometry to determine the glycosylation status of the glycoproteins (An et al., 2013; Illiano et al., 2020). These techniques have been used to characterize the glycans found on HA during vaccine production (An et al., 2013). I would also investigate the particle:PFU ratio generated by 6-TG treated cells and compare this ratio to virus produced by untreated cells. I would quantify the HA units, the foci forming units, and PFUs to enumerate particle production. I could also perform a qPCR to quantify the amount of viral RNA present in the cellular supernatant from infected cells and compare this to PFU production. These data would determine whether the virus particles that are generated from infected cells are fully infectious and potentially identify the defect in N-linked glycosylation.

6.5 Further Characterization of IAV RdRp Adaptation Mutations in the Mouse Model will Confirm an Increase in Virus Fitness

In Chapter 5, I demonstrated that the PA E349G substitution significantly improved polymerase activity in both the minigenome replicon assay and in rescued virus. To further characterize the substitutions effect on host adaptation, I would infect mice with recombinant viruses that contain the specific adaptation mutations. I would

generate a virus for each unique polymerase mutation, allowing analysis of the substitution on virus replication within the mouse. I would collect the BALF from infected mice to enumerate virus production. Furthermore, I would generate a virus with paired substitutions, as to analyze if the mutations are working in concert with each other. Analyzing virus replication harbouring the individual mutations would allow me to compare the substitutions to the wildtype virus in the context of viral infection. I would expect these data will confirm that the RdRp adaptation mutations increase viral fitness in the mouse model. This will also allow me to determine whether PB1 mutations affect virus replication in the mouse lung.

6.6 Further Studying the Effects of RdRp Mutations on Viral Polymerase Activity Will Identify Key Viral Processes

The PA E349G substitution flanks the PA oligomerization domain that is required for higher order structures between two polymerase complexes. This domain, which forms dimers of heterotrimers, aids in the synthesis of cRNA and vRNA. What effect does the PA E349G mutation have on the RdRp? I would answer this by analyzing the synthesis of vRNA and cRNA with the PA E349G substitution and compare it to parental polymerase activity. Preliminary results indicated that CA/07-MA produced more vRNA over time compared to the parental virus (Slaine et al., 2018). Analyzing the synthesis of cRNA and vRNA will allow me to quantify genome replication. vRNA and cRNA can be analyzed from the minigenome replicon assay directly, allowing me to quantify at which step the PA E349G polymerase is enhanced. Total RNA would be extracted from transfected cells and cDNA would be synthesized for the positive sense (cRNA and

mRNA) and negative sense (vRNA) RNA. qPCR or radio-labeled primers would allow me to quantify the concentration of the different types of viral RNA between wild-type polymerase and PA E349G substituted polymerase (Robb et al., 2009). It is possible that the PA E349G substitution results in greater accumulation of both cRNA and vRNA, which then would create more mRNA and subsequently synthesize more viral protein. Furthermore, these experiments would allow me to analyze cRNA and vRNA levels in human and mouse cell lines, potentially identifying a new adaptation mechanism in the polymerase complex. These data would further our understanding of IAV RdRp function and genome replication.

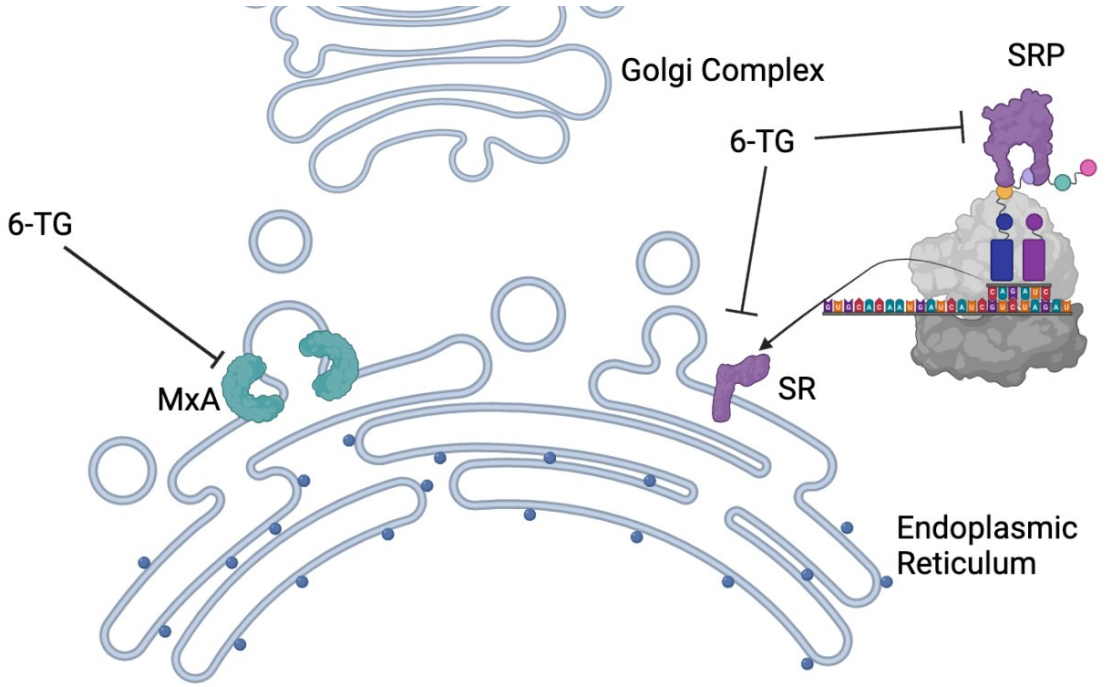

Figure 6.1: Potential GTPases that 6-TG may be inhibiting in the secretory pathway.
6-TG may impair the localization of the nascent polypeptide to the ER by inhibiting the signal recognition particle (SRP) or the SRP receptor (SR). 6-TG may impair dynamin like GTPases (Human MxA), which may be responsible for the tubulation and excision of vesicles budding from the ER. Image was created with BioRender.com

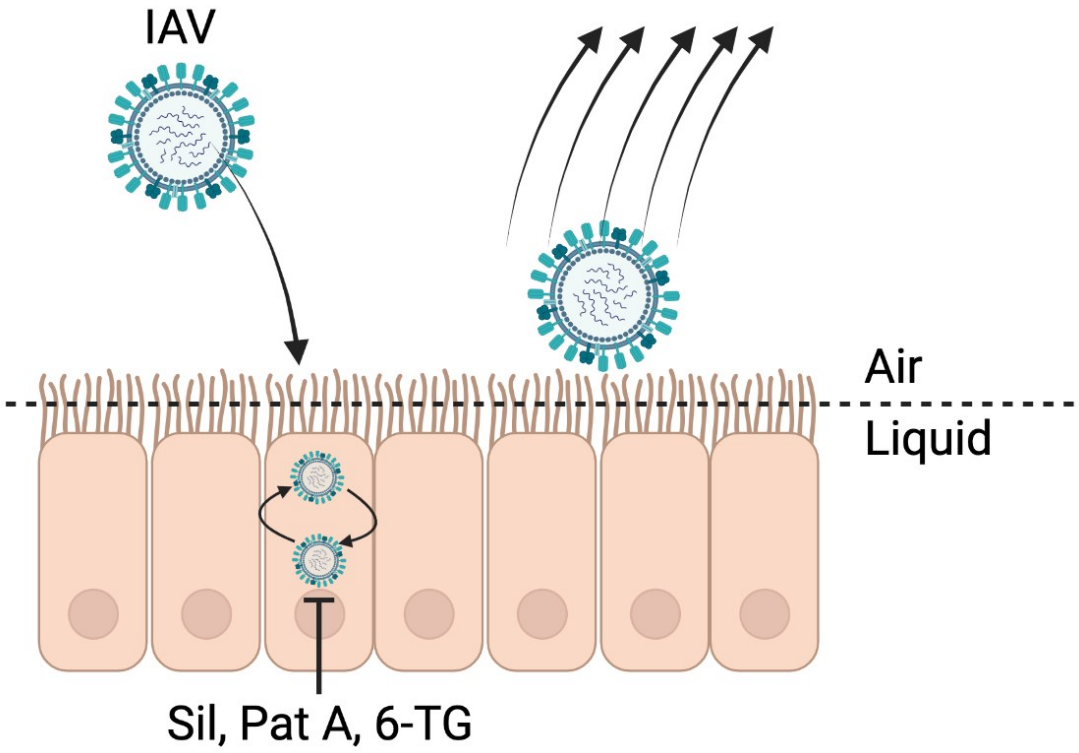

Figure 6.2: Illustration of the air-liquid interface model using primary cell lines. Using the 3D model with primary airway cells allows polarization of cells. Cells would be infected with IAV and treated with the HTA silvestrol (Sil), pateamine A (Pat A), and 6-Thioguanine (6-TG). Image was created with BioRender.com

BIBLIOGRAPHY

Abdul Jabbar, M., & Nayak, D. P. (1987). Signal processing, glycosylation, and secretion of mutant hemagglutinins of a human influenza virus by Saccharomyces cerevisiae. *Molecular and Cellular Biology*, *7*(4), 1476–1485. https://doi.org/10.1128/mcb.7.4.1476

Accola, M. A., Huang, B., Al Masri, A., & McNiven, M. A. (2002). The Antiviral Dynamin Family Member, MxA, Tubulates Lipids and Localizes to the Smooth Endoplasmic Reticulum*. *Journal of Biological Chemistry*, *277*(24), 21829–21835. https://doi.org/10.1074/jbc.M201641200

Ai, W., Zhang, J., Zalloum, W. A., Jia, R., Cherukupalli, S., Ding, X., Sun, Z., Sun, L., Jiang, X., Ma, X., Li, Z., Wang, D., Huang, B., Zhan, P., & Liu, X. (2020). Discovery of novel “Dual-site” binding oseltamivir derivatives as potent influenza virus neuraminidase inhibitors. *European Journal of Medicinal Chemistry*, *191*, 112147. https://doi.org/10.1016/j.ejmech.2020.112147

Akopian, D., Shen, K., Zhang, X., & Shan, S. (2013). Signal Recognition Particle: An essential protein targeting machine. *Annual Review of Biochemistry*, *82*, 693–721. https://doi.org/10.1146/annurev-biochem-072711-164732

Al-Beltagi, S., Preda, C. A., Goulding, L. V., James, J., Pu, J., Skinner, P., Jiang, Z., Wang, B. L., Yang, J., Banyard, A. C., Mellits, K. H., Gershkovich, P., Hayes, C. J., Nguyen-Van-Tam, J., Brown, I. H., Liu, J., & Chang, K.-C. (2021). Thapsigargin Is a Broad-Spectrum Inhibitor of Major Human Respiratory Viruses: Coronavirus, Respiratory Syncytial Virus and Influenza A Virus. *Viruses*, *13*(2). https://doi.org/10.3390/v13020234

Amin-Wetzel, N., Saunders, R. A., Kamphuis, M. J., Rato, C., Preissler, S., Harding, H. P., & Ron, D. (2017). A J-Protein Co-chaperone Recruits BiP to Monomerize IRE1 and Repress the Unfolded Protein Response. *Cell*, *171*(7), 1625-1637.e13. https://doi.org/10.1016/j.cell.2017.10.040

An, Y., Rininger, J. A., Jarvis, D. L., Jing, X., Ye, Z., Aumiller, J. J., Eichelberger, M., & Cipollo, J. F. (2013). Comparative Glycomics Analysis of Influenza Hemagglutinin (H5N1) Produced in Vaccine Relevant Cell Platforms. *Journal of Proteome Research*, *12*(8), 3707–3720. https://doi.org/10.1021/pr400329k

Anand, A. A., & Walter, P. (2020). Structural insights into ISRIB, a memory-enhancing inhibitor of the integrated stress response. *The FEBS Journal*, *287*(2), 239–245. https://doi.org/10.1111/febs.15073

Aragón, T., de la Luna, S., Novoa, I., Carrasco, L., Ortín, J., & Nieto, A. (2000). Eukaryotic translation initiation factor 4GI is a cellular target for NS1 protein, a translational activator of influenza virus. *Molecular and Cellular Biology*, *20*(17), 6259–6268. https://doi.org/10.1128/MCB.20.17.6259-6268.2000

Arias-Mireles, B. H., de Rozieres, C. M., Ly, K., & Joseph, S. (2018). RNA Modulates the Interaction between Influenza A Virus NS1 and Human PABP1. *Biochemistry*, *57*(26), 3590–3598. https://doi.org/10.1021/acs.biochem.8b00218

Bacher, G., Pool, M., & Dobberstein, B. (1999). The Ribosome Regulates the Gtpase of the β-Subunit of the Signal Recognition Particle Receptor. *Journal of Cell Biology*, *146*(4), 723–730. https://doi.org/10.1083/jcb.146.4.723

Back, S. H., Lee, K., Vink, E., & Kaufman, R. J. (2006). Cytoplasmic IRE1alpha-mediated XBP1 mRNA splicing in the absence of nuclear processing and endoplasmic reticulum stress. *The Journal of Biological Chemistry*, *281*(27), 18691–18706. https://doi.org/10.1074/jbc.M602030200

Bao, D., Xue, R., Zhang, M., Lu, C., Ma, T., Ren, C., Zhang, T., Yang, J., Teng, Q., Li, X., Li, Z., & Liu, Q. (2021). N-Linked Glycosylation Plays an Important Role in Budding of Neuraminidase Protein and Virulence of Influenza Viruses. *Journal of Virology*, *95*(3). https://doi.org/10.1128/JVI.02042-20

Baranovich, T., Wong, S.-S., Armstrong, J., Marjuki, H., Webby, R. J., Webster, R. G., & Govorkova, E. A. (2013). T-705 (favipiravir) induces lethal mutagenesis in influenza A H1N1 viruses in vitro. *Journal of Virology*, *87*(7), 3741–3751. https://doi.org/10.1128/JVI.02346-12

Barman, S., & Nayak, D. P. (2000). Analysis of the Transmembrane Domain of Influenza Virus Neuraminidase, a Type II Transmembrane Glycoprotein, for Apical Sorting and Raft Association. *Journal of Virology*, *74*(14), 6538–6545. https://doi.org/10.1128/JVI.74.14.6538-6545.2000

Barry, J. M. (2004). The site of origin of the 1918 influenza pandemic and its public health implications. *Journal of Translational Medicine*, *2*, 3. https://doi.org/10.1186/1479-5876-2-3

Bashir, S., Banday, M., Qadri, O., Bashir, A., Hilal, N., Nida-I-Fatima, null, Rader, S., & Fazili, K. M. (2021). The molecular mechanism and functional diversity of UPR signaling sensor IRE1. *Life Sciences*, *265*, 118740. https://doi.org/10.1016/j.lfs.2020.118740

Bauer, D. L. V., Tellier, M., Martínez-Alonso, M., Nojima, T., Proudfoot, N. J., Murphy, S., & Fodor, E. (2018). Influenza Virus Mounts a Two-Pronged Attack on Host RNA Polymerase II Transcription. *Cell Reports*, *23*(7), 2119-2129.e3. https://doi.org/10.1016/j.celrep.2018.04.047

Bauer, L., Lyoo, H., van der Schaar, H. M., Strating, J. R., & van Kuppeveld, F. J. (2017). Direct-acting antivirals and host-targeting strategies to combat enterovirus infections. *Current Opinion in Virology*, *24*, 1–8. https://doi.org/10.1016/j.coviro.2017.03.009

Bayoumy, A. B., van Liere, E. L. S. A., Simsek, M., Warner, B., Loganayagam, A., Sanderson, J. D., Anderson, S., Nolan, J., de Boer, N. K., Mulder, C. J. J., & Ansari, A. (2020). Efficacy, safety and drug survival of thioguanine as maintenance treatment for inflammatory bowel disease: A retrospective multi-centre study in the United Kingdom. *BMC Gastroenterology*, *20*(1), 296. https://doi.org/10.1186/s12876-020-01441-6

B'chir, W., Maurin, A.-C., Carraro, V., Averous, J., Jousse, C., Muranishi, Y., Parry, L., Stepien, G., Fafournoux, P., & Bruhat, A. (2013). The eIF2α/ATF4 pathway is essential for stress-induced autophagy gene expression. *Nucleic Acids Research*, *41*(16), 7683–7699. https://doi.org/10.1093/nar/gkt563

Beale, R., Wise, H., Stuart, A., Ravenhill, B. J., Digard, P., & Randow, F. (2014). A LC3-Interacting Motif in the Influenza A Virus M2 Protein Is Required to Subvert Autophagy and Maintain Virion Stability. *Cell Host & Microbe*, *15*(2), 239–247. https://doi.org/10.1016/j.chom.2014.01.006

Behillil, S., May, F., Fourati, S., Luyt, C.-E., Chicheportiche, T., Sonneville, R., Tandjaoui-Lambiotte, Y., Roux, D., Guérin, L., Mayaux, J., Maury, E., Ferré, A., Georger, J.-F., Voiriot, G., Enouf, V., van der Werf, S., Dessap, A. M., & de Prost, N. (2020). Oseltamivir Resistance in Severe Influenza A(H1N1)pdm09 Pneumonia and Acute Respiratory Distress Syndrome: A French Multicenter Observational Cohort Study. *Clinical Infectious Diseases: An Official Publication of the Infectious Diseases Society of America*, *71*(4), 1089–1091. https://doi.org/10.1093/cid/ciz904

Belser, J. A., Eckert, A. M., Huynh, T., Gary, J. M., Ritter, J. M., Tumpey, T. M., & Maines, T. R. (2020). A Guide for the Use of the Ferret Model for Influenza Virus Infection. *The American Journal of Pathology*, *190*(1), 11–24. https://doi.org/10.1016/j.ajpath.2019.09.017

Belser, J. A., Jayaraman, A., Raman, R., Pappas, C., Zeng, H., Cox, N. J., Katz, J. M., Sasisekharan, R., & Tumpey, T. M. (2011). Effect of D222G mutation in the hemagglutinin protein on receptor binding, pathogenesis and transmissibility of the 2009 pandemic H1N1 influenza virus. *PloS One*, *6*(9), e25091. http://dx.doi.org.ezproxy.library.dal.ca/10.1371/journal.pone.0025091

Belser, J. A., Katz, J. M., & Tumpey, T. M. (2011). The ferret as a model organism to study influenza A virus infection. *Disease Models & Mechanisms*, *4*(5), 575–579. https://doi.org/10.1242/dmm.007823

Belshaw, R., Sanjuán, R., & Pybus, O. G. (2011). Viral mutation and substitution: Units and levels. *Current Opinion in Virology*, *1*(5), 430–435. https://doi.org/10.1016/j.coviro.2011.08.004

Bertram, S., Glowacka, I., Steffen, I., Kühl, A., & Pöhlmann, S. (2010). Novel insights into proteolytic cleavage of influenza virus hemagglutinin. *Reviews in Medical Virology*, *20*(5), 298–310. https://doi.org/10.1002/rmv.657

Bhagwat, A. R., Le Sage, V., Nturibi, E., Kulej, K., Jones, J., Guo, M., Tae Kim, E., Garcia, B. A., Weitzman, M. D., Shroff, H., & Lakdawala, S. S. (2020). Quantitative live cell imaging reveals influenza virus manipulation of Rab11A transport through reduced dynein association. *Nature Communications*, *11*(1), 23. https://doi.org/10.1038/s41467-019-13838-3

Bier, K., York, A., & Fodor, E. (2011). Cellular cap-binding proteins associate with influenza virus mRNAs. *The Journal of General Virology*, *92*(Pt 7), 1627–1634. https://doi.org/10.1099/vir.0.029231-0

Blum, L., Geisslinger, G., Parnham, M. J., Grünweller, A., & Schiffmann, S. (2020). Natural antiviral compound silvestrol modulates human monocyte-derived macrophages and dendritic cells. *Journal of Cellular and Molecular Medicine*. https://doi.org/10.1111/jcmm.15360

Boda, B., Benaoudia, S., Huang, S., Bonfante, R., Wiszniewski, L., Tseligka, E. D., Tapparel, C., & Constant, S. (2018). Antiviral drug screening by assessing epithelial functions and innate immune responses in human 3D airway epithelium model. *Antiviral Research*, *156*, 72–79. https://doi.org/10.1016/j.antiviral.2018.06.007

Brázda, V., Porubiaková, O., Cantara, A., Bohálová, N., Coufal, J., Bartas, M., Fojta, M., & Mergny, J.-L. (2021). G-quadruplexes in H1N1 influenza genomes. *BMC Genomics*, *22*(1), 77. https://doi.org/10.1186/s12864-021-07377-9

Brito Querido, J., Sokabe, M., Kraatz, S., Gordiyenko, Y., Skehel, J. M., Fraser, C. S., & Ramakrishnan, V. (2020). Structure of a human 48S translational initiation complex. *Science (New York, N.Y.)*, *369*(6508), 1220–1227. https://doi.org/10.1126/science.aba4904

Bronk, J. R., Lister, N., & Shaw, M. I. (1988). Transport and metabolism of 6-thioguanine and 6-mercaptopurine in mouse small intestine. *Clinical Science (London, England: 1979)*, *74*(6), 629–638. https://doi.org/10.1042/cs0740629

Brooke, C. B. (2017). Population diversity and collective interactions during influenza virus infection. *Journal of Virology*, *91*(22), e01164. https://doi.org/10.1128/JVI.01164-17

Brooke, C. B., Ince, W. L., Wrammert, J., Ahmed, R., Wilson, P. C., Bennink, J. R., & Yewdell, J. W. (2013). Most influenza a virions fail to express at least one essential viral protein. *Journal of Virology*, *87*(6), 3155–3162. https://doi.org/10.1128/JVI.02284-12

Brown, E. G. (1990). Increased virulence of a mouse-adapted variant of influenza A/FM/1/47 virus is controlled by mutations in genome segments 4, 5, 7, and 8. *Journal of Virology*, *64*(9), 4523–4533.

Bull, J. J., Meyers, L. A., & Lachmann, M. (2005). Quasispecies Made Simple. *PLoS Computational Biology*, *1*(6). https://doi.org/10.1371/journal.pcbi.0010061

Buratowski, S. (2009). Progression through the RNA polymerase II CTD cycle. *Molecular Cell*, *36*(4), 541–546. https://doi.org/10.1016/j.molcel.2009.10.019

Burchenal, J. H., Murphy, M. L., Ellison, R. R., Sykes, M. P., Tan, T. C., Leone, L. A., Karnofsky, D. A., Craver, L. F., Dargeon, H. W., & Rhoads, C. P. (1953). Clinical Evaluation of a New Antimetabolite, 6-Mercaptopurine, in the Treatment of Leukemia and Allied Diseases. *Blood*, *8*(11), 965–999. https://doi.org/10.1182/blood.V8.11.965.965

Burgui, I., Aragón, T., Ortín, J., & Nieto, A. (2003). PABP1 and eIF4GI associate with influenza virus NS1 protein in viral mRNA translation initiation complexes. *The Journal of General Virology*, *84*(Pt 12), 3263–3274. https://doi.org/10.1099/vir.0.19487-0

Bussey, K. A., Desmet, E. A., Mattiacio, J. L., Hamilton, A., Bradel-Tretheway, B., Bussey, H. E., Kim, B., Dewhurst, S., & Takimoto, T. (2011). PA Residues in the 2009 H1N1 Pandemic Influenza Virus Enhance Avian Influenza Virus Polymerase Activity in Mammalian Cells ▿ . *Journal of Virology*, *85*(14), 7020–7028. https://doi.org/10.1128/JVI.00522-11

Calfon, M., Zeng, H., Urano, F., Till, J. H., Hubbard, S. R., Harding, H. P., Clark, S. G., & Ron, D. (2002). IRE1 couples endoplasmic reticulum load to secretory capacity by processing the XBP-1 mRNA. *Nature*, *415*(6867), 92–96. https://doi.org/10.1038/415092a

Carrique, L., Fan, H., Walker, A. P., Keown, J. R., Sharps, J., Staller, E., Barclay, W. S., Fodor, E., & Grimes, J. M. (2020). Host ANP32A mediates the assembly of the influenza virus replicase. *Nature*, *587*(7835), 638–643. https://doi.org/10.1038/s41586-020-2927-z

Casalegno, J.-S., Bouscambert-Duchamp, M., Caro, V., Schuffenecker, I., Sabatier, M., Traversier, A., Valette, M., Lina, B., Ferraris, O., & Escuret, V. (2010). Oseltamivir-resistant influenza A(H1N1) viruses in south of France, 2007/2009. *Antiviral Research*, *87*(2), 242–248. https://doi.org/10.1016/j.antiviral.2010.05.010

Casao, A., Mata-Campuzano, M., Ordás, L., Cebrián-Pérez, J. A., Muiño-Blanco, T., & Martínez-Pastor, F. (2015). Cleaved PARP-1, an Apoptotic Marker, can be Detected in Ram Spermatozoa. *Reproduction in Domestic Animals = Zuchthygiene*, *50*(4), 688–691. https://doi.org/10.1111/rda.12549

Caspersen, C., Pedersen, P. S., & Treiman, M. (2000). The Sarco/Endoplasmic Reticulum Calcium-ATPase 2b Is an Endoplasmic Reticulum Stress-inducible Protein *. *Journal of Biological Chemistry*, *275*(29), 22363–22372. https://doi.org/10.1074/jbc.M001569200

Cauldwell, A. V., Long, J. S., Moncorgé, O., & Barclay, W. S. (2014). Viral determinants of influenza A virus host range. *The Journal of General Virology*, *95*(Pt 6), 1193–1210. https://doi.org/10.1099/vir.0.062836-0

Cencic, R., & Pelletier, J. (2016). Hippuristanol—A potent steroid inhibitor of eukaryotic initiation factor 4A. *Translation (Austin, Tex.)*, *4*(1), e1137381. https://doi.org/10.1080/21690731.2015.1137381

Chambers, J. M., Lindqvist, L. M., Webb, A., Huang, D. C. S., Savage, G. P., & Rizzacasa, M. A. (2013). Synthesis of biotinylated episilvestrol: Highly selective targeting of the translation factors eIF4AI/II. *Organic Letters*, *15*(6), 1406–1409. https://doi.org/10.1021/ol400401d

Chen, R., & Holmes, E. C. (2006). Avian influenza virus exhibits rapid evolutionary dynamics. *Molecular Biology and Evolution*, *23*(12), 2336–2341. https://doi.org/10.1093/molbev/msl102

Chen, W.-L., Pan, L., Kinghorn, A. D., Swanson, S. M., & Burdette, J. E. (2016). Silvestrol induces early autophagy and apoptosis in human melanoma cells. *BMC Cancer*, *16*, 17. https://doi.org/10.1186/s12885-015-1988-0

Chen, Y., & Brandizzi, F. (2013). IRE1: ER stress sensor and cell fate executor. *Trends in Cell Biology*, *23*(11), 547–555. https://doi.org/10.1016/j.tcb.2013.06.005

Cherepanova, N., Shrimal, S., & Gilmore, R. (2016). N-linked glycosylation and homeostasis of the endoplasmic reticulum. *Current Opinion in Cell Biology*, *41*, 57–65. https://doi.org/10.1016/j.ceb.2016.03.021

Cheung, P. P. H., Watson, S. J., Choy, K.-T., Fun Sia, S., Wong, D. D. Y., Poon, L. L. M., Kellam, P., Guan, Y., Malik Peiris, J. S., & Yen, H.-L. (2014). Generation and characterization of influenza A viruses with altered polymerase fidelity. *Nature Communications*, *5*, 4794. https://doi.org/10.1038/ncomms5794

Chiang, C., Chen, G.-W., & Shih, S.-R. (2008). Mutations at Alternative 5′ Splice Sites of M1 mRNA Negatively Affect Influenza A Virus Viability and Growth Rate. *Journal of Virology*, *82*(21), 10873–10886. https://doi.org/10.1128/JVI.00506-08

Chitalia, V. C., & Munawar, A. H. (2020). A painful lesson from the COVID-19 pandemic: The need for broad-spectrum, host-directed antivirals. *Journal of Translational Medicine*, *18*(1), 390. https://doi.org/10.1186/s12967-020-02476-9

Chitwood, P. J., Juszkiewicz, S., Guna, A., Shao, S., & Hegde, R. S. (2018). EMC Is Required to Initiate Accurate Membrane Protein Topogenesis. *Cell*, *175*(6), 1507-1519.e16. https://doi.org/10.1016/j.cell.2018.10.009

Cho, H., Ahn, S. H., Kim, K. M., & Kim, Y. K. (2013). Non-structural protein 1 of influenza viruses inhibits rapid mRNA degradation mediated by double-stranded RNA-binding protein, staufen1. *FEBS Letters*, *587*(14), 2118–2124. https://doi.org/10.1016/j.febslet.2013.05.029

Chu, J., Galicia-Vázquez, G., Cencic, R., Mills, J. R., Katigbak, A., Porco, J. A., & Pelletier, J. (2016). CRISPR-Mediated Drug-Target Validation Reveals Selective Pharmacological Inhibition of the RNA Helicase, eIF4A. *Cell Reports*, *15*(11), 2340–2347. https://doi.org/10.1016/j.celrep.2016.05.005

Ciampor, F., Cmarko, D., Cmarková, J., & Závodská, E. (1995). Influenza virus M2 protein and haemagglutinin conformation changes during intracellular transport. *Acta Virologica*, *39*(3), 171–181.

Clerici, M., Faini, M., Aebersold, R., & Jinek, M. (2017). Structural insights into the assembly and polyA signal recognition mechanism of the human CPSF complex. *ELife*, *6*, e33111. https://doi.org/10.7554/eLife.33111

Coe, H., & Michalak, M. (2010). ERp57, a multifunctional endoplasmic reticulum resident oxidoreductase. *The International Journal of Biochemistry & Cell Biology*, *42*(6), 796–799. https://doi.org/10.1016/j.biocel.2010.01.009

Copeland, C. S., Zimmer, K. P., Wagner, K. R., Healey, G. A., Mellman, I., & Helenius, A. (1988). Folding, trimerization, and transport are sequential events in the biogenesis of influenza virus hemagglutinin. *Cell*, *53*(2), 197–209. https://doi.org/10.1016/0092-8674(88)90381-9

Cortese, M., Lee, J.-Y., Cerikan, B., Neufeldt, C. J., Oorschot, V. M. J., Köhrer, S., Hennies, J., Schieber, N. L., Ronchi, P., Mizzon, G., Romero-Brey, I., Santarella-Mellwig, R., Schorb, M., Boermel, M., Mocaer, K., Beckwith, M. S., Templin, R. M., Gross, V., Pape, C., … Bartenschlager, R. (2020). Integrative Imaging Reveals SARS-CoV-2-Induced Reshaping of Subcellular Morphologies. *Cell Host & Microbe*, *28*(6), 853-866.e5. https://doi.org/10.1016/j.chom.2020.11.003

Costa, T., Chaves, A. J., Valle, R., Darji, A., van Riel, D., Kuiken, T., Majó, N., & Ramis, A. (2012). Distribution patterns of influenza virus receptors and viral attachment patterns in the respiratory and intestinal tracts of seven avian species. *Veterinary Research*, *43*, 28. https://doi.org/10.1186/1297-9716-43-28

Costa-Mattioli, M., & Walter, P. (2020). The integrated stress response: From mechanism to disease. *Science*, *368*(6489). https://doi.org/10.1126/science.aat5314

Cox, J. S., Shamu, C. E., & Walter, P. (1993). Transcriptional induction of genes encoding endoplasmic reticulum resident proteins requires a transmembrane protein kinase. *Cell*, *73*(6), 1197–1206. https://doi.org/10.1016/0092-8674(93)90648-a

Cox, J. S., & Walter, P. (1996). A novel mechanism for regulating activity of a transcription factor that controls the unfolded protein response. *Cell*, *87*(3), 391–404. https://doi.org/10.1016/s0092-8674(00)81360-4

Credle, J. J., Finer-Moore, J. S., Papa, F. R., Stroud, R. M., & Walter, P. (2005). On the mechanism of sensing unfolded protein in the endoplasmic reticulum. *Proceedings of the National Academy of Sciences of the United States of America*, *102*(52), 18773–18784. https://doi.org/10.1073/pnas.0509487102

Cui, W., Li, J., Ron, D., & Sha, B. (2011). The structure of the PERK kinase domain suggests the mechanism for its activation. *Acta Crystallographica. Section D, Biological Crystallography*, *67*(Pt 5), 423–428. https://doi.org/10.1107/S0907444911006445

D, P., I, T., G, F., C, B., B, B., S, W., D, S., S, T., Pr, G., Xr, B., & Mf, N. (2006). Azathioprine suppresses ezrin-radixin-moesin-dependent T cell-APC conjugation through inhibition of Vav guanosine exchange activity on Rac proteins. *Journal of Immunology (Baltimore, Md. : 1950)*, *176*(1). https://doi.org/10.4049/jimmunol.176.1.640

Dadonaite, B., Gilbertson, B., Knight, M. L., Trifkovic, S., Rockman, S., Laederach, A., Brown, L. E., Fodor, E., & Bauer, D. L. V. (2019). The structure of the influenza A virus genome. *Nature Microbiology*, *4*(11), 1781–1789. https://doi.org/10.1038/s41564-019-0513-7

Dadonaite, B., Vijayakrishnan, S., Fodor, E., Bhella, D., & Hutchinson, E. C. (2016). Filamentous influenza viruses. *The Journal of General Virology*, *97*(8), 1755–1764. https://doi.org/10.1099/jgv.0.000535

Daniels, R., Kurowski, B., Johnson, A. E., & Hebert, D. N. (2003). N-linked glycans direct the cotranslational folding pathway of influenza hemagglutinin. *Molecular Cell*, *11*(1), 79–90. https://doi.org/10.1016/s1097-2765(02)00821-3

Davies, B. E. (2010). Pharmacokinetics of oseltamivir: An oral antiviral for the treatment and prophylaxis of influenza in diverse populations. *Journal of Antimicrobial Chemotherapy*, *65*(Suppl 2), ii5–ii10. https://doi.org/10.1093/jac/dkq015

Davis, A. R., Hiti, A. L., & Nayak, D. P. (1980). Influenza defective interfering viral RNA is formed by internal deletion of genomic RNA. *Proceedings of the National Academy of Sciences of the United States of America*, *77*(1), 215–219. https://doi.org/10.1073/pnas.77.1.215

Davis, C. W., Jackson, K. J. L., McCausland, M. M., Darce, J., Chang, C., Linderman, S. L., Chennareddy, C., Gerkin, R., Brown, S. J., Wrammert, J., Mehta, A. K., Cheung, W. C., Boyd, S. D., Waller, E. K., & Ahmed, R. (2020). Influenza vaccine-induced human bone marrow plasma cells decline within a year after vaccination. *Science (New York, N.Y.)*, *370*(6513), 237–241. https://doi.org/10.1126/science.aaz8432

Davis, D., Yuan, H., Liang, F.-X., Yang, Y.-M., Westley, J., Petzold, C., Dancel-Manning, K., Deng, Y., Sall, J., & Sehgal, P. B. (2019). Human Antiviral Protein MxA Forms Novel Metastable Membraneless Cytoplasmic Condensates Exhibiting Rapid Reversible Tonicity-Driven Phase Transitions. *Journal of Virology*, *93*(22), e01014-19. https://doi.org/10.1128/JVI.01014-19

de Boer, N. K. H., Reinisch, W., Teml, A., van Bodegraven, A. A., Schwab, M., Lukas, M., Ochsenkühn, T., Petritsch, W., Knoflach, P., Almer, S., van der Merwe, S. W., Herrlinger, K. R., Seiderer, J., Vogelsang, H., & Mulder, C. J. J. (2006). 6-Thioguanine Treatment in Inflammatory Bowel Disease: A Critical Appraisal by a European 6-TG Working Party. *Digestion*, *73*(1), 25–31. https://doi.org/10.1159/000091662

de Lucas, S., Peredo, J., Marión, R. M., Sánchez, C., & Ortín, J. (2010). Human Staufen1 protein interacts with influenza virus ribonucleoproteins and is required for efficient virus multiplication. *Journal of Virology*, *84*(15), 7603–7612. https://doi.org/10.1128/JVI.00504-10

Derijks, L. J. J., Gilissen, L. P. L., Engels, L. G. J. B., Bos, L. P., Bus, P. J., Lohman, J. J. H. M., van Deventer, S. J. H., Hommes, D. W., & Hooymans, P. M. (2006). Pharmacokinetics of 6-thioguanine in patients with inflammatory bowel disease. *Therapeutic Drug Monitoring*, *28*(1), 45–50. https://doi.org/10.1097/01.ftd.0000179839.71138.6d

Dharan, N. J., Gubareva, L. V., Meyer, J. J., Okomo-Adhiambo, M., McClinton, R. C., Marshall, S. A., St George, K., Epperson, S., Brammer, L., Klimov, A. I., Bresee, J. S., Fry, A. M., & Oseltamivir-Resistance Working Group. (2009). Infections with oseltamivir-resistant influenza A(H1N1) virus in the United States. *JAMA*, *301*(10), 1034–1041. https://doi.org/10.1001/jama.2009.294

Diab-Assaf, M., Abou-khouzam, R., Saadallah-Zeidan, N., Habib, K., Bitar, N., Karam, W., Liagre, B., Harakeh, S., & Azar, R. (2015). Expression of eukaryotic initiation factor 4E and 4E binding protein 1 in colorectal carcinogenesis. *International Journal of Clinical and Experimental Pathology*, *8*(1), 404–413.

Dias, A., Bouvier, D., Crépin, T., McCarthy, A. A., Hart, D. J., Baudin, F., Cusack, S., & Ruigrok, R. W. H. (2009). The cap-snatching endonuclease of influenza virus polymerase resides in the PA subunit. *Nature*, *458*(7240), 914–918. https://doi.org/10.1038/nature07745

Donnelly, N., Gorman, A. M., Gupta, S., & Samali, A. (2013). The eIF2α kinases: Their structures and functions. *Cellular and Molecular Life Sciences: CMLS*, *70*(19), 3493–3511. https://doi.org/10.1007/s00018-012-1252-6

Duan, M., Hibbs, M. L., & Chen, W. (2017). The contributions of lung macrophage and monocyte heterogeneity to influenza pathogenesis. *Immunology and Cell Biology*, *95*(3), 225–235. https://doi.org/10.1038/icb.2016.97

Egorov, A., Brandt, S., Sereinig, S., Romanova, J., Ferko, B., Katinger, D., Grassauer, A., Alexandrova, G., Katinger, H., & Muster, T. (1998). Transfectant influenza A viruses with long deletions in the NS1 protein grow efficiently in Vero cells. *Journal of Virology*, *72*(8), 6437–6441. https://doi.org/10.1128/JVI.72.8.6437-6441.1998

Ek, S., W, L., & Br, M. (1993). A single amino acid in the PB2 gene of influenza A virus is a determinant of host range. *Journal of Virology*, *67*(4), 1761–1764. https://doi.org/10.1128/jvi.67.4.1761-1764.1993

Elder, K. T., Bye, J. M., Skehel, J. J., Waterfield, M. D., & Smith, A. E. (1979). In vitro synthesis, glycosylation, and membrane insertion of influenza virus haemagglutinin. *Virology*, *95*(2), 343–350. https://doi.org/10.1016/0042-6822(79)90489-6

Elgner, F., Sabino, C., Basic, M., Ploen, D., Grünweller, A., & Hildt, E. (2018). Inhibition of Zika Virus Replication by Silvestrol. *Viruses*, *10*(4). https://doi.org/10.3390/v10040149

Engler, C., Gruetzner, R., Kandzia, R., & Marillonnet, S. (2009). Golden Gate Shuffling: A One-Pot DNA Shuffling Method Based on Type IIs Restriction Enzymes. *PLoS ONE*, *4*(5). https://doi.org/10.1371/journal.pone.0005553

Fan, H., Walker, A. P., Carrique, L., Keown, J. R., Serna Martin, I., Karia, D., Sharps, J., Hengrung, N., Pardon, E., Steyaert, J., Grimes, J. M., & Fodor, E. (2019). Structures of influenza A virus RNA polymerase offer insight into viral genome replication. *Nature*, *573*(7773), 287–290. https://doi.org/10.1038/s41586-019-1530-7

Farrar, J. D. (2014). Type I Interferons in Immunity. In *Reference Module in Biomedical Sciences*. Elsevier. https://doi.org/10.1016/B978-0-12-801238-3.00120-3

Fink, E. E., Moparthy, S., Bagati, A., Bianchi-Smiraglia, A., Lipchick, B. C., Wolff, D. W., Roll, M. V., Wang, J., Liu, S., Bakin, A. V., Kandel, E. S., Lee, A.-H., & Nikiforov, M. A. (2018). XBP1-KLF9 Axis Acts as a Molecular Rheostat to Control the Transition from Adaptive to Cytotoxic Unfolded Protein Response. *Cell Reports*, *25*(1), 212-223.e4. https://doi.org/10.1016/j.celrep.2018.09.013

Flahault, A., & Zylberman, P. (2010). Influenza pandemics: Past, present and future challenges. *Public Health Reviews*, *32*, 319–340. https://doi.org/10.1007/BF03391605

Fodor, E., Mingay, L. J., Crow, M., Deng, T., & Brownlee, G. G. (2003). A single amino acid mutation in the PA subunit of the influenza virus RNA polymerase promotes the generation of defective interfering RNAs. *Journal of Virology*, *77*(8), 5017–5020. https://doi.org/10.1128/jvi.77.8.5017-5020.2003

Forbes, N. E., Ping, J., Dankar, S. K., Jia, J.-J., Selman, M., Keleta, L., Zhou, Y., & Brown, E. G. (2012). Multifunctional Adaptive NS1 Mutations Are Selected upon Human Influenza Virus Evolution in the Mouse. *PLOS ONE*, *7*(2), e31839. https://doi.org/10.1371/journal.pone.0031839

Foster, K. A., Oster, C. G., Mayer, M. M., Avery, M. L., & Audus, K. L. (1998). Characterization of the A549 cell line as a type II pulmonary epithelial cell model for drug metabolism. *Experimental Cell Research*, *243*(2), 359–366. https://doi.org/10.1006/excr.1998.4172

Frabutt, D. A., Wang, B., Riaz, S., Schwartz, R. C., & Zheng, Y.-H. (2018). Innate Sensing of Influenza A Virus Hemagglutinin Glycoproteins by the Host Endoplasmic Reticulum (ER) Stress Pathway Triggers a Potent Antiviral Response via ER-Associated Protein Degradation. *Journal of Virology*, *92*(1). https://doi.org/10.1128/JVI.01690-17

Freiden, P. J., Gaut, J. R., & Hendershot, L. M. (1992). Interconversion of three differentially modified and assembled forms of BiP. *The EMBO Journal*, *11*(1), 63–70.

Frosi, Y., Usher, R., Lian, D. T. G., Lane, D. P., & Brown, C. J. (2019). Monitoring flux in signalling pathways through measurements of 4EBP1-mediated eIF4F complex assembly. *BMC Biology*, *17*(1), 40. https://doi.org/10.1186/s12915-019-0658-0

Fulda, S., Honer, M., Menke-Moellers, I., & Berthold, F. (1995). Antiproliferative potential of cytostatic drugs on neuroblastoma cells in vitro. *European Journal of Cancer (Oxford, England: 1990)*, *31A*(4), 616–621. https://doi.org/10.1016/0959-8049(95)00055-n

Gack, M. U., Albrecht, R. A., Urano, T., Inn, K.-S., Huang, I.-C., Carnero, E., Farzan, M., Inoue, S., Jung, J. U., & García-Sastre, A. (2009). Influenza A virus NS1 targets the ubiquitin ligase TRIM25 to evade recognition by the host viral RNA sensor RIG-I. *Cell Host & Microbe*, *5*(5), 439–449. https://doi.org/10.1016/j.chom.2009.04.006

Galicia-Vázquez, G., Cencic, R., Robert, F., Agenor, A. Q., & Pelletier, J. (2012). A cellular response linking eIF4AI activity to eIF4AII transcription. *RNA (New York, N.Y.)*, *18*(7), 1373–1384. https://doi.org/10.1261/rna.033209.112

Gamblin, S. J., & Skehel, J. J. (2010). Influenza Hemagglutinin and Neuraminidase Membrane Glycoproteins. *The Journal of Biological Chemistry*, *285*(37), 28403–28409. https://doi.org/10.1074/jbc.R110.129809

Gao, B., Gong, X., Fang, S., Weng, W., Wang, H., Chu, H., Sun, Y., Meng, C., Tan, L., Song, C., Qiu, X., Liu, W., Forlenza, M., Ding, C., & Liao, Y. (2021). Inhibition of anti-viral stress granule formation by coronavirus endoribonuclease nsp15 ensures efficient virus replication. *PLoS Pathogens*, *17*(2). https://doi.org/10.1371/journal.ppat.1008690

García-García, C., Frieda, K. L., Feoktistova, K., Fraser, C. S., & Block, S. M. (2015). RNA BIOCHEMISTRY. Factor-dependent processivity in human eIF4A DEAD-box helicase. *Science (New York, N.Y.)*, *348*(6242), 1486–1488. https://doi.org/10.1126/science.aaa5089

Gaucherand, L., Porter, B. K., Levene, R. E., Price, E. L., Schmaling, S. K., Rycroft, C. H., Kevorkian, Y., McCormick, C., Khaperskyy, D. A., & Gaglia, M. M. (2019). The Influenza A Virus Endoribonuclease PA-X Usurps Host mRNA Processing Machinery to Limit Host Gene Expression. *Cell Reports*, *27*(3), 776-792.e7. https://doi.org/10.1016/j.celrep.2019.03.063

Gaymard, A., Le Briand, N., Frobert, E., Lina, B., & Escuret, V. (2016). Functional balance between neuraminidase and haemagglutinin in influenza viruses. *Clinical Microbiology and Infection: The Official Publication of the European Society of Clinical Microbiology and Infectious Diseases*, *22*(12), 975–983. https://doi.org/10.1016/j.cmi.2016.07.007

Gething, M. J., McCammon, K., & Sambrook, J. (1986). Expression of wild-type and mutant forms of influenza hemagglutinin: The role of folding in intracellular transport. *Cell*, *46*(6), 939–950. https://doi.org/10.1016/0092-8674(86)90076-0

Ghafari, M., Lumby, C. K., Weissman, D. B., & Illingworth, C. J. R. (2020). Inferring Transmission Bottleneck Size from Viral Sequence Data Using a Novel Haplotype Reconstruction Method. *Journal of Virology*, *94*(13), e00014-20. https://doi.org/10.1128/JVI.00014-20

Ghoneim, H. E., Thomas, P. G., & McCullers, J. A. (2013). Depletion of alveolar macrophages during influenza infection facilitates bacterial superinfections. *Journal of Immunology (Baltimore, Md.: 1950)*, *191*(3), 1250–1259. https://doi.org/10.4049/jimmunol.1300014

Ghosh, A., & Lima, C. D. (2010). Enzymology of RNA cap synthesis. *Wiley Interdisciplinary Reviews. RNA*, *1*(1), 152–172. https://doi.org/10.1002/wrna.19

Glitscher, M., Himmelsbach, K., Woytinek, K., Johne, R., Reuter, A., Spiric, J., Schwaben, L., Grünweller, A., & Hildt, E. (2018). Inhibition of Hepatitis E Virus Spread by the Natural Compound Silvestrol. *Viruses*, *10*(6). https://doi.org/10.3390/v10060301

Goldhill, D. H., Te Velthuis, A. J. W., Fletcher, R. A., Langat, P., Zambon, M., Lackenby, A., & Barclay, W. S. (2018). The mechanism of resistance to favipiravir in influenza. *Proceedings of the National Academy of Sciences of the United States of America*, *115*(45), 11613–11618. https://doi.org/10.1073/pnas.1811345115

Gonatopoulos-Pournatzis, T., & Cowling, V. H. (2014). Cap-binding complex (CBC). *The Biochemical Journal*, *457*(2), 231–242. https://doi.org/10.1042/BJ20131214

Goñi, N., Iriarte, A., Comas, V., Soñora, M., Moreno, P., Moratorio, G., Musto, H., & Cristina, J. (2012). Pandemic influenza A virus codon usage revisited: Biases, adaptation and implications for vaccine strain development. *Virology Journal*, *9*, 263. https://doi.org/10.1186/1743-422X-9-263

Goulding, L. V., Yang, J., Jiang, Z., Zhang, H., Lea, D., Emes, R. D., Dottorini, T., Pu, J., Liu, J., & Chang, K.-C. (2020). Thapsigargin at Non-Cytotoxic Levels Induces a Potent Host Antiviral Response that Blocks Influenza A Virus Replication. *Viruses*, *12*(10). https://doi.org/10.3390/v12101093

Grabherr, R., & Ernst, W. (2010). Baculovirus for eukaryotic protein display. *Current Gene Therapy*, *10*(3), 195–200. https://doi.org/10.2174/156652310791321297

Greenbaum, B. D., Rabadan, R., & Levine, A. J. (2009). Patterns of oligonucleotide sequences in viral and host cell RNA identify mediators of the host innate immune system. *PloS One*, *4*(6), e5969. https://doi.org/10.1371/journal.pone.0005969

Grimm, D., Staeheli, P., Hufbauer, M., Koerner, I., Martínez-Sobrido, L., Solórzano, A., García-Sastre, A., Haller, O., & Kochs, G. (2007). Replication fitness determines high virulence of influenza A virus in mice carrying functional Mx1 resistance gene. *Proceedings of the National Academy of Sciences*, *104*(16), 6806–6811. https://doi.org/10.1073/pnas.0701849104

Gu, H., Fan, R. L. Y., Wang, D., & Poon, L. L. M. (2019). Dinucleotide evolutionary dynamics in influenza A virus. *Virus Evolution*, *5*(2), vez038. https://doi.org/10.1093/ve/vez038

Guo, J., Gao, X., Liu, B., Li, Y., Liu, W., Lu, J., Liu, C., Xue, R., & Li, X. (2020). Mouse adaptation of the H9N2 avian influenza virus causes the downregulation of genes related to innate immune responses and ubiquitin-mediated proteolysis in mice. *Medical Microbiology and Immunology*, *209*(2), 151–161. https://doi.org/10.1007/s00430-020-00656-4

Gupta, S. V., Sass, E. J., Davis, M. E., Edwards, R. B., Lozanski, G., Heerema, N. A., Lehman, A., Zhang, X., Jarjoura, D., Byrd, J. C., Pan, L., Chan, K. K., Kinghorn, A. D., Phelps, M. A., Grever, M. R., & Lucas, D. M. (2011). Resistance to the translation initiation inhibitor silvestrol is mediated by ABCB1/P-glycoprotein overexpression in acute lymphoblastic leukemia cells. *The AAPS Journal*, *13*(3), 357–364. https://doi.org/10.1208/s12248-011-9276-7

Haga, R. B., & Ridley, A. J. (2016). Rho GTPases: Regulation and roles in cancer cell biology. *Small GTPases*, *7*(4), 207–221. https://doi.org/10.1080/21541248.2016.1232583

Haller, O., & Kochs, G. (2020). Mx genes: Host determinants controlling influenza virus infection and trans-species transmission. *Human Genetics*, *139*(6–7), 695–705. https://doi.org/10.1007/s00439-019-02092-8

Hamilton, K., Sun, Y., & Tong, L. (2019). Biophysical characterizations of the recognition of the AAUAAA polyadenylation signal. *RNA (New York, N.Y.)*, *25*(12), 1673–1680. https://doi.org/10.1261/rna.070870.119

Harding, H. P., Zhang, Y., Bertolotti, A., Zeng, H., & Ron, D. (2000). Perk Is Essential for Translational Regulation and Cell Survival during the Unfolded Protein Response. *Molecular Cell*, *5*(5), 897–904. https://doi.org/10.1016/S1097-2765(00)80330-5

Harding, H. P., Zhang, Y., & Ron, D. (1999). Protein translation and folding are coupled by an endoplasmic-reticulum-resident kinase. *Nature*, *397*(6716), 271–274. https://doi.org/10.1038/16729

Harding, H. P., Zhang, Y., Zeng, H., Novoa, I., Lu, P. D., Calfon, M., Sadri, N., Yun, C., Popko, B., Paules, R., Stojdl, D. F., Bell, J. C., Hettmann, T., Leiden, J. M., & Ron, D. (2003). An integrated stress response regulates amino acid metabolism and resistance to oxidative stress. *Molecular Cell*, *11*(3), 619–633. https://doi.org/10.1016/s1097-2765(03)00105-9

Harlen, K. M., & Churchman, L. S. (2017). The code and beyond: Transcription regulation by the RNA polymerase II carboxy-terminal domain. *Nature Reviews. Molecular Cell Biology*, *18*(4), 263–273. https://doi.org/10.1038/nrm.2017.10

Hassan, I. H., Zhang, M. S., Powers, L. S., Shao, J. Q., Baltrusaitis, J., Rutkowski, D. T., Legge, K., & Monick, M. M. (2012). Influenza A viral replication is blocked by inhibition of the inositol-requiring enzyme 1 (IRE1) stress pathway. *The Journal of Biological Chemistry*, *287*(7), 4679–4689. https://doi.org/10.1074/jbc.M111.284695

Hay, A. J., Gregory, V., Douglas, A. R., & Lin, Y. P. (2001). The Evolution of Human Influenza Viruses. *Philosophical Transactions: Biological Sciences*, *356*(1416), 1861–1870.

He, G., Massarella, J., & Ward, P. (1999). Clinical pharmacokinetics of the prodrug oseltamivir and its active metabolite Ro 64-0802. *Clinical Pharmacokinetics*, *37*(6), 471–484. https://doi.org/10.2165/00003088-199937060-00003

Heaton, B. E., Kennedy, E. M., Dumm, R. E., Harding, A. T., Sacco, M. T., Sachs, D., & Heaton, N. S. (2017). A CRISPR Activation Screen Identifies a Pan-avian Influenza Virus Inhibitory Host Factor. *Cell Reports*, *20*(7), 1503–1512. https://doi.org/10.1016/j.celrep.2017.07.060

Hellen, C. U. T., & Sarnow, P. (2001). Internal ribosome entry sites in eukaryotic mRNA molecules. *Genes & Development*, *15*(13), 1593–1612. https://doi.org/10.1101/gad.891101

Heneghan, C. J., Onakpoya, I., Jones, M. A., Doshi, P., Del Mar, C. B., Hama, R., Thompson, M. J., Spencer, E. A., Mahtani, K. R., Nunan, D., Howick, J., & Jefferson, T. (2016). Neuraminidase inhibitors for influenza: A systematic review and meta-analysis of regulatory and mortality data. *Health Technology Assessment (Winchester, England)*, *20*(42), 1–242. https://doi.org/10.3310/hta20420

Herfst, S., Schrauwen, E. J. A., Linster, M., Chutinimitkul, S., de Wit, E., Munster, V. J., Sorrell, E. M., Bestebroer, T. M., Burke, D. F., Smith, D. J., Rimmelzwaan, G. F., Osterhaus, A. D. M. E., & Fouchier, R. A. M. (2012). Airborne transmission of influenza A/H5N1 virus between ferrets. *Science (New York, N.Y.)*, *336*(6088), 1534–1541. https://doi.org/10.1126/science.1213362

Higa, A., Taouji, S., Lhomond, S., Jensen, D., Fernandez-Zapico, M. E., Simpson, J. C., Pasquet, J.-M., Schekman, R., & Chevet, E. (2014). Endoplasmic Reticulum Stress-Activated Transcription Factor ATF6α Requires the Disulfide Isomerase PDIA5 To Modulate Chemoresistance. *Molecular and Cellular Biology*, *34*(10), 1839–1849. https://doi.org/10.1128/MCB.01484-13

Hinnebusch, A. G. (2011). Molecular mechanism of scanning and start codon selection in eukaryotes. *Microbiology and Molecular Biology Reviews: MMBR*, *75*(3), 434–467, first page of table of contents. https://doi.org/10.1128/MMBR.00008-11

Hinte, F., van Anken, E., Tirosh, B., & Brune, W. (2020). Repression of viral gene expression and replication by the unfolded protein response effector XBP1u. *ELife*, *9*. https://doi.org/10.7554/eLife.51804

Hirst, G. K. (1947). STUDIES ON THE MECHANISM OF ADAPTATION OF INFLUENZA VIRUS TO MICE. *Journal of Experimental Medicine*, *86*(5), 357–366. https://doi.org/10.1084/jem.86.5.357

Hitomi, J., Katayama, T., Taniguchi, M., Honda, A., Imaizumi, K., & Tohyama, M. (2004). Apoptosis induced by endoplasmic reticulum stress depends on activation of caspase-3 via caspase-12. *Neuroscience Letters*, *357*(2), 127–130. https://doi.org/10.1016/j.neulet.2003.12.080

Hoffmann, E., Neumann, G., Kawaoka, Y., Hobom, G., & Webster, R. G. (2000). A DNA transfection system for generation of influenza A virus from eight plasmids. *Proceedings of the National Academy of Sciences*, *97*(11), 6108–6113. https://doi.org/10.1073/pnas.100133697

Hoffmann, E., Stech, J., Guan, Y., Webster, R. G., & Perez, D. R. (2001). Universal primer set for the full-length amplification of all influenza A viruses. *Archives of Virology*, *146*(12), 2275–2289. https://doi.org/10.1007/s007050170002

Hoffmann, H.-H., Schneider, W. M., Blomen, V. A., Scull, M. A., Hovnanian, A., Brummelkamp, T. R., & Rice, C. M. (2017). Diverse Viruses Require the Calcium Transporter SPCA1 for Maturation and Spread. *Cell Host & Microbe*, *22*(4), 460-470.e5. https://doi.org/10.1016/j.chom.2017.09.002

Hogue, B. G., & Nayak, D. P. (1992). Synthesis and processing of the influenza virus neuraminidase, a type II transmembrane glycoprotein. *Virology*, *188*(2), 510–517. https://doi.org/10.1016/0042-6822(92)90505-j

Hogue, B. G., & Nayak, D. P. (1994). Deletion mutation in the signal anchor domain activates cleavage of the influenza virus neuraminidase, a type II transmembrane protein. *The Journal of General Virology*, *75 (Pt 5)*, 1015–1022. https://doi.org/10.1099/0022-1317-75-5-1015

Holcik, M., & Pestova, T. V. (2007). Translation mechanism and regulation: Old players, new concepts. *EMBO Reports*, *8*(7), 639–643. https://doi.org/10.1038/sj.embor.7400988

Hollien, J., Lin, J. H., Li, H., Stevens, N., Walter, P., & Weissman, J. S. (2009). Regulated Ire1-dependent decay of messenger RNAs in mammalian cells. *The Journal of Cell Biology*, *186*(3), 323–331. https://doi.org/10.1083/jcb.200903014

Honce, R., & Schultz-Cherry, S. (2019). Impact of Obesity on Influenza A Virus Pathogenesis, Immune Response, and Evolution. *Frontiers in Immunology*, *10*, 1071. https://doi.org/10.3389/fimmu.2019.01071

Hu, J., & Rapoport, T. A. (2016). Fusion of the endoplasmic reticulum by membrane-bound GTPases. *Seminars in Cell & Developmental Biology*, *60*, 105–111. https://doi.org/10.1016/j.semcdb.2016.06.001

Huang, B. Y., & Fernández, I. S. (2020). Long-range interdomain communications in eIF5B regulate GTP hydrolysis and translation initiation. *Proceedings of the National Academy of Sciences of the United States of America*, *117*(3), 1429–1437. https://doi.org/10.1073/pnas.1916436117

Hull, J. D., Gilmore, R., & Lamb, R. A. (1988). Integration of a small integral membrane protein, M2, of influenza virus into the endoplasmic reticulum: Analysis of the internal signal-anchor domain of a protein with an ectoplasmic NH2 terminus. *The Journal of Cell Biology*, *106*(5), 1489–1498. https://doi.org/10.1083/jcb.106.5.1489

Ibricevic, A., Pekosz, A., Walter, M. J., Newby, C., Battaile, J. T., Brown, E. G., Holtzman, M. J., & Brody, S. L. (2006). Influenza virus receptor specificity and cell tropism in mouse and human airway epithelial cells. *Journal of Virology*, *80*(15), 7469–7480. https://doi.org/10.1128/JVI.02677-05

Ichikawa, A., Kuba, K., Morita, M., Chida, S., Tezuka, H., Hara, H., Sasaki, T., Ohteki, T., Ranieri, V. M., dos Santos, C. C., Kawaoka, Y., Akira, S., Luster, A. D., Lu, B., Penninger, J. M., Uhlig, S., Slutsky, A. S., & Imai, Y. (2013). CXCL10-CXCR3 enhances the development of neutrophil-mediated fulminant lung injury of viral and nonviral origin. *American Journal of Respiratory and Critical Care Medicine*, *187*(1), 65–77. https://doi.org/10.1164/rccm.201203-0508OC

Illiano, A., Pinto, G., Melchiorre, C., Carpentieri, A., Faraco, V., & Amoresano, A. (2020). Protein Glycosylation Investigated by Mass Spectrometry: An Overview. *Cells*, *9*(9), E1986. https://doi.org/10.3390/cells9091986

Ilyushina, N. A., Khalenkov, A. M., Seiler, J. P., Forrest, H. L., Bovin, N. V., Marjuki, H., Barman, S., Webster, R. G., & Webby, R. J. (2010). Adaptation of pandemic H1N1 influenza viruses in mice. *Journal of Virology*, *84*(17), 8607–8616. https://doi.org/10.1128/JVI.00159-10

Imai, M., Watanabe, T., Hatta, M., Das, S. C., Ozawa, M., Shinya, K., Zhong, G., Hanson, A., Katsura, H., Watanabe, S., Li, C., Kawakami, E., Yamada, S., Kiso, M., Suzuki, Y., Maher, E. A., Neumann, G., & Kawaoka, Y. (2012). Experimental adaptation of an influenza H5 HA confers respiratory droplet transmission to a reassortant H5 HA/H1N1 virus in ferrets. *Nature*, *486*(7403), 420–428. https://doi.org/10.1038/nature10831

Influenza A virus defective viral genomes are inefficiently packaged into virions relative to wild-type genomic RNAs | bioRxiv. (n.d.). Retrieved May 21, 2021, from https://www.biorxiv.org/content/10.1101/2021.05.13.444068v1

Ito, T., Couceiro, J. N., Kelm, S., Baum, L. G., Krauss, S., Castrucci, M. R., Donatelli, I., Kida, H., Paulson, J. C., Webster, R. G., & Kawaoka, Y. (1998). Molecular basis for the generation in pigs of influenza A viruses with pandemic potential. *Journal of Virology*, *72*(9), 7367–7373. https://doi.org/10.1128/JVI.72.9.7367-7373.1998

Ivanov, P., Kedersha, N., & Anderson, P. (2019). Stress Granules and Processing Bodies in Translational Control. *Cold Spring Harbor Perspectives in Biology*, *11*(5), a032813. https://doi.org/10.1101/cshperspect.a032813

Iwasaki, S., Floor, S. N., & Ingolia, N. T. (2016). Rocaglates convert DEAD-box protein eIF4A into a sequence-selective translational repressor. *Nature*, *534*(7608), 558–561. https://doi.org/10.1038/nature17978

Iwata, S., Masuhara, K., Umeki, N., Sako, Y., & Maruta, S. (2016). Interaction of a novel fluorescent GTP analogue with the small G-protein K-Ras. *The Journal of Biochemistry*, *159*(1), 41–48. https://doi.org/10.1093/jb/mvv071

Jagger, B. W., Wise, H. M., Kash, J. C., Walters, K.-A., Wills, N. M., Xiao, Y.-L., Dunfee, R. L., Schwartzman, L. M., Ozinsky, A., Bell, G. L., Dalton, R. M., Lo, A., Efstathiou, S., Atkins, J. F., Firth, A. E., Taubenberger, J. K., & Digard, P. (2012). An overlapping protein-coding region in influenza A virus segment 3 modulates the host response. *Science (New York, N.Y.)*, *337*(6091), 199–204. https://doi.org/10.1126/science.1222213

Janda, C. Y., Li, J., Oubridge, C., Hernández, H., Robinson, C. V., & Nagai, K. (2010). Recognition of a signal peptide by the signal recognition particle. *Nature*, *465*(7297), 507–510. https://doi.org/10.1038/nature08870

Jefferson, T., Jones, M. A., Doshi, P., Del Mar, C. B., Hama, R., Thompson, M. J., Spencer, E. A., Onakpoya, I. J., Mahtani, K. R., Nunan, D., Howick, J., & Heneghan, C. J. (2014). Neuraminidase inhibitors for preventing and treating influenza in adults and children. *The Cochrane Database of Systematic Reviews*, *2014*(4). https://doi.org/10.1002/14651858.CD008965.pub4

Jharap, B., de Boer, N., Vos, R., Smid, K., Zwiers, A., Peters, G., Mulder, C., Wilhelm, A., & van Bodegraven, A. (2011). Biotransformation of 6-thioguanine in inflammatory bowel disease patients: A comparison of oral and intravenous administration of 6-thioguanine. *British Journal of Pharmacology*, *163*(4), 722–731. https://doi.org/10.1111/j.1476-5381.2011.01265.x

Johnston, B. P., Pringle, E. S., & McCormick, C. (2019). KSHV activates unfolded protein response sensors but suppresses downstream transcriptional responses to support lytic replication. *PLoS Pathogens*, *15*(12), e1008185. https://doi.org/10.1371/journal.ppat.1008185

Joshi, A., Newbatt, Y., McAndrew, P. C., Stubbs, M., Burke, R., Richards, M. W., Bhatia, C., Caldwell, J. J., McHardy, T., Collins, I., & Bayliss, R. (2015). Molecular mechanisms of human IRE1 activation through dimerization and ligand binding. *Oncotarget*, *6*(15), 13019–13035. https://doi.org/10.18632/oncotarget.3864

Jurkin, J., Henkel, T., Nielsen, A. F., Minnich, M., Popow, J., Kaufmann, T., Heindl, K., Hoffmann, T., Busslinger, M., & Martinez, J. (2014). The mammalian tRNA ligase complex mediates splicing of XBP1 mRNA and controls antibody secretion in plasma cells. *The EMBO Journal*, *33*(24), 2922–2936. https://doi.org/10.15252/embj.201490332

Jwa, M., & Chang, P. (2012). PARP16 is a tail-anchored endoplasmic reticulum protein required for the PERK- and IRE1α-mediated unfolded protein response. *Nature Cell Biology*, *14*(11), 1223–1230. https://doi.org/10.1038/ncb2593

Karlas, A., Machuy, N., Shin, Y., Pleissner, K.-P., Artarini, A., Heuer, D., Becker, D., Khalil, H., Ogilvie, L. A., Hess, S., Mäurer, A. P., Müller, E., Wolff, T., Rudel, T., & Meyer, T. F. (2010). Genome-wide RNAi screen identifies human host factors crucial for influenza virus replication. *Nature*, *463*(7282), 818–822. https://doi.org/10.1038/nature08760

Kearse, M., Moir, R., Wilson, A., Stones-Havas, S., Cheung, M., Sturrock, S., Buxton, S., Cooper, A., Markowitz, S., Duran, C., Thierer, T., Ashton, B., Meintjes, P., & Drummond, A. (2012). Geneious Basic: An integrated and extendable desktop software platform for the organization and analysis of sequence data. *Bioinformatics*, *28*(12), 1647–1649. https://doi.org/10.1093/bioinformatics/bts199

Kedersha, N., Chen, S., Gilks, N., Li, W., Miller, I. J., Stahl, J., & Anderson, P. (2002). Evidence that ternary complex (eIF2-GTP-tRNA(i)(Met))-deficient preinitiation complexes are core constituents of mammalian stress granules. *Molecular Biology of the Cell*, *13*(1), 195–210. https://doi.org/10.1091/mbc.01-05-0221

Kedersha, N., Panas, M. D., Achorn, C. A., Lyons, S., Tisdale, S., Hickman, T., Thomas, M., Lieberman, J., McInerney, G. M., Ivanov, P., & Anderson, P. (2016). G3BP-Caprin1-USP10 complexes mediate stress granule condensation and associate with 40S subunits. *The Journal of Cell Biology*, *212*(7), 845–860. https://doi.org/10.1083/jcb.201508028

Kedersha, N., Panas, M. D., Achorn, C. A., Lyons, S., Tisdale, S., Hickman, T., Thomas, M., Lieberman, J., McInerney, G. M., Ivanov, P., & Anderson, P. (2020). Correction: G3BP-Caprin1-USP10 complexes mediate stress granule condensation and associate with 40S subunits. *The Journal of Cell Biology*, *219*(1). https://doi.org/10.1083/jcb.20150802809202019c

Keestra-Gounder, A. M., Byndloss, M. X., Seyffert, N., Young, B. M., Chávez-Arroyo, A., Tsai, A. Y., Cevallos, S. A., Winter, M. G., Pham, O. H., Tiffany, C. R., de Jong, M. F., Kerrinnes, T., Ravindran, R., Luciw, P. A., McSorley, S. J., Bäumler, A. J., & Tsolis, R. M. (2016). NOD1/NOD2 signaling links ER stress with inflammation. *Nature*, *532*(7599), 394–397. https://doi.org/10.1038/nature17631

Khaperskyy, D. A., Emara, M. M., Johnston, B. P., Anderson, P., Hatchette, T. F., & McCormick, C. (2014). Influenza a virus host shutoff disables antiviral stress-induced translation arrest. *PLoS Pathogens*, *10*(7), e1004217. https://doi.org/10.1371/journal.ppat.1004217

Khaperskyy, D. A., Hatchette, T. F., & McCormick, C. (2012). Influenza A virus inhibits cytoplasmic stress granule formation. *FASEB Journal: Official Publication of the Federation of American Societies for Experimental Biology*, *26*(4), 1629–1639. https://doi.org/10.1096/fj.11-196915

Khaperskyy, D. A., Schmaling, S., Larkins-Ford, J., McCormick, C., & Gaglia, M. M. (2016). Selective Degradation of Host RNA Polymerase II Transcripts by Influenza A Virus PA-X Host Shutoff Protein. *PLoS Pathogens*, *12*(2), e1005427. https://doi.org/10.1371/journal.ppat.1005427

Kim, S., Hwang, B. Y., Su, B.-N., Chai, H., Mi, Q., Kinghorn, A. D., Wild, R., & Swanson, S. M. (2007). Silvestrol, a potential anticancer rocaglate derivative from Aglaia foveolata, induces apoptosis in LNCaP cells through the mitochondrial/apoptosome pathway without activation of executioner caspase-3 or -7. *Anticancer Research*, *27*(4B), 2175–2183.

Klenk, H.-D., Rott, R., Orlich, M., & Blödorn, J. (1975). Activation of influenza A viruses by trypsin treatment. *Virology*, *68*(2), 426–439. https://doi.org/10.1016/0042-6822(75)90284-6

Knoops, K., Kikkert, M., Worm, S. H. E. van den, Zevenhoven-Dobbe, J. C., Meer, Y. van der, Koster, A. J., Mommaas, A. M., & Snijder, E. J. (2008). SARS-Coronavirus Replication Is Supported by a Reticulovesicular Network of Modified Endoplasmic Reticulum. *PLOS Biology*, *6*(9), e226. https://doi.org/10.1371/journal.pbio.0060226

Koelle, K., Cobey, S., Grenfell, B., & Pascual, M. (2006). Epochal Evolution Shapes the Phylodynamics of Interpandemic Influenza A (H3N2) in Humans. *Science*, *314*(5807), 1898–1903. https://doi.org/10.1126/science.1132745

Kolb, P. S., Ayaub, E. A., Zhou, W., Yum, V., Dickhout, J. G., & Ask, K. (2015). The therapeutic effects of 4-phenylbutyric acid in maintaining proteostasis. *The International Journal of Biochemistry & Cell Biology*, *61*, 45–52. https://doi.org/10.1016/j.biocel.2015.01.015

Koshimichi, H., Ishibashi, T., Kawaguchi, N., Sato, C., Kawasaki, A., & Wajima, T. (2018). Safety, Tolerability, and Pharmacokinetics of the Novel Anti-influenza Agent Baloxavir Marboxil in Healthy Adults: Phase I Study Findings. *Clinical Drug Investigation*, *38*(12), 1189–1196. https://doi.org/10.1007/s40261-018-0710-9

Kosik, I., & Yewdell, J. W. (2019). Influenza Hemagglutinin and Neuraminidase: Yin–Yang Proteins Coevolving to Thwart Immunity. *Viruses*, *11*(4). https://doi.org/10.3390/v11040346

Kozlov, G., & Gehring, K. (2020). Calnexin cycle—Structural features of the ER chaperone system. *The FEBS Journal*, *287*(20), 4322–4340. https://doi.org/10.1111/febs.15330

Krishnamoorthy, T., Pavitt, G. D., Zhang, F., Dever, T. E., & Hinnebusch, A. G. (2001). Tight binding of the phosphorylated alpha subunit of initiation factor 2 (eIF2alpha) to the regulatory subunits of guanine nucleotide exchange factor eIF2B is required for inhibition of translation initiation. *Molecular and Cellular Biology*, *21*(15), 5018–5030. https://doi.org/10.1128/MCB.21.15.5018-5030.2001

Kumar, N., Khandelwal, N., Kumar, R., Chander, Y., Rawat, K. D., Chaubey, K. K., Sharma, S., Singh, S. V., Riyesh, T., Tripathi, B. N., & Barua, S. (2019). Inhibitor of Sarco/Endoplasmic Reticulum Calcium-ATPase Impairs Multiple Steps of Paramyxovirus Replication. *Frontiers in Microbiology*, *10*. https://doi.org/10.3389/fmicb.2019.00209

Kutter, J. S., Spronken, M. I., Fraaij, P. L., Fouchier, R. A., & Herfst, S. (2018). Transmission routes of respiratory viruses among humans. *Current Opinion in Virology*, *28*, 142–151. https://doi.org/10.1016/j.coviro.2018.01.001

Kuznetsov, G., Xu, Q., Rudolph-Owen, L., Tendyke, K., Liu, J., Towle, M., Zhao, N., Marsh, J., Agoulnik, S., Twine, N., Parent, L., Chen, Z., Shie, J.-L., Jiang, Y., Zhang, H., Du, H., Boivin, R., Wang, Y., Romo, D., & Littlefield, B. A. (2009). Potent in vitro and in vivo anticancer activities of des-methyl, des-amino pateamine A, a synthetic analogue of marine natural product pateamine A. *Molecular Cancer Therapeutics*, *8*(5), 1250–1260. https://doi.org/10.1158/1535-7163.MCT-08-1026

Lai, A. L., & Freed, J. H. (2015). The Interaction between Influenza HA Fusion Peptide and Transmembrane Domain Affects Membrane Structure. *Biophysical Journal*, *109*(12), 2523–2536. https://doi.org/10.1016/j.bpj.2015.10.044

Lakadamyali, M., Rust, M. J., & Zhuang, X. (2004). Endocytosis of influenza viruses. *Microbes and Infection / Institut Pasteur*, *6*(10), 929–936. https://doi.org/10.1016/j.micinf.2004.05.002

Lakdawala, S. S., Lamirande, E. W., Suguitan, A. L., Wang, W., Santos, C. P., Vogel, L., Matsuoka, Y., Lindsley, W. G., Jin, H., & Subbarao, K. (2011). Eurasian-Origin Gene Segments Contribute to the Transmissibility, Aerosol Release, and Morphology of the 2009 Pandemic H1N1 Influenza Virus. *PLoS Pathogens*, *7*(12). https://doi.org/10.1371/journal.ppat.1002443

Lakdawala, S. S., Wu, Y., Wawrzusin, P., Kabat, J., Broadbent, A. J., Lamirande, E. W., Fodor, E., Altan-Bonnet, N., Shroff, H., & Subbarao, K. (2014). Influenza a virus assembly intermediates fuse in the cytoplasm. *PLoS Pathogens*, *10*(3), e1003971. https://doi.org/10.1371/journal.ppat.1003971

Lam, H. C., Bi, X., Sreevatsan, S., & Boley, D. (2017). Evolution and Vaccination of Influenza Virus. *Journal of Computational Biology: A Journal of Computational Molecular Cell Biology*, *24*(8), 787–798. https://doi.org/10.1089/cmb.2017.0025

Landeras-Bueno, S., Fernández, Y., Falcón, A., Oliveros, J. C., & Ortín, J. (2016). Chemical Genomics Identifies the PERK-Mediated Unfolded Protein Stress Response as a Cellular Target for Influenza Virus Inhibition. *MBio*, *7*(2), e00085-16. https://doi.org/10.1128/mBio.00085-16

Lee, K. P. K., Dey, M., Neculai, D., Cao, C., Dever, T. E., & Sicheri, F. (2008). Structure of the dual enzyme Ire1 reveals the basis for catalysis and regulation in nonconventional RNA splicing. *Cell*, *132*(1), 89–100. https://doi.org/10.1016/j.cell.2007.10.057

Legate, K. R., & Andrews, D. W. (2003). The beta-subunit of the signal recognition particle receptor is a novel GTP-binding protein without intrinsic GTPase activity. *The Journal of Biological Chemistry*, *278*(30), 27712–27720. https://doi.org/10.1074/jbc.M302158200

Levene, R. E., Shrestha, S. D., & Gaglia, M. M. (2021). The influenza A virus host shutoff factor PA-X is rapidly turned over in a strain-specific manner. *Journal of Virology*, JVI.02312-20. https://doi.org/10.1128/JVI.02312-20

Lewy, T. G., Grabowski, J. M., & Bloom, M. E. (2017). BiP: Master Regulator of the Unfolded Protein Response and Crucial Factor in Flavivirus Biology. *The Yale Journal of Biology and Medicine*, *90*(2), 291–300.

Leyva-Grado, V. H., Churchill, L., Wu, M., Williams, T. J., Taishi, P., Majde, J. A., & Krueger, J. M. (2009). Influenza Virus- and Cytokine-Immunoreactive Cells in the Murine Olfactory and Central Autonomic Nervous Systems before and after Illness Onset. *Journal of Neuroimmunology*, *211*(1–2), 73–83. https://doi.org/10.1016/j.jneuroim.2009.03.016

Li, B., Clohisey, S. M., Chia, B. S., Wang, B., Cui, A., Eisenhaure, T., Schweitzer, L. D., Hoover, P., Parkinson, N. J., Nachshon, A., Smith, N., Regan, T., Farr, D., Gutmann, M. U., Bukhari, S. I., Law, A., Sangesland, M., Gat-Viks, I., Digard, P., … Hacohen, N. (2020). Genome-wide CRISPR screen identifies host dependency factors for influenza A virus infection. *Nature Communications*, *11*(1), 164. https://doi.org/10.1038/s41467-019-13965-x

Li, F. C. K., Choi, B. C. K., Sly, T., & Pak, A. W. P. (2008). Finding the real case-fatality rate of H5N1 avian influenza. *Journal of Epidemiology & Community Health*, *62*(6), 555–559. https://doi.org/10.1136/jech.2007.064030

Li, J., Ishaq, M., Prudence, M., Xi, X., Hu, T., Liu, Q., & Guo, D. (2009). Single mutation at the amino acid position 627 of PB2 that leads to increased virulence of an H5N1 avian influenza virus during adaptation in mice can be compensated by multiple mutations at other sites of PB2. *Virus Research*, *144*(1–2), 123–129. https://doi.org/10.1016/j.virusres.2009.04.008

Li, Z., Watanabe, T., Hatta, M., Watanabe, S., Nanbo, A., Ozawa, M., Kakugawa, S., Shimojima, M., Yamada, S., Neumann, G., & Kawaoka, Y. (2009). Mutational analysis of conserved amino acids in the influenza A virus nucleoprotein. *Journal of Virology*, *83*(9), 4153–4162. https://doi.org/10.1128/JVI.02642-08

Limburg, H., Harbig, A., Bestle, D., Stein, D. A., Moulton, H. M., Jaeger, J., Janga, H., Hardes, K., Koepke, J., Schulte, L., Koczulla, A. R., Schmeck, B., Klenk, H.-D., & Böttcher-Friebertshäuser, E. (2019). TMPRSS2 Is the Major Activating Protease of Influenza A Virus in Primary Human Airway Cells and Influenza B Virus in Human Type II Pneumocytes. *Journal of Virology*, *93*(21). https://doi.org/10.1128/JVI.00649-19

Lin, X., Zhou, J., Zhang, Y., Wu, J., Zhang, F., Li, Z., Zhang, Y., Bi, S., Shu, Y., & Wang, Y. (2009). Oseltamivir boosts 2009 H1N1 virus infectivity in vitro. *Biochemical and Biophysical Research Communications*, *390*(4), 1305–1308. https://doi.org/10.1016/j.bbrc.2009.10.142

Linxweiler, M., Schick, B., & Zimmermann, R. (2017). Let's talk about Secs: Sec61, Sec62 and Sec63 in signal transduction, oncology and personalized medicine. *Signal Transduction and Targeted Therapy*, *2*, 17002. https://doi.org/10.1038/sigtrans.2017.2

Lipsitch, M. (2018). Why Do Exceptionally Dangerous Gain-of-Function Experiments in Influenza? *Methods in Molecular Biology (Clifton, N.J.)*, *1836*, 589–608. https://doi.org/10.1007/978-1-4939-8678-1_29

Liu, X., Bushnell, D. A., & Kornberg, R. D. (2013). RNA polymerase II transcription: Structure and mechanism. *Biochimica Et Biophysica Acta*, *1829*(1), 2–8. https://doi.org/10.1016/j.bbagrm.2012.09.003

Liu, Y. (2020). A code within the genetic code: Codon usage regulates co-translational protein folding. *Cell Communication and Signaling: CCS*, *18*(1), 145. https://doi.org/10.1186/s12964-020-00642-6

Low, W.-K., Dang, Y., Schneider-Poetsch, T., Shi, Z., Choi, N. S., Merrick, W. C., Romo, D., & Liu, J. O. (2005). Inhibition of eukaryotic translation initiation by the marine natural product pateamine A. *Molecular Cell*, *20*(5), 709–722. https://doi.org/10.1016/j.molcel.2005.10.008

Low, W.-K., Dang, Y., Schneider-Poetsch, T., Shi, Z., Choi, N. S., Rzasa, R. M., Shea, H. A., Li, S., Park, K., Ma, G., Romo, D., & Liu, J. O. (2007). Isolation and identification of eukaryotic initiation factor 4A as a molecular target for the marine natural product Pateamine A. *Methods in Enzymology*, *431*, 303–324. https://doi.org/10.1016/S0076-6879(07)31014-8

Lu, Y., Liang, F.-X., & Wang, X. (2014). A synthetic biology approach identifies the mammalian UPR RNA ligase RtcB. *Molecular Cell*, *55*(5), 758–770. https://doi.org/10.1016/j.molcel.2014.06.032

Lu, Y.-N., Kavianpour, S., Zhang, T., Zhang, X., Nguyen, D., Thombre, R., He, L., & Wang, J. (2021). MARK2 phosphorylates eIF2α in response to proteotoxic stress. *PLoS Biology*, *19*(3), e3001096. https://doi.org/10.1371/journal.pbio.3001096

Luczo, J. M., Stambas, J., Durr, P. A., Michalski, W. P., & Bingham, J. (2015). Molecular pathogenesis of H5 highly pathogenic avian influenza: The role of the haemagglutinin cleavage site motif. *Reviews in Medical Virology*, *25*(6), 406–430. https://doi.org/10.1002/rmv.1846

Lukarska, M., Fournier, G., Pflug, A., Resa-Infante, P., Reich, S., Naffakh, N., & Cusack, S. (2017). Structural basis of an essential interaction between influenza polymerase and Pol II CTD. *Nature*, *541*(7635), 117–121. https://doi.org/10.1038/nature20594

Luo, W., Tian, L., Gan, Y., Chen, E., Shen, X., Pan, J., Irwin, D. M., Chen, R.-A., & Shen, Y. (2020). The fit of codon usage of human-isolated avian influenza A viruses to human. *Infection, Genetics and Evolution: Journal of Molecular Epidemiology and Evolutionary Genetics in Infectious Diseases*, *81*, 104181. https://doi.org/10.1016/j.meegid.2020.104181

Manzoor, R., Igarashi, M., & Takada, A. (2017). Influenza A Virus M2 Protein: Roles from Ingress to Egress. *International Journal of Molecular Sciences*, *18*(12). https://doi.org/10.3390/ijms18122649

Mao, T., Shao, M., Qiu, Y., Huang, J., Zhang, Y., Song, B., Wang, Q., Jiang, L., Liu, Y., Han, J.-D. J., Cao, P., Li, J., Gao, X., Rui, L., Qi, L., Li, W., & Liu, Y. (2011). PKA phosphorylation couples hepatic inositol-requiring enzyme 1alpha to glucagon signaling in glucose metabolism. *Proceedings of the National Academy of Sciences of the United States of America*, *108*(38), 15852–15857. https://doi.org/10.1073/pnas.1107394108

Maquat, L. E., Hwang, J., Sato, H., & Tang, Y. (2010). CBP80-Promoted mRNP Rearrangements during the Pioneer Round of Translation, Nonsense-Mediated mRNA Decay, and Thereafter. *Cold Spring Harbor Symposia on Quantitative Biology*, *75*, 127–134. https://doi.org/10.1101/sqb.2010.75.028

Marciniak, S. J., Yun, C. Y., Oyadomari, S., Novoa, I., Zhang, Y., Jungreis, R., Nagata, K., Harding, H. P., & Ron, D. (2004). CHOP induces death by promoting protein synthesis and oxidation in the stressed endoplasmic reticulum. *Genes & Development*, *18*(24), 3066–3077. https://doi.org/10.1101/gad.1250704

Matrosovich, M., Matrosovich, T., Garten, W., & Klenk, H.-D. (2006). New low-viscosity overlay medium for viral plaque assays. *Virology Journal*, *3*, 63. https://doi.org/10.1186/1743-422X-3-63

Matsuoka, Y., Lamirande, E. W., & Subbarao, K. (2009). The mouse model for influenza. *Current Protocols in Microbiology*, *Chapter 15*, Unit 15G.3. https://doi.org/10.1002/9780471729259.mc15g03s13

Matsuzaki, Y., Sugawara, K., Takashita, E., Muraki, Y., Hongo, S., Katsushima, N., Mizuta, K., & Nishimura, H. (2004). Genetic diversity of influenza B virus: The frequent reassortment and cocirculation of the genetically distinct reassortant viruses in a community. *Journal of Medical Virology*, *74*(1), 132–140. https://doi.org/10.1002/jmv.20156

Matthews, J. H., Maass, D. R., Northcote, P. T., Atkinson, P. H., & Teesdale-Spittle, P. H. (2013). The cellular target specificity of pateamine A. *Zeitschrift Fur Naturforschung. C, Journal of Biosciences*, *68*(9–10), 406–415. https://doi.org/10.1515/znc-2013-9-1008

McCormick, C., & Khaperskyy, D. A. (2017). Translation inhibition and stress granules in the antiviral immune response. *Nature Reviews. Immunology*, *17*(10), 647–660. https://doi.org/10.1038/nri.2017.63

McCracken, S., Fong, N., Rosonina, E., Yankulov, K., Brothers, G., Siderovski, D., Hessel, A., Foster, S., Shuman, S., & Bentley, D. L. (1997). 5'-Capping enzymes are targeted to pre-mRNA by binding to the phosphorylated carboxy-terminal domain of RNA polymerase II. *Genes & Development*, *11*(24), 3306–3318. https://doi.org/10.1101/gad.11.24.3306

McCullough, K. D., Martindale, J. L., Klotz, L. O., Aw, T. Y., & Holbrook, N. J. (2001). Gadd153 sensitizes cells to endoplasmic reticulum stress by down-regulating Bcl2 and perturbing the cellular redox state. *Molecular and Cellular Biology*, *21*(4), 1249–1259. https://doi.org/10.1128/MCB.21.4.1249-1259.2001

McGinnis, J., Laplante, J., Shudt, M., & George, K. S. (2016). Next generation sequencing for whole genome analysis and surveillance of influenza A viruses. *Journal of Clinical Virology: The Official Publication of the Pan American Society for Clinical Virology*, *79*, 44–50. https://doi.org/10.1016/j.jcv.2016.03.005

Mehle, A., & Doudna, J. A. (2009). Adaptive strategies of the influenza virus polymerase for replication in humans. *Proceedings of the National Academy of Sciences of the United States of America*, *106*(50), 21312–21316. https://doi.org/10.1073/pnas.0911915106

Meng, B., Bentley, K., Marriott, A. C., Scott, P. D., Dimmock, N. J., & Easton, A. J. (2017). Unexpected complexity in the interference activity of a cloned influenza defective interfering RNA. *Virology Journal*, *14*(1), 138. https://doi.org/10.1186/s12985-017-0805-6

Merrick, W. C., & Pavitt, G. D. (2018). Protein Synthesis Initiation in Eukaryotic Cells. *Cold Spring Harbor Perspectives in Biology*, *10*(12). https://doi.org/10.1101/cshperspect.a033092

Meyer, D., Sielaff, F., Hammami, M., Böttcher-Friebertshäuser, E., Garten, W., & Steinmetzer, T. (2013). Identification of the first synthetic inhibitors of the type II transmembrane serine protease TMPRSS2 suitable for inhibition of influenza virus activation. *The Biochemical Journal*, *452*(2), 331–343. https://doi.org/10.1042/BJ20130101

Miller, J. D., Tajima, S., Lauffer, L., & Walter, P. (1995). The beta subunit of the signal recognition particle receptor is a transmembrane GTPase that anchors the alpha subunit, a peripheral membrane GTPase, to the endoplasmic reticulum membrane. *The Journal of Cell Biology*, *128*(3), 273–282. https://doi.org/10.1083/jcb.128.3.273

Moore, E. C., & LePAGE, G. A. (1958). The metabolism of 6-thioguanine in normal and neoplastic tissues. *Cancer Research*, *18*(9), 1075–1083.

Morishima, N., Nakanishi, K., Takenouchi, H., Shibata, T., & Yasuhiko, Y. (2002). An endoplasmic reticulum stress-specific caspase cascade in apoptosis. Cytochrome c-independent activation of caspase-9 by caspase-12. *The Journal of Biological Chemistry*, *277*(37), 34287–34294. https://doi.org/10.1074/jbc.M204973200

Moscona, A. (2005). Neuraminidase inhibitors for influenza. *The New England Journal of Medicine*, *353*(13), 1363–1373. https://doi.org/10.1056/NEJMra050740

Müller, C., Schulte, F. W., Lange-Grünweller, K., Obermann, W., Madhugiri, R., Pleschka, S., Ziebuhr, J., Hartmann, R. K., & Grünweller, A. (2018). Broad-spectrum antiviral activity of the eIF4A inhibitor silvestrol against corona- and picornaviruses. *Antiviral Research*, *150*, 123–129. https://doi.org/10.1016/j.antiviral.2017.12.010

Nakagawa, T., & Yuan, J. (2000). Cross-talk between two cysteine protease families. Activation of caspase-12 by calpain in apoptosis. *The Journal of Cell Biology*, *150*(4), 887–894. https://doi.org/10.1083/jcb.150.4.887

Nakagawa, T., Zhu, H., Morishima, N., Li, E., Xu, J., Yankner, B. A., & Yuan, J. (2000). Caspase-12 mediates endoplasmic-reticulum-specific apoptosis and cytotoxicity by amyloid-beta. *Nature*, *403*(6765), 98–103. https://doi.org/10.1038/47513

Nakahigashi, K., Takai, Y., Shiwa, Y., Wada, M., Honma, M., Yoshikawa, H., Tomita, M., Kanai, A., & Mori, H. (2014). Effect of codon adaptation on codon-level and gene-level translation efficiency in vivo. *BMC Genomics*, *15*, 1115. https://doi.org/10.1186/1471-2164-15-1115

Narasaraju, T., Yang, E., Samy, R. P., Ng, H. H., Poh, W. P., Liew, A.-A., Phoon, M. C., van Rooijen, N., & Chow, V. T. (2011). Excessive neutrophils and neutrophil extracellular traps contribute to acute lung injury of influenza pneumonitis. *The American Journal of Pathology*, *179*(1), 199–210. https://doi.org/10.1016/j.ajpath.2011.03.013

Nebigil, C. G., Moog, C., Vagner, S., Benkirane-Jessel, N., Smith, D. R., & Désaubry, L. (2020). Flavaglines as natural products targeting eIF4A and prohibitins: From traditional Chinese medicine to antiviral activity against coronaviruses. *European Journal of Medicinal Chemistry*, *203*, 112653. https://doi.org/10.1016/j.ejmech.2020.112653

Nelson, J. A., & Vidale, E. (1986). Formation of 6-thioguanine and 6-mercaptopurine from their 9-alkyl derivatives in mice. *Cancer Research*, *46*(1), 137–140.

Nemeroff, M. E., Barabino, S. M., Li, Y., Keller, W., & Krug, R. M. (1998). Influenza virus NS1 protein interacts with the cellular 30 kDa subunit of CPSF and inhibits 3'end formation of cellular pre-mRNAs. *Molecular Cell*, *1*(7), 991–1000. https://doi.org/10.1016/s1097-2765(00)80099-4

Neumann, G., Watanabe, T., Ito, H., Watanabe, S., Goto, H., Gao, P., Hughes, M., Perez, D. R., Donis, R., Hoffmann, E., Hobom, G., & Kawaoka, Y. (1999). Generation of influenza A viruses entirely from cloned cDNAs. *Proceedings of the National Academy of Sciences of the United States of America*, *96*(16), 9345–9350. https://doi.org/10.1073/pnas.96.16.9345

Newman, J. R. S., & Keating, A. E. (2003). Comprehensive identification of human bZIP interactions with coiled-coil arrays. *Science (New York, N.Y.)*, *300*(5628), 2097–2101. https://doi.org/10.1126/science.1084648

Nicholson, D. W., Ali, A., Thornberry, N. A., Vaillancourt, J. P., Ding, C. K., Gallant, M., Gareau, Y., Griffin, P. R., Labelle, M., & Lazebnik, Y. A. (1995). Identification and inhibition of the ICE/CED-3 protease necessary for mammalian apoptosis. *Nature*, *376*(6535), 37–43. https://doi.org/10.1038/376037a0

Nj, D., Ew, R., Pd, S., & Ac, M. (2008). Influenza virus protecting RNA: An effective prophylactic and therapeutic antiviral. *Journal of Virology*, *82*(17), 8570–8578. https://doi.org/10.1128/jvi.00743-08

Nobusawa, E., & Sato, K. (2006). Comparison of the mutation rates of human influenza A and B viruses. *Journal of Virology*, *80*(7), 3675–3678. https://doi.org/10.1128/JVI.80.7.3675-3678.2006

Noshi, T., Kitano, M., Taniguchi, K., Yamamoto, A., Omoto, S., Baba, K., Hashimoto, T., Ishida, K., Kushima, Y., Hattori, K., Kawai, M., Yoshida, R., Kobayashi, M., Yoshinaga, T., Sato, A., Okamatsu, M., Sakoda, Y., Kida, H., Shishido, T., & Naito, A. (2018). In vitro characterization of baloxavir acid, a first-in-class cap-dependent endonuclease inhibitor of the influenza virus polymerase PA subunit. *Antiviral Research*, *160*, 109–117. https://doi.org/10.1016/j.antiviral.2018.10.008

Novoa, I., Zeng, H., Harding, H. P., & Ron, D. (2001). Feedback inhibition of the unfolded protein response by GADD34-mediated dephosphorylation of eIF2alpha. *The Journal of Cell Biology*, *153*(5), 1011–1022. https://doi.org/10.1083/jcb.153.5.1011

Numajiri Haruki, A., Naito, T., Nishie, T., Saito, S., & Nagata, K. (2011). Interferon-inducible antiviral protein MxA enhances cell death triggered by endoplasmic reticulum stress. *Journal of Interferon & Cytokine Research: The Official Journal of the International Society for Interferon and Cytokine Research*, *31*(11), 847–856. https://doi.org/10.1089/jir.2010.0132

Oancea, I., Png, C. W., Das, I., Lourie, R., Winkler, I. G., Eri, R., Subramaniam, N., Jinnah, H. A., McWhinney, B. C., Levesque, J.-P., McGuckin, M. A., Duley, J. A., & Florin, T. H. J. (2013). A novel mouse model of veno-occlusive disease provides strategies to prevent thioguanine-induced hepatic toxicity. *Gut*, *62*(4), 594–605. https://doi.org/10.1136/gutjnl-2012-302274

Odagiri, T., & Tashiro, M. (1997). Segment-specific noncoding sequences of the influenza virus genome RNA are involved in the specific competition between defective interfering RNA and its progenitor RNA segment at the virion assembly step. *Journal of Virology*, *71*(3), 2138–2145. https://doi.org/10.1128/JVI.71.3.2138-2145.1997

Ohuchi, R., Ohuchi, M., Garten, W., & Klenk, H. D. (1997). Oligosaccharides in the stem region maintain the influenza virus hemagglutinin in the metastable form required for fusion activity. *Journal of Virology*, *71*(5), 3719–3725.

Oikawa, D., Tokuda, M., Hosoda, A., & Iwawaki, T. (2010). Identification of a consensus element recognized and cleaved by IRE1 alpha. *Nucleic Acids Research*, *38*(18), 6265–6273. https://doi.org/10.1093/nar/gkq452

Onomoto, K., Jogi, M., Yoo, J.-S., Narita, R., Morimoto, S., Takemura, A., Sambhara, S., Kawaguchi, A., Osari, S., Nagata, K., Matsumiya, T., Namiki, H., Yoneyama, M., & Fujita, T. (2012). Critical role of an antiviral stress granule containing RIG-I and PKR in viral detection and innate immunity. *PloS One*, *7*(8), e43031. https://doi.org/10.1371/journal.pone.0043031

Osada, N., Kohara, A., Yamaji, T., Hirayama, N., Kasai, F., Sekizuka, T., Kuroda, M., & Hanada, K. (2014). The genome landscape of the african green monkey kidney-derived vero cell line. *DNA Research: An International Journal for Rapid Publication of Reports on Genes and Genomes*, *21*(6), 673–683. https://doi.org/10.1093/dnares/dsu029

Oyadomari, S., & Mori, M. (2004). Roles of CHOP/GADD153 in endoplasmic reticulum stress. *Cell Death & Differentiation*, *11*(4), 381–389. https://doi.org/10.1038/sj.cdd.4401373

Paget, J., Spreeuwenberg, P., Charu, V., Taylor, R. J., Iuliano, A. D., Bresee, J., Simonsen, L., Viboud, C., & Global Seasonal Influenza-associated Mortality Collaborator Network and GLaMOR Collaborating Teams*. (2019). Global mortality associated with seasonal influenza epidemics: New burden estimates and predictors from the GLaMOR Project. *Journal of Global Health*, *9*(2), 020421. https://doi.org/10.7189/jogh.09.020421

Pakos-Zebrucka, K., Koryga, I., Mnich, K., Ljujic, M., Samali, A., & Gorman, A. M. (2016). The integrated stress response. *EMBO Reports*, *17*(10), 1374–1395. https://doi.org/10.15252/embr.201642195

Palese, P. (2004). Influenza: Old and new threats. *Nature Medicine*, *10*(12), S82–S87. https://doi.org/10.1038/nm1141

Panthu, B., Terrier, O., Carron, C., Traversier, A., Corbin, A., Balvay, L., Lina, B., Rosa-Calatrava, M., & Ohlmann, T. (2017). The NS1 Protein from Influenza Virus Stimulates Translation Initiation by Enhancing Ribosome Recruitment to mRNAs. *Journal of Molecular Biology*, *429*(21), 3334–3352. https://doi.org/10.1016/j.jmb.2017.04.007

Paules, C., & Subbarao, K. (2017). Influenza. *Lancet (London, England)*, *390*(10095), 697–708. https://doi.org/10.1016/S0140-6736(17)30129-0

Pauly, M. D., Procario, M. C., & Lauring, A. S. (2017). A novel twelve class fluctuation test reveals higher than expected mutation rates for influenza A viruses. *ELife*, *6*. https://doi.org/10.7554/eLife.26437

Pearce, D. C., Pallaghy, P. K., McCaw, J. M., McVernon, J., & Mathews, J. D. (2011). Understanding mortality in the 1918–1919 influenza pandemic in England and Wales. *Influenza and Other Respiratory Viruses*, *5*(2), 89–98. https://doi.org/10.1111/j.1750-2659.2010.00186.x

Pearse, B. R., & Hebert, D. N. (2010). Lectin chaperones help direct the maturation of glycoproteins in the endoplasmic reticulum. *Biochimica Et Biophysica Acta*, *1803*(6), 684–693. https://doi.org/10.1016/j.bbamcr.2009.10.008

Petrova, V. N., & Russell, C. A. (2018). The evolution of seasonal influenza viruses. *Nature Reviews Microbiology*, *16*(1), 47–60. https://doi.org/10.1038/nrmicro.2017.118

Pflug, A., Guilligay, D., Reich, S., & Cusack, S. (2014). Structure of influenza A polymerase bound to the viral RNA promoter. *Nature*, *516*(7531), 355–360. https://doi.org/10.1038/nature14008

Pflug, A., Lukarska, M., Resa-Infante, P., Reich, S., & Cusack, S. (2017). Structural insights into RNA synthesis by the influenza virus transcription-replication machine. *Virus Research*, *234*, 103–117. https://doi.org/10.1016/j.virusres.2017.01.013

Pharo, E. A., Williams, S. M., Boyd, V., Sundaramoorthy, V., Durr, P. A., & Baker, M. L. (2020). Host-Pathogen Responses to Pandemic Influenza H1N1pdm09 in a Human Respiratory Airway Model. *Viruses*, *12*(6), E679. https://doi.org/10.3390/v12060679

Phipps, K. L., Marshall, N., Tao, H., Danzy, S., Onuoha, N., Steel, J., & Lowen, A. C. (2017). Seasonal H3N2 and 2009 Pandemic H1N1 Influenza A Viruses Reassort Efficiently but Produce Attenuated Progeny. *Journal of Virology*, *91*(17). https://doi.org/10.1128/JVI.00830-17

Pleschka, S., Jaskunas, R., Engelhardt, O. G., Zürcher, T., Palese, P., & García-Sastre, A. (1996). A plasmid-based reverse genetics system for influenza A virus. *Journal of Virology*, *70*(6), 4188–4192. https://doi.org/10.1128/JVI.70.6.4188-4192.1996

Plumb, R., Zhang, Z.-R., Appathurai, S., & Mariappan, M. (2015). A functional link between the co-translational protein translocation pathway and the UPR. *ELife*, *4*. https://doi.org/10.7554/eLife.07426

Pobre, K. F. R., Poet, G. J., & Hendershot, L. M. (2019). The endoplasmic reticulum (ER) chaperone BiP is a master regulator of ER functions: Getting by with a little help from ERdj friends. *The Journal of Biological Chemistry*, *294*(6), 2098–2108. https://doi.org/10.1074/jbc.REV118.002804

Poon, L. L., Pritlove, D. C., Fodor, E., & Brownlee, G. G. (1999). Direct evidence that the poly(A) tail of influenza A virus mRNA is synthesized by reiterative copying of a U track in the virion RNA template. *Journal of Virology*, *73*(4), 3473–3476. https://doi.org/10.1128/JVI.73.4.3473-3476.1999

Prasad, V., Suomalainen, M., Jasiqi, Y., Hemmi, S., Hearing, P., Hosie, L., Burgert, H.-G., & Greber, U. F. (2020). The UPR sensor IRE1α and the adenovirus E3-19K glycoprotein sustain persistent and lytic infections. *Nature Communications*, *11*(1), 1997. https://doi.org/10.1038/s41467-020-15844-2

Preissler, S., Rato, C., Yan, Y., Perera, L. A., Czako, A., & Ron, D. (n.d.). Calcium depletion challenges endoplasmic reticulum proteostasis by destabilising BiP-substrate complexes. *ELife*, *9*, e62601. https://doi.org/10.7554/eLife.62601

Preissler, S., & Ron, D. (2019). Early Events in the Endoplasmic Reticulum Unfolded Protein Response. *Cold Spring Harbor Perspectives in Biology*, *11*(4), a033894. https://doi.org/10.1101/cshperspect.a033894

Prevo, R., Tiwana, G. S., Maughan, T. S., Buffa, F. M., McKenna, W. G., & Higgins, G. S. (2017). Depletion of signal recognition particle 72kDa increases radiosensitivity. *Cancer Biology & Therapy*, *18*(6), 425–432. https://doi.org/10.1080/15384047.2017.1323587

Promlek, T., Ishiwata-Kimata, Y., Shido, M., Sakuramoto, M., Kohno, K., & Kimata, Y. (2011). Membrane aberrancy and unfolded proteins activate the endoplasmic reticulum stress sensor Ire1 in different ways. *Molecular Biology of the Cell*, *22*(18), 3520–3532. https://doi.org/10.1091/mbc.E11-04-0295

Proudfoot, N. J., Furger, A., & Dye, M. J. (2002). Integrating mRNA Processing with Transcription. *Cell*, *108*(4), 501–512. https://doi.org/10.1016/S0092-8674(02)00617-7

Qi, L., Tsai, B., & Arvan, P. (2017). New Insights into the Physiological Role of Endoplasmic Reticulum-Associated Degradation. *Trends in Cell Biology*, *27*(6), 430–440. https://doi.org/10.1016/j.tcb.2016.12.002

Qiu, Y., Mao, T., Zhang, Y., Shao, M., You, J., Ding, Q., Chen, Y., Wu, D., Xie, D., Lin, X., Gao, X., Kaufman, R. J., Li, W., & Liu, Y. (2010). A crucial role for RACK1 in the regulation of glucose-stimulated IRE1alpha activation in pancreatic beta cells. *Science Signaling*, *3*(106), ra7. https://doi.org/10.1126/scisignal.2000514

Raj, K., Kaur, K., Gupta, G. D., & Singh, S. (2021). Current understanding on molecular drug targets and emerging treatment strategy for novel coronavirus-19. *Naunyn-Schmiedeberg's Archives of Pharmacology*. https://doi.org/10.1007/s00210-021-02091-5

Rajendran, S., Lakshminarayanan, A., Ramanathan, G., & Subramanian Shanmugam, S. K. (2020). Antioxidant Antagonises Chemotherapeutic Drug Effect in Lung Cancer Cell Line A549. *Asian Pacific Journal of Cancer Prevention: APJCP*, *21*(4), 1019–1023. https://doi.org/10.31557/APJCP.2020.21.4.1019

Rambaut, A., Pybus, O. G., Nelson, M. I., Viboud, C., Taubenberger, J. K., & Holmes, E. C. (2008). The genomic and epidemiological dynamics of human influenza A virus. *Nature*, *453*(7195), 615–619. https://doi.org/10.1038/nature06945

Rambout, X., & Maquat, L. E. (2020). The nuclear cap-binding complex as choreographer of gene transcription and pre-mRNA processing. *Genes & Development*, *34*(17–18), 1113–1127. https://doi.org/10.1101/gad.339986.120

Rapiejko, P. J., & Gilmore, R. (1994). Signal sequence recognition and targeting of ribosomes to the endoplasmic reticulum by the signal recognition particle do not require GTP. *Molecular Biology of the Cell*, *5*(8), 887–897. https://doi.org/10.1091/mbc.5.8.887

Reed, L., & Muench, H. (1938). *A SIMPLE METHOD OF ESTIMATING FIFTY PER CENT ENDPOINTS*. https://doi.org/10.1093/OXFORDJOURNALS.AJE.A118408

Reid, A. H., Fanning, T. G., Hultin, J. V., & Taubenberger, J. K. (1999). Origin and evolution of the 1918 "Spanish" influenza virus hemagglutinin gene. *Proceedings of the National Academy of Sciences*, *96*(4), 1651–1656.

Reinacher, M., Bonin, J., Narayan, O., & Scholtissek, C. (1983). Pathogenesis of neurovirulent influenza A virus infection in mice. Route of entry of virus into brain determines infection of different populations of cells. *Laboratory Investigation; a Journal of Technical Methods and Pathology*, *49*(6), 686–692.

Renaud, C., Kuypers, J., & Englund, J. A. (2011). Emerging oseltamivir resistance in seasonal and pandemic influenza A/H1N1. *Journal of Clinical Virology*, *52*(2), 70–78. https://doi.org/10.1016/j.jcv.2011.05.019

Richard, M., & Fouchier, R. A. M. (2016). Influenza A virus transmission via respiratory aerosols or droplets as it relates to pandemic potential. *FEMS Microbiology Reviews*, *40*(1), 68–85. https://doi.org/10.1093/femsre/fuv039

Robb, N. C., Smith, M., Vreede, F. T., & Fodor, E. (2009). NS2/NEP protein regulates transcription and replication of the influenza virus RNA genome. *The Journal of General Virology*, *90*(Pt 6), 1398–1407. https://doi.org/10.1099/vir.0.009639-0

Roberts, P. C., Garten, W., & Klenk, H. D. (1993). Role of conserved glycosylation sites in maturation and transport of influenza A virus hemagglutinin. *Journal of Virology*, *67*(6), 3048–3060. https://doi.org/10.1128/JVI.67.6.3048-3060.1993

Roberts, R. L., Wallace, M. C., Seinen, M. L., van Bodegraven, A. A., Krishnaprasad, K., Jones, G. T., van Rij, A. M., Baird, A., Lawrance, I. C., Prosser, R., Bampton, P., Grafton, R., Simms, L. A., Studd, C., Bell, S. J., Kennedy, M. A., Halliwell, J., Gearry, R. B., Radford-Smith, G., … Barclay, M. L. (2018). Nonsynonymous Polymorphism in Guanine Monophosphate Synthetase Is a Risk Factor for Unfavorable Thiopurine Metabolite Ratios in Patients With Inflammatory Bowel Disease. *Inflammatory Bowel Diseases*, *24*(12), 2606–2612. https://doi.org/10.1093/ibd/izy163

Rogers, G. N., & Paulson, J. C. (1983). Receptor determinants of human and animal influenza virus isolates: Differences in receptor specificity of the H3 hemagglutinin based on species of origin. *Virology*, *127*(2), 361–373. https://doi.org/10.1016/0042-6822(83)90150-2

Rolling, T., Koerner, I., Zimmermann, P., Holz, K., Haller, O., Staeheli, P., & Kochs, G. (2009). Adaptive Mutations Resulting in Enhanced Polymerase Activity Contribute to High Virulence of Influenza A Virus in Mice. *Journal of Virology*, *83*(13), 6673–6680. https://doi.org/10.1128/JVI.00212-09

Ron, D., & Hubbard, S. R. (2008). How IRE1 Reacts to ER Stress. *Cell*, *132*(1), 24–26. https://doi.org/10.1016/j.cell.2007.12.017

Rowe, T., Banner, D., Farooqui, A., Ng, D. C. K., Kelvin, A. A., Rubino, S., Huang, S. S. H., Fang, Y., & Kelvin, D. J. (2010). In vivo ribavirin activity against severe pandemic H1N1 Influenza A/Mexico/4108/2009. *The Journal of General Virology*, *91*(Pt 12), 2898–2906. https://doi.org/10.1099/vir.0.024323-0

Rozo, M., & Gronvall, G. K. (2015). The Reemergent 1977 H1N1 Strain and the Gain-of-Function Debate. *MBio*, *6*(4). https://doi.org/10.1128/mBio.01013-15

Ruggiano, A., Foresti, O., & Carvalho, P. (2014). Quality control: ER-associated degradation: protein quality control and beyond. *The Journal of Cell Biology*, *204*(6), 869–879. https://doi.org/10.1083/jcb.201312042

Russell, C. J., Hu, M., & Okda, F. A. (2018). Influenza Hemagglutinin Protein Stability, Activation, and Pandemic Risk. *Trends in Microbiology*, *26*(10), 841–853. https://doi.org/10.1016/j.tim.2018.03.005

Rutkovsky, A. C., Yeh, E. S., Guest, S. T., Findlay, V. J., Muise-Helmericks, R. C., Armeson, K., & Ethier, S. P. (2019). Eukaryotic initiation factor 4E-binding protein as an oncogene in breast cancer. *BMC Cancer*, *19*. https://doi.org/10.1186/s12885-019-5667-4

Sadlish, H., Galicia-Vazquez, G., Paris, C. G., Aust, T., Bhullar, B., Chang, L., Helliwell, S. B., Hoepfner, D., Knapp, B., Riedl, R., Roggo, S., Schuierer, S., Studer, C., Porco, J. A., Pelletier, J., & Movva, N. R. (2013). Evidence for a functionally relevant rocaglamide binding site on the eIF4A:RNA complex. *ACS Chemical Biology*, *8*(7), 1519–1527. https://doi.org/10.1021/cb400158t

Saira, K., Lin, X., DePasse, J. V., Halpin, R., Twaddle, A., Stockwell, T., Angus, B., Cozzi-Lepri, A., Delfino, M., Dugan, V., Dwyer, D. E., Freiberg, M., Horban, A., Losso, M., Lynfield, R., Wentworth, D. N., Holmes, E. C., Davey, R., Wentworth, D. E., … INSIGHT FLU003 Study Group. (2013). Sequence analysis of in vivo defective interfering-like RNA of influenza A H1N1 pandemic virus. *Journal of Virology*, *87*(14), 8064–8074. https://doi.org/10.1128/JVI.00240-13

Saito, T., Taylor, G., & Webster, R. G. (1995). Steps in maturation of influenza A virus neuraminidase. *Journal of Virology*, *69*(8), 5011–5017. https://doi.org/10.1128/JVI.69.8.5011-5017.1995

Sanjana, N. E., Shalem, O., & Zhang, F. (2014). Improved vectors and genome-wide libraries for CRISPR screening. *Nature Methods*, *11*(8), 783–784. https://doi.org/10.1038/nmeth.3047

Sato, R., Okura, T., Kawahara, M., Takizawa, N., Momose, F., & Morikawa, Y. (2019). Apical Trafficking Pathways of Influenza A Virus HA and NA via Rab17- and Rab23-Positive Compartments. *Frontiers in Microbiology*, *10*, 1857. https://doi.org/10.3389/fmicb.2019.01857

Schilling, M., Gravenstein, S., Drinka, P., Cox, N., Krause, P., Povinelli, L., & Shult, P. (2004). Emergence and Transmission of Amantadine-Resistant Influenza A in a Nursing Home. *Journal of the American Geriatrics Society*, *52*(12), 2069–2073. https://doi.org/10.1111/j.1532-5415.2004.52567.x

Schimmel, P. (2018). The emerging complexity of the tRNA world: Mammalian tRNAs beyond protein synthesis. *Nature Reviews. Molecular Cell Biology*, *19*(1), 45–58. https://doi.org/10.1038/nrm.2017.77

Schlautmann, L. P., & Gehring, N. H. (2020). A Day in the Life of the Exon Junction Complex. *Biomolecules*, *10*(6). https://doi.org/10.3390/biom10060866

Schmidt, M. F. (1982). Acylation of viral spike glycoproteins: A feature of enveloped RNA viruses. *Virology*, *116*(1), 327–338. https://doi.org/10.1016/0042-6822(82)90424-x

Schnell, J. R., & Chou, J. J. (2008). Structure and mechanism of the M2 proton channel of influenza A virus. *Nature*, *451*(7178), 591–595. https://doi.org/10.1038/nature06531

Schwarz, D. S., & Blower, M. D. (2016). The endoplasmic reticulum: Structure, function and response to cellular signaling. *Cellular and Molecular Life Sciences: CMLS*, *73*(1), 79–94. https://doi.org/10.1007/s00018-015-2052-6

Sehgal, P., Szalai, P., Olesen, C., Praetorius, H. A., Nissen, P., Christensen, S. B., Engedal, N., & Møller, J. V. (2017). Inhibition of the sarco/endoplasmic reticulum (ER) Ca2+-ATPase by thapsigargin analogs induces cell death via ER Ca2+ depletion and the unfolded protein response. *The Journal of Biological Chemistry*, *292*(48), 19656–19673. https://doi.org/10.1074/jbc.M117.796920

Serna Martin, I., Hengrung, N., Renner, M., Sharps, J., Martínez-Alonso, M., Masiulis, S., Grimes, J. M., & Fodor, E. (2018). A Mechanism for the Activation of the Influenza Virus Transcriptase. *Molecular Cell*, *70*(6), 1101-1110.e4. https://doi.org/10.1016/j.molcel.2018.05.011

Seyedpour, S., Khodaei, B., Loghman, A. H., Seyedpour, N., Kisomi, M. F., Balibegloo, M., Nezamabadi, S. S., Gholami, B., Saghazadeh, A., & Rezaei, N. (2021). Targeted therapy strategies against SARS-CoV-2 cell entry mechanisms: A systematic review of in vitro and in vivo studies. *Journal of Cellular Physiology*, *236*(4), 2364–2392. https://doi.org/10.1002/jcp.30032

Shen, J., Chen, X., Hendershot, L., & Prywes, R. (2002). ER stress regulation of ATF6 localization by dissociation of BiP/GRP78 binding and unmasking of Golgi localization signals. *Developmental Cell*, *3*(1), 99–111. https://doi.org/10.1016/s1534-5807(02)00203-4

Shen, P., Reineke, L. C., Knutsen, E., Chen, M., Pichler, M., Ling, H., & Calin, G. A. (2018). Metformin blocks MYC protein synthesis in colorectal cancer via mTOR-4EBP-eIF4E and MNK1-eIF4G-eIF4E signaling. *Molecular Oncology*, *12*(11), 1856–1870. https://doi.org/10.1002/1878-0261.12384

Shi, R. Z., Lyons, S. D., & Christopherson, R. I. (1998). Metabolic effects of thiopurine derivatives against human CCRF-CEM leukaemia cells. *The International Journal of Biochemistry & Cell Biology*, *30*(8), 885–895. https://doi.org/10.1016/s1357-2725(98)00053-3

Shih, S. R., Nemeroff, M. E., & Krug, R. M. (1995). The choice of alternative 5' splice sites in influenza virus M1 mRNA is regulated by the viral polymerase complex. *Proceedings of the National Academy of Sciences of the United States of America*, *92*(14), 6324–6328. https://doi.org/10.1073/pnas.92.14.6324

Shin, J.-Y., Wey, M., Umutesi, H. G., Sun, X., Simecka, J., & Heo, J. (2016). Thiopurine Prodrugs Mediate Immunosuppressive Effects by Interfering with Rac1 Protein Function. *The Journal of Biological Chemistry*, *291*(26), 13699–13714. https://doi.org/10.1074/jbc.M115.694422

Shiraki, K., & Daikoku, T. (2020). Favipiravir, an anti-influenza drug against life-threatening RNA virus infections. *Pharmacology & Therapeutics*, *209*, 107512. https://doi.org/10.1016/j.pharmthera.2020.107512

Short, K. R., Kroeze, E. J. B. V., Fouchier, R. A. M., & Kuiken, T. (2014). Pathogenesis of influenza-induced acute respiratory distress syndrome. *The Lancet. Infectious Diseases*, *14*(1), 57–69. https://doi.org/10.1016/S1473-3099(13)70286-X

Shoulders, M. D., Ryno, L. M., Genereux, J. C., Moresco, J. J., Tu, P. G., Wu, C., Yates, J. R., Su, A. I., Kelly, J. W., & Wiseman, R. L. (2013). Stress-independent activation of XBP1s and/or ATF6 reveals three functionally diverse ER proteostasis environments. *Cell Reports*, *3*(4), 1279–1292. https://doi.org/10.1016/j.celrep.2013.03.024

Simms, C. L., Thomas, E. N., & Zaher, H. S. (2017). Ribosome-based quality control of mRNA and nascent peptides. *Wiley Interdisciplinary Reviews. RNA*, *8*(1). https://doi.org/10.1002/wrna.1366

Slaine, P. D., Kleer, M., Duguay, B. A., Pringle, E. S., Kadijk, E., Ying, S., Balgi, A., Roberge, M., McCormick, C., & Khaperskyy, D. A. (2021). Thiopurines activate an antiviral unfolded protein response that blocks influenza A virus glycoprotein accumulation. *Journal of Virology*. https://doi.org/10.1128/JVI.00453-21

Slaine, P. D., Kleer, M., Smith, N. K., Khaperskyy, D. A., & McCormick, C. (2017). Stress Granule-Inducing Eukaryotic Translation Initiation Factor 4A Inhibitors Block Influenza A Virus Replication. *Viruses*, *9*(12). https://doi.org/10.3390/v9120388

Slaine, P. D., MacRae, C., Kleer, M., Lamoureux, E., McAlpine, S., Warhuus, M., Comeau, A. M., McCormick, C., Hatchette, T., & Khaperskyy, D. A. (2018). Adaptive Mutations in Influenza A/California/07/2009 Enhance Polymerase Activity and Infectious Virion Production. *Viruses*, *10*(5). https://doi.org/10.3390/v10050272

Steen, P. V. den, Rudd, P. M., Dwek, R. A., & Opdenakker, G. (1998). Concepts and Principles of O-Linked Glycosylation. *Critical Reviews in Biochemistry and Molecular Biology*, *33*(3), 151–208. https://doi.org/10.1080/10409239891204198

Stevens, J., Blixt, O., Glaser, L., Taubenberger, J. K., Palese, P., Paulson, J. C., & Wilson, I. A. (2006). Glycan Microarray Analysis of the Hemagglutinins from Modern and Pandemic Influenza Viruses Reveals Different Receptor Specificities. *Journal of Molecular Biology*, *355*(5), 1143–1155. https://doi.org/10.1016/j.jmb.2005.11.002

Su, W.-C., Chen, Y.-C., Tseng, C.-H., Hsu, P. W.-C., Tung, K.-F., Jeng, K.-S., & Lai, M. M. C. (2013). Pooled RNAi screen identifies ubiquitin ligase Itch as crucial for influenza A virus release from the endosome during virus entry. *Proceedings of the National Academy of Sciences of the United States of America*, *110*(43), 17516–17521. https://doi.org/10.1073/pnas.1312374110

Sun, X., Tse, L. V., Ferguson, A. D., & Whittaker, G. R. (2010). Modifications to the hemagglutinin cleavage site control the virulence of a neurotropic H1N1 influenza virus. *Journal of Virology*, *84*(17), 8683–8690. https://doi.org/10.1128/JVI.00797-10

Surviladze, Z., Ursu, O., Miscioscia, F., Curpan, R., Halip, L., Bologa, C., Oprea, T., Waller, A., Strouse, J., Salas, V., Wu, Y., Edwards, B., Wandinger-Ness, A., & Sklar, L. (2010). Three small molecule pan activator families of Ras-related GTPases. In *Probe Reports from the NIH Molecular Libraries Program*. National Center for Biotechnology Information (US). http://www.ncbi.nlm.nih.gov/books/NBK47359/

Sutton, T. C., Finch, C., Shao, H., Angel, M., Chen, H., Capua, I., Cattoli, G., Monne, I., & Perez, D. R. (2014). Airborne transmission of highly pathogenic H7N1 influenza virus in ferrets. *Journal of Virology*, *88*(12), 6623–6635. https://doi.org/10.1128/JVI.02765-13

Sweet, C., & Smith, H. (1980). Pathogenicity of influenza virus. *Microbiological Reviews*, *44*(2), 303–330.

Tabas, I., & Ron, D. (2011). Integrating the mechanisms of apoptosis induced by endoplasmic reticulum stress. *Nature Cell Biology*, *13*(3), 184–190. https://doi.org/10.1038/ncb0311-184

Takashita, E., Ichikawa, M., Morita, H., Ogawa, R., Fujisaki, S., Shirakura, M., Miura, H., Nakamura, K., Kishida, N., Kuwahara, T., Sugawara, H., Sato, A., Akimoto, M., Mitamura, K., Abe, T., Yamazaki, M., Watanabe, S., Hasegawa, H., & Odagiri, T. (2019). Human-to-Human Transmission of Influenza A(H3N2) Virus with Reduced Susceptibility to Baloxavir, Japan, February 2019. *Emerging Infectious Diseases*, *25*(11), 2108–2111. https://doi.org/10.3201/eid2511.190757

Tashiro, M., Ciborowski, P., Klenk, H. D., Pulverer, G., & Rott, R. (1987). Role of Staphylococcus protease in the development of influenza pneumonia. *Nature*, *325*(6104), 536–537. https://doi.org/10.1038/325536a0

Te Velthuis, A. J. W., Long, J. S., & Barclay, W. S. (2018). Assays to Measure the Activity of Influenza Virus Polymerase. *Methods in Molecular Biology (Clifton, N.J.)*, *1836*, 343–374. https://doi.org/10.1007/978-1-4939-8678-1_17

Thakur, A., Gaikwad, S., Vijjamarri, A. K., & Hinnebusch, A. G. (2020). EIF2α interactions with mRNA control accurate start codon selection by the translation preinitiation complex. *Nucleic Acids Research*, *48*(18), 10280–10296. https://doi.org/10.1093/nar/gkaa761

To, J., & Torres, J. (2019). Viroporins in the Influenza Virus. *Cells*, *8*(7). https://doi.org/10.3390/cells8070654

Toots, M., & Plemper, R. K. (2020). Next-generation direct-acting influenza therapeutics. *Translational Research*, *220*, 33–42. https://doi.org/10.1016/j.trsl.2020.01.005

Tsuru, A., Fujimoto, N., Takahashi, S., Saito, M., Nakamura, D., Iwano, M., Iwawaki, T., Kadokura, H., Ron, D., & Kohno, K. (2013). Negative feedback by IRE1β optimizes mucin production in goblet cells. *Proceedings of the National Academy of Sciences of the United States of America*, *110*(8), 2864–2869. https://doi.org/10.1073/pnas.1212484110

Tumpey, T. M., Basler, C. F., Aguilar, P. V., Zeng, H., Solórzano, A., Swayne, D. E., Cox, N. J., Katz, J. M., Taubenberger, J. K., Palese, P., & García-Sastre, A. (2005). Characterization of the reconstructed 1918 Spanish influenza pandemic virus. *Science (New York, N.Y.)*, *310*(5745), 77–80. https://doi.org/10.1126/science.1119392

Van Poucke, S. G. M., Nicholls, J. M., Nauwynck, H. J., & Van Reeth, K. (2010). Replication of avian, human and swine influenza viruses in porcine respiratory explants and association with sialic acid distribution. *Virology Journal*, *7*, 38. https://doi.org/10.1186/1743-422X-7-38

Vasilijevic, J., Zamarreño, N., Oliveros, J. C., Rodriguez-Frandsen, A., Gómez, G., Rodriguez, G., Pérez-Ruiz, M., Rey, S., Barba, I., Pozo, F., Casas, I., Nieto, A., & Falcón, A. (2017). Reduced accumulation of defective viral genomes contributes to severe outcome in influenza virus infected patients. *PLOS Pathogens*, *13*(10), e1006650. https://doi.org/10.1371/journal.ppat.1006650

Vattem, K. M., & Wek, R. C. (2004). Reinitiation involving upstream ORFs regulates ATF4 mRNA translation in mammalian cells. *Proceedings of the National Academy of Sciences of the United States of America*, *101*(31), 11269–11274. https://doi.org/10.1073/pnas.0400541101

Velappan, N., Micheva-Viteva, S., Adikari, S. H., Waldo, G. S., Lillo, A. M., & Bradbury, A. R. M. (2020). Selection and verification of antibodies against the cytoplasmic domain of M2 of influenza, a transmembrane protein. *MAbs*, *12*(1), 1843754. https://doi.org/10.1080/19420862.2020.1843754

Villareal, V. A., Rodgers, M. A., Costello, D. A., & Yang, P. L. (2015). Targeting host lipid synthesis and metabolism to inhibit dengue and hepatitis C viruses. *Antiviral Research*, *124*, 110–121. https://doi.org/10.1016/j.antiviral.2015.10.013

Visher, E., Whitefield, S. E., McCrone, J. T., Fitzsimmons, W., & Lauring, A. S. (2016). The Mutational Robustness of Influenza A Virus. *PLoS Pathogens*, *12*(8), e1005856. https://doi.org/10.1371/journal.ppat.1005856

Volmer, R., Ploeg, K. van der, & Ron, D. (2013). Membrane lipid saturation activates endoplasmic reticulum unfolded protein response transducers through their transmembrane domains. *Proceedings of the National Academy of Sciences*, *110*(12), 4628–4633. https://doi.org/10.1073/pnas.1217611110

Wang, P., Li, J., Tao, J., & Sha, B. (2018). The luminal domain of the ER stress sensor protein PERK binds misfolded proteins and thereby triggers PERK oligomerization. *Journal of Biological Chemistry*, *293*(11), 4110–4121. https://doi.org/10.1074/jbc.RA117.001294

Wang, Q., Li, L., & Ye, Y. (2006). Regulation of retrotranslocation by p97-associated deubiquitinating enzyme ataxin-3. *The Journal of Cell Biology*, *174*(7), 963–971. https://doi.org/10.1083/jcb.200605100

Watanabe, T., Kawakami, E., Shoemaker, J. E., Lopes, T. J. S., Matsuoka, Y., Tomita, Y., Kozuka-Hata, H., Gorai, T., Kuwahara, T., Takeda, E., Nagata, A., Takano, R., Kiso, M., Yamashita, M., Sakai-Tagawa, Y., Katsura, H., Nonaka, N., Fujii, H., Fujii, K., … Kawaoka, Y. (2014). Influenza virus-host interactome screen as a platform for antiviral drug development. *Cell Host & Microbe*, *16*(6), 795–805. https://doi.org/10.1016/j.chom.2014.11.002

Weiland, J. E., Davis, W. B., Holter, J. F., Mohammed, J. R., Dorinsky, P. M., & Gadek, J. E. (1986). Lung neutrophils in the adult respiratory distress syndrome. Clinical and pathophysiologic significance. *The American Review of Respiratory Disease*, *133*(2), 218–225. https://doi.org/10.1164/arrd.1986.133.2.218

Welkers, M. R. A., Pawestri, H. A., Fonville, J. M., Sampurno, O. D., Pater, M., Holwerda, M., Han, A. X., Russell, C. A., Jeeninga, R. E., Setiawaty, V., de Jong, M. D., & Eggink, D. (2019). Genetic diversity and host adaptation of avian H5N1 influenza viruses during human infection. *Emerging Microbes & Infections*, *8*(1), 262–271. https://doi.org/10.1080/22221751.2019.1575700

Wennerberg, K., Rossman, K. L., & Der, C. J. (2005). The Ras superfamily at a glance. *Journal of Cell Science*, *118*(Pt 5), 843–846. https://doi.org/10.1242/jcs.01660

Wheeler, J. R., Matheny, T., Jain, S., Abrisch, R., & Parker, R. (2016). Distinct stages in stress granule assembly and disassembly. *ELife*, *5*, e18413. https://doi.org/10.7554/eLife.18413

Wille, M., & Holmes, E. C. (2020). The Ecology and Evolution of Influenza Viruses. *Cold Spring Harbor Perspectives in Medicine*, *10*(7). https://doi.org/10.1101/cshperspect.a038489

Wilson, I. A., Skehel, J. J., & Wiley, D. C. (1981). Structure of the haemagglutinin membrane glycoprotein of influenza virus at 3 A resolution. *Nature*, *289*(5796), 366–373. https://doi.org/10.1038/289366a0

Wolfe, A. L., Singh, K., Zhong, Y., Drewe, P., Rajasekhar, V. K., Sanghvi, V. R., Mavrakis, K. J., Jiang, M., Roderick, J. E., Van der Meulen, J., Schatz, J. H., Rodrigo, C. M., Zhao, C., Rondou, P., de Stanchina, E., Teruya-Feldstein, J., Kelliher, M. A., Speleman, F., Porco, J. A., … Wendel, H.-G. (2014). RNA G-quadruplexes cause eIF4A-dependent oncogene translation in cancer. *Nature*, *513*(7516), 65–70. https://doi.org/10.1038/nature13485

Wong, E. H. M., Smith, D. K., Rabadan, R., Peiris, M., & Poon, L. L. M. (2010). Codon usage bias and the evolution of influenza A viruses. Codon Usage Biases of Influenza Virus. *BMC Evolutionary Biology*, *10*, 253. https://doi.org/10.1186/1471-2148-10-253

Wu, J., Chen, S., Liu, H., Zhang, Z., Ni, Z., Chen, J., Yang, Z., Nie, Y., & Fan, D. (2018). Tunicamycin specifically aggravates ER stress and overcomes chemoresistance in multidrug-resistant gastric cancer cells by inhibiting N-glycosylation. *Journal of Experimental & Clinical Cancer Research: CR*, *37*(1), 272. https://doi.org/10.1186/s13046-018-0935-8

Wu, Y., Wu, Y., Tefsen, B., Shi, Y., & Gao, G. F. (2014). Bat-derived influenza-like viruses H17N10 and H18N11. *Trends in Microbiology*, *22*(4), 183–191. https://doi.org/10.1016/j.tim.2014.01.010

Xu, L., Bao, L., Li, F., Lv, Q., Ma, Y., Zhou, J., Xu, Y., Deng, W., Zhan, L., Zhu, H., Ma, C., Shu, Y., & Qin, C. (2011). Adaption of Seasonal H1N1 Influenza Virus in Mice. *PLOS ONE*, *6*(12), e28901. https://doi.org/10.1371/journal.pone.0028901

Xu, L., Bao, L., Lv, Q., Deng, W., Ma, Y., Li, F., Zhan, L., Zhu, H., Ma, C., & Qin, C. (2010). A single-amino-acid substitution in the HA protein changes the replication and pathogenicity of the 2009 pandemic A (H1N1) influenza viruses in vitro and in vivo. *Virology Journal*, *7*, 325. https://doi.org/10.1186/1743-422X-7-325

Xu, Z., Zhou, R., Jin, M., & Chen, H. (2010). Selection pressure on the hemagglutinin gene of influenza A (H1N1) virus: Adaptation to human and swine hosts in Asia. *Acta Virologica*, *54*(2), 113–118. https://doi.org/10.4149/av_2010_02_113

Yamamoto, K., & Ichikawa, S. (2019). Tunicamycin: Chemical synthesis and biosynthesis. *The Journal of Antibiotics*, *72*(12), 924–933. https://doi.org/10.1038/s41429-019-0200-1

Yamamoto, K., Yoshida, H., Kokame, K., Kaufman, R. J., & Mori, K. (2004). Differential contributions of ATF6 and XBP1 to the activation of endoplasmic reticulum stress-responsive cis-acting elements ERSE, UPRE and ERSE-II. *Journal of Biochemistry*, *136*(3), 343–350. https://doi.org/10.1093/jb/mvh122

Yángüez, E., Castello, A., Welnowska, E., Carrasco, L., Goodfellow, I., & Nieto, A. (2011). Functional impairment of eIF4A and eIF4G factors correlates with inhibition of influenza virus mRNA translation. *Virology*, *413*(1), 93–102. https://doi.org/10.1016/j.virol.2011.02.012

Yángüez, E., Rodriguez, P., Goodfellow, I., & Nieto, A. (2012). Influenza virus polymerase confers independence of the cellular cap-binding factor eIF4E for viral mRNA translation. *Virology*, *422*(2), 297–307. https://doi.org/10.1016/j.virol.2011.10.028

Ye, J., Rawson, R. B., Komuro, R., Chen, X., Davé, U. P., Prywes, R., Brown, M. S., & Goldstein, J. L. (2000). ER stress induces cleavage of membrane-bound ATF6 by the same proteases that process SREBPs. *Molecular Cell*, *6*(6), 1355–1364. https://doi.org/10.1016/s1097-2765(00)00133-7

Yewdell, J. W., Yellen, A., & Bächi, T. (1988). Monoclonal antibodies localize events in the folding, assembly, and intracellular transport of the influenza virus hemagglutinin glycoprotein. *Cell*, *52*(6), 843–852. https://doi.org/10.1016/0092-8674(88)90426-6

Yin, Y., Chen, S., Hakim, M. S., Wang, W., Xu, L., Dang, W., Qu, C., Verhaar, A. P., Su, J., Fuhler, G. M., Peppelenbosch, M. P., & Pan, Q. (2018). 6-Thioguanine inhibits rotavirus replication through suppression of Rac1 GDP/GTP cycling. *Antiviral Research*, *156*, 92–101. https://doi.org/10.1016/j.antiviral.2018.06.011

Yoshida, H., Matsui, T., Yamamoto, A., Okada, T., & Mori, K. (2001). XBP1 mRNA is induced by ATF6 and spliced by IRE1 in response to ER stress to produce a highly active transcription factor. *Cell*, *107*(7), 881–891. https://doi.org/10.1016/s0092-8674(01)00611-0

Yoshida, H., Okada, T., Haze, K., Yanagi, H., Yura, T., Negishi, M., & Mori, K. (2000). ATF6 activated by proteolysis binds in the presence of NF-Y (CBF) directly to the cis-acting element responsible for the mammalian unfolded protein response. *Molecular and Cellular Biology*, *20*(18), 6755–6767. https://doi.org/10.1128/mcb.20.18.6755-6767.2000

Zhang, H., Nakajima, S., Kato, H., Gu, L., Yoshitomi, T., Nagai, K., Shinmori, H., Kokubo, S., & Kitamura, M. (2013). Selective, potent blockade of the IRE1 and ATF6 pathways by 4-phenylbutyric acid analogues. *British Journal of Pharmacology*, *170*(4), 822–834. https://doi.org/10.1111/bph.12306

Zhang, X., & Wang, Y. (2016). Glycosylation quality control by the Golgi structure. *Journal of Molecular Biology*, *428*(16), 3183–3193. https://doi.org/10.1016/j.jmb.2016.02.030

Zhang, Z., Hu, S., Li, Z., Wang, X., Liu, M., Guo, Z., Li, S., Xiao, Y., Bi, D., & Jin, H. (2011). Multiple amino acid substitutions involved in enhanced pathogenicity of LPAI H9N2 in mice. *Infection, Genetics and Evolution: Journal of Molecular Epidemiology and Evolutionary Genetics in Infectious Diseases*, *11*(7), 1790–1797. https://doi.org/10.1016/j.meegid.2011.07.025

Zheng, B., Chan, K.-H., Zhang, A. J. X., Zhou, J., Chan, C. C. S., Poon, V. K. M., Zhang, K., Leung, V. H. C., Jin, D.-Y., Woo, P. C. Y., Chan, J. F. W., To, K. K. W., Chen, H., & Yuen, K.-Y. (2010). D225G mutation in hemagglutinin of pandemic influenza H1N1 (2009) virus enhances virulence in mice. *Experimental Biology and Medicine (Maywood, N.J.)*, *235*(8), 981–988. https://doi.org/10.1258/ebm.2010.010071

Zost, S. J., Parkhouse, K., Gumina, M. E., Kim, K., Diaz Perez, S., Wilson, P. C., Treanor, J. J., Sant, A. J., Cobey, S., & Hensley, S. E. (2017). Contemporary H3N2 influenza viruses have a glycosylation site that alters binding of antibodies elicited by egg-adapted vaccine strains. *Proceedings of the National Academy of Sciences of the United States of America*, *114*(47), 12578–12583. https://doi.org/10.1073/pnas.1712377114

Zyryanova, A. F., Kashiwagi, K., Rato, C., Harding, H. P., Crespillo-Casado, A., Perera, L. A., Sakamoto, A., Nishimoto, M., Yonemochi, M., Shirouzu, M., Ito, T., & Ron, D. (2021). ISRIB Blunts the Integrated Stress Response by Allosterically Antagonising the Inhibitory Effect of Phosphorylated eIF2 on eIF2B. *Molecular Cell*, *81*(1), 88-103.e6. https://doi.org/10.1016/j.molcel.2020.10.031